

Mimicking the [Fe] Hydrogenase Active Site:

Transition Metal Frustrated Lewis Pairs for the Heterolytic Cleavage of Dihydrogen



Mimicking the [Fe] Hydrogenase Active Site:
Transition Metal Frustrated Lewis Pairs for the
Heterolytic Cleavage of Dihydrogen

Mimicking the [Fe] Hydrogenase Active Site: Transition Metal Frustrated Lewis Pairs for the Heterolytic Cleavage of Dihydrogen

Dissertation

zur Erlangung des mathematisch-naturwissenschaftlichen
Doktorgrades
„Doctor rerum naturalium“
der Georg-August-Universität Göttingen

im Promotionsprogramm Chemie
der Georg-August University School of Science (GAUSS)

vorgelegt von

Kai Felix Kalz

aus Celle

Göttingen 2014

Betreuungsausschuss

Prof. Dr. Franc Meyer	<i>Institut für Anorganische Chemie, Universität Göttingen</i>
Prof. Dr. Ulf Diederichsen	<i>Institut für Organische und Biomolekulare Chemie, Universität Göttingen</i>
Prof. Dr. Ebbe Nordlander	<i>Chemical Center – Chemical Physics, Lunds Universitet</i>

Referent

Prof. Dr. Franc Meyer	<i>Institut für Anorganische Chemie, Universität Göttingen</i>
-----------------------	--

Korreferent

Prof. Dr. Ulf Diederichsen	<i>Institut für Organische und Biomolekulare Chemie, Universität Göttingen</i>
----------------------------	--

Weitere Mitglieder der Prüfungskommission

Prof. Dr. Guido Clever	<i>Institut für Anorganische Chemie, Universität Göttingen</i>
Prof. Dr. Sven Schneider	<i>Institut für Anorganische Chemie, Universität Göttingen</i>
Jun.-Prof. Dr. Ricardo Mata	<i>Institut für Physikalische Chemie, Universität Göttingen</i>
Dr. Inke Siewert	<i>Institut für Anorganische Chemie, Universität Göttingen</i>

Tag der mündlichen Prüfung: 28.07.2014

Coverdesign: Niels Kalz

Bibliografische Information der Deutschen Nationalbibliothek

Die Deutsche Nationalbibliothek verzeichnet diese Publikation in der Deutschen Nationalbibliografie; detaillierte bibliografische Daten sind im Internet über <http://dnb.d-nb.de> abrufbar.

1. Aufl. - Göttingen : Cuvillier, 2014
Zugl.: Göttingen, Univ., Diss., 2014

© CUVILLIER VERLAG, Göttingen 2014
Nonnenstieg 8, 37075 Göttingen
Telefon: 0551-54724-0
Telefax: 0551-54724-21
www.cuvillier.de

Alle Rechte vorbehalten. Ohne ausdrückliche Genehmigung des Verlages ist es nicht gestattet, das Buch oder Teile daraus auf fotomechanischem Weg (Fotokopie, Mikrokopie) zu vervielfältigen.

1. Auflage, 2014

Gedruckt auf umweltfreundlichem, säurefreiem Papier aus nachhaltiger Forstwirtschaft

ISBN 978-3-95404-890-8
eISBN 978-3-7369-4890-7

Contents

1	Introduction	1
1.1	Hydrogen – Fuel of the Future?	2
1.2	Basic Principles of Dihydrogen Activation	3
1.3	Frustrated Lewis Pairs (FLPs)	5
1.3.1	General Concept	6
1.3.2	Mechanism of H ₂ Activation in FLPs	8
1.3.3	Transition Metal-Based FLPs	9
1.4	Hydrogenases – The Natural Hydrogen Economy	11
1.4.1	[FeFe] and [NiFe] Hydrogenases	12
1.4.2	The [Fe] Hydrogenase – A Novel Kind of Hydrogenase	15
1.5	Model Complexes: Learning from Nature	21
1.6	Objective	24
2	Mimicking the Natural Hydride Acceptor Methenyl-H₄MPT⁺	27
2.1	Hydride Acceptors in Biology and Chemistry	28
2.1.1	Imidazolium Ions as Hydride Acceptor Molecules	28
2.1.2	Models for N ⁵ ,N ¹⁰ -Methenyltetrahydrofolate	29
2.2	Synthesis of Imidazolinium Ions	31
2.2.1	General Strategy	32
2.2.2	Synthesis of Amidines	34
2.2.3	Formation of the Imidazolinium Heterocycle	35
2.2.4	Further Attempts to Synthesize Imidazolinium Salts	37
2.3	Properties of Imidazolinium Ions	40
2.3.1	Structural Parameters of Imidazolinium Ions	41
2.3.2	Electrochemical Properties of Imidazolinium Ions	44
2.3.3	Reactivity of Imidazolinium Ions	47
2.4	Conclusion	51
3	The Chemistry of Amidines: Isomers and Silver Complexes	53
3.1	General Aspects of Amidines	54
3.1.1	Classification of Amidines	54
3.1.2	Isomerism in Amidines	55
3.1.3	Molecular Association	57
3.2	Structural Parameters of Amidines	58

3.3	The Chemistry of Amidines in Solution	61
3.3.1	Temperature and Concentration Dependencies	62
3.3.2	Identification of Isomers	68
3.4	The Coordination Chemistry of Amidines	78
3.4.1	General Aspects	78
3.4.2	Amidinat silver(I) Complexes	79
3.5	Summary	83
4	The Transition Metal Lewis Base	85
4.1	The Choice and Synthesis of a Suitable Lewis Base	86
4.1.1	General Aspects	86
4.1.2	Synthesis of Carbonyl Metalates	87
4.1.3	Alternative Metal Complexes	88
4.2	Revisiting the Synthesis of $K[CpRu(CO)_2]$ (KRp)	90
4.2.1	A Revised Synthetic Protocol	90
4.2.2	Isotope Labeling	91
4.2.3	Elucidating the Structure and Further Properties of KRp	92
4.3	Rs – A Metalate with Interesting Properties	94
4.3.1	IR Spectroscopy	95
4.3.2	Mass Spectrometry and UV/Vis Spectroscopy	96
4.3.3	Solid-State ^{13}C MAS NMR Spectroscopy	97
4.3.4	Elemental Analysis and Bulk Morphology	101
4.3.5	Conclusion	103
4.4	Summary and Outlook	103
5	Transition Metal Frustrated Lewis Pairs	105
5.1	Synthesis of Transition Metal Frustrated Lewis Pairs	106
5.1.1	Proof of Principle: Synthesis of $[Im^{-2H}]^+Fp^-$	107
5.1.2	Imidazolium-Based Lewis Pairs Lacking Frustration	108
5.2	Nucleophilic Substitution Reactions	110
5.2.1	The adduct $[Fp-C_6F_4MesIm]^+$	110
5.2.2	Mechanistic Details	113
5.2.3	A Second Example: Ruthenium Adduct $[Rp-TolFIm]^+$	114
5.2.4	Consequences for Reactions with H_2 and Other Substrates	117
5.3	Electron Transfer Reactions	118
5.3.1	General Considerations	118
5.3.2	Electron Transfer between $TolFIm^+Br^-$ and KFp	119
5.3.3	Structure of the Radical TolFIm	121
5.3.4	Competing ET and Nucleophilic Substitution Reactions	122
5.3.5	Dihydrogen Splitting Despite Other Reactivities?	124
5.4	Further Examples and Unclear Reactions	126
5.5	$TolFIm^+Br^-$ and Rs : A Novel H_2 Splitting System	128
5.5.1	DFT Calculations	128
5.5.2	Advantages of Rs and H/D Exchange Reactions	130
5.5.3	Heterolytic Splitting of Dihydrogen	131
5.6	Summary and Conclusion	137

6 Experimental Section	139
6.1 General Considerations	139
6.2 Synthesis of Amidines	141
6.3 Synthesis of Bisamidinatodisilver(I) Complexes	149
6.4 Synthesis of Imidazolium Salt [Im ^{-2H}] ⁺ Br ⁻	151
6.5 Synthesis of Imidazolinium Salts	152
6.6 Synthesis of Imidazolidines	160
6.7 Synthesis of Carbonyl Metalates	163
6.8 Attempted Syntheses of Transition Metal FLPs	166
6.9 Reactions with H ₂ or D ₂	170
6.10 Reactions with Other Substrates	172
6.11 DFT Calculations	172
Bibliography	175
List of Abbreviations	197
Appendix	201
Structures of Important Compounds	203
Crystallographic Data	206
Electron Microprobe Analysis	214
Additional NMR Data	215
List of Scientific Contributions	219
Acknowledgments	221
Curriculum Vitae	223

1

Introduction

Abstract Hydrogen is the most abundant element on earth, but only a very small fraction of it is found as molecular gas H₂. Nevertheless, entire ecosystems are powered by this fuel in nature, raising mankind's hope that sustainable alternatives for the use of fossil fuels exist. Improved systems producing and activating the H₂ molecule have to be developed in order to pave the way for a hydrogen economy, which could satisfy the ever-increasing demand for energy of our society. This chapter provides the theoretical background on the activation of dihydrogen introducing "classical" transition metal-based systems and the so-called frustrated Lewis pairs (FLPs), a class of novel catalysts which has become increasingly popular in the last years. Furthermore, information on a group of naturally-occurring enzymes called hydrogenases is provided. Due to their astonishing high efficiency in producing or activating dihydrogen, hydrogenases are ideal prototypes that could trigger the development of a new era of H₂ activation catalysts featuring unforeseen efficiencies.

1.1 Hydrogen – Fuel of the Future?

In a world as dependent on the availability of energy as ours, the most urgent scientific and technical challenge is to assure a secure and environmentally benign supply of energy.^[1] Facing an ever-increasing demand for energy which currently comprises roughly 16.3 TW per year and which is projected to reach 20 TW in 2030, to double by 2050 and to triple by the end of the century,^[1,2] this challenge represents an enormous problem to solve. Furthermore, a development towards a renewable supply of energy has to occur since only finite resources of fossil fuels are available and combustion of oil, natural gas or coal poses severe problems to the environment and earth's climate by emission of carbon dioxide. And yet, the sun annually provides 100 000 TW of solar energy to our planet, hence only a little more than one hour of sunlight could in principle satisfy our annual energy requirements.^[2] Methods to capture this energy exist but their efficiencies are still insufficient to represent a serious alternative to fossil fuels.

An attractive approach to utilize solar energy is its storage in the form of chemical bonds – like in natural photosynthesis. However, the construction of a so-called “artificial leaf” which is able to efficiently collect and convert solar energy remains an enormous scientific challenge.^[3–5] The hydrogen (H₂) molecule – from organometallic chemists frequently called dihydrogen – is the central energy carrier in an envisioned scenario of alternative energy supplies focusing on sustainable methods to produce, store and consume energy. This aspired scenario has been coined “hydrogen economy”,^[6–8] but problems connected with its realization still persist despite the effort of research already spent on this topic. Accordingly, efficient and sustainable methods to produce H₂ and to recover the energy stored in this molecule have to be developed by the basic science.^[1] In addition to this, novel hydrogen storage materials have to be found in order to guarantee a safe and practical possibility to use dihydrogen as an energy vector, especially in automotive applications.^[9,10] Nevertheless, once the problems are overcome, dihydrogen could be the ideal energy carrier since its energy density is 142 MJ kg⁻¹, which is more than three times larger than that of liquid hydrocarbons.^[9] Furthermore, H₂ is a clean fuel as the only exhaust gas one obtains when burning it with dioxygen is water. A reaction of H₂ and O₂ in a controlled way, for example in a fuel cell, could thus be the key to a sustainable energy supply in the future. However, novel catalysts have to be developed in order to make both the production and energetic exploitation of H₂ more efficient.

Dihydrogen is not only important as a future energy carrier, but even today vast quantities are used in chemical reactions. All crude oil is treated with H₂ within the refining process and hundreds of million tons of ammonia are synthesized every year by the Haber-Bosch process.^[11] A common problem of the presently available methods to achieve these transformations is the fact that often expensive and non-abundant metals as for example platinum have to be used. The main reason for this is the high H–H bond energy of 436 kJ mol⁻¹.^[12] Consequently, reactions involving H₂ usually afford the

input of considerable amounts of energy. Despite this fundamental drawback, catalytic hydrogenations constitute the majority of human-made chemical reactions in the world. Facing the enormous amounts of dihydrogen used in chemical processes, the need for more efficient catalysts becomes even more apparent.

At the present time, nearly all hydrogen gas required for chemical transformations is produced by reactions from carbon feedstocks (fossil fuels and biomass).^[13] The most relevant method is the endothermic steam reforming of methane which is conducted at a nickel catalyst at elevated temperatures and converts natural gas (CH_4 and H_2O) to synthesis gas (CO and H_2). Further amounts of dihydrogen can be obtained by the water-gas shift reaction producing CO_2 and H_2 from CO and H_2O .^[13] It is important to note that this industrial production of dihydrogen is not sustainable since fossil fuels are used to generate H_2 . In a long-term view, energetically unfavored splitting of water by electrolysis or solar power has to evolve into an attractive alternative to steam reforming processes in order to produce H_2 in a sustainable way. However, a massive effort of scientific research is still required in order to improve existing dihydrogen-producing systems. Inspiration for these novel catalysts might come from naturally occurring enzymes (see section 1.4).

1.2 Basic Principles of Dihydrogen Activation

The activation of small molecules like dihydrogen is most commonly conducted at transition metal centers since the availability of d orbitals allows for a variety of possible orbital interactions, ultimately leading to the activation of chemical bonds.^[14] The tuneability in terms of electron configuration and oxidation state are further advantages of transition metals in catalytic reactions. Soon after the discovery of the first metal complex containing a dihydrogen ligand, $\text{W}(\text{CO})_3(\text{P}^i\text{Pr}_3)_2(\eta^2\text{-H}_2)$, by Kubas *et al.* in 1984,^[15] the theoretical foundation for understanding bond formation with a hydrogen molecule was laid. This led to a reinvestigation of known dihydride complexes and soon further dihydrogen complexes appeared in literature.^[16] As an extension of the Chatt-Dewar-Duncanson model for complexes with unsaturated alkene or alkyne ligands (“ π -complexes”), the bonding situation found in H_2 complexes has been termed “ σ -complex”, indicating that a σ bond interacts with a metal center.^[17] Analogous to the three-center two-electron (3c-2e) bonding in carbocations and boranes, this binding can be called nonclassical.^[16] The set of possible orbital interactions of a transition metal M with the typically *side-on* coordinated H_2 molecule is depicted in Figure 1.1. In principle two synergistic orbital interactions, donation of electron density from the bonding σ orbital of dihydrogen into a vacant d orbital (d_{z^2}) of the metal and $\text{M} \rightarrow \text{H}_2$ backdonation into the antibonding σ^* orbital, contribute to an overall binding interaction.

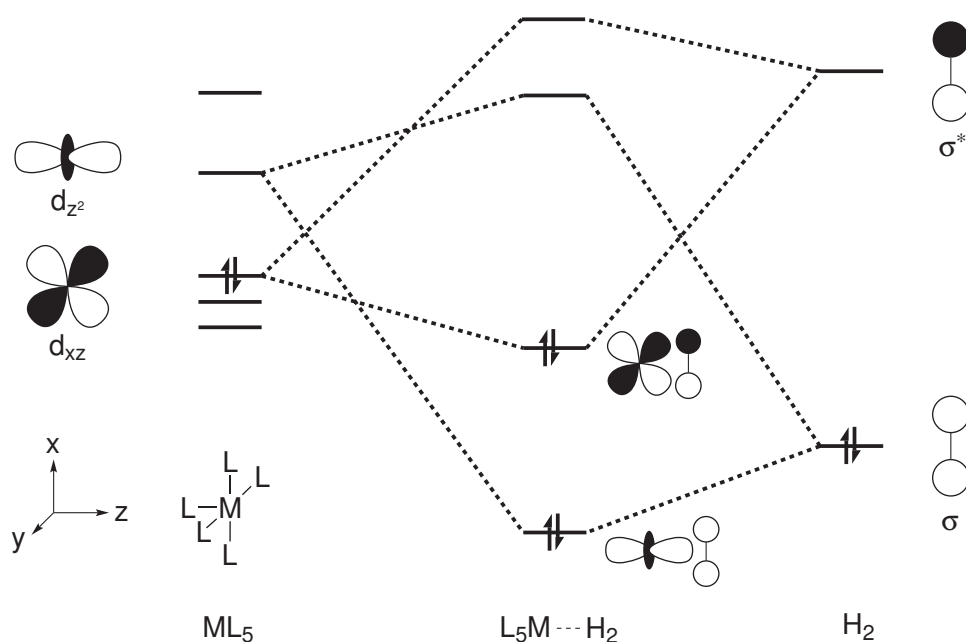


Figure 1.1. Orbital interactions in an octahedral $M-H_2$ σ -complex with a *side-on* coordinated dihydrogen ligand. Adapted with permission from Kubas *et al.*,^[18] © 2007 American Chemical Society.

Homolytic and Heterolytic Splitting of H_2

Considering backdonation of metal d electrons into the antibonding H_2 orbital is not only crucial to the understanding of the stabilization of a metal- H_2 σ -complex, in fact it is also the key to comprehend activation of the H-H single bond. If the electron density donated into the σ^* orbital is large enough, the H-H bond is cleaved homolytically and a dihydride complex is formed. However, no sharp separation between H_2 and dihydride complexes exist, but rather a continuum of different H-H bond distances (Figure 1.2). The elongation of the H-H bond depends (analogously to the degree of olefin activation described by the Chatt-Dewar-Duncanson model) on the degree of backdonation from the metal center.^[16] Astonishingly, the very strong H-H bond can be stretched to more than twice its length in molecular H_2 during its activation at a metal center. Powerful methods to probe the degree of activation of the H_2 molecule in metal complexes are neutron diffraction and nuclear magnetic resonance (NMR) spectroscopy, permitting a direct determination of the H-H bond distance and, respectively, the measurement of coupling constants J_{HD} in HD-substituted complexes or T_1 relaxation times.^[18]

The type of bond activation associated with a high degree of backdonation of electron density into the H_2 σ^* orbital culminates in a homolytic splitting of the dihydrogen molecule. By this, the oxidation state of the metal increases by two and overall an oxidative addition takes place. Furthermore, the total coordination number of the complex increases by one. On the contrary, neither the oxidation state of the metal nor the coordination number changes when a heterolytic cleavage of the dihydrogen molecule

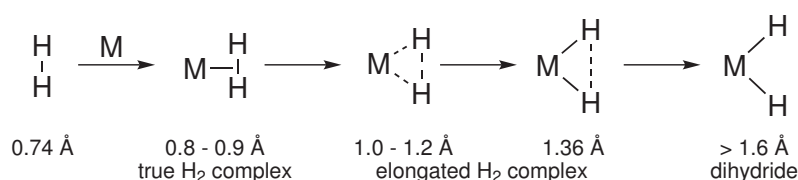


Figure 1.2. Stretching of H–H bond distances for a series of M–H₂ complexes. Adapted with permission from Kubas *et al.*,^[16] © 2001 Elsevier.

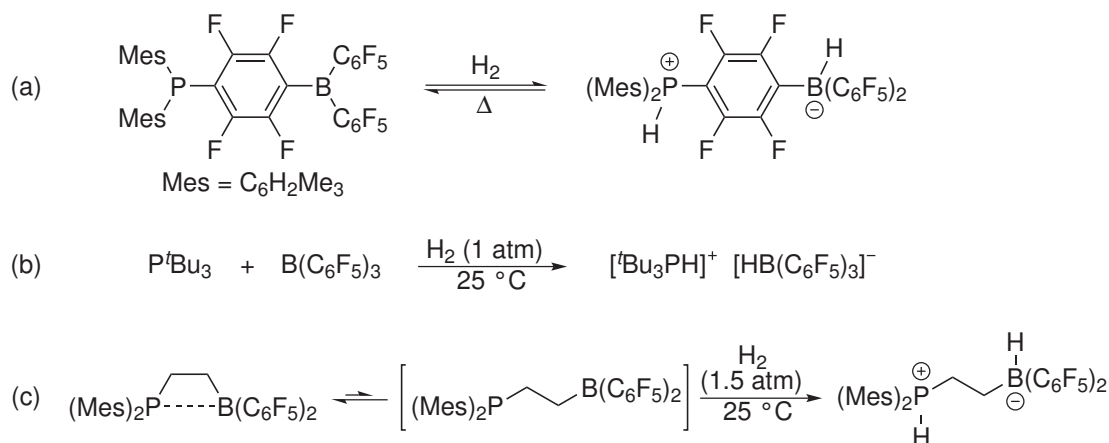
occurs. In this case the H–H bond is not split into equal parts, but formation of a hydride ion (H[−]) and a proton can be observed. Typically the hydride ion coordinates to the metal center (thereby decreasing the overall charge of the complex by −1) and the remaining proton is accepted by an internal or external base.^[19] Whether a homolytic or heterolytic splitting of the H₂ molecule occurs, is governed by the electronic properties of the complex. Electron-rich metal centers favor the homolytic cleavage since the extent of backdonation is typically relatively large, whereas electron-poor/electrophilic metals mostly show heterolytic cleavage of H₂. Here, backdonation is weak and most of the overall bonding interaction can be attributed to a strong H₂→M σ-donation.^[16,18] In such complexes, the H₂ molecule is usually highly polarized. Indeed, coordinating H₂ to a highly electrophilic cationic metal usually leads to an increase of its acidity by up to several orders of magnitude.^[18] Once H₂ is homolytically or heterolytically activated, protons and/or hydride ions can be transferred to a substrate, providing the basis for a large array of homogeneous industrial processes. Metal complexes which have been successfully applied in large-scale industrial catalytic hydrogenations include such prominent examples as Wilkinson’s rhodium-based catalyst RhCl(PPh₃)₃ or the ruthenium-based Noyori systems.^[20,21]

1.3 Frustrated Lewis Pairs (FLPs)

Until relatively recently in the history of dihydrogen activation, chemists assumed that only transition metals were able to cleave the very stable H–H bond. This belief was fundamentally shattered when a series of metal-free systems were discovered at the beginning of the 21st century. Bertrand *et al.* reported that stable singlet carbenes can mimic to some extent the reactivity of transition metals by nucleophilically activating dihydrogen or even ammonia under very mild conditions.^[22] Even more groundbreaking was the development of the concept of frustrated Lewis pairs (FLPs) which was popularized by the groups of Stephan and Erker.^[23–27] The discovery of a phosphine-borane that was able to reversibly activate dihydrogen by Stephan *et al.*^[28] in 2006 and subsequent publication of related intermolecular^[29] and intramolecular^[30] systems paved the way for a new era of hydrogen activation already foreshadowing unforeseen applications.^[31]

1.3.1 General Concept

The first systems represented in Scheme 1.1 had in common that an electron-deficient borane was combined with a Lewis basic phosphine. Contrary to the widely accepted understanding that combination of a Lewis acid and a Lewis base would inevitably lead to the formation of a Lewis acid–base adduct, the reactivity inherent to FLPs was not quenched by adduct formation. Instead, steric constraints prevented the system from forming unreactive adducts and enabled the use of FLPs for bond activation. The first intramolecular system^[28] (example (a) in Scheme 1.1) was shown to reversibly incorporate dihydrogen. The Lewis acidic borane accepts a hydride ion and the phosphine Lewis base is protonated to yield a zwitterionic phosphonium borate. Hence the H₂ molecule is cleaved heterolytically. Further studies led to the discovery of the FLP shown in Scheme 1.1 (b). Here, a combination of B(C₆F₅)₃ and tri-(*tert*-butyl)phosphine afforded an FLP which could activate dihydrogen under mild conditions.^[29] The group of Erker developed the linked FLP shown in example (c) of Scheme 1.1, which could also achieve a metal-free activation of H₂ despite interaction of the phosphine and borane moieties.^[30,32] In solution, rupture of the weak P...B bond gives the intramolecular FLP which was also shown to be suitable for H₂ activation. From a thermodynamic view, intramolecular FLPs have several advantages since the critical step in the thermodynamic cycle, the association of the reaction partners, involves a considerable loss of entropy in the case of intermolecular systems.^[33,34] For this problem, the notion “termolecularity trap” has been used.^[35]



Scheme 1.1. Several frustrated Lewis pairs and their reactivity with H₂: (a) First FLP published by Stephan *et al.*,^[28] (b) an intermolecular^[29] and (c) a second intramolecular^[30] system.

The prospect of a hydrogenation catalysis no longer dependent on expensive and toxic metals led to an increased scientific interest in this particular field of research. Consequently, the insights into this fascinating topic grew rapidly and were summarized several times.^[23,27,36–38] In the course of further uncovering FLP reactivity, the early systems were modified and it was soon realized that the concept of frustrated Lewis

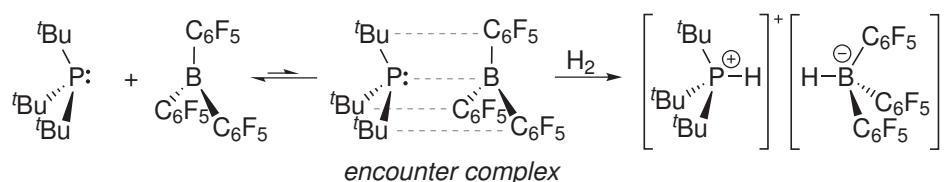
pairs was suitable to describe the activation of dihydrogen by a number of other systems. However, most modifications targeted the Lewis basic component and it was demonstrated that also nitrogen bases^[23,39] and N-heterocyclic carbenes (NHCs)^[40–44] were able to assist in the heterolytic cleavage of H₂. On the contrary, the borane Lewis acid was not subjected to much variation since this mostly lowered the reactivity of the obtained systems.^[45–47] Only few systems were reported that did not involve boranes with strongly electron-withdrawing substituents for FLP-type chemistry.^[48–52] A relatively recent development in this respect is the utilization of aluminum in FLP-type chemistry. These compounds show interesting properties and can be used in the activation of organic and inorganic molecules.^[53–64]

When developing novel FLP systems it is important to consider the dual importance of optimizing structural and electronic features of both the Lewis acid and the Lewis base.^[65,66] On the one hand, the reaction partners should have bulky residues in order to prevent the formation of simple Lewis adducts, and on the other hand the cumulative acid–base strength of the system should be high enough to enable the heterolytic cleavage of H₂.^[33] In principle it is possible to use a relatively weak Lewis base, but this requires a very electron-deficient Lewis acid as counterpart which is normally achieved by incorporating particularly electron-withdrawing substituents. By careful adjustment of steric (principle of “size exclusion”)^[66] and electronic^[67,68] properties it is also possible to add chemoselectivity or functional group tolerance to the system.

Besides dihydrogen also various other substrates have been used in reactions with FLPs. Particularly important is the activation of CO₂^[69–74] as it represents a potent greenhouse gas and simultaneously a sustainable source for the production of basic chemicals (e. g. carboxylic acids, methanol).^[75] Furthermore, FLPs were found to activate other small molecules such as THF,^[23] CO,^[76–78] alkenes,^[79] alkynes,^[80] silanes,^[81] halogens,^[82] N₂O,^[83–86] NO^[87,88] and SO₂.^[89] Even activity in polymerization reactions has been demonstrated for FLP systems.^[90,91] Besides this, FLP chemistry has now reached the point where it becomes interesting also for organic chemists and the chemical industry because FLP-based catalysts can be used for the transformation of organic substrates. In fact, a number of metal-free catalytic hydrogenations have been developed and are now available for reactions performed under mild conditions including substrates as imines,^[92] nitriles,^[92] aziridines,^[92] alkenes,^[93,94] alkynes,^[95] N-based heterocycles^[96] and many more. FLP catalysts have been optimized for hydrogenation reactions and surprisingly simple systems including for example ethers as Lewis bases have been developed.^[97] Even more astonishingly, first attempts to implement chirality have been successful and it was found that chiral FLPs can be used in asymmetric hydrogenations.^[98] Hydrogenation reactions mediated by FLPs have been comprehensively summarized recently.^[99–101]

1.3.2 Mechanism of H₂ Activation in FLPs

Despite a considerable amount of scientific contributions to this field, the mechanism of H₂ activation mediated by FLPs still remains a matter of debate. In their first publication on this topic,^[28] Stephan *et al.* speculated that the heterolytic splitting of dihydrogen might be initiated by *side-on* coordination of H₂ to the boron center and subsequent addition of H₂ to the B–C bond prior to reaction with the Lewis base. However, calculations showed that the activation barrier for such adduct formation in FLPs is rather high^[102,103] and no experimental proof for an interaction of boron with H₂ was found.^[29] Consequently, coordination of H₂ to the boron Lewis acid can be considered rather unlikely. In addition to *side-on* coordination to the boron center, also *end-on* coordination to the phosphine Lewis base was proposed based on the observation of phosphine-hydrogen adducts in low-temperature matrix-isolation experiments.^[104,105] However, the adducts were extremely unstable. The most probable mechanism of heterolytic H₂ splitting in phosphine-borane FLPs is represented in Scheme 1.2 and has been originally proposed by Pápai *et al.* in 2008.^[102] Instead of forming unreactive Lewis acid–base adducts, the two components of an FLP exhibit secondary interactions which lead to a weak association. In such an “encounter complex” the prevailing interactions are H⋯F interactions which is in line with the earlier observation of attractive dispersion forces in phosphine-borane addition products.^[106] Very recently, in addition to highly sophisticated computational investigations,^[107] even experimental proof for the association *via* weak dispersion interactions has been obtained by means of NMR spectroscopy.^[108]



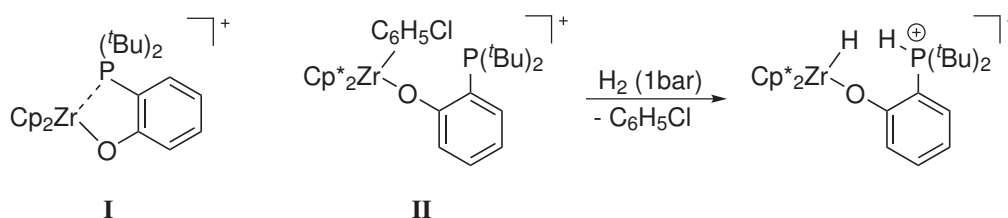
Scheme 1.2. Most probable mechanism of hydrogen splitting mediated by FLPs. Formation of a loosely bound encounter complex precedes the actual H₂ splitting step.

After formation of the encounter complex, the H₂ molecule enters the system and interacts with both reactive centers of the FLP. The true nature of this interaction is still under debate, but the signs increasingly point to a polarization of the H₂ molecule as part of the shifting of electron density from the phosphine to the boron center. In the course of this shifting, the H₂ σ* orbital accepts electron density from the phosphine and simultaneously electron density is donated from the H₂ σ orbital to the electrophilic borane. Consequently, the H–H bond is weakened and ultimately cleaved in a concerted way resulting in the formation of the phosphonium borate.^[102,109] In the transition state, a non-linear arrangement of the H₂ molecule has been found by structural and theoretical studies.^[110,111] A second concept has been proposed by Grimme *et al.* in 2010.^[112]

According to this model, a transfer of electrons is not necessarily required in order to activate dihydrogen. Instead, the electric field generated by the donor and acceptor atoms of the FLP might be sufficient for polarizing the H₂ molecule and finally leads to the observed heterolytic cleavage of dihydrogen. However, a number of subsequent theoretical calculations found only small contributions of the polarization effect to the overall interaction energy.^[113,114] Indeed, Pápai *et al.* recently showed in a comparative study that the electric field theory can be seriously questioned.^[115] Hence it can be assumed that H₂ activation in FLPs is the result of orbital interactions which involve the shifting of electron density.

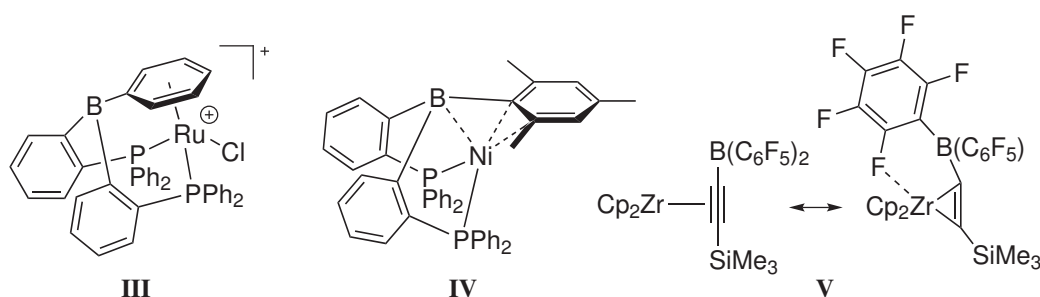
1.3.3 Transition Metal-Based FLPs

Still in its infancy, frustrated Lewis pair chemistry has not focused much on transition metals since scientists were eager to develop main group alternatives for transition metal-based catalysts. Nevertheless, indications that the FLP concept is also important in the realm of transition metal chemistry got stronger especially in the last few years. Indeed, FLP-type reactivity represents an exiting approach to achieve novel activation pathways and reactivity patterns in transition metal chemistry. Of high importance in this field were the contributions of Wass *et al.* demonstrating that some early transition metals are able to act as Lewis acids in FLP-type chemistry.^[116] The cationic zirconocene-phosphinoaryloxy complex **I** depicted in Scheme 1.3 showed for example reactivity in the dehydrogenation reactions of amine boranes. The related chlorobenzene adduct of the pentamethylcyclopentadienyl derivative **II** could even cleave the dihydrogen molecule.^[117] In general, these two and other systems developed by the group of Wass were shown to react for example with H₂, CO₂, CO, amine boranes, alkenes, alkynes, ethers or acetone and thus they represent “typical” FLPs, at least concerning their reaction pattern.^[116,118] Not only did these systems show a markedly higher reactivity than classical main group FLPs in many cases, additionally they featured unprecedented reactivities as for example CO reduction or C-halide cleavage in alkyl halides.^[118] Today also neutral or cationic lanthanum,^[118] titanium^[119,120] or hafnium complexes^[120] showing FLP reactivity are available. A comprehensive review about this chemistry has appeared recently.^[116,121]



Scheme 1.3. Zirconocene-phosphinoaryloxy complexes featuring FLP-type chemistry (Cp = C₅H₅, Cp* = C₅Me₅).^[117]

Expanding the FLP concept to the group of transition metals was an intriguing approach and soon other examples appeared in literature. However, most of the systems were restricted to electron-deficient transition metal centers as exemplified by further scandium-,^[122–124] zirconium-,^[125–128] hafnium-,^[129] ruthenium-,^[130] platinum-,^[131] or zinc-based^[132] complexes. A different approach to incorporate transition metals also makes use of the Lewis acidity of metal centers and their ability to facilitate a nucleophilic attack at a coordinated ligand. An example in which the metal fragment acts as a mere bystander was recently reported by Stephan and co-workers, demonstrating that complex **III** in Scheme 1.4 readily accepts a hydride ion at the phenyl ring when a phosphine base and H₂ are added.^[133] Such ancillary transition metal centers are not directly involved in the FLP reaction itself, but they are nevertheless essential for creating the actual Lewis acidic center. In addition to this, also cases are known in which the (still Lewis acidic) metal center assists in the formation of the carbon-based Lewis base, for example in ruthenium acetylides.^[134] On the contrary, in some other exemplary cases, the metal fragment is the substrate (transformations occur in the ligand sphere) or provides only the structural framework for activation.^[135]



Scheme 1.4. Examples for transition metal complexes showing FLP-type reactivity.

In contrast to Lewis acidic metal centers, Lewis basic transition metal fragments appear only rarely in literature, although the topic of metal-only Lewis pairs including transition metal Lewis bases was addressed recently by a review focusing on metal-metal dative bonding.^[136] In FLP-type chemistry, transition metal Lewis bases did not play a decisive role until now. However, some examples already exist where the metal fragment shows a Lewis basic character. The potential of certain platinum complexes^[137] to act as Lewis bases in reactions with fluoroboranes was recently demonstrated and furthermore also rhenium hydride/borane FLPs in which the metal hydride is the Lewis base were published.^[138] A promising concept to achieve Lewis basicity directly at the transition metal center is to incorporate boranes as ligands in the environment of the metal.^[139] Complex **IV** in Scheme 1.4 featuring close interactions with the boron atom and two carbon atoms of the mesityl ring for example cleaves H₂ heterolytically. In the course of the reaction the hydride ion is accepted by the borane yielding a bridging B–H–Ni hydrido ligand and the nickel center gets protonated.^[140] Furthermore, an intramolecular boron Lewis acid/zirconocene pair with a weak Zr...F contact (compound **V** in Scheme 1.4) was reported to react with a variety of small molecules.^[141,142]

As has been pointed out by Owen,^[139] many metal-borane complexes are not “frustrated” in the original sense since in most cases a direct bonding interaction between metal and borane moiety exists. This aspect is a general problem when talking about transition metal FLPs since – as seen above – also many ligand-assisted reactions at metal centers involving internal bases can be regarded as FLP-type transformations.^[121] In analogy to the known cooperative effects in transition metal catalysis, these systems have been termed “cooperative Lewis pairs” by Wass and co-workers due to the absence of steric factors preventing adduct formation.^[121] Indeed, in many cases H₂ cleavage by transition metal FLPs and ligand-assisted hydrogenation reactions are not so easily categorized and intermediate cases exist.^[116] Nevertheless, keeping the FLP concept in mind when considering such systems is useful since it permits a new view on already existing catalysts and could lead to their improvement. While the pool of transition metals offers new possibilities to extend the set of Lewis acids and Lewis bases in FLP-type reactions, the boundaries between “classical” FLP chemistry and cooperative activation by metals and ligands become increasingly blurred. Carrying FLP chemistry to extremes by expanding the concept to transition metals, might lead to interesting new developments in catalysis.

1.4 Hydrogenases – The Natural Hydrogen Economy

Despite the many efforts already made, establishing a sustainable energy supply including dihydrogen as the primary energy carrier still remains an enormous challenge. Efficient ways to produce, store and activate the H₂ molecule have to be found in order to replace fossil fuels as driving force of our society. In this respect nature is already far ahead of our development since the estimated global amount of dihydrogen produced and consumed in nature adds up to roughly 0.3 billion tons per year.^[143] Invariably, the concentrations of H₂ encountered by microorganisms are extremely low and therefore the enzymes involved in its metabolism feature high affinities and efficiencies. Indeed, dihydrogen is a valuable energy source or a sink of redundant electrons for many anaerobic or – less frequently – aerobic microorganisms with diverse metabolisms.^[144,145] Among those microorganisms engaged in H₂ metabolism are mainly bacteria and archaea, but also some eukaryotes.

Most of the processes consuming or producing dihydrogen are performed by an ancient group of enzymes named hydrogenases which catalyze the reversible reaction $\text{H}_2 \rightleftharpoons \text{H}^+ + \text{H}^- \rightleftharpoons 2\text{H}^+ + 2\text{e}^-$.^[146,147] From the isotope exchange reaction $\text{H}_2 + \text{D}_2\text{O} \rightleftharpoons \text{HD} + \text{HDO}$ it was inferred that hydrogenases cleave the H₂ molecule in a heterolytic way.^[148] According to the metal content of the active site, hydrogenases can be classified into [FeFe], [NiFe] or [Fe] hydrogenases. Although the three types of hydrogenases represent phylogenetically distinct classes,^[145] a unifying structural motif for activation or production of H₂ can be recognized in the enzymes since all of them harbor Fe^{II} metal ions in their active sites.^[143,149,150] Another common feature

is the presence of highly toxic CO or CN⁻ ligands which were previously considered completely abiological.^[151] Even though the reversible formation of H₂ from protons and electrons looks like a simple reaction, its realization is not so easily achieved since the standard redox potential $E^\circ(\text{H}_2/\text{H}^+)$ amounts to -414 mV at pH 7, a value below the potential of common redox mediators.^[152] This is why highly specialized enzymes with complex active centers are necessary to mediate the reaction. Facing the astonishingly high efficiencies of these biological systems, scientists try to discover the general concepts behind H₂ activation and to develop novel catalysts inspired by nature.^[143,153,154] As a consequence of the rapid developments in the field especially within the last two decades, a number of general reviews covering the most diverse aspects of hydrogenases such as their structure and function,^[146,147,150,155-157] occurrence and classification,^[145,158] physiological^[152,159] and chemical aspects,^[151,160,161] synthetic model compounds,^[149,162,163] computational studies,^[164] O₂ tolerance,^[165,166] biosynthesis,^[167] and electrocatalytic properties^[168,169] appeared in the literature. Very recently, an extensive review covering the different facets of hydrogenases was published.^[170] The following sections summarize the essential characteristics of the three classes of hydrogenases before focusing on approaches to design novel catalysts reminiscent of the naturally occurring systems.

1.4.1 [FeFe] and [NiFe] Hydrogenases

The first bacterial enzyme capable of activating molecular hydrogen was already observed in 1931 and coined “hydrogenase” by Stephenson and Stickland.^[171] However, the interest in this particular class of enzymes did not start to intensify until the 1990s after the publication of the first crystal structures of [FeFe] and [NiFe] hydrogenase enzymes.^[172-174] Subsequently, the significance of hydrogenase enzymes for the development of future H₂ production or activation catalysts was recognized and publications in this field increased rapidly.

Although, in principle, all hydrogenases work bidirectionally as isolated enzymes, the situation does not represent a true equilibrium process in living organisms because the physiological conditions provided by the cell mostly decide on the preferred direction of the reaction.^[170] [FeFe] hydrogenases preferentially catalyze the formation of dihydrogen from protons and electrons, whereas [NiFe] hydrogenases are mainly found in organisms performing the oxidation of H₂.^[175] Extremely high activities for H₂ generation are found in [FeFe] hydrogenases, but the enzymes only work under strictly anaerobic conditions.^[165,175] Under optimum conditions for example a single [FeFe] hydrogenase enzyme from *Desulfovibrio desulfuricans* is able to produce 9000 molecules of H₂ per second at 30 °C.^[175,176] In contrast to [FeFe] hydrogenases, [NiFe] hydrogenases are not irreversibly destroyed by O₂ and some variants are even active under aerobic conditions.^[165] However, the activity of [NiFe] hydrogenases is usually lower.

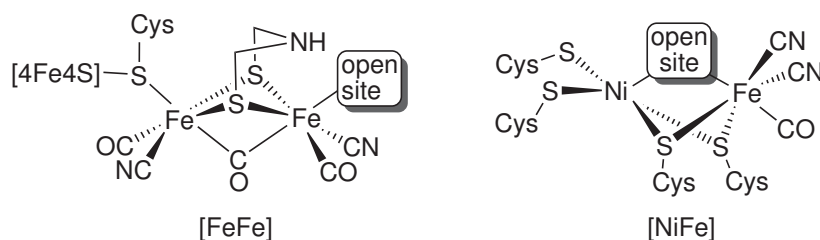


Figure 1.3. Structures of the active sites of [FeFe] and [NiFe] hydrogenases.^[159]

Figure 1.3 depicts the structures of the active sites of [FeFe] and [NiFe] hydrogenases. First indications of the presence of toxic CO and CN⁻ ligands obtained by IR spectroscopy^[177] startled the scientific community and established an astonishing connection between the chemistry of hydrogenases and traditional organometallic chemistry.^[18,151] Because of their high sensitivity towards dioxygen, these organometallic centers normally lie deeply buried within the protein scaffold and pathways for the transport of reactants and products as well as for electrons are necessary.^[170]

[FeFe] Hydrogenases

Most [FeFe] hydrogenases are monomeric and consist of a single catalytic subunit only.^[145] The active site shown in Figure 1.3 is also called “H-cluster” and consists of two iron atoms which are bridged by a CO molecule and a dithiolate ligand containing an amino group. Each of the two metals is further coordinated by a CN⁻ ligand and an additional CO molecule. The so-called proximal iron atom is linked to a [4Fe4S] cluster *via* a bridging cysteine (Cys) sulfur ensuring a pathway for electron transport. The distance of the proximal iron to the [4Fe4S] cluster amounts to approximately 4 Å. The other iron atom – the so-called distal iron atom – is believed to be the binding site of inhibitors like CO or O₂, as well as of dihydrogen. In the history of exploring [FeFe] hydrogenase activity, there has been some considerable debate on the identity of the bridgehead atom of the dithiolate ligand. Meanwhile, strong experimental and theoretical evidence confirms the presence of an NH group rather than the presence of the previously proposed oxygen atom or CH₂ group.^[178–181] By accepting or donating a proton, the NH group plays an important role in the catalytic cycle.^[170] Considering that the [4Fe4S] cluster might be present in its oxidized [4Fe4S]²⁺ or reduced [4Fe4S]⁺ form and that the binuclear part has three possible redox states (Fe^{II}Fe^{II}, Fe^IFe^{II}, Fe^IFe^I), a total of six redox states are imaginable for the H-cluster.^[170] However, not all of these redox states actually occur under physiological conditions. Most probably, the H_{ox} ([4Fe4S]²⁺–Fe^{II}Fe^I) and the H_{red} ([4Fe4S]²⁺–Fe^IFe^I) states are essential components of the catalytic cycle.^[146] Recently, a super-reduced state H_{sred} ([4Fe4S]⁺–Fe^IFe^I) has been identified^[182] and considered as part of the catalytic cycle.^[170,183]

In the quest for biomimetic catalysts, an impressive number of structural and functional models for the [FeFe] hydrogenase has been designed and especially in the last few

years an extremely high level of sophistication has been reached.^[170] A recent example of a complete [FeFe] hydrogenase model is described in section 1.5.^[184] Besides the general reviews cited above, some additional review articles exist which exclusively treat the [FeFe] hydrogenase and its model compounds.^[185–189]

[NiFe] Hydrogenases

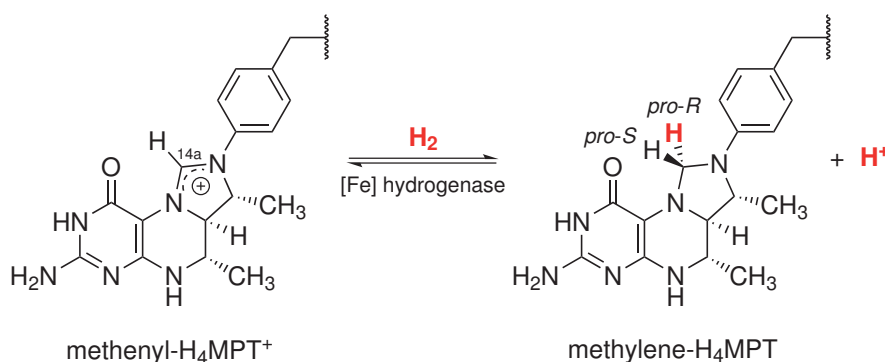
In contrast to mostly monomeric [FeFe] hydrogenases, almost all [NiFe] hydrogenase enzymes consist of a large subunit harboring the active site, and a small subunit accommodating the iron-sulfur (FeS) clusters of the electron transport chain.^[174] Different hydrophobic gas channels^[190] and proton transfer pathways have been identified in [NiFe] hydrogenases.^[170] The active site of standard [NiFe] hydrogenases (Figure 1.3) consists of a nickel and an iron atom which are bridged by two cysteine sulfur atoms. Furthermore, the Ni center is coordinated by two additional cysteine residues and the Fe center features two CN⁻ and one CO ligand. In a distance of approximately 11 Å to the redox active Ni atom, a [4Fe4S] cluster is located which belongs to the small subunit of the enzyme and takes care of the transport of electrons.^[170] In certain oxygen-tolerant [NiFe] hydrogenases the proximal FeS cluster is not a [4Fe4S] cluster but a unique [4Fe3S] cluster.^[191–193] The possibility of this cluster to access a superoxidized state and to deliver two electrons back to the active site in order to reduce O₂ is assumed to be the reason for the retention of hydrogenase activity even in the presence of dioxygen.^[191–198] The so-called [NiFeSe] hydrogenases are a subclass of [NiFe] hydrogenases in which one of the terminal cysteine residues coordinating the Ni atom is replaced by a selenocysteine. In comparison to “normal” [NiFe] hydrogenases, these enzymes usually exhibit a significantly higher catalytic activity.^[199]

The catalytic cycle performed by [NiFe] hydrogenases has been the subject of intense debate and in the course of its exploration more than ten different states or intermediates of the active site have been identified.^[200] The main differences between these structures relate to the oxidation state of nickel (Ni^I, Ni^{II} or Ni^{III}) and the nature of the ligand occupying the open coordination site in Figure 1.3. However, in principle only three states possess a special relevance for the catalytic cycle: In the active state of the enzyme, the so-called Ni-SI_a state, no additional bridging ligand exists and the open site remains empty. The oxidation states of the metals are Ni^{II}Fe^{II}. Heterolytic splitting of H₂ yields several different Ni-R states carrying a hydride ion in the bridge between the Ni^{II} and the Fe^{II} centers. The proton is attached to the sulfur of a terminal cysteine residue. Release of this proton and an electron leads to the formation of the paramagnetic Ni-C state still featuring a hydride bridge and a Ni^{III}Fe^{II} oxidation state. Finally, the catalytic cycle is closed by removing the second proton and electron.^[170,200] Also in the case of [NiFe] hydrogenases, great progress in modeling the structure and reactivity of the natural systems has been achieved in recent years and meanwhile also a remarkable functional model of the [NiFe] hydrogenase has been synthesized (see

section 1.5).^[201] A few specialized reviews document the rapid developments in the field.^[202–205]

1.4.2 The [Fe] Hydrogenase – A Novel Kind of Hydrogenase

[Fe] hydrogenase – systematically named H₂-forming methylenetetrahydromethanopterin dehydrogenase (Hmd) – differs from the other two types of hydrogenases in the fact that it does not contain any nickel or iron-sulfur clusters. Furthermore, the enzyme does not catalyze the formation of dihydrogen from protons and electrons or the oxidation of H₂. Instead, it promotes the reversible hydride transfer from H₂ to N⁵,N¹⁰-methenyltetrahydromethanopterin (methenyl-H₄MPT⁺) yielding N⁵,N¹⁰-methylenetetrahydromethanopterin (methylene-H₄MPT) and a proton. Contrary to [FeFe] and [NiFe] hydrogenases, a direct transfer of electrons is not observed in the [Fe] hydrogenase. The reaction is an important step in the production of methane from CO₂ in many methanogenic archaea.^[159,206] The transfer of a hydride ion occurs stereospecifically to the *pro-R* side of the substrate at carbon atom C^{14a} which is derived from CO₂ (Scheme 1.5).^[207]



Scheme 1.5. Stereospecific hydride transfer from H₂ to methenyl-H₄MPT⁺ catalyzed by [Fe] hydrogenase.

Since its discovery in 1990,^[208,209] the understanding of [Fe] hydrogenase has experienced substantial breaks. Indeed, the enzyme was initially believed to be a purely organic hydrogenation catalyst and it took quite some time until the crucial role of an iron-based cofactor was recognized in 2004.^[210] Nevertheless, the prospect to discover novel concepts of H₂ activation fueled the curiosity of the scientific community and meanwhile even details on for example the biosynthesis of the [Fe] hydrogenase are available.^[211–213] A series of reviews represents the cornerstones of the evolution that took place in the understanding of [Fe] hydrogenase.^[214–219]

The Enzyme and its Substrate

Tetrahydromethanopterin (H_4MPT) is a tetrahydrofolate analogue and acts as a carbon carrier for C_1 units in various groups of microorganisms (Figure 1.4).^[220,221] In methanogenesis it may carry C_1 units in different oxidation levels.

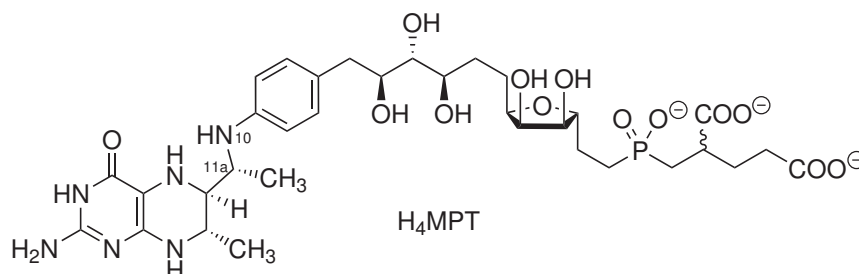


Figure 1.4. Structure of tetrahydromethanopterin (H_4MPT).

An example for a process in which tetrahydromethanopterin is involved is the aforementioned interconversion of methenyl- H_4MPT^+ and methylene- H_4MPT , the reaction performed by the [Fe] hydrogenase (Scheme 1.5). The structure of methylene- H_4MPT has been elucidated by means of NMR spectroscopy and differences between the solution structure and the structure in the enzyme have been identified. In solution, the imidazolidine ring adopts an envelope conformation with the flap at the N^{10} nitrogen atom, whereas for the structures of enzyme-bound methylene- H_4MPT different puckered conformations have been found.^[222–225] In the crystal structure of [Fe] hydrogenase cocrystallized with the substrate,^[226] methylene- H_4MPT is present in a rather extended conformation with the kink at the C^{11a} carbon atom of the imidazolidine ring (for details see chapter 2.3.3).

The structure of the [Fe] hydrogenase apoenzyme (the enzyme without the cofactor) has been determined for the first time in 2006, establishing the fact that the enzyme can be present either in an open or in a closed conformation.^[227] The homodimeric protein consists of two peripheral and one central globular unit, while the latter is composed of segments of both subunits. Each of the two identical subunits features a molecular mass of roughly 38 kDa and the two clefts between the globular units harbor the active sites of the enzyme. After it became clear that the active site of the enzyme was not of purely organic origin but contained a functional iron-based cofactor instead,^[210,228] attempts focused on the crystallization of the holoenzyme containing the intact cofactor. However, this was hampered because of the cofactor's acute light- and temperature-sensitivity. In contrast to this, the purified enzyme was still active in the presence of dioxygen, but cyanide or high concentrations of carbon monoxide also deactivated the enzyme.^[210] The O_2 tolerance of [Fe] hydrogenase was examined in detail.^[229] The breakthrough in the crystallization attempts came with the work of Shima *et al.* who revealed the crystal structure of an active enzyme which was obtained by reconstituting heterologously produced apoenzyme with the labile cofactor extracted from a native enzyme.^[230–232]

Figure 1.5 depicts the protein structure of the [Fe] hydrogenase cocrystallized with the substrate methylene- H_4 MPT.^[233]

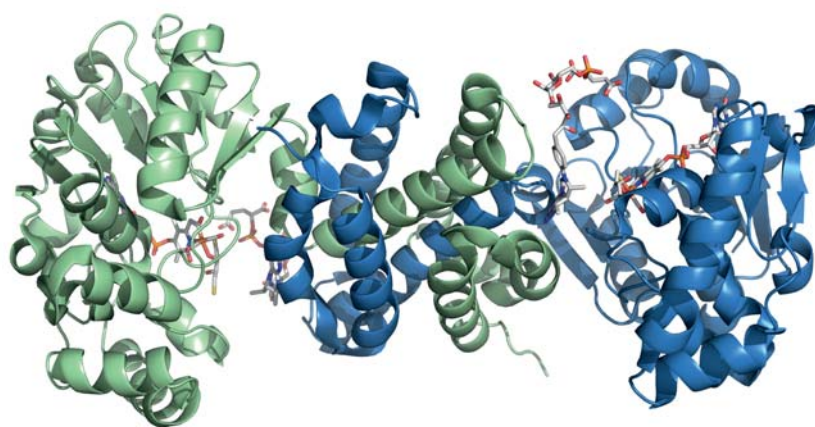


Figure 1.5. Protein structure of the mutated [Fe] hydrogenase from *Methanocaldococcus jannaschii* reconstituted with the cofactor and cocrystallized with methylene- H_4 MPT.^[226] The protein model was generated from the X-ray structure (Protein Data Bank accession code 3H65).

The Active Site of [Fe] Hydrogenase

Before crystallographic data on the active site was available, investigations conducted independently from the crystallization attempts revealed that the cofactor of [Fe] hydrogenase contained CO ligands which were most probably bound to Fe^{II} .^[234] Mössbauer and EPR investigations subsequently confirmed that iron was present in a low oxidation state, either low-spin Fe^0 or low-spin Fe^{II} .^[235] Apart from this, the structure of the light-inactivation product was determined by means of NMR measurements.^[236] Furthermore, X-ray absorption spectroscopy (XAS) provided first hints on the coordination geometry of the active site.^[237] A *cis*-arrangement of the CO ligands and a low-spin $Fe(II)$ oxidation state was also supported by further IR and Mössbauer measurements,^[238] as well as by means of ^{57}Fe nuclear resonance vibrational spectroscopy (NRVS).^[239]

According to the current understanding of the [Fe] hydrogenase, the active site of the enzyme consists of an iron guanylylpyridinol cofactor (FeGP cofactor) that features a unique coordination motif (Figure 1.6).^[226] The central iron atom is coordinated by two CO molecules, one cysteine sulfur atom and a guanylylpyridinol moiety. The latter is bound *via* the pyridinol nitrogen atom and an acyl group which is a rather unusual coordination motif in biological systems. The position *trans* to the acyl ligand is considered to be the site of substrate binding.^[226,240]

In the first crystal structure of [Fe] hydrogenase including the cofactor,^[230] the acyl binding motif was not considered. Instead, the guanylylpyridinol moiety was thought

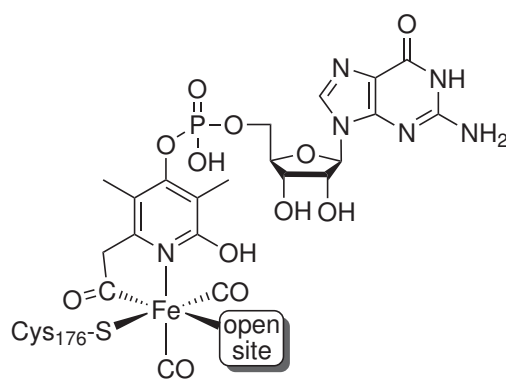


Figure 1.6. Structure of the FeGP cofactor.

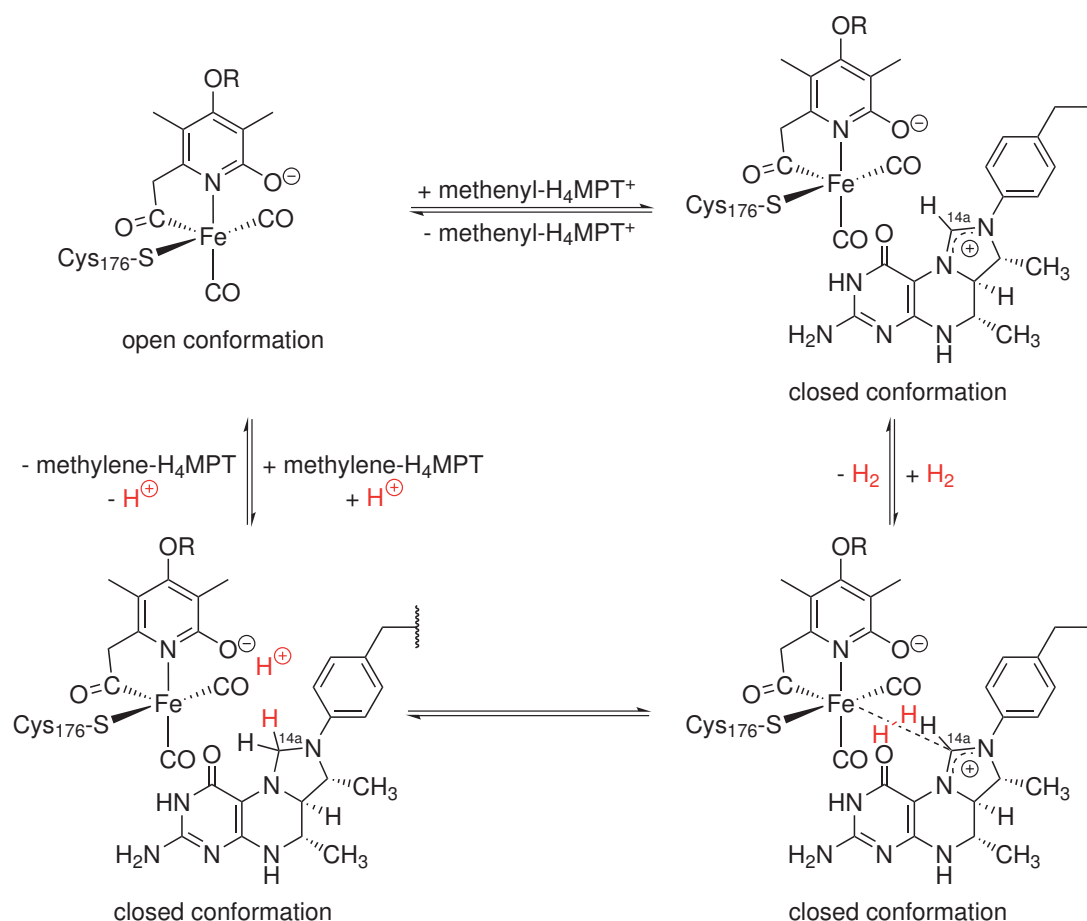
to bind only in a monodentate way *via* the pyridinol's nitrogen atom and to possess a non-coordinating carboxyl instead of an acyl group. The additional coordination site was supposed to be occupied by a water molecule. Hiromoto *et al.* later revised the structure based on studies of a mutated enzyme because evidence for an acyl ligand was found in the new protein structure.^[241] Reevaluation of the original crystallographic data indeed led to an improved quality of the data fit, resulting in the active site structure shown in Figure 1.6. Subsequently, experimental evidence for this novel structure was gathered, for example by further XAS measurements,^[242] IR spectroscopy and mass spectrometry.^[243]

Mechanism of H₂ activation in [Fe] hydrogenase

In order to elucidate the mechanism of H₂ activation in [Fe] hydrogenase, numerous experiments including isotope labeling experiments have been conducted. The experiments revealed that [Fe] hydrogenase differs from the other two classes of hydrogenases in the facts that it does not reduce electron acceptors (e. g. artificial dyes) and that it catalyzes the exchange between H₂ and H₂O only in the presence of methenyl-H₄MPT⁺ or methylene-H₄MPT.^[209,244] Like in the other hydrogenases, a heterolytic splitting of H₂ takes place, yielding a hydride ion and a proton.^[209,214] Although these general aspects of H₂ splitting in the [Fe] hydrogenase were clear relatively early after the discovery of the novel hydrogenase, the exact mechanism remained elusive for a long time. In order to explain the activity of the enzyme considering the apparent absence of a transition metal, the concept of superelectrophilic activation was put forward by Berkessel and Thauer in 1995.^[245] According to their proposal, methenyl-H₄MPT⁺ gets protonated at a nitrogen atom during reaction yielding a dication which should exhibit enhanced electrophilicity at its C^{14a} carbon atom. The increased carbocationic character at this position then permits hydride abstraction from molecular hydrogen. Further studies revealed that the splitting of H₂ requires a base which helps to cleave the H–H bond in a concerted, bifunctional manner.^[246] A detailed conformational analysis explained the observed stereoselectivity.^[222]

Along with the realization that the FeGP cofactor was essential for hydrogenase activity and after unraveling the first crystal structure of an active [Fe] hydrogenase enzyme,^[230] a series of further attempts to understand the mechanism of dihydrogen activation was initiated. Computational modeling of the reaction by Yang and Hall^[247] predicted a trigger mechanism in which the presence or absence of the substrate regulates the donor strength of a simplified pyridone moiety. Reinterpretation of the crystallographic data and subsequent proposal of an acyl group in the cofactor^[241] led to a new model in which the acyl ligation was considered.^[248] The model features strong Fe–H...H–O interactions which were considered responsible for the lacking exchange with water or H₂/D₂ in the absence of the substrate. A key step in the proposed mechanism is the proton transfer to the coordinated cysteine sulfur atom or alternatively to the pyridinol oxygen atom after heterolytic cleavage of the H₂ molecule. Complementary calculations by Dey *et al.* elucidated the effect of the internal ligands on the binding properties of [Fe] hydrogenase.^[249] More recently, the mechanism proposed by Yang and Hall was revisited by Reiher *et al.* taking also dispersion interactions between the active site and the hydride acceptor molecule into account.^[250] By this means, a lower energy barrier for the hydride transfer step was calculated and the protonation of the pyridinol oxygen after heterolytic cleavage of the H₂ molecule was found to be kinetically favored compared to protonation at the cysteine sulfur atom.

Further information on the mechanism of H₂ activation was gained by modeling the closed form of the enzyme in the presence of methylene-H₄MPT. Based on the enzyme-substrate complex in which the enzyme was found in its open form, Shima *et al.* reported a computer model of the closed form of the enzyme featuring a distance of 3 Å between the metal center of the FeGP cofactor and the C^{14a} carbon atom of methylene-H₄MPT.^[226] In contrast to a distance of 9.3 Å which was found in the crystal structure of the open form, the authors considered this distance to be appropriate for hydride transfer. Subsequently, a catalytic mechanism for the splitting of dihydrogen in the [Fe] hydrogenase was proposed taking into account the rearrangement of the enzyme structure upon substrate binding (Scheme 1.6): In the absence of any substrate, the enzyme is present in an open conformation. Arrival of the substrate methenyl-H₄MPT⁺ then triggers the closure of the cleft resulting in an arrangement in which the iron cofactor and the substrate are directly opposite to each other. Simultaneously to the conformational changes in the enzyme, also the substrate might be activated by the structural changes resulting in an increased carbocationic character of the C^{14a} carbon atom as proposed earlier.^[245,246] After this, the H₂ molecule supplied by a hydrophobic channel binds *side-on* to iron, gets polarized and is finally cleaved heterolytically. The hydride ion is transferred to the C^{14a} carbon atom of the substrate while the proton might be accepted by either the cysteine sulfur atom or the pyridinol hydroxylate group. The catalytic cycle is closed by release of methylene-H₄MPT, removal of the proton and transition to the open conformation of the enzyme. The conformational change required for H₂ activation in the proposed mechanism was indeed later confirmed by circular dichroism (CD) spectroscopy.^[251]



Scheme 1.6. Catalytic mechanism of hydrogen activation in the [Fe] hydrogenase proposed by Shima and co-workers involving a conformational change of the enzyme upon substrate binding.^[226]

Despite the progress already made in understanding the [Fe] hydrogenase, the details of the mechanism of dihydrogen activation still remain uncertain. The often proposed *side-on* coordination of H_2 to the Lewis acidic metal center still leaves some open questions since this would normally lower the $\text{p}K_{\text{a}}$ of dihydrogen and hence complicate a hydride transfer to the substrate.^[18,149] Furthermore, one would expect an exchange of the thus activated H_2 with water also in the absence of substrate which is not observed in the [Fe] hydrogenase.^[252] However, considering the influence of the carbocation, *side-on* coordination becomes again more feasible. In a possible scenario of hydrogen activation H_2 is captured in between the Lewis acidic metal center and the positively charged carbon atom prior to splitting of the H–H bond.^[252] In such a mechanism, the carbocation is assumed to resemble a second transition metal center.

As has been pointed out by Vogt *et al.* the low-spin iron could not only act as a Lewis acid but in principle also as a Lewis base during the catalytic cycle.^[252] This would make an *end-on* binding mode of the H_2 molecule conceivable and could also explain why the hydride acceptor is required in order to observe the mentioned exchange activities.

1.5 Model Complexes: Learning from Nature

A promising approach to develop more efficient catalysts for the transformations of H_2 is to model the active sites of enzymes. By designing low molecular weight models, chemists try to simplify the complex protein scaffold and to unravel the general concepts behind the enzymes' activities. Mimicking the reactivity of the natural systems often is an important part in understanding the catalysis. Hydrogenases provide considerable inspiration for the fabrication of novel H_2 -producing or H_2 -activating catalysts since they feature earth-abundant metals (Ni, Fe) as well as high efficiencies.^[154,253–255] Unraveling the concepts behind dihydrogen activation and production in hydrogenases could therefore be an important step towards solving the world's energy problem. With the advent of low molecular weight models of hydrogenases, first success in the quest for robust biomimetic catalysts has been achieved. Figure 1.7 depicts a selection of hydrogenase-inspired systems. Complex **VI** synthesized by Rauchfuss *et al.* represents the first complete model system which contains all of the functional components of the active site of the [FeFe] hydrogenase: a reactive diiron center, a bridging amine ligand and a decamethylferrocenyl moiety as a one-electron redox module.^[184,256] In the presence of oxidant and base, this system is able to catalytically oxidize the H_2 molecule. Recently, Ogo and co-workers reported the [NiFe] hydrogenase model **VII** mimicking for the first time the bidirectional behavior of the enzyme.^[201,257] Oxidation of dihydrogen as well as production of H_2 are possible provided that a strong base and, respectively, a strong acid are added. The intermediary formed hydride complex can

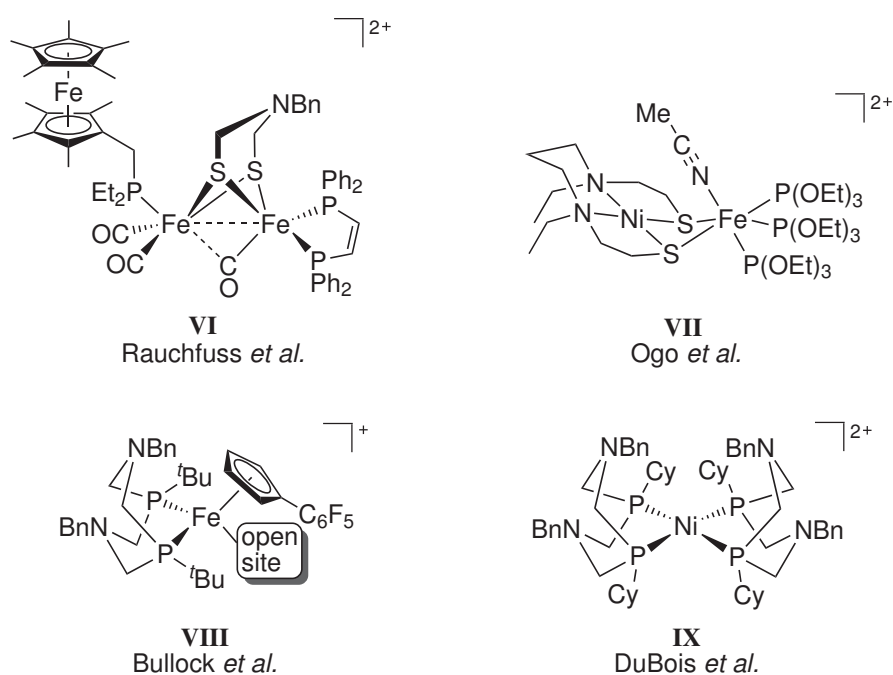


Figure 1.7. Selection of bioinspired catalysts for the formation or oxidation of dihydrogen (Bn = CH_2Ph , Cy = cyclohexyl).

either be oxidized by common electron acceptors like methyl viologen or protonated by acids to recover compound **VII**. Iron complex **VIII** is able to split a dihydrogen molecule coordinating to the open site in a heterolytic way.^[258] In the splitting process, the proton is first transferred to the amine base located in the ligand sphere before subsequent deprotonation by an added external base. Oxidation of the complex then liberates the second proton.^[258] Although the compound is mononuclear, it nevertheless mimics essential features of the active site of the [FeFe] hydrogenase and catalyzes the oxidation of H₂ with relatively high efficiencies. Very recently, the product of H₂ heterolysis performed by a complex similar to compound **VIII** featuring slight modifications in the ligand system was even characterized by means of X-ray crystallography.^[259] The solid state structure showed a remarkably short H ··· H distance of 1.489(10) Å in the Fe–H ··· H–N moiety.

Very important in the context of mimicking hydrogenase activity is the work of DuBois and co-workers.^[260] Using diphosphine-based ligands, the group synthesized several functional hydrogenase models based on abundant and inexpensive transition metals like iron, nickel or cobalt. An example for such a complex is compound **IX** in Figure 1.7. Applying some general principles derived from hydrogenase activity, surprisingly high efficiencies could be obtained.^[154,260–263] These design principles are: (i) presence of an open coordination site at the metal, (ii) presence of a pendant base close to the metal center functioning as proton relay and (iii) energetic matching of hydride acceptor ability of the metal and proton acceptor ability of the base. The role of the pendant amine base constituting the second coordination sphere has been analyzed in detail^[260,264] and corresponding basic groups have for example also been implemented into model systems **VII** and **VIII**.

Model Complexes for the [Fe] Hydrogenase Active Site

The systems presented in this section show that already first steps towards understanding the reactivity of hydrogenases are made. Unfortunately, the yields and turnover numbers of the models systems still leave room for improvements and technological applications are yet to come. Model complexes for the [Fe] hydrogenase could offer new perspectives for the development of even more efficient catalysts since the presently available systems are largely based on [FeFe] and [NiFe] hydrogenases.

Mimicking the active site of the [Fe] hydrogenase began even before the first crystal structure of an active enzyme was uncovered. Royer *et al.* reported the synthesis of iridium complex **X** which contains an analogue of the guanylylpyridone cofactor (Figure 1.8) and showed that the complex is active in the dehydrogenation reaction of 1-phenylethanol to acetophenone.^[265] Furthermore, studies on rather simple CO-containing models helped to interpret the experimental findings related to [Fe] hydrogenase and contributed to the elucidation of the active site structure and oxidation state.^[216,218,219,238,242,266–269] After the discovery that the active site of the [Fe] hydrogenase contains a rather unusual acyl binding motif, more elaborate complexes representing

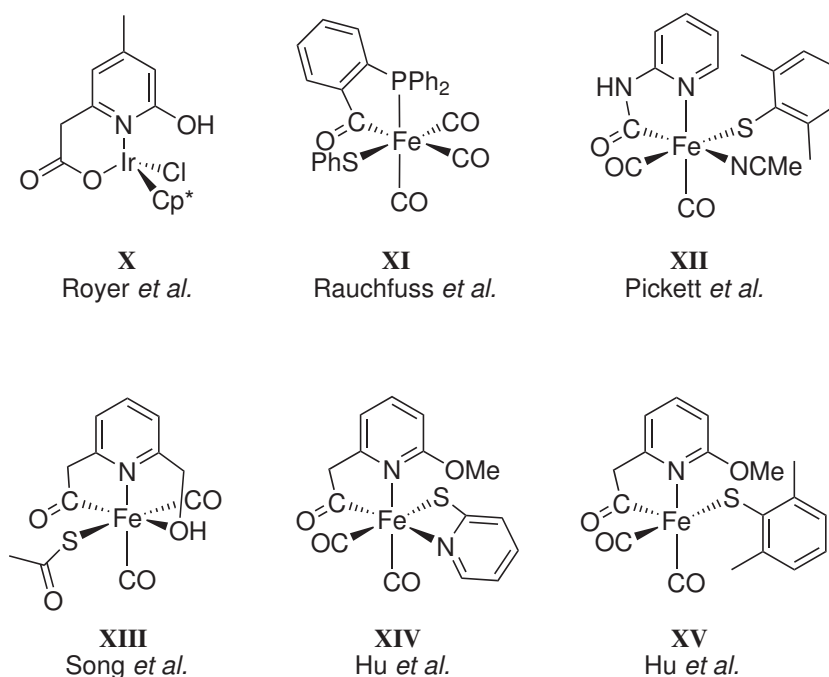


Figure 1.8. Selected models for the active site of [Fe] hydrogenase ($\text{Cp}^* = \text{C}_5\text{Me}_5$).

more accurate models occurred in literature. Today already a large body of model compounds exists, featuring a *cis*-arrangement of CO ligands, coordination of a pyridine and/or thiolate moiety as well as acyl ligation. Figure 1.8 depicts a selection of model complexes for the active site of [Fe] hydrogenase. Rauchfuss *et al.* obtained one of the first model complexes containing an acyl ligand, complex **XI**, by oxidative addition of phosphine-modified thioesters to an Fe^0 carbonyl.^[270,271] Complex **XII** was synthesized by Pickett *et al.* and contains a carbamoyl group as surrogate for the acyl group found in the natural enzyme.^[272,273] Song and co-workers used Collman's reagent $\text{Na}_2[\text{Fe}(\text{CO})_4]$ to synthesize compound **XIII** *via* a nucleophilic substitution reaction.^[274] In their model, a hydroxymethyl group was present for the first time. A similar (but dinuclear) complex featuring an acylmethylpyridinol ligand with very close resemblance to the active site of [Fe] hydrogenase was recently obtained by a similar approach.^[275] Also very important in the field of [Fe] hydrogenase model complexes is the work of Hu and co-workers. Complex **XIV** represents an early example of a model involving an acylmethylpyridinyl ligand.^[276] Only one year later the same group published the first pentacoordinate iron complex **XV** with very close resemblance to the active site of the enzyme.^[277] The model complex was investigated thoroughly by computational methods^[278] and the reversible protonation of the thiolate ligand was demonstrated experimentally.^[279] The reactivity of the complex with water parallels the decomposition of the FeGP cofactor.^[280] Subsequently, similar pentacoordinate complexes were synthesized^[281] and recently even the synthesis of an analogous compound featuring an acylmethylpyridinol ligand was accomplished.^[282] A review on model compounds containing iron-acyl ligation has been published lately.^[283]

1.6 Objective

Despite the progress made in modeling the active sites of hydrogenases, until now no model compound exists that mimics the reactivity of the [Fe] hydrogenase – the heterolytic splitting of dihydrogen. This is hardly surprising since the known models focus on the structural modeling of the FeGP cofactor and neglect the substrate methenyl- H_4MPT^+ completely. A truly functional model should also include the hydride acceptor since it is required for the reactivity of the enzyme.^[209] This work now aims at synthesizing the first functional model for the [Fe] hydrogenase considering also a hydride acceptor molecule. By this, further insights into the mechanism of H_2 activation by the [Fe] hydrogenase are expected. Since significant parallels between the [Fe] hydrogenase and the other types of hydrogenase enzymes exist,^[284] the discovery of mechanistic details for the [Fe] hydrogenase could also contribute to the understanding of [FeFe] and [NiFe] hydrogenases in general. Finally, new insights into dihydrogen activation and formation could probably lead to the development of even more efficient catalysts.

In order to design a functional model for the [Fe] hydrogenase, this project intends to make use of the analogy between the active site of the enzyme and the chemistry of frustrated Lewis pairs. As has been pointed out in chapter 1.4.2, the iron center in the [Fe] hydrogenase could not only act as a Lewis acid but in principle also as a Lewis base during the catalytic cycle.^[252] This brings into mind the concept of frustrated Lewis pairs since, from a chemical point of view, the hydride acceptor methenyl- H_4MPT^+ can be regarded as a Lewis acid while the FeGp cofactor represents a base that becomes

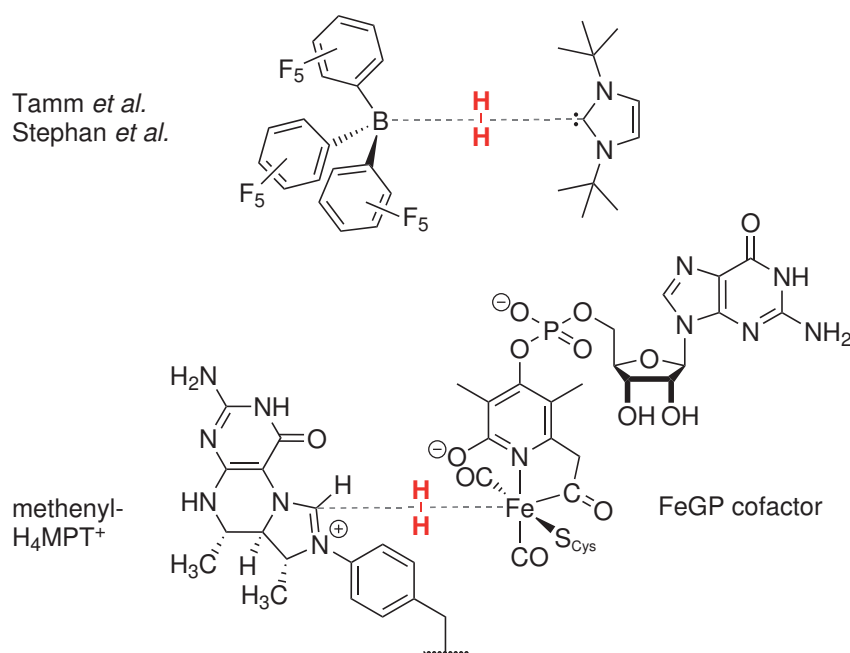
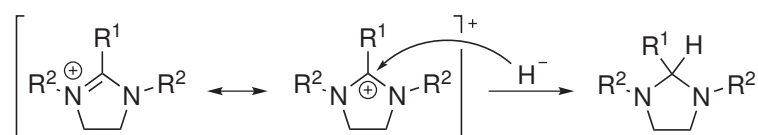


Figure 1.9. Comparison between a carbene FLP (top),^[40,41] and the active site of [Fe] hydrogenase (bottom).

protonated during the H₂ splitting process. In this picture, notable parallels especially to the FLP systems using an N-heterocyclic carbene as base developed by Tamm^[40] and Stephan^[41] are evident (Figure 1.9).

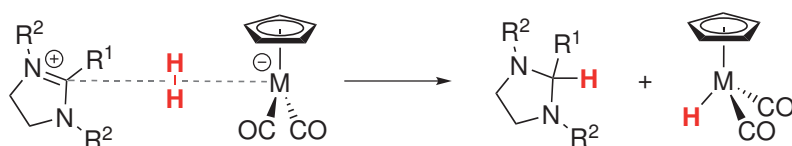
The challenge this work has to face is twofold: First, a suitable hydride acceptor molecule needs to be synthesized which is able to accept the hydride ion originating from the heterolytic splitting of dihydrogen. Second, this molecule has to be combined with a transition metal Lewis base that can accept the proton after H₂ cleavage. To achieve this, a series of imidazolium ions will be synthesized and their properties – particularly with regard to their hydride acceptor abilities – will be tested. Imidazolium ions are attractive candidates to act as hydride acceptors in the envisioned reaction with H₂ since they were found to add nucleophiles like the hydride ion to their reactive C² carbon atoms (Scheme 1.7).^[285–289] Also methenyl-H₄MPT⁺ which accepts the hydride ion originating from the heterolytic cleavage of H₂ in the [Fe] hydrogenase is an imidazolium ion and hence an analogy to the natural system exists. As the imidazolium ions will be subjected to a base, it is necessary to substitute the proton which occupies the C² position in the natural prototype methenyl-H₄MPT⁺ for a different moiety R¹ in the imidazolium ions. Otherwise, deprotonation by the base would yield the respective carbenes.



Scheme 1.7. Formation of an imidazolidine *via* addition of a H⁻ nucleophile to the C² carbon atom of an imidazolium ion.

As transition metal bases, mainly the carbonyl metalates K[CpFe(CO)₂] (**KFp**) and K[CpRu(CO)₂] (**KRp**) will be considered. In analogy to the active site of the [Fe] hydrogenase, these complexes possess a group 8 transition metal and several CO ligands. Although the structural similarity to the FeGP cofactor is only present rudimentarily, the metalates nevertheless feature a low oxidation state (0) of the central metal atom and can thus be protonated to yield the hydride complexes HFeCp(CO)₂ (**HFp**) and HRuCp(CO)₂ (**HRp**), respectively. Consequently, the function of the FeGP cofactor is emulated in a simplified way.

By combining the imidazolium ions and the carbonyl metalates, a heterolytic splitting reaction of H₂ according to Scheme 1.8 is envisaged. In case of a successful reaction, the targeted model system would be the first functional model for the [Fe] hydrogenase



Scheme 1.8. Concept of this work (M = Fe, Ru).

active site. Simultaneously, the scope of transition metal frustrated Lewis pairs would be significantly extended to also include transition metal Lewis bases. In summary, the presented system could shed a new light on the heterolytic splitting of H_2 and stimulate the development of more efficient H_2 activation catalysts.

2

Mimicking the Natural Hydride Acceptor Methenyl- H_4MPT^+

Abstract The enzyme [Fe] hydrogenase cleaves the dihydrogen molecule very efficiently and subsequently transfers the hydride ion to the acceptor molecule methenyl- H_4MPT^+ . As outlined in the previous chapter, the purpose of the work in hand also comprises the synthesis of small molecule analogs of the natural hydride acceptor molecule. Efforts in this direction focused on the synthesis of appropriate imidazolium ions, but also an imidazolium ion was considered. This chapter summarizes the performed synthetic steps as well as properties of the obtained molecules with regard to their envisaged role as hydride acceptors.

2.1 Hydride Acceptors in Biology and Chemistry

Molecules which are involved in transfer reactions of a hydride ion can be found ubiquitously in biological systems – a prominent example for this type of molecules being the coenzyme nicotinamide adenine dinucleotide (phosphate) $NAD(P)^+/NAD(P)H$ – and their corresponding transformations are essential for life. Since the [Fe] hydrogenase has attracted the interest of the scientific community only relatively recently, model systems for the coenzyme methenyl- H_4MPT^+ have not emerged in the literature so far. However, first experiences in this field of research have already been gained in the framework of a diploma thesis^[290] elucidating the potential of imidazolium ions for modeling the reactivity of the cofactor. Furthermore, models for related hydride acceptor molecules like the N^5, N^{10} -methenyltetrahydrofolate already exist. This section is meant to summarize the experiments performed in the preliminary stages of this project. Additionally it covers the research on models for hydride acceptor molecules similar to methenyl- H_4MPT^+ .

2.1.1 Imidazolium Ions as Hydride Acceptor Molecules

The purpose of a diploma thesis^[290] dealing with the synthesis and examination of model compounds for the [Fe] hydrogenase active site was *inter alia* to gather first experiences with the chemistry of methenyl- H_4MPT^+ mimics. In a first attempt to understand the natural hydride acceptor, the three imidazolium ions depicted in Figure 2.1 were synthesized. Unfortunately, either undesired electron transfer reactions (benzimidazolium compounds) or no reactivity at all (remaining imidazolium compound) were observed when the imidazolium halides were reacted with models for the FeGP cofactor.

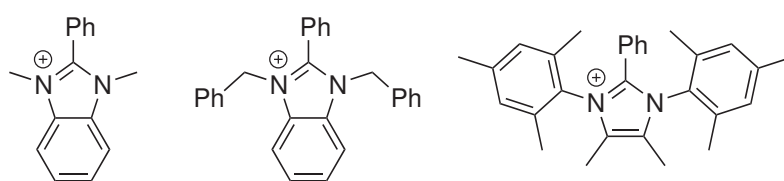
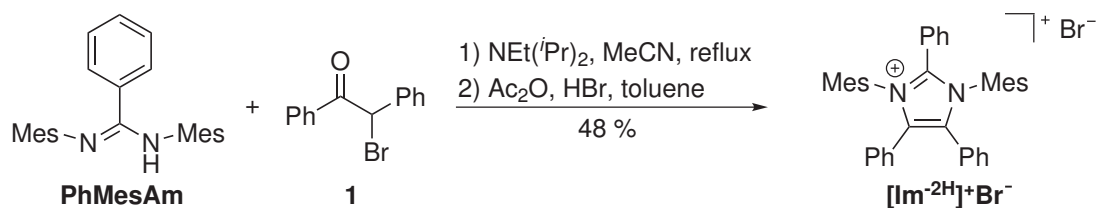


Figure 2.1. Imidazolium ions synthesized in the course of a diploma thesis dealing with the modeling of the methenyl- H_4MPT^+ cofactor and its reactivity.^[290]

In the preliminary stages of this work, another try was made at synthesizing appropriate imidazolium ions. Following the reaction presented in Scheme 2.1, compound $[Im^{-2H}]^+ Br^-$ was synthesized in a yield of 48 % by a modified literature procedure^[291] designed for the synthesis of C^2 -unsubstituted imidazolium salts. The required α -bromoketone **1** was obtained by following a modified synthetic protocol^[291,292] as well, and the preparation of amidine **PhMesAm** is described in section 2.2.2. Exchange of the bromide counteranion for PF_6^- by stirring a DCM solution of the compound over



Scheme 2.1. Synthesis of imidazolium salt $[\text{Im}^{-2\text{H}}]^+\text{Br}^-$ (Mes = 2,4,6-trimethylphenyl).

KPF₆ and subsequent recrystallization from mixtures of chlorobenzene and *n*-pentane yielded crystals suitable for X-ray crystallography. The solid state structure obtained in this way is represented in Figure 2.2. As it turned out later, the reactivity of imidazolium salt $[\text{Im}^{-2\text{H}}]^+\text{Br}^-$ was inadequate and an uptake of a hydride ion was not observed in model reactions analogous to section 2.3.3. One reason for the lack of desired reactivity of the synthesized imidazolium ions might be the heterocycle itself, as the positive charge can be stabilized very efficiently by its aromatic system. A reaction with the hydride ion would interrupt the aromatic system. Consequently, nucleophiles do not readily attack the central C² carbon atom. For this reasons, improved hydride acceptor molecules were developed in the framework of this work. Corresponding efforts focused on the synthesis of imidazolinium ions as both improved electrochemical properties and a better reactivity were anticipated. Matters of reactivity of these systems will be discussed in chapter 2.3.3. Since also methenyl-H₄MPT⁺ features an imidazolinium heterocycle, these more advanced models emulate the natural system even more precisely.

2.1.2 Models for N⁵,N¹⁰-Methenyltetrahydrofolate

Although model systems explicitly mimicking the coenzyme methenyl-H₄MPT⁺ do not yet exist in the literature, related hydride-accepting molecules have been synthesized in the course of developing analogs to the different derivatives of tetrahydrofolic acid. Tetrahydrofolate (vitamin B₉) and its related molecules, the so-called folates, are essential cofactors that facilitate the transfer of one-carbon units in the biosynthetic pathways of important biomolecules like amino acids (methionine, serine, glycine) and nucleobases (purine, pyrimidine).^[293,294] One of the intermediates in the metabolism of tetrahydrofolic acid is N⁵,N¹⁰-methenyltetrahydrofolate which has stimulated the development of imidazolinium ions as suitable small molecule mimics modeling the transfer of one-carbon units to various substrates. Figure 2.3 depicts the cofactor N⁵,N¹⁰-methenyltetrahydrofolate and some exemplary model compounds synthesized in order to mimic its reactivity.^[285,286,295]

Most of the model compounds feature an imidazolinium ion bearing two different substituents at the nitrogen atoms in order to emulate the situation found in the natural cofactor more accurately, but also symmetrical imidazolinium ions have been reported. The model systems were subjected to reactions with a large variety of reagents as for

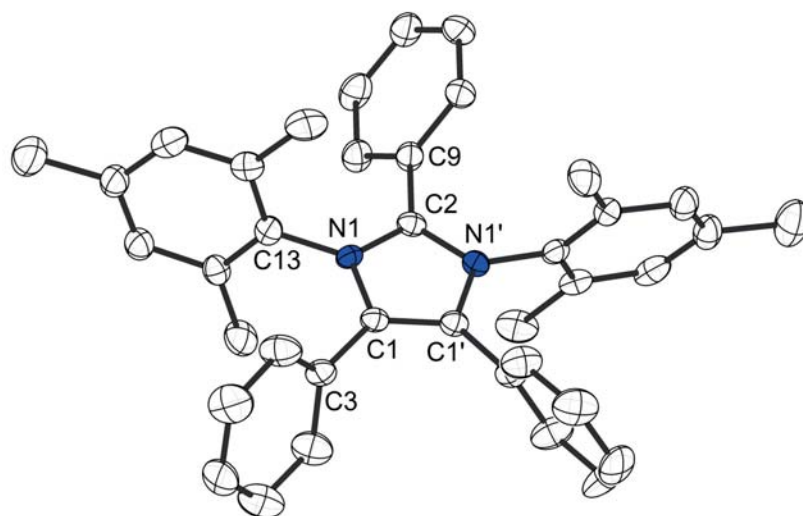


Figure 2.2. Thermal displacement ellipsoids (shown at 50 % probability) of the molecular structure of imidazolium salt $[Im^{2H}]^+PF_6^-$. The PF_6^- counteranion as well as hydrogen atoms are omitted for clarity. Symmetry operations used to generate equivalent atoms ('): $1.5 - x, y, 1.5 - z$. Selected bond length [\AA] and angles [$^\circ$]: N1–C1 1.408(4), N1–C2 1.341(4), N1–C13 1.449(4), C1–C1' 1.364(7), C1–C13 1.469(5), C2–C9 1.478(6); N1–C2–N1' 108.0(4), C1–N1–C2 109.4(3), N1–C1–C1' 106.6(2), N1–C2–C9 126.0(2).

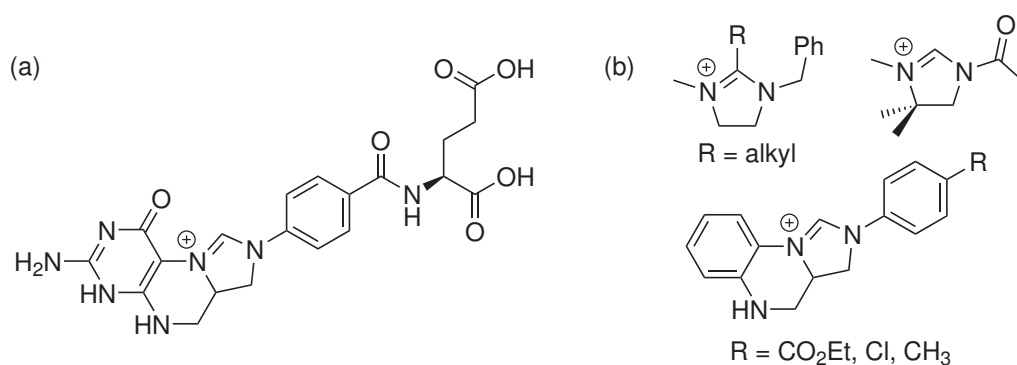
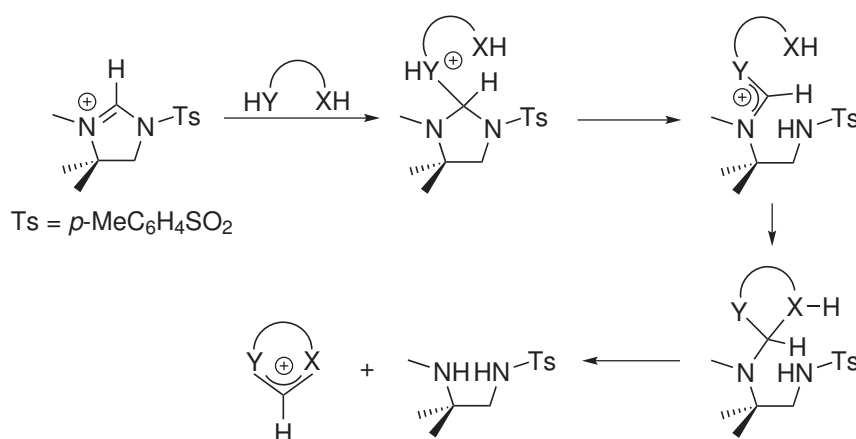


Figure 2.3. The cofactor N^5, N^{10} -methenyltetrahydrofolate (a) and selected imidazolium ions serving as its model compounds.^[285,286,295]

example hydride ions,^[285–289] carbon nucleophiles,^[285–287] and water or the hydroxide ion^[295–298] in order to understand the chemistry of the natural prototype. In an attempt to explain the occurrence of over-reduction products (giving ethylenediamines) and different hydrolysis products, systematic studies on the influences of the different substituents were conducted.^[288,289,299] As in the cofactor, it was noticed that the C² carbon atom could be easily transferred to other molecules yielding for example ketones^[285,287] and also more complex molecules by utilizing bifunctional nucleophiles to cleave the heterocycle (Scheme 2.2).^[300] Indeed, the natural system has inspired chemists to benefit from corresponding molecules in a large variety of chemical transformations.^[301]



Scheme 2.2. Transfer of a one-carbon unit by reaction of a bifunctional nucleophile with an imidazolinium ion.^[300]

2.2 Synthesis of Imidazolinium Ions

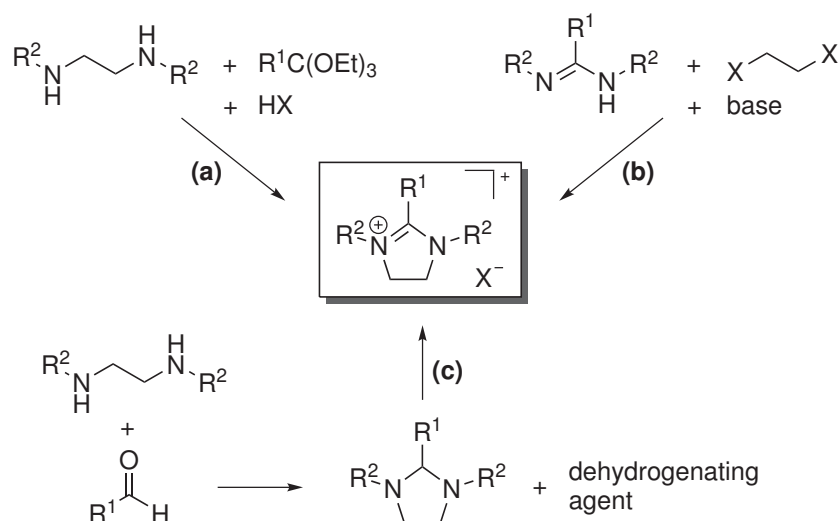
Imidazolinium ions were considered promising candidates for mimicking the hydride acceptor methenyl-H₄MPT⁺ since also in the natural system an imidazolinium heterocycle is present. In comparison with the structurally related imidazolium ion, the imidazolinium ion was expected to show a higher tendency to accept a hydride ion as the aromaticity does not extend over the whole ring system. As a consequence, the hydride uptake is not associated with a disruption of aromaticity in the heterocycle. Furthermore, the experiences made with the synthesis of model compounds for N⁵,N¹⁰-methenyltetrahydrofolate clearly demonstrate that imidazolinium ions are able to accept a hydride ion. Additionally they have the potential to transfer the one-carbon unit. The following sections describe the general approach as well as experimental details aiming at the synthesis of imidazolinium ions suitable for the task to act as hydride acceptors in the heterolytic cleavage of dihydrogen.

2.2.1 General Strategy

As already mentioned in the objective of this thesis, a necessary prerequisite for the targeted imidazolium ions is the presence of a substituent in the C^2 position. The reason for this is that a proton in this position would be relatively acidic and readily deprotonated if an appropriate base was present to yield the respective N-heterocyclic carbene. The substituent in this position should on the one hand be inert towards the attack of a nucleophile or base, and on the other hand it should also feature a certain steric demand in order to protect the reactive C^2 position against the direct attack of a Lewis base resulting in the formation of a Lewis acid–base adduct. At the same time the shielding effect should not be too high as a hydride ion originating from the heterolytic cleavage reaction of dihydrogen should still have free access to the C^2 carbon atom. Mainly three strategies for the preparation of imidazolium ions have been applied in synthetic chemistry (Scheme 2.3):

- (a) Orthoester Method** Probably the most common method for the preparation of imidazolium salts is the orthoester method which involves the reaction of a diamine (or diimine)^[302] with an orthoester to close the heterocyclic ring system.^[303] This synthetic strategy has been widely used for the synthesis of imidazolium ions bearing no substituent in the C^2 position as precursors for N-heterocyclic carbenes,^[304–307] but also imidazolium ions with C^2 substituents have been synthesized *via* this route.^[303,308] The required diamine is typically obtained by a reductive amination with glyoxal or by palladium-catalyzed C–N coupling.^[309,310] This method is often relatively elaborate and suffers from purification problems of the unstable diamines.^[309]
- (b) Amidine Method** The amidine method is a relatively new method to build up the imidazolium heterocycle and circumvents the sometimes tedious synthesis of appropriate diamines. The strategy comprises the reaction of amidines with so-called "di-electrophiles" and a variety of possible reaction partners like cyclic sulfates,^[311] 1,2-dichloroethane,^[309] 1,2-dibromoethane,^[302] (2-bromoethyl)diphenylsulfonium triflate^[310] and epoxides^[312] have been identified. It has been shown that the method can be applied very generally and also the synthesis of larger heterocycles,^[302,313] as well as of backbone-substituted imidazolium salts,^[312,314] has been demonstrated. However, only imidazolium ions without substituent in the C^2 position have been synthesized so far, mainly because the scientific interest focused on the synthesis of precursors for N-heterocyclic carbenes.
- (c) Imidazolidine Method** A rather exotic route to imidazolium ions is the oxidation/dehydrogenation of imidazolidines. After condensation of a suitably substituted ethylenediamine and an aldehyde, the resulting imidazolidine is reacted with a dehydrogenating agent in order to formally remove a hydride ion.^[315–319] For this purpose for example *N*-bromosuccinimide (NBS), *N*-bromoacetamide

(NBA), *N*-iodosuccinimide (NIS),^[318] 1,3-dibromo-5,5-dimethylhydantoin (DBDMH),^[320] quinones and azo compounds,^[317] or CCl_4 ^[316] have been used. In this way, also imidazolinium salts substituted in their C^2 position have been prepared.^[317–319] This method is particularly interesting as it provides the possibility to make the heterolytic splitting of H_2 envisaged in this project catalytic. The dehydrogenation of imidazolidines obtained from the splitting reaction by one of the reagents mentioned above would recover the imidazolinium ion and thereby close the catalytic cycle.

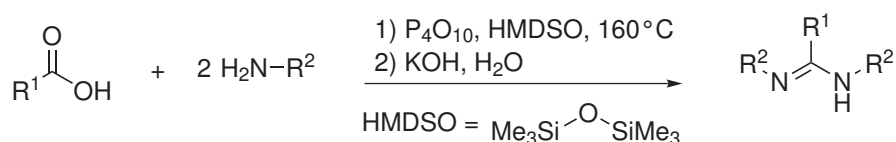


Scheme 2.3. Synthesis of imidazolinium ions through the orthoester (a), the amidine (b) and the imidazolidine method (c).

A fourth method to prepare imidazolinium salts is the addition of substituents to appropriate imidazolines. This route has not been considered here since it has mostly been restricted to alkylation reactions. Also the preparation of the required imidazolines is often not straightforward and sometimes affords the use of expensive palladium catalysts.^[310,321] On the contrary, the amidine method (b) is very attractive for the preparation of a large variety of hydride acceptor molecules because it offers a comparatively simple route to differently substituted imidazolinium ions which does not depend on the availability of appropriate diamines. Although imidazolinium ions featuring C^2 substituents have not been prepared by this method before, it seems likely that the method can be modified to also include a C^2 substituent by using appropriate amidines. For this reason, the amidine method was chosen to synthesize the desired hydride acceptors and as it turned out later, synthesis of C^2 -substituted imidazolinium salts is indeed possible pursuing this approach. The following sections describe the syntheses of appropriate amidines and imidazolinium salts *via* the amidine route, but also the efforts aiming at alternative synthetic procedures are summarized.

2.2.2 Synthesis of Amidines

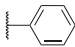
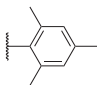

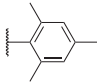
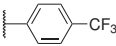
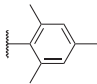
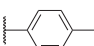
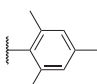
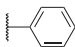
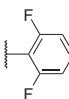
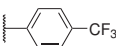
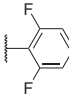
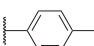
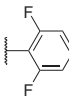
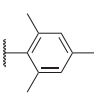
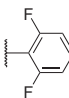
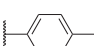

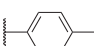
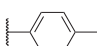
Amidines are an extremely versatile group of chemical compounds and their usefulness in a large variety of (catalytic) reactions has been demonstrated.^[322,323] Furthermore, they display a rich coordination chemistry and amidine complexes with many different main group elements and transition metals have been reported (for details see chapter 3.4). As a consequence, various methods for the preparation of amidines exist and reviews on their synthesis have been published several times.^[324–327] Among the many syntheses of amidines, a convenient method for the preparation of N,N' -disubstituted amidines bearing also a substituent at the carbon atom is the condensation reaction of a carboxylic acid and aromatic amines (Scheme 2.4). This reaction is conducted in the presence of polyphosphoric acid trimethylsilyl ester (PPSE) at 160 °C.^[328] PPSE is a soluble mixture of different tetraphosphoric acid trimethylsilyl esters^[329] which can be readily prepared from phosphorus pentoxide and hexamethyldisiloxane (HMDSO).^[330]



Scheme 2.4. Synthesis of amidines by using PPSE.^[328]

Making use of modified existing literature procedures,^[328,331,332] a variety of symmetrical amidines with different substituents could be prepared from benzoic acid derivatives and anilines. Table 2.1 depicts an overview of the synthesized amidines which are abbreviated according to their substituents at the carbon and the nitrogen atoms, respectively. By using PPSE, the amidines could be prepared in good to excellent yields, provided that the workup procedures were modified to match the demands of the different substituents (for details see Experimental Section). All obtained products were characterized carefully, however the NMR spectra were rather complicated as a mixture of different isomers was encountered in solution. This observation prompted us to look into the chemistry of amidines more thoroughly, and hence the properties of amidines in the solid state and in solution, as well as their coordination chemistry, will be covered separately in chapter 3.

Table 2.1: Overview over the synthesized amidines.

amidine	R ¹	R ²	yield
PhMesAm			82 %
C ₆ F ₅ MesAm			87 %
CF ₃ PhMesAm			87 %
TolMesAm			74 %
PhFAM			90 %
CF ₃ PhFAM			79 %
TolFAM			86 %
MesFAM			77 %
TolFTolAm			58 %
TolTolAm			62 %

2.2.3 Formation of the Imidazolinium Heterocycle

The desired imidazolinium salts were prepared according to reaction (b) in Scheme 2.3 by a reaction of the respective amidines with 1,2-dibromoethane in the presence of a mild base at reflux temperature (131 °C). In similar reactions with formamidines,^[309,310] ethyldiisopropylamine (Hünig's base) proved to be a suitable base to deprotonate the amidine and thus also in the present case this base was employed. As it turned out, the targeted C²-substituted imidazolinium salts were accessible *via* this route in moderate yields. An overview of the synthesized imidazolinium salt as well as the obtained yields is depicted in Table 2.2. The nomenclature is analogous to the amidine systems and the counterion is included.

Table 2.2: Overview over the synthesized imidazolium bromides. Yields marked with an asterisk were obtained from reactions without an additional base. Hence, the maximum yield in those cases is 50 %

imidazolium salt	R ¹	R ²	yield
PhMesIm⁺Br⁻			85 %
C₆F₅MesIm⁺Br⁻			38 %
CF₃PhMesIm⁺Br⁻			39 %
TolMesIm⁺Br⁻			66 %
PhFIm⁺Br⁻			28 %
TolFIm⁺Br⁻			39 [*] /52 %
MesFIm⁺Br⁻			60 %
TolFTolIm⁺Br⁻			39 % [*]
TolTolIm⁺Br⁻			71 %

Bertrand and co-workers had reported that imidazolium ions were not accessible by the reaction of formamidines with 1,2-dibromoethane due to HBr elimination.^[311] However, optimized conditions including the use of MeCN as the solvent and K₂CO₃ as a base showed that in principle such a reaction is possible.^[302] This work shows that, contrary to these reports, 1,2-dibromoethane can be readily used in the reactions with benzamidines. In fact, this reaction represents an attractive route to C²-substituted imidazolium salts. Nevertheless, the reactions were found highly dependent on the utilized amidine which was reflected in a large variance of the obtained yields. Consequently each synthesis was optimized as effectively as possible. This sometimes afforded a change of the applied base (e. g. CsCO₃ was used in the synthesis of C₆F₅MesIm⁺Br⁻), an adjustment of temperature and/or reaction time, or modifications of the workup

procedure. For **TolFIm⁺Br⁻** and **TolFTollIm⁺Br⁻** it was possible to refrain from using a base since in principle, also the amidine can act as a base in the reaction.^[309] The maximum yield is then 50 % since half of the amount of amidine gets protonated in the course of the reaction yielding the respective amidinium cation. The advantage of such a reaction is that the amidine can be recovered after isolation of the product and reused in additional runs of the reaction permitting an overall higher yield. Details of the experimental procedures can be found in chapter 6.5.

Interestingly, it was not possible to obtain an imidazolinium salt starting from amidine **CF₃PhFAm**, in which both R¹ and R² have electron-withdrawing CF₃- or F-substituents, by a reaction with 1,2-dibromoethane in the presence of a base. Although the imidazolinium salt could be detected in the reaction mixture by means of NMR spectroscopy and ESI mass spectrometry, it could not be isolated as a pure compound. A reason for this is that **CF₃PhFAm** seems to be extraordinarily unstable compared to the other imidazolinium ions synthesized in this project. Under workup conditions, the imidazolinium ion obviously decomposes to yield a mixture of products which hampers the purification process.

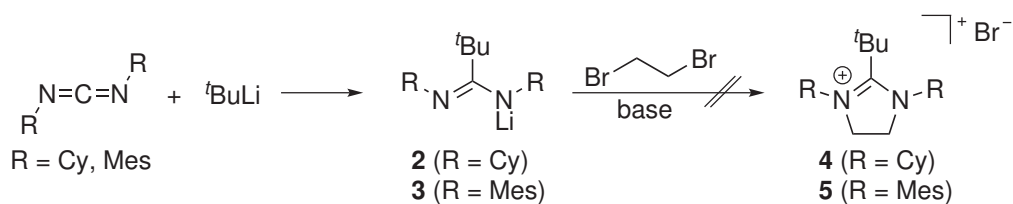
2.2.4 Further Attempts to Synthesize Imidazolinium Salts

Besides the syntheses already described in the sections above, additional attempts to produce C²-substituted imidazolinium salts were conducted, albeit with less success. The following paragraphs summarize the efforts to synthesize appropriate imidazolinium ions featuring also aliphatic substituents.

Alternative Methods to Synthesize Amidines

Since it is known that aliphatic amines do not readily react with carboxylic acids in the presence of PPSE,^[328] alternative procedures had to be found in order to gain access to amidines featuring also aliphatic residues at their carbon and nitrogen atoms. At first glance, the nucleophilic attack of an organolithium reagent at the carbon atom of a carbodiimide offers a promising alternative to the PPSE method. Subsequent reaction of the obtained lithium amidinate with 1,2-dibromoethane should then yield the respective imidazolinium salt according to the amidine method (Scheme 2.5). Carbodiimides can for example be readily obtained from thioureas,^[333] a few of them are even commercially available. Following a published literature procedure,^[334] Li[^tBuC(NCy)₂] (**2**) was synthesized from commercially available dicyclohexylcarbodiimide. Analogous reaction of the mesityl-substituted carbodiimide which was obtained from the corresponding thiourea^[335] led to the formation of amidinate **3**.

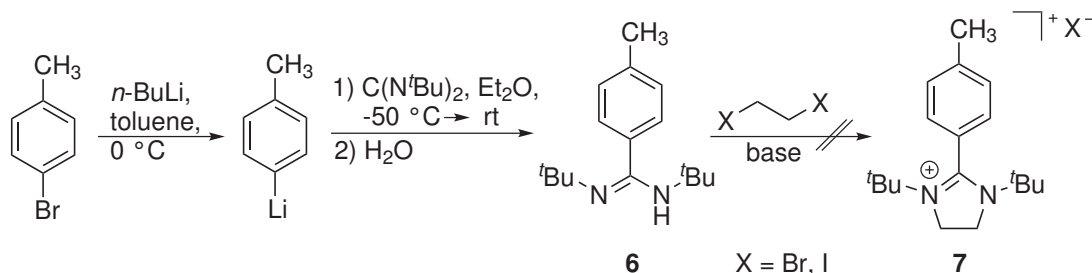
However, when both amidinates were subjected to reactions with 1,2-dibromoethane in the presence of a base (usually ethyldiisopropylamine), no formation of imidazolinium salts **4** and **5** was observed. NMR spectroscopy and ESI mass spectrometry merely



Scheme 2.5. Synthesis of imidazolium salts following the carbodiimide method (Cy = cyclohexyl, Mes = 2,4,6-trimethylphenyl).

showed the presence of the respective amidines or their decomposition products. A possible reason for this might be that the lithium amidinates are not present in the required *E-anti* form in solution (for nomenclature of isomers see section 3.1.2) due to enhanced steric repulsion between the relatively bulky *tert*-butyl and cyclohexyl/mesityl groups. Only when an arrangement of the substituents as shown in Scheme 2.5 is possible, the reaction forming an imidazolium ion can be achieved.

An alternative route to imidazolium ions starting from an aryl bromide and a carbodiimide is shown in Scheme 2.6. Commercially available di-*tert*-butylcarbodiimide was treated with *p*-tolyllithium which can be readily obtained from *p*-bromotoluene by reaction with lithium powder or *n*-butyllithium.^[336,337] Aqueous workup yielded the amidine **6**, but in the subsequent reaction with 1,2-dibromoethane no product formation was observed. Efforts to facilitate the formation of imidazolium ion **7** by using 1,2-diiodoethane instead of 1,2-dibromoethane were unsuccessful as well.

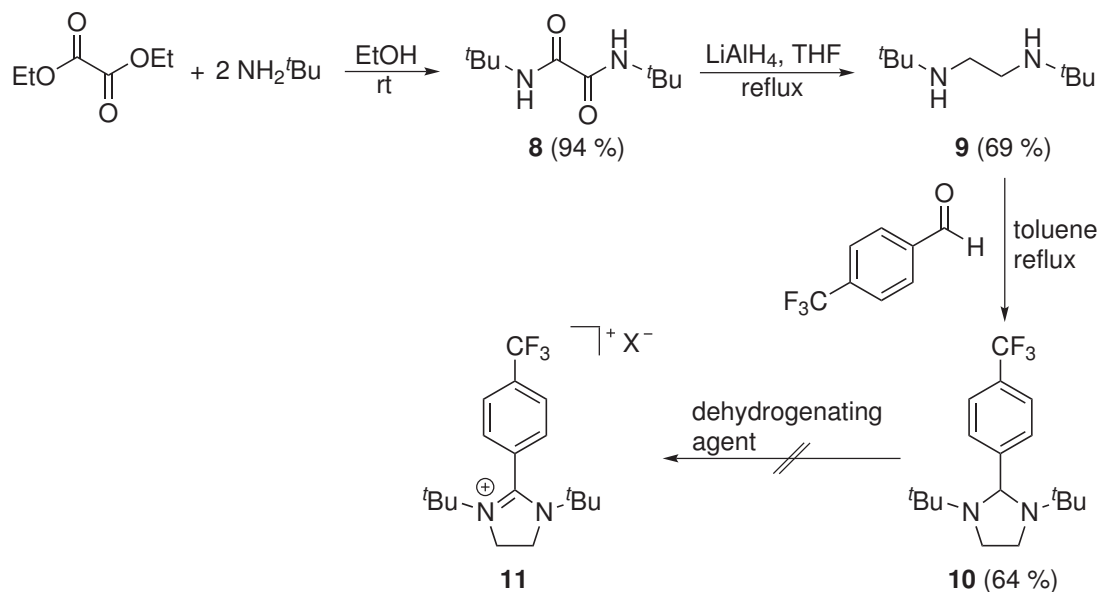


Scheme 2.6. Alternative synthesis of imidazolium salts *via* carbodiimides.

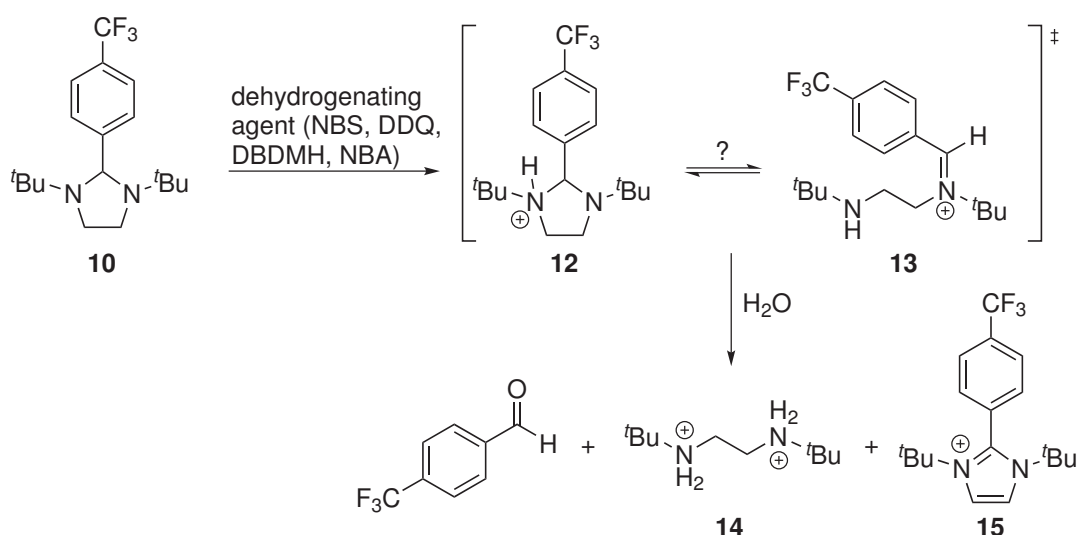
Imidazolidine Route

As the previously mentioned route was not appropriate to provide alkyl-substituted imidazolium ions, further attempts were made to achieve this goal. According to Scheme 2.7, a reaction of diethyl oxalate with *tert*-butylamine and subsequent reduction of the obtained diamide **8** with LiAlH_4 gave *N,N'*-di-*tert*-butyl-1,2-ethylenediamine (**9**). By this method, which was performed according to a modified literature procedure,^[338] diamide **8** was synthesized in a yield of 94 % and diamine **9** in a yield of 69 %. In the following condensation reaction with 4-(trifluoromethyl)benzaldehyde in toluene, imidazolidine **10** could be synthesized in a yield of 64 %. Unfortunately, analogous reactions

of diamine **9** with pentafluorobenzaldehyde turned out to be unsuccessful and complex mixtures of different products were obtained under different reaction conditions. A possible explanation for this could be that the pentafluorophenyl-substituted imidazolidine is not stable under the applied reaction conditions. This is not surprising as it is known that in some cases pentafluorophenyl-substituted imidazolidines might lose pentafluorobenzene to produce carbenes. Similar imidazolidines have in fact been used as air-stable precursors for carbenes.^[339,340] The generated carbene might then undergo a variety of reactions leading to the different observed products.



Scheme 2.7. Attempted synthesis of imidazolinium salts *via* the imidazolidine route.



Scheme 2.8. Intermediate and detected products in the reaction of imidazolidine **10** with dehydrogenating agents

Imidazolidine **10** was subjected to reactions with various dehydrogenating agents such as NBS, NCS, NBA, DBDMH, 2,3-dichloro-5,6-dicyano-1,4-benzoquinone (DDQ), and CCl₄ (for a review of literature on dehydrogenating agents see section 2.2.1). However, the formation of an imidazolinium ion **11** was not observed in any of the performed reactions. Instead, reactions with NBS, DDQ, DBDMH or NBA led to the formation of imidazolium ion **15**, the protonated diamine **14** and 4-(trifluoromethyl)benzaldehyde as could be verified by means of NMR spectroscopy and mass spectrometry (Scheme 2.8). Besides these products, the reaction mixtures contained – depending on the applied dehydrogenating agent – varying amounts of other (decomposition) products. Reactions with NCS or CCl₄ gave only decomposition products. When oxygen- and moisture-free conditions were maintained throughout the reaction, an intermediate could be detected which was tentatively assigned to the structure of the protonated imidazolidine **12**. For this compound, NMR spectra showed the presence of two chemically inequivalent *tert*-butyl groups as well as four inequivalent protons belonging to the two CH₂ groups. Furthermore, a coupling of 5 Hz between the C² proton and the NH group was observed. To our knowledge, a similar intermediate has not been reported before, but a simple ring opening reaction would produce iminium ion **13** which has been proposed as an intermediate in the reductive cleavage of similar imidazolidines.^[288] The origin of the proton for this reaction must be the reaction of the dehydrogenating agent with imidazolidine **10**. Consequently, the dehydrogenating agent oxidizes the imidazolinium ion in this reaction to give imidazolium ion **15** and protons, which in turn leads to the formation of the observed decomposition products *via* hydrolysis of the protonated imidazolidine **12**.

In summary, the imidazolidine route does not seem to be suitable for the formation of the targeted imidazolinium ions. The ability of the imidazolidine nitrogen atoms to be easily protonated, especially if electron-donating *tert*-butyl groups are used as substituents, obviously promotes the decomposition of the heterocycle. The decomposition occurs when dehydrogenating agents are used in the synthesis of imidazolinium ions, most likely *via* preceding protonation of the imidazolidine.

2.3 Properties of Imidazolinium Ions

With the compounds depicted in Table 2.2, a large variety of imidazolinium ions was synthesized. In order to evaluate their potential in a heterolytic cleavage reaction of dihydrogen, the imidazolinium salts were examined in terms of their structural and electrochemical properties. Furthermore, their reactivities were investigated. The following sections summarize the X-ray diffraction and cyclic voltammetry measurements which were conducted in order to elucidate the structural and electrochemical properties of the imidazolinium ions. Additionally, the behavior of the synthesized imidazolinium ions in model reactions with the hydride ion as well as the implications of the obtained results for the suitability as hydride acceptor molecules are discussed.

2.3.1 Structural Parameters of Imidazolinium Ions

For most of the synthesized imidazolinium salts, crystals suitable for X-ray crystallography were obtained by recrystallization from mixtures of DCM or CHCl_3 and Et_2O . An overview of the obtained crystal structures is presented in Figure 2.4, where the bromide counterions of the depicted imidazolinium ions are not shown. The figure does not contain molecular structures of **TolMesIm**⁺ and **TolFTolIm**⁺ although crystals of both compounds were obtained by diffusing Et_2O into DCM solutions of the respective compounds. A reason for this is the fact that the quality of the measured crystal structures was not sufficient. Only when a disorder model was applied to the structures, better *R*-factors were obtained. For reasons not yet entirely clear, the crystal structure of **TolMesIm**⁺**Br**⁻ contained a small fraction of molecules which were halogenated at the *ortho*-methyl groups of the mesityl rings, presumably by chlorine atoms. The exact proportion of chlorination could not be determined. Likewise, compound **TolFTolIm**⁺**Br**⁻ was partly contaminated with molecules showing a fluorine atom at the methyl group of the *para*-tolyl ring. Also in this case the origin of the unexpected fluorine atoms could not be clarified. However, assuming a content of 25 % of additionally fluorinated molecules led to a significant improvement of the crystallographic data. Recrystallization of both imidazolinium ions did not remove the impurities. In sharp contrast to this, the contamination of the compounds could not be verified by means of ESI mass spectrometry, and also elemental analysis of the products showed satisfactory results in favor of the presence of uncontaminated samples. Probably, halogenation occurred during crystallization or – more likely – the additionally halogenated molecules are only present to a very small fraction in the bulk material, but crystallize in preference from solutions of the respective compounds.

Selected bond lengths and bond angles for the imidazolinium ions are depicted in Table 2.3. All imidazolinium ions have in common that the central imidazolinium heterocycle is more or less planar. Only minor deviations from planarity can be recognized as one of the two CH_2 carbon atoms is slightly displaced above a plane spanned by the two nitrogen atoms and the C^2 carbon atom, while the other carbon atom is located slightly below this plane. The deviations are in a range of 0.04 to 0.14 Å and the maximum is found in compound **PhFIm**⁺**Br**⁻. Furthermore, the aromatic residues at the nitrogen atoms as well as the aromatic ring at the C^2 carbon atom are not located in a common plane with the heterocycle. Instead, the substituents are tilted against the imidazolinium ring. The dihedral angles Im-*N*Ar and Im- C^2 Ar between these planes are included in Table 2.3 as well.

All in all the C^2 -N bond lengths vary from 1.32 to 1.34 Å and can thus be classified as a borderline case between “regular” C-N single and C=N double bonds.^[341] The bond lengths for the two C^2 -N bonds within one imidazolinium ion differ only slightly, while **TolFTolIm**⁺ showed the largest difference (0.02 Å). However, the effect of the partial fluorination at the tolyl substituent (see above) remains unclear. In the case of imidazolinium ion **PhMesIm**⁺, equal bond lengths are observed as the two nitrogen atoms

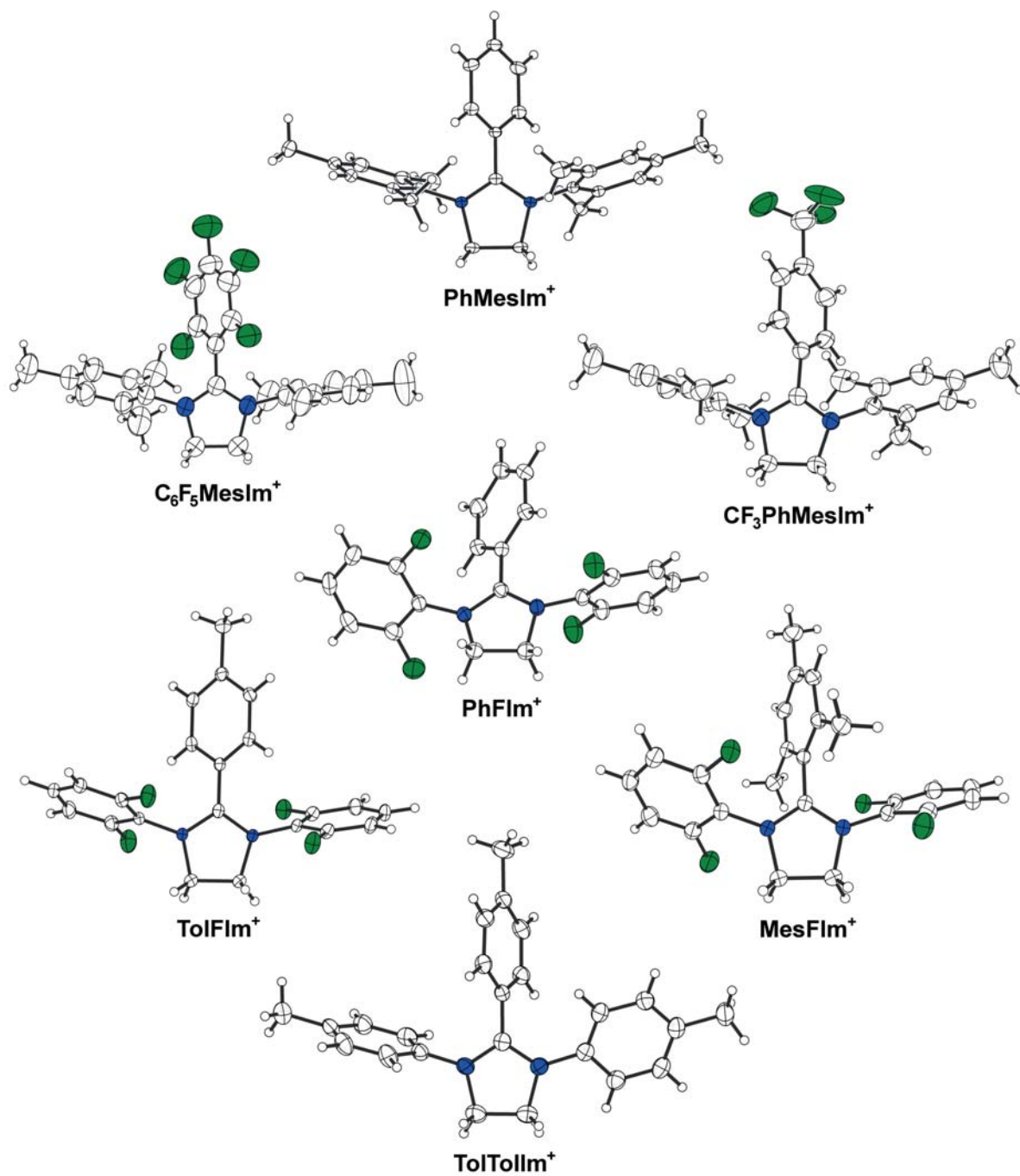


Figure 2.4. Thermal displacement ellipsoids (shown at 50 % probability) of molecular structures of imidazolium salts. Bromide anions are omitted and hydrogen atoms are displayed as ball-and-stick representation with fixed radii of 0.135 Å.

Table 2.3: Selected bond lengths [Å] and angles [°] of the solid state structures of the imidazolinium ions. (*) The crystal structure of **TolFTolIm⁺** was refined applying a disorder model (see text). The quality of the crystal structure of **TolMesIm⁺** was not sufficient for a reliable determination of bond lengths and angles.

compound	d(C ² -N)	d(C ² -C _{Ar})	∠(N-C ² =N)	∠(Im-NAr)	∠(Im-C ² Ar)
PhMesIm⁺	1.322(2) 1.322(2)	1.485(3)	112.2(2)	75.3(1) 75.3(1)	44.1(1)
C₆F₅MesIm⁺	1.327(4) 1.324(4)	1.479(5)	112.8(3)	76.0(3) 77.7(3)	55.1(2)
CF₃PhMesIm⁺	1.323(3) 1.320(3)	1.479(3)	112.6(2)	82.2(2) 81.8(1)	59.4(2)
PhFIm⁺	1.331(3) 1.330(3)	1.464(3)	110.7(2)	75.2(2) 67.4(2)	43.8(2)
TolFIm⁺	1.334(2) 1.330(2)	1.461(2)	110.5(1)	65.5(2) 78.3(1)	36.0(2)
MesFIm⁺	1.331(3) 1.323(2)	1.478(3)	110.9(2)	62.0(2) 62.1(2)	68.0(2)
TolTolIm⁺	1.319(3) 1.335(3)	1.470(3)	111.6(2)	42.9(2) 62.3(3)	64.8(1)
TolFTolIm⁺ (*)	1.323(4) 1.343(4)	1.466(5)	110.9(3)	55.8(2) 63.8(3)	42.5(3)

are related by symmetry (symmetry operation used to generate equivalent atoms: $-x, -x + y, 0.333 - z$). The C²-C_{Ar} distances range from 1.46 to 1.49 Å, the comparably short C-C distance being indicative of a (at least partly) conjugated system including the imidazolinium heterocycle and the aromatic ring at the C² carbon atom. The shortest bond lengths are observed for imidazolinium ions bearing fluorine-substituted aromatic groups at the nitrogen atoms. Consequently, electron-withdrawing groups at the nitrogen atoms obviously intensify the electron deficiency at the C² carbon atom which is at least partly compensated by electron density from the C²-substituent leading to a shorter C²-C_{Ar} bond length. The mesityl group in imidazolinium ion **MesFIm⁺** counteracts this trend. The associated C²-C_{Ar} bond length is lengthened, presumably because of steric reasons. As becomes clear from the structural data of imidazolinium ion **CF₃PhMesIm⁺** an electron-withdrawing substituent in the C² position does not lead to a shorter C²-C_{Ar} bond distance. This is an important discovery since it makes clear that the substituents have differing electronic influences on the imidazolinium heterocycle depending on their position.

The N-C²=N bond angles are in a range between 110.5 and 112.8°. The smaller ones are found in imidazolinium ions with electron-withdrawing substituents at the nitrogen atoms. Since **TolTolIm⁺** shows a comparably large N-C²=N angle, it can be suspected,

that electronic effects are the main cause for the observed trend. The dihedral angles for the twisting of the imidazolinium plane against the planes of the aromatic N-substituents $\angle(\text{Im}-N\text{Ar})$ collected in Table 2.3 indicate that mesityl substituents induce a certain steric strain in the molecule as the observed variance is relatively small. Seemingly, the mesityl substituents are more or less fixed in a certain position close to 90° to avoid steric repulsion. However, rotation is easier for the other substituents as is reflected by the variance of dihedral angles. Concerning the C^2 substituent, the largest dihedral angle is found for the mesityl substituent as well, again hinting at steric reasons. As already recognized beforehand, electron-withdrawing substituents at the nitrogen atoms lead to an enhanced displacement of electron density of the aromatic ring into the imidazolinium heterocycle. Besides a shorter C^2-C_{Ar} bond length, this fact is also reflected by a smaller $\text{Im}-C^2\text{Ar}$ dihedral angle indicative of a more pronounced delocalization between the two ring systems.

2.3.2 Electrochemical Properties of Imidazolinium Ions

When designing hydride acceptor molecules for the use in the heterolytic splitting reaction of dihydrogen, it is important to consider possible side reactions which could occur under experimental conditions. In the present case, a conceivable scenario would be the direct electron transfer from the Lewis basic to the Lewis acidic site. Although the targeted reaction mechanism does not include a transfer of electrons, such a reaction cannot be excluded, especially as relatively electron-rich metal centers will be involved in the reaction. Consequently, the electrochemical properties of the synthesized imidazolinium ions were explored by means of cyclic voltammetry (CV) which was conducted at a PerkinElmer 263A potentiostat, using a glassy carbon working electrode, a silver quasi-reference electrode and a platinum counter electrode. All measurements were performed in 0.1 M solutions of NBu_4PF_6 in MeCN at room temperature. Decamethylferrocene (FeCp_2^*) was added as internal standard. All measured redox potentials are referenced *vs.* the $\text{FeCp}_2/\text{FeCp}_2^+$ (Fc/Fc^+) redox couple ($\text{FeCp}_2^*/\text{FeCp}_2^{*+}$ *vs.* Fc/Fc^+ : 0.510 V in MeCN).^[342] The cyclic voltammograms obtained for the imidazolinium ions bearing mesityl or tolyl substituents at their nitrogen atoms are compiled in Figure 2.5. The remaining imidazolinium ions featuring electron-withdrawing fluorine-substituted aromatic rings at the nitrogen atoms are depicted in Figure 2.6. As anticipated, the imidazolinium ions were readily reduced giving rise to mostly reversible reduction waves at potentials lower than -1.5 V. For compounds $\text{C}_6\text{F}_5\text{MesIm}^+\text{Br}^-$ and $\text{TolTolIm}^+\text{Br}^-$ irreversible waves were measured and only reductive peak potentials E_p^{red} could be determined. Obviously, the two compounds are not stable in their one-electron-reduced form and decomposition or reaction to other species is faster than re-oxidation in the cyclic voltammetry experiment. In order to compare these two imidazolinium salts to the remaining imidazolinium bromides, for which a calculation of standard potentials E° was possible, the standard potentials were estimated by adding

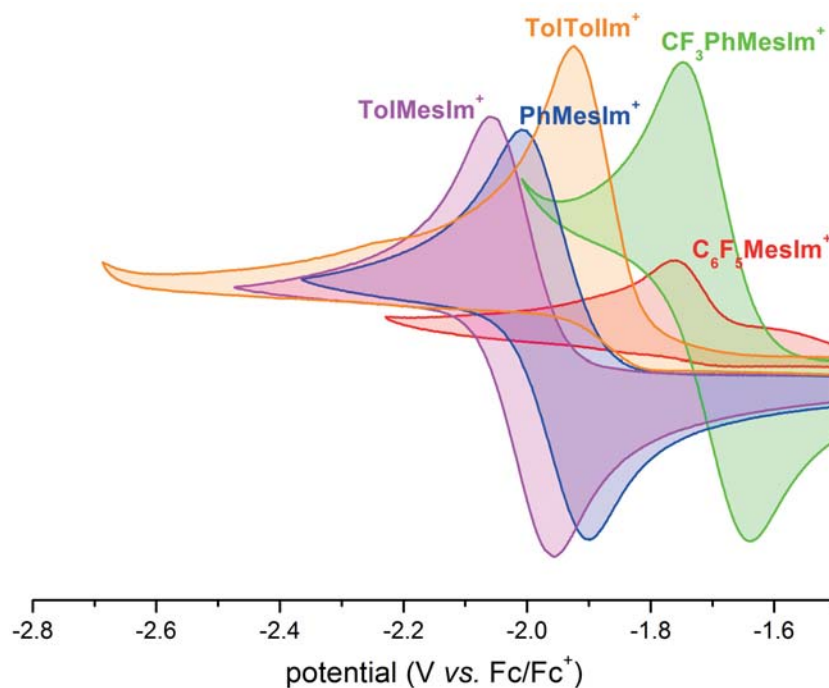


Figure 2.5. Cyclic voltammograms of the *N*-mesityl-substituted imidazolinium bromides and **TolTolIm⁺Br⁻**. The measurements were performed in 0.1 M NBu₄PF₆ solutions (MeCN) at a scan rate of 100 mV s⁻¹ and the potentials are referenced *vs.* the Fc/Fc⁺ redox couple.

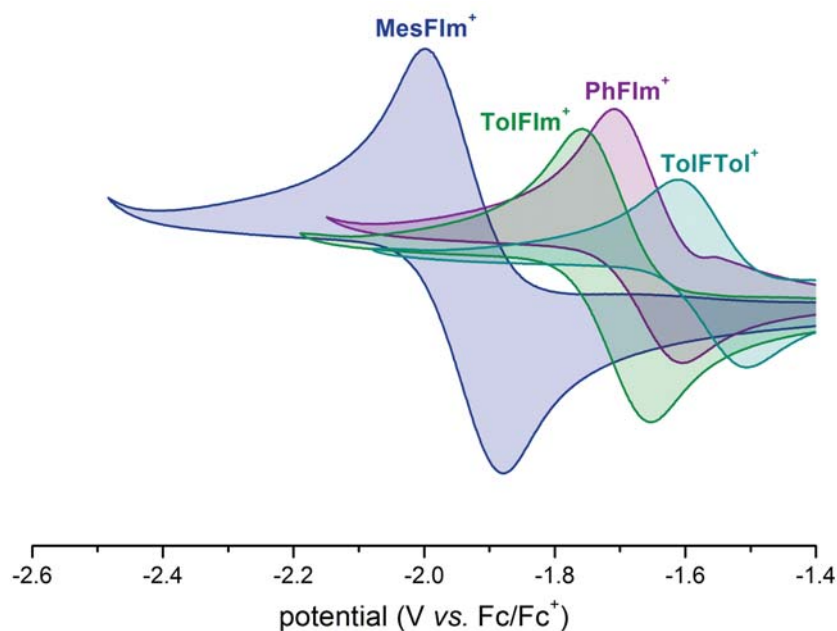


Figure 2.6. Cyclic voltammograms of the imidazolinium bromides bearing fluorine-substituted aromatic rings at the nitrogen atoms. The measurements were performed in 0.1 M NBu₄PF₆ solutions (MeCN) at a scan rate of 100 mV s⁻¹ and the potentials are referenced *vs.* the Fc/Fc⁺ redox couple.

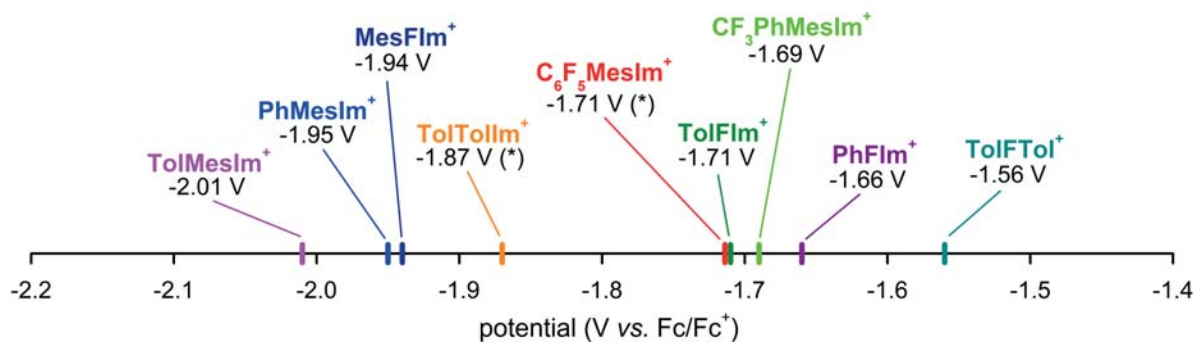


Figure 2.7. Standard potentials E° and estimated standard potentials (marked with an asterisk, for details see text) of the synthesized imidazolinium salts referenced *vs.* the Fc/Fc⁺ redox couple.

a value of 0.05 V to the measured peak potentials E_p^{red} . This potential corresponds to the half of the mean difference between reductive and oxidative peak potentials of the imidazolinium salts featuring reversible reduction waves. The estimated standard potentials E° of **C₆F₅MesIm⁺Br⁻** and **TolTollm⁺Br⁻** as well as the standard potentials of the remaining imidazolinium salts are summarized in Figure 2.7. When looking at the obtained results, it becomes clear that fluorine-substituted imidazolinium ions generally show higher potentials than imidazolinium ions lacking a fluorine substituent, irrespective of the exact site of the fluorination (aromatic ring at the C² carbon atom or at the nitrogen atoms). This behavior is expected, as the electron-withdrawing effect of the fluorine atoms should lead to an imidazolinium ring which is more electron-deficient and can thus be reduced more easily. Imidazolinium salt **TolFTollm⁺Br⁻** has the highest reduction potential and should readily accept an electron. Seemingly, an exception to this rule is **MesFlm⁺Br⁻** which features an unexpectedly low redox potential of -1.94 V, comparable to the other mesityl-substituted imidazolinium ions in Figure 2.5. An explanation for this could be that the mesityl substituent at the C² carbon atom complicates the reduction by its steric demand. The most probable site of reduction is the C² carbon atom, and an uptake of an electron at this position should induce a structural rearrangement in the imidazolinium heterocycle which is hampered by the mesityl group.

After examination of the electrochemical reduction potentials, the focus now turns towards the reactivity of the synthesized imidazolinium ions. Special attention will be devoted to the reduction of the imidazolinium salts with hydride ions, a reaction that is fundamentally important for the targeted heterolytic cleavage of dihydrogen.

2.3.3 Reactivity of Imidazolinium Ions

The electrophilic character of the C² carbon atom makes the imidazolinium ion a potential reaction partner for a variety of nucleophiles such as the hydride ion,^[285–289,315,343] carbon nucleophiles,^[285–287] and water or the hydroxide ion.^[295–298,343,344] For the heterolytic splitting of dihydrogen envisaged in this project, this electrophilic character of the imidazolinium salt is desired as it should lead to a polarization of the H₂ molecule and thus to an uptake of the subsequently generated hydride ion. Before starting the eventual reactions with dihydrogen, the synthesized imidazolinium ions were examined with respect to the electrophilicities of their C² carbon atoms. As a first hint for the reactivity, the ¹³C NMR chemical shifts of the C² carbon atoms were compared since they can be correlated to the electronic environment at this position. Although other effects as for example local magnetic fields have to be considered, it can be assumed that the chemical shift δ is higher (the signal is shifted to lower field) for C² carbon atoms with a lower electron density since the structures of the imidazolinium ions are all very similar. From the chemical shifts depicted in Table 2.4 it is evident that the imidazolinium ions featuring electron-withdrawing fluorine substituents at the nitrogen atoms generally show a higher chemical shift of the C² carbon atom, this being indicative of a more electrophilic character of the carbon atom. The highest shift is found for imidazolinium ion **MesFIm⁺Br⁻** which suggests that electron-donating substituents at the C² carbon atom further enhance this effect. On the contrary, electron-withdrawing substituents in the C²-position seem to attenuate the electrophilic character since **C₆F₅MesIm⁺Br⁻** and **CF₃PhMesIm⁺Br⁻** display the lowest chemical shifts of all examined imidazolinium ions. At first glance this is surprising since these two imidazolinium ions are among the group of compounds displaying the highest reduction potentials in the CV

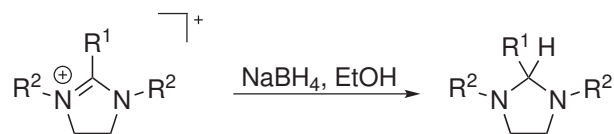
Table 2.4: ¹³C NMR chemical shifts of the C² carbon atoms of the synthesized imidazolinium ions in CDCl₃ providing a first hint at the electrophilicities of the C² positions. For comparison, also the chemical shift of imidazolium ion [**Im^{-2H}**]⁺**Br⁻** (in CD₂Cl₂) is given.

compound	¹³ C- δ (C ²)
PhMesIm⁺Br⁻	165.6 ppm
C₆F₅MesIm⁺Br⁻	157.8 ppm
CF₃PhMesIm⁺Br⁻	164.4 ppm
TolMesIm⁺Br⁻	165.6 ppm
TolTolIm⁺Br⁻	164.5 ppm
PhFIm⁺Br⁻	169.6 ppm
TolFIm⁺Br⁻	169.6 ppm
MesFIm⁺Br⁻	170.1 ppm
TolFTolIm⁺Br⁻	169.9 ppm
[Im^{-2H}]⁺Br⁻	144.5 ppm

measurements. A possible explanation for this trend could be that electron-donating substituents at the C^2 carbon atom as well as electron-withdrawing substituents at the nitrogen atoms stabilize the resonance structure with a positive formal charge at the carbon atom. In contrast to this, the complementary resonance structure with a positive formal charge at one of the nitrogen atoms is stabilized when the electron-withdrawing substituent is located at the C^2 -position and the electron-donating groups at the nitrogen atoms. The structural data of the imidazolium ions obtained by X-ray crystallography corroborate this assumption since also in the crystal structures, N-fluorine-substituted compounds were found to have shorter C^2-C_{Ar} bond length, which is also indicative of an enhanced electrophilicity of the C^2 carbon atom (see section 2.3.1). The fact that the C^2 chemical shift of imidazolium ion $[Im^{2H}]^+Br^-$ (which is represented as well in Table 2.4) is significantly lower than the chemical shifts of all imidazolium ions, provides additional evidence for the conclusion drawn above that imidazolium ions are generally more reactive towards nucleophiles than imidazolium ions.

In order to explore the hydride acceptor capacities of imidazolium ions more thoroughly, the synthesized imidazolium salts were subjected to reactions with $NaBH_4$ in EtOH (Scheme 2.9). As in the planned heterolytic splitting reaction of dihydrogen, the imidazolium ions should be readily reduced to give the corresponding imidazolidines. Unfortunately, all of the mesityl-substituted imidazolidines were not converted into the respective imidazolidines by this procedure and remained unchanged in solution. Only for imidazolium ion $CF_3PhMesIm^+Br^-$ traces of the corresponding imidazolidine were identified in solution, but isolation of the compound failed. The reason for this is most probably connected to both the steric bulk of the mesityl substituents as well as to electronic effects. As has been already demonstrated, the N-mesityl-substituted imidazolium ions mostly feature relatively low ^{13}C NMR chemical shifts for the C^2 carbon atoms. This could explain the low electrophilicity of the mesityl-substituted imidazolium ions and the fact that reactions with the H^- nucleophile do not take place. The imidazolium salt $MesFIm^+Br^-$ seems to be special in this respect since it shows the highest shift of the C^2 carbon atom in the ^{13}C NMR measurements. However, a reaction with $NaBH_4$ was not observed under the experimental conditions. A reason for this could be that the reactive C^2 carbon atom is shielded by the bulky mesityl C^2 -substituent. By this, a reaction with the H^- nucleophile is prevented. Whether steric reasons are also crucial for the imidazolium ions featuring mesityl substituents at the nitrogen atoms cannot be judged ultimately. Most probably, a combination of steric and electronic factors is responsible for the lack of reactivity.

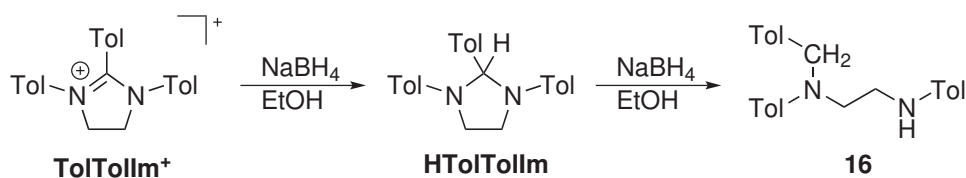
The remaining imidazolium ions with fluorine-substituted aromatic residues $PhFIm^+$, $TolFIm^+$ and $TolFTolIm^+$ were readily reduced at room temperature and the corre-



Scheme 2.9. Reaction of imidazolium ions with $NaBH_4$ producing imidazolidines.

sponding imidazolidines **HPhFIm**, **HTolFIm** and **HTolFTolIm** were formed in a quantitative yield. This is understandable since the high chemical shifts of the C² carbon atoms observed in the ¹³C NMR measurements indicate a high electrophilicity. Furthermore, the high reduction potentials and the structural parameters derived from the crystal structures support the estimation of relatively electrophilic C² carbon atoms.

Like the imidazolinium salts with electron-withdrawing substituents at the nitrogen atoms, also **TolTolIm**⁺**Br**⁻ reacted with NaBH₄ in EtOH. However, the reaction did not proceed as smoothly as in the previous cases and the imidazolidine was contaminated with varying amounts of a by-product. Based on the obtained NMR data, the side product was tentatively assigned to the structure of over-reduction product **16** in Scheme 2.10, since it is known that in certain cases alkaline borohydrides might cleave the imidazolidine ring, giving rise to ethylenediamines.^[286,288,289] As this reactivity hints at an insufficient stability of the corresponding imidazolidine, compound **TolTolIm**⁺**Br**⁻ is probably not the ideal candidate for a reaction with dihydrogen, especially as possible catalytic reactions are hampered due to this additional reactivity.



Scheme 2.10. Reaction of imidazolinium ion **TolTolIm**⁺ with NaBH₄ resulting in the formation of imidazolidine **HTolTolIm** and over-reduction product **16**.

The structural changes that occur in the imidazolinium heterocycle upon accepting a hydride ion can be illustrated exemplarily by considering the solid state structure of imidazolidine **HTolFIm** since it was possible to obtain crystals suitable for X-ray crystallography by slow evaporation of a CHCl₃ solution of the compound.^[345] From the crystallographic data represented in Figure 2.8 it becomes clear that the almost planar imidazolinium heterocycle of **TolFIm**⁺ experiences severe structural changes upon accepting a hydride ion. In the solid state, **HTolFIm** adopts an envelope conformation in which one carbon atom is located significantly above (0.55 Å) the plane defined by both N atoms and the C² carbon atom. In sharp contrast to this, the imidazolinium ion is nearly planar as already discussed in section 2.3.1.

The envelope conformation found for **HTolFIm** parallels to some extent what was already found in the [Fe] hydrogenase for the structure of methylene-H₄MPT bound in an enzyme-substrate complex. In the open form of the enzyme, a similar geometry of the reduced hydride acceptor molecule was found (Figure 2.9).^[226] However, in the enzyme-substrate complex, the imidazolidine ring is slightly more planar as the respective carbon atom is only 0.37 Å above the plane through both nitrogen atoms (N⁵ and N¹⁰) and the central carbon atom (C^{14a}; atom labeling according to the reference^[226]). Besides this, the orientation of the phenyl substituent at the nitrogen atom differs. These

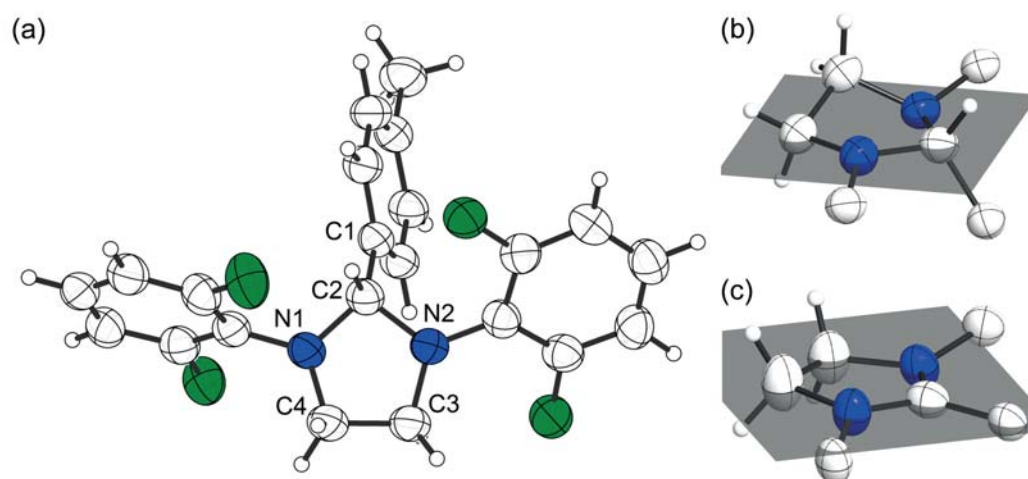


Figure 2.8. (a) Thermal displacement ellipsoids (shown at 50 % probability) of the molecular structure of imidazolidine **HTolFIm**. Hydrogen atoms are displayed as ball-and-stick representation with fixed radii of 0.135 Å. Selected bond length [Å] and angles [°]: N1–C2 1.472(2), C1–C2 1.516(3), C2–N2 1.480(2), N2–C3 1.465(2), C3–C4 1.509(3), C4–N1 1.468(2); N1–C2–N2 101.4(2), N1–C1–C2 111.4(2), C1–C2–N2 114.1(2); (b) imidazolidine ring of **HTolFIm** and plane through both nitrogen atoms and the C² carbon; (c) the imidazolinium heterocycle of **TolFIm**⁺ for comparison.

structural differences between natural prototype and model compound may be related to the annulated ring system in methylene- H_4MPT and/or the protein environment imposing a more planar conformation on the imidazolidine ring. In fact, the hydride transfer might be facilitated in the natural system as structural changes are minimized during reaction.^[223] Imposing a certain degree of non-planarity to an imidazolinium ion might thus be a key to enhancing its hydride acceptor ability in even more potent model systems.

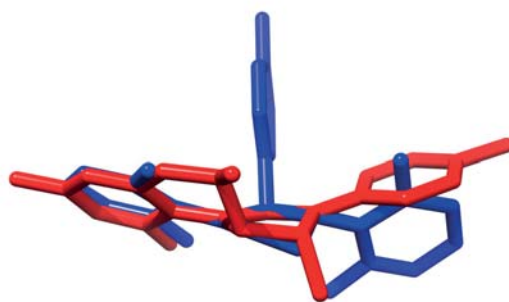


Figure 2.9. Superposition of **HTolFIm** (blue) and central fragment of methylene- H_4MPT (red) as found in the crystal structure of the enzyme-substrate complex.^[226]

2.4 Conclusion

In summary, various imidazolium salts bearing different aromatic substituents have been successfully synthesized. In order to get an impression of their suitability as models for the hydride acceptor methenyl- H_4MPT^+ found in the [Fe] hydrogenase, a series of investigations was carried out. Structural aspects were elucidated by means of X-ray crystallography while CV measurements gave some indications of the electrochemical properties of the imidazolium ions. Finally, matters of reactivity were addressed by subjecting the compounds to model reactions with the H^- nucleophile. The reactions showed that in general a good correlation between the electrophilicity of the imidazolium ion and the ^{13}C NMR chemical shift of the C^2 carbon atom can be expected. However, steric aspects have to be considered as well since bulky substituents like the mesityl group might block the access to the electrophilic carbon atom. In general, the obtained results indicate that electron-withdrawing substituents at the nitrogen atoms and electron-donating substituents at the C^2 carbon atom increase the electrophilicity of the imidazolium ion. As has been shown in reactions with NaBH_4 , the three imidazolium ions **PhIm** $^+$, **TolIm** $^+$ and **TolTolIm** $^+$ can readily be reduced by a hydride ion to yield the corresponding imidazolidines. This demonstrates that imidazolium ions are suitable hydride acceptors that can in principle mimic the uptake of a hydride ion by methenyl- H_4MPT^+ . Whether also the hydrogen splitting reaction performed by the [Fe] hydrogenase can be mimicked by imidazolium-based systems will be investigated in chapter 5.

3

The Chemistry of Amidines: Isomers and Silver Complexes

Abstract In the context of this project, a large variety of amidines as precursors for imidazolium and imidazolinium salts has been synthesized. Despite their relatively simple structures, these compounds exhibit surprisingly complex NMR spectra. A reason for this is the fact that amidines are able to adopt different isomeric or tautomeric forms which might also exist simultaneously in solution. In this chapter, the often complex mixtures of isomers are examined in more detail by means of X-ray diffraction and NMR spectroscopy. Some of the amidines synthesized in the course of this work are furthermore able to form dinuclear silver(I) complexes and hence provide an example for the applicability of amidines in classical coordination chemistry.

3.1 General Aspects of Amidines

Amidines are a well-known and extensively described class of compounds in literature with a first comprehensive review dating back to the 1940s.^[324] Since then, different aspects of their chemistry have been elucidated and even summarized in two books on this topic.^[346,347] As many amidines are biologically active, they often show antiviral, antifungal and antibacterial properties. Furthermore, some tranquilizing drugs and potential chemotherapeutics contain the amidine moiety.^[348,349] However, despite their constantly recurring presence in literature they still hold many surprises and mysteries since in most cases amidines feature a relatively complicated chemistry in solution. All of the synthesized compounds showed complex NMR spectra, which were found to be dependent on temperature, solvent, pH as well as on the concentration. In this section, a general overview over the different subclasses of amidines and their possibilities of isomerism and tautomerism is given. As the synthesized amidines are exclusively symmetrically *N,N'*-disubstituted amidines, the focus will be on this particular group of amidines.

3.1.1 Classification of Amidines

Amidines are the nitrogen analogues of carboxylic acids and esters, having both a C=N double bond and an amide-like C–N single bond (Figure 3.1). The possibility of protonation at the imino nitrogen atom makes the amidine a nitrogen base, which can be protonated to yield the symmetric amidinium cation. In very acidic media also a second protonation is possible, while in strong alkaline solutions deprotonation gives an anion (as long as at least one of the residues R^2 – R^4 is a proton).^[350] Charges can be delocalized and thus stabilized very efficiently by the N=C–N-unit.

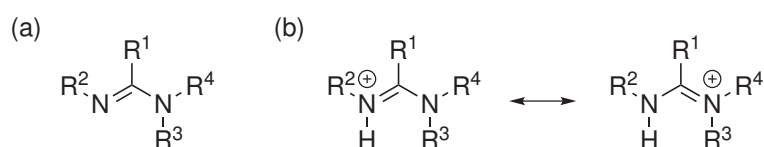


Figure 3.1. General chemical structures of amidines (a) and amidinium ions (b).

Depending on the number of substituents and the substitution pattern at the nitrogen atoms, amidines can be classified into five groups: unsubstituted ($R^2 = R^3 = R^4 = H$), monosubstituted (one of the residues R^2 or R^3 or $R^4 \neq H$), *N,N'*-disubstituted ($R^4 = H$), *N,N*-disubstituted ($R^2 = H$) and trisubstituted amidines (R^2 , R^3 and $R^4 \neq H$). The nature of substituent R^1 is irrelevant for this nomenclature, yet in the chemical literature often trivial names are used for amidines with different substituents R^1 . Accordingly, amidines with $R^1 = H$, Me or Ph are often called formamidines, acetamidines or benzamidines. Besides acyclic amidines, also cyclic amidines – with the N=C–N-unit partly or fully incorporated into a ring system – are known.

3.1.2 Isomerism in Amidines

All groups of amidines mentioned above exhibit configurational (*E/Z*) isomerism with respect to the C=N double bond. Furthermore, rotation about the C–N single bond leads to two different conformational isomers (*syn* or *anti*).^[350,351] In fact, rotational isomerism plays an important role for amidines as the C–N single bond has partial double bond character and consequently the rotational energy barriers are relatively high compared to other systems. Monosubstituted and *N,N'*-disubstituted amidines may additionally show tautomerism.^[350] The amidines synthesized in the course of this work are exclusively symmetric *N,N'*-disubstituted amidines and therefore the different types of isomerism will be further illustrated by using the example of this subclass of amidines. Figure 3.2 shows the isomers possible for amidines with the same substituents at both nitrogen atoms and the possibilities of interconversion *via* C=N isomerization (a), C–N rotation (b) or tautomerization (c). It is important to mention that for the *E/Z* and *syn/anti* nomenclature it is always presumed that substituent R¹ has a lower priority according to the Cahn-Ingold-Prelog sequence rules than the nitrogen substituent, which in fact is not necessarily true in every case.^[352]

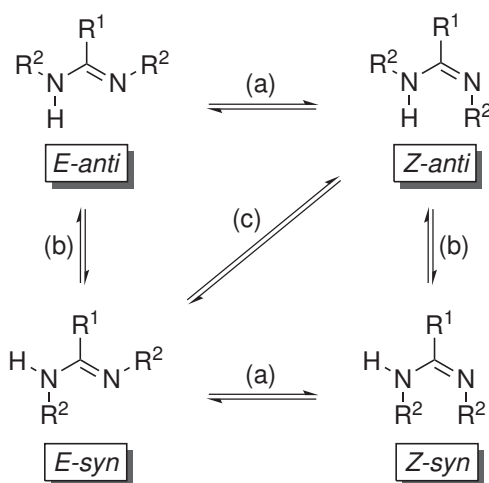


Figure 3.2. Possible isomeric forms of symmetric *N,N'*-disubstituted amidines which are linked by C=N isomerization (a), C–N rotation (b) or tautomerism (c).

In most amidines the *E* isomer is energetically favored over the *Z* isomer, however the type and number of substituents may change this very general trend by steric or electronic effects.^[350,352–356] According to this, the *Z* isomer for example is favored as the steric bulk of the substituent R¹ increases.^[357,358] Similarly, also the presence of rotational isomers depends on the substituents, but solvent effects have to be considered as well.^[359]

Mechanisms of Isomerization in Amidines

As already briefly mentioned, isomerization in amidines may occur *via* rotation about the C=N double bond or by C–N rotation (possibilities (a) and (b) in Figure 3.2). However, the activation energy for rotation about the C=N double bond is generally estimated to be too high to occur at room temperature and hence no equilibrium of *E* and *Z* isomers should be operative in amidines.^[360,361] Reliable experimental data on this topic are only scarcely available, but in specific cases the barrier to rotation might be lowered due to bond delocalization in the amidine moiety and an associated weakening of the C=N double bond.^[352] It has been proposed that C–N rotation might also be catalyzed by acids which are able to protonate the imino nitrogen atom and hence also weaken the C=N double bond.^[362] An alternative mechanism for C=N isomerization is inversion at the doubly bonded nitrogen atom involving a linear transition state. For some trisubstituted amidines this has been postulated and an activation energy of 105 to 109 kJ mol⁻¹ has been determined.^[352]

On the contrary, rotation about the C–N single bond is usually fast and in most cases reduced temperatures have to be applied to study this rotation. Experimentally determined rotational barriers about the C–N bond normally lie in the range of 50 – 80 kJ mol⁻¹.^[352,359,363–366] In some cases this barrier is lowered due to steric bulk of the substituents, which causes a destabilization of the planar ground state and thus facilitates C–N rotation.^[352]

A third possibility of isomerization in amidines is tautomerism, which describes the transfer of a proton from the amino to the imino nitrogen atom (possibility (c) in Figure 3.2). According to this, the *E-syn* and *Z-anti* isomers depicted in Figure 3.2 are linked by tautomerism, whereas transfer of the proton from one nitrogen atom to the other for the *E-anti* and *Z-syn* isomers would yield the respective identical structures. For many years, tautomerism – especially of amidines with different substituents at the nitrogen atoms – was (and still is) a controversially discussed issue in the scientific world.^[367] However, the different views on the identities of the predominant forms of amidines and their interconversion processes in solution soon met with the general conclusion that in most cases an equilibrium of different isomers exists and that tautomerism has to be considered.^[360] Investigations on the tautomerism of formamidines by Limbach *et al.* for example showed that both *E-syn* and *E-anti* isomers exist in solution, but only the *E-anti* isomer was involved in a fast tautomeric process which was promoted by the formation of a cyclic dimer.^[356,368] Further examples for the significance of tautomerism in amidines exist, but its actual manifestation is diverse and often discussed controversially.^[356,369–372] Prototropic tautomerism is a very fast reaction and might be facilitated by intermolecular hydrogen bonding.^[367]

For symmetrically *N,N'*-disubstituted amidines essentially two general ideas about the interconversion processes in solution exist: In particular because of the general estimation that *E/Z* isomerization is very unlikely to occur at room temperature, the opinion that only rotational isomerism with respect to the C–N single bond has to be the main

isomerization process, was widely accepted and various IR measurements seemed to support this hypothesis.^[361,373] On the other hand, Prevoršek *et al.* very early suggested – after analysis of extensive IR measurements – that tautomerism in symmetrically *N,N'*-disubstituted amidines could lead to configurational (*E/Z*) and conformational (*syn/anti*) isomerism at the same time in the case that *E-syn* and *Z-anti* isomers are involved in the equilibrium.^[374] Later, NMR measurements by Krechl *et al.* confirmed the presence of *E-syn* and *Z-anti* tautomers in very diluted CDCl₃ solutions of *N,N'*-diphenylacetamidine and also the formation of dimers in concentrated solutions as well as in the solid state was suggested.^[375] The question whether rotational isomerism or tautomerism (or a combination of both mechanisms) is responsible for the often complicated situation found in solution of *N,N'*-disubstituted amidines cannot be answered ultimately and has to be investigated in every specific case. Considering the diverse and sometimes even confusing influences on the possibilities of isomerization in amidines, the situation of the synthesized amidines is examined more thoroughly in the following chapters 3.2 and 3.3.

3.1.3 Molecular Association

Apart from the different kinds of isomerism mentioned in the last section, also intermolecular interactions might complicate the evaluation of NMR spectra of amidines. As soon as there is at least one proton bound to a nitrogen atom, amidines are able to form dimers or polymers *via* intermolecular hydrogen bonding networks.^[349,350,361,376] The extent to which this happens mostly depends on the nature of the substituents and the substitution pattern, temperature, concentration and the solvent.^[359,361,362] In apolar solvents the formation of intermolecular aggregates is more likely than in polar solvents, where amidine...solvent interactions are favored.^[360] For some amidines, interactions with chloroform have been reported.^[362] In Figure 3.3 the possibilities of intermolecular interactions – cyclic or linear aggregation – are illustrated for symmetrically *N,N'*-disubstituted amidines. Linear dimers or polymers are possible for all isomers, whereas a cyclic dimer can only be realized for the *E-anti* isomer.

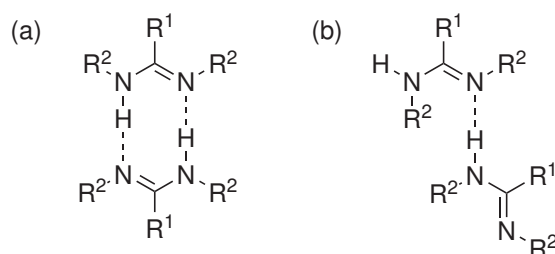


Figure 3.3. Cyclic dimer (a) and an example for a linear association (b) formed by amidines.

The molecular association of amidines with carboxylic acids has been studied several times.^[349,375–378] In the reported cases, formation of dimeric associates comprising

exclusively the *E-anti* isomer in a cyclic complex with the carboxylic acid has been observed.

3.2 Structural Parameters of Amidines

In order to set a starting point for the examination of the isomeric composition of amidines in solution, this section will focus on the solid state structures of amidines obtained by X-ray crystallography which has been used several times in literature to characterize amidines.^[350,355,379] In the course of the preparation of amidines as precursors for imidazolium and imidazolinium ions, crystals suitable for X-ray crystallography of several amidines were obtained either by recrystallization from mixtures of ethanol and water or by slow evaporation of chloroform or dichloromethane solutions of the respective amidines. All in all seven different amidine solid state structures could be determined by means of X-ray crystallography and all of them showed molecular association supported by hydrogen bonds. In almost all cases hydrogen-bonded dimers are present in the crystal structure (Figure 3.4), and only in the case of **TolTolAm** the formation of a linear polymer was observed (Figure 3.5). As becomes clear from the molecular structures, not all of the possible isomers mentioned in Figure 3.2 are actually present in the solid state. The *E-anti* isomer for example seems to be energetically unfavored as it is not present in any of the structures. Also the *Z-syn* isomer was found only for **TolFam**. The *E-syn* isomer on the contrary seems to be energetically favorable as all of the amidines adopt this conformation.

Different structural parameters can be used in order to compare the solid state structures of amidines. According to Häfelinger and Kuske^[350] a valuable parameter is the difference of CN bond distances $\Delta_{\text{CN}} = d(\text{C}-\text{N}) - d(\text{C}=\text{N})$, which is a direct measure of conjugation and is equal to zero in a fully conjugated system due to bond equalization. In a system with Δ_{CN} significantly distinct from zero, conjugation may be hampered because of electronic or steric reasons. Table 3.1 shows Δ_{CN} for the obtained molecular structures, the C–N and C=N bond length $d(\text{C}-\text{N})$ and $d(\text{C}=\text{N})$, the N–C=N bond angle as well as the isomer(s) present in the crystal structure for each of the amidines crystallized. All in all, the C–N bond lengths vary from 1.32 – 1.38 Å, the C=N bond lengths from 1.28 – 1.32 Å and the N–C=N bond angles from 118 – 128°. For such a small group of structurally very similar amidines this might be regarded as a relatively large variability of structural parameters. It is important to notice that for **C₆F₅MesAm**, **PhMesAm**, and **MesFam** it was not possible to differentiate between *Z-anti* and *E-syn* isomer and therefore only one set of bond length and bond angle is given for each amidine. A reason for this is that in these cases the isomers are substantially disordered in the crystal lattice and hence only averaged values can be determined, an observation that has been made before for related systems.^[355] Hence the fact that Δ_{CN} is very close to zero does not necessarily mean that those amidines exhibit a large degree of

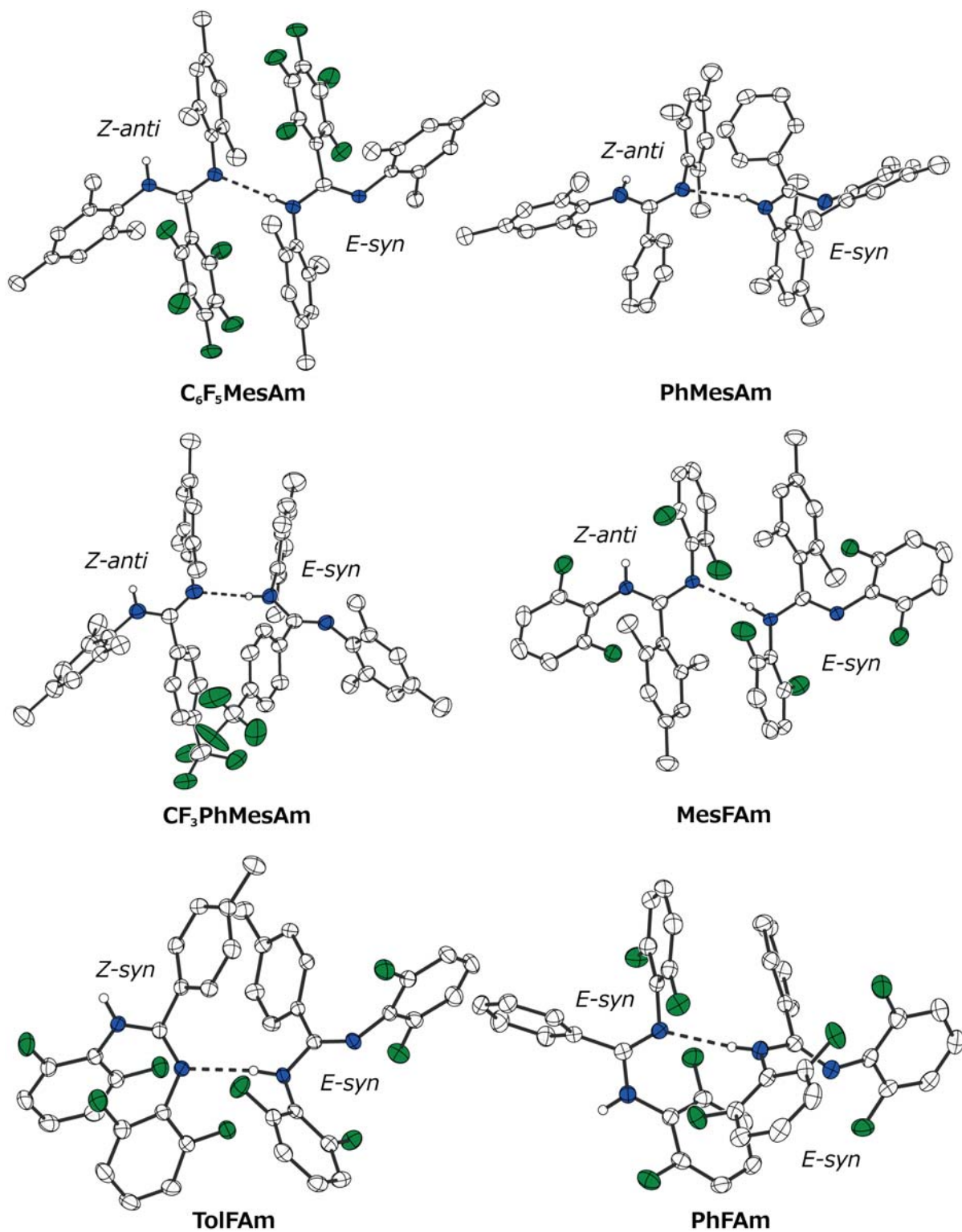


Figure 3.4. Thermal displacement ellipsoids (shown at 50 % probability) of molecular structures of different amidines illustrating the dimer formation in the solid state. Hydrogen atoms except for hydrogen atoms involved in hydrogen bonding (ball-and-stick representation with fixed radii of 0.135 Å) are omitted for reasons of clarity.

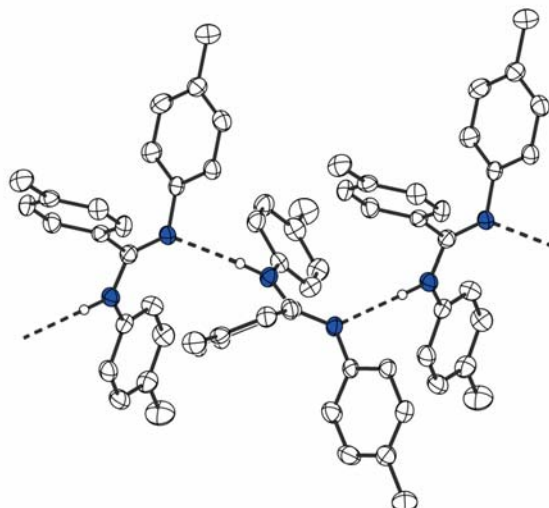


Figure 3.5. Thermal displacement ellipsoids (shown at 50 % probability) of the solid state structure of a linear polymer of amidine **TolTolAm**. Hydrogen atoms except for hydrogen atoms involved in hydrogen bonding (ball-and-stick representation with fixed radii of 0.135 Å) are omitted for reasons of clarity.

conjugation. In these particular cases, small Δ_{CN} values are rather a consequence of the structural conditions in the crystal lattice.

For **CF₃PhMesAm**, **TolFam**, and **PhFam** it was possible to measure the parameters for both individual amidines of the dimer as they were not significantly disordered. In the solid state, **CF₃PhMesAm** exists as both *Z-anti* and *E-syn* isomers, **TolFam** as pair of *Z-syn* and *E-syn* isomers and **PhFam** exclusively as *E-syn* isomer, while one could even discriminate hydrogen-bond-accepting and -donating amidine.

The **PhFam** isomer accepting the hydrogen bond has a longer C=N bond and a shorter C–N bond, hence the delocalization is more pronounced and Δ_{CN} is smaller. The hy-

Table 3.1: Structural parameters of the amidines. Hydrogen bond acceptors (acc.) and donors (don.) are marked where distinct bond length were determined. (*) Δ_{CN} of these amidines may be blurred by disorder in the crystal.

amidine	isomer(s)	d(C–N)/Å	d(C=N)/Å	$\angle(\text{N–C=N})$	$\Delta_{\text{CN}}/\text{Å}$
C₆F₅MesAm	<i>Z-anti, E-syn</i>	1.324(2)	1.317(2)	124.5(1)°	0.008(3)*
PhMesAm	<i>Z-anti, E-syn</i>	1.330(2)	1.329(2)	120.8(2)°	0.001(4)*
CF₃PhMesAm	<i>Z-anti</i> (acc.)	1.351(3)	1.292(3)	126.0(2)°	0.059(6)
	<i>E-syn</i> (don.)	1.360(3)	1.282(3)	121.1(2)°	0.078(6)
MesFam	<i>Z-anti, E-syn</i>	1.338(3)	1.322(4)	121.3(3)°	0.016(7)*
TolFam	<i>Z-syn</i> (acc.)	1.374(2)	1.293(2)	128.3(1)°	0.082(3)
	<i>E-syn</i> (don.)	1.368(2)	1.289(2)	118.2(1)°	0.079(3)
PhFam	<i>E-syn</i> (acc.)	1.360(2)	1.291(2)	120.0(1)°	0.069(4)
	<i>E-syn</i> (don.)	1.379(2)	1.285(2)	119.7(1)°	0.094(4)
TolTolAm	<i>E-syn</i>	1.363(2)	1.297(2)	122.1(2)°	0.066(4)

drogen bond-donating amidine on the other hand has the largest Δ_{CN} value of all investigated amidines. As the only amidine, **TolFAm** is also present in its *Z-syn* isomer. This isomer has the largest N–C=N bond angle of all isomers, presumably because of steric interactions between the aromatic rings. The smallest N–C=N bond angle can be found in the *E-syn* isomer of **TolFAm**, this possibly being a result of packing forces operative in the crystal lattice. In contrast to all the other amidines mentioned before, **TolTolAm** only exists as a single isomer – namely the *E-syn* isomer – forming not a dimeric aggregate, but a linear polymer in the solid state. Whether this is a consequence of steric and/or electronic effects cannot be judged from the available data.

3.3 The Chemistry of Amidines in Solution

The chemistry of amidines in solution is often characterized by a complex behavior with respect to the presence of different isomers or aggregates, which is not necessarily identical to the situation found in the solid state. Consequently, the crystal structures analyzed in chapter 3.2 have only limited significance for the respective dissolved amidines. Historically, this problem was addressed by means of IR spectroscopy^[360,380] which turned out to be a powerful tool to investigate molecular association of amidines in solution by hydrogen bonding, and tautomerism particularly of monosubstituted amidines. In some specific cases IR spectra might also provide indirect evidence concerning the configuration of the double bond.^[362] However, IR spectroscopy in most cases only gave contradictory estimations on the identities of the observed isomers and failed completely in assigning different rotamers. In hand with its evolution to a routine analytical method and the development of advanced 2D measurements, NMR spectroscopy also shed some new light on the chemistry of amidines in solution. Extensive analysis of ^1H and ^{13}C NMR data on amidines enabled the derivation of additivity parameters for the calculation of chemical shifts.^[354,362] Subsequently, also elaborate 2D NMR measurements were used in order to identify the isomers of amidines and amidinium ions present in solution.^[357,381,382] Therefore, this section will focus on NMR spectroscopy in order to investigate the synthesized amidines. Amidines **C₆F₅MesAm**, **CF₃PhMesAm**, **TolFAm**, and **TolTolAm** will serve as examples for the very diverse behavior of amidines in solution.

3.3.1 Temperature and Concentration Dependencies

C₆F₅MesAm Amidines in solution often show temperature as well as concentration dependence, as frequently equilibria between different isomers or aggregation phenomena exist. Not surprisingly, also amidine **C₆F₅MesAm** exhibits temperature-dependent NMR spectra in CDCl₃ solution as shown in Figure 3.6.

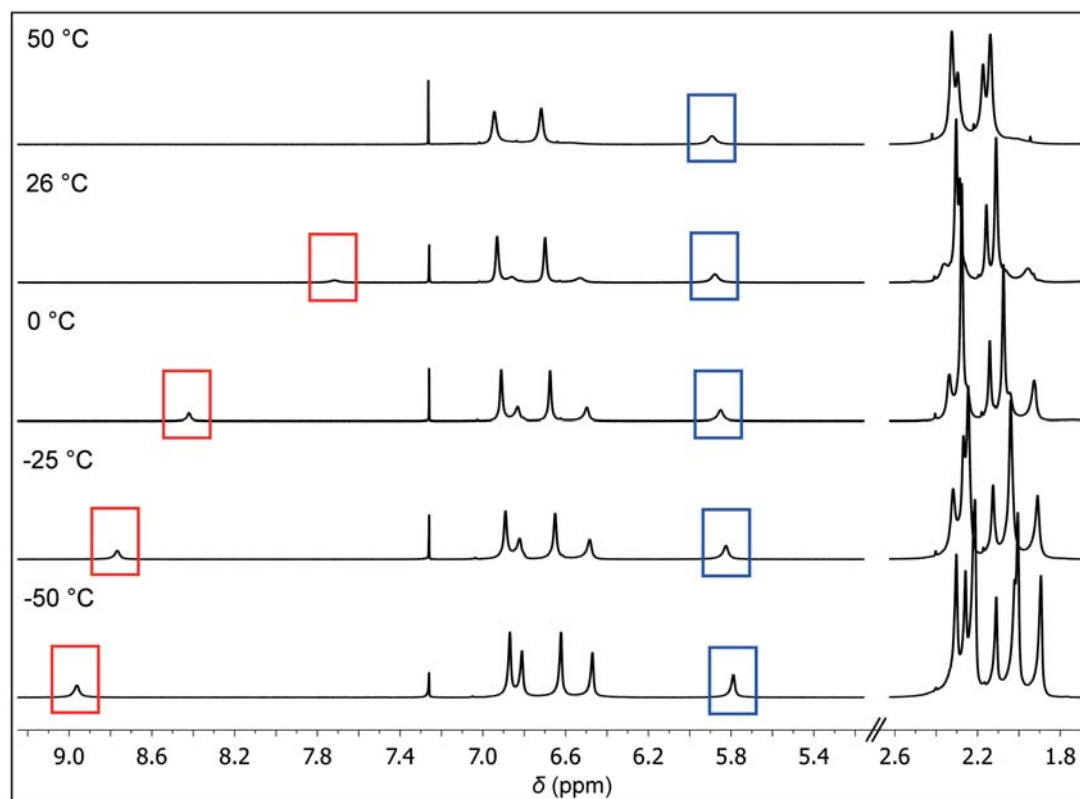


Figure 3.6. NMR spectra of **C₆F₅MesAm** in CDCl₃ at 50, 26, 0, –25, and –50 °C (top to bottom). The NH protons of the major and minor isomer are marked with a blue and a red box, respectively.

At high temperatures (50 °C) only one set of signals is present with a chemical shift for the NH proton of 5.9 ppm. Upon cooling of the solution down to –50 °C, a second set of signals occurs which also increases in intensity from a ratio of 1:0.3 (26 °C) over 1:0.4 (0 °C) and 1:0.6 (–25 °C) to 1:0.7 (–50 °C) as the temperature drops. It is interesting to note that the chemical shift for the NH proton of the growing species gradually shifts over a large range from 7.7 to 9.0 ppm whereas the chemical shift of the other NH proton remains more or less constant (only a small shift from 5.9 to 5.8 ppm can be observed). In principle this behavior is also found for solutions of different concentrations of **C₆F₅MesAm** in CDCl₃. Starting with a very dilute solution (0.03 M) and a ratio of 1:0.2, the ratio grows in favor of the second species, finally reaching an amount of 1:0.5 at a 0.20 M concentration. Simultaneously, also the chemical shift for the NH proton of the second species shifts from 7.2 to 8.2 ppm. Especially the strong concentration dependence and the rather large shifting of the NH proton are indicative of a molecular

association phenomenon. In which way this might be connected to different isomers in solution will be discussed in section 3.3.2.

From the temperature dependence of the ratio of the two isomers A and B, the thermodynamic parameters of the isomerization reaction $A \rightleftharpoons B$ can be obtained. According to the equation

$$\ln K_{\text{eq}} = -\frac{\Delta H^\circ}{RT} + \frac{\Delta S^\circ}{R} \quad \text{with the equilibrium constant } K_{\text{eq}} = \frac{[B]_{\text{eq}}}{[A]_{\text{eq}}} \quad (3.1)$$

a plot of $\ln K_{\text{eq}}$ vs. $1/T$ allows for a determination of both the standard enthalpy ΔH° and the standard entropy ΔS° of the reaction. For amidine **C₆F₅MesAm**, this plot is shown in Figure 3.7. From the slope of the linear fit, a ΔH° value of $6.4 \pm 0.9 \text{ kJ mol}^{-1}$ was calculated while the slope gave a standard entropy ΔS° of $31 \pm 4 \text{ J K}^{-1} \text{ mol}^{-1}$.

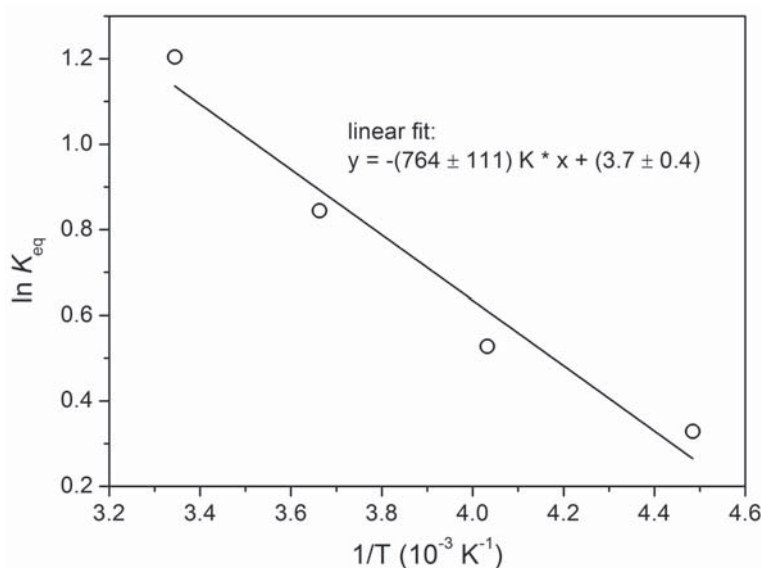


Figure 3.7. Linear fit of the $\ln K_{\text{eq}}$ vs. $1/T$ plot of amidine **C₆F₅MesAm**.

CF₃PhMesAm The NMR spectra of **CF₃PhMesAm** in CDCl_3 were difficult to examine in terms of different isomers because already at room temperature only one species prevailed in solution. The second isomer was difficult to characterize spectroscopically as its signal intensity was very low. The ratio between the two isomers did not exceed 1:0.1 over the whole temperature range. However, upon changing the solvent from CDCl_3 to CD_2Cl_2 the ratio was completely shifted. Now two clearly distinguishable isomers were observed which were present in a ratio of 1:0.4 at room temperature (Figure 3.8). In sharp contrast to amidine **C₆F₅MesAm** however, this ratio was not significantly altered upon cooling of the solution to a temperature as low as -90°C where the isomers still showed a ratio of 1:0.5. As seen before for **C₆F₅MesAm**, a temperature-dependent shifting of the signals was recognized.

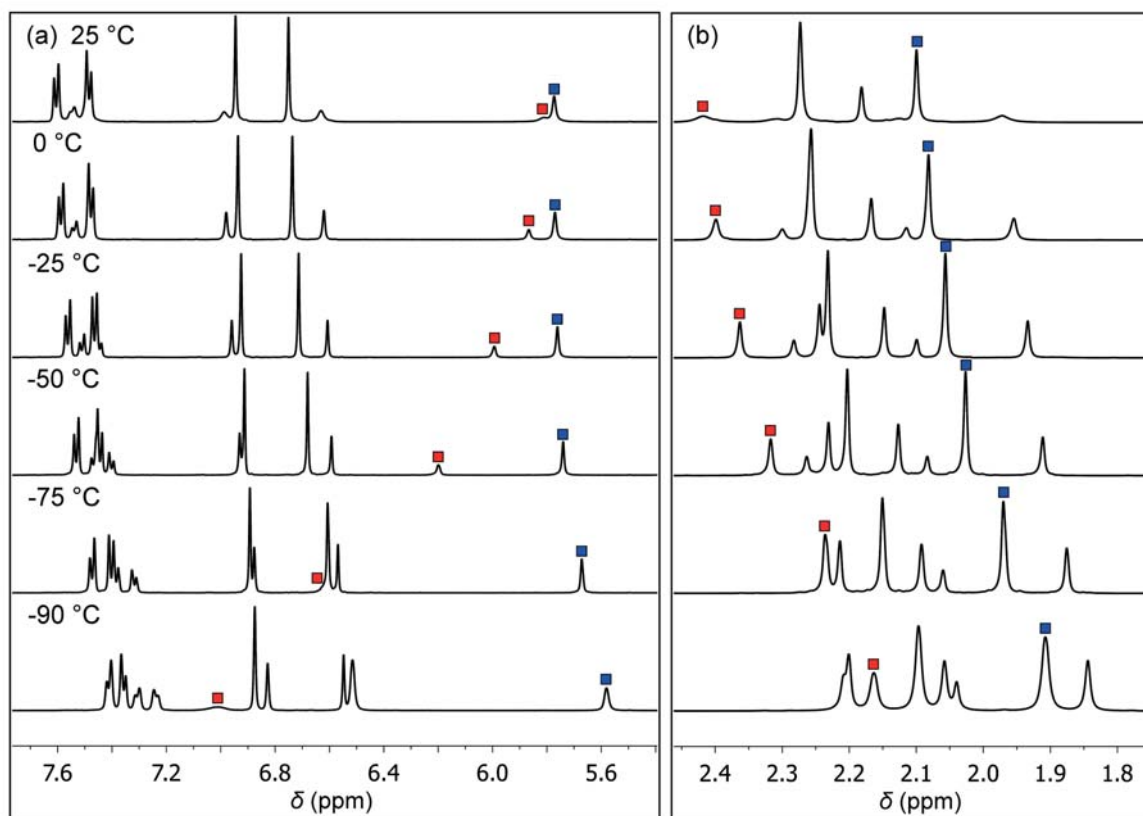


Figure 3.8. NMR spectra of $\text{CF}_3\text{PhMesAm}$ in CD_2Cl_2 at 25, 0, -25, -50, -75, and -90 °C (top to bottom) in (a) the aromatic and (b) the methyl region. In (a) the NH protons and in (b) the *o*-NHMe-CH₃ protons of the major (blue) and the minor isomer (red) are highlighted.

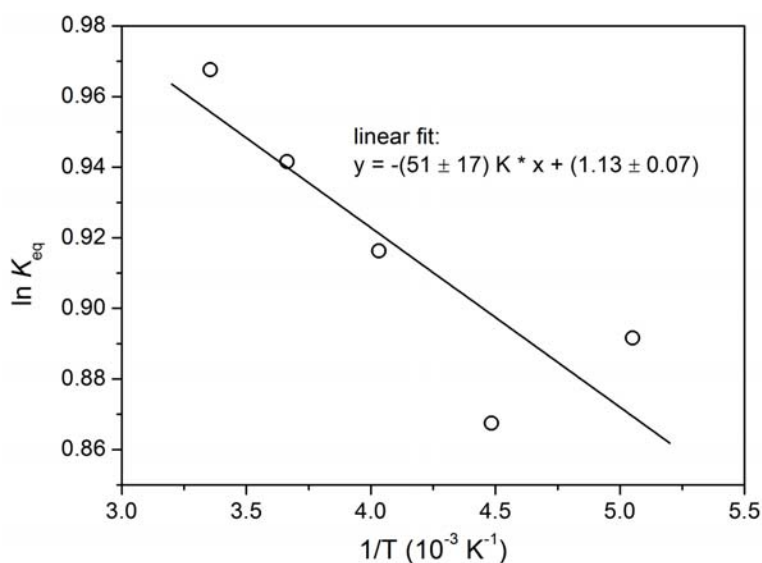


Figure 3.9. Linear fit of the $\ln K_{\text{eq}}$ vs. $1/T$ plot of amidine $\text{CF}_3\text{PhMesAm}$.

The NMR spectra from 0.03 to 0.20 M concentrations in CD_2Cl_2 reinforce the picture obtained from the NMR spectra at variable temperatures. Also in this case a ratio of 1:0.4 remains rather constant, hence **CF₃PhMesAm** shows almost no temperature or concentration dependence with respect to the ratio of both isomers present in solution. However, the chemical shifts of the signals depend on temperature and concentration. At low temperatures the concentration dependence is even more pronounced. As for amidine **C₆F₅MesAm**, also for **CF₃PhMesAm** the thermodynamic parameters of the isomerization reaction were calculated using equation 3.1. The linear fit of the $\ln K_{\text{eq}}$ vs. $1/T$ plot shown in Figure 3.9 gave a standard enthalpy ΔH° of $0.4 \pm 0.1 \text{ kJ mol}^{-1}$ and a standard entropy ΔS° of $9.4 \pm 0.6 \text{ J K}^{-1} \text{ mol}^{-1}$. ΔH° is very close to zero since the ratio of the two isomers does not change significantly over the examined temperature range.

TolFAm Similar to the NMR spectra at variable temperatures of **CF₃PhMesAm**, also the NMR spectra of **TolFAm** in CDCl_3 show a constant ratio of two isomers (1:0.4) as well as a shifting of the signals at different temperatures. In contrast to **CF₃PhMesAm** however, the NH protons of both isomers shift to lower field. Surprisingly, the shift for the major isomer is more apparent than the one for the minor isomer, hence an obvious difference to the previously examined amidines exists.

The spectra at different concentrations from 0.03 to 0.20 M solutions feature a constant ratio of 1:0.4 of the two isomers. Furthermore, no clearly visible shift of the signals can be noticed as the concentration rises. From these observations concerning temperature and concentration it is already clear that one has to deal with a different situation in solution than in the cases of the previously mentioned amidines.

Like in the case of amidine **CF₃PhMesAm**, ΔH° is expected to be relatively close to zero since the ratio of the two isomers remains rather constant when changing the

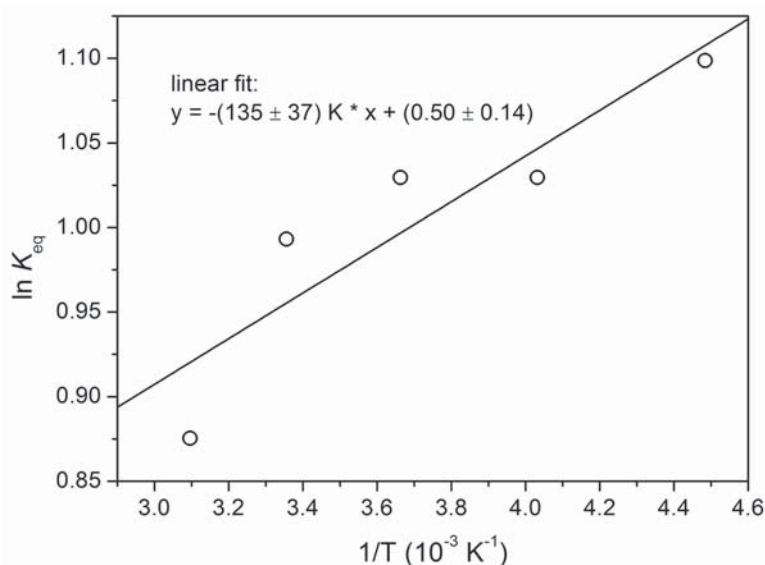


Figure 3.10. Linear fit of the $\ln K_{\text{eq}}$ vs. $1/T$ plot of amidine **TolFAm**.

temperature. Indeed, the thermodynamic parameters obtained from the linear fit of the $\ln K_{\text{eq}}$ vs. $1/T$ plot (Figure 3.10) gave a standard enthalpy ΔH° of $-1.1 \pm 0.3 \text{ kJ mol}^{-1}$. The calculated standard entropy ΔS° was $4 \pm 1 \text{ J K}^{-1} \text{ mol}^{-1}$.

TolTolAm The NMR spectrum of **TolTolAm** in CD_2Cl_2 turned out to be marked by relatively broad signals, indicative of a fast exchange of different species at room temperature. Even at very low temperatures (-90°C) the signals – in particular those of the minor isomer – narrow only slightly. Furthermore, the ratio of both isomers is only 1:0.2 which hampers a detailed analysis, especially as the signals of the minor isomer are partly obscured by signals of the major isomer. This situation improves when changing the solvent to CDCl_3 . At high temperatures the signals are still broad, but at low temperatures they become sharp and a second set of signals becomes visible (Figure 3.11). In contrast to the amidines mentioned above, no major shifting of the signals is observed as the temperature decreases. The ratio of isomers is nearly 1:1 at -50°C .

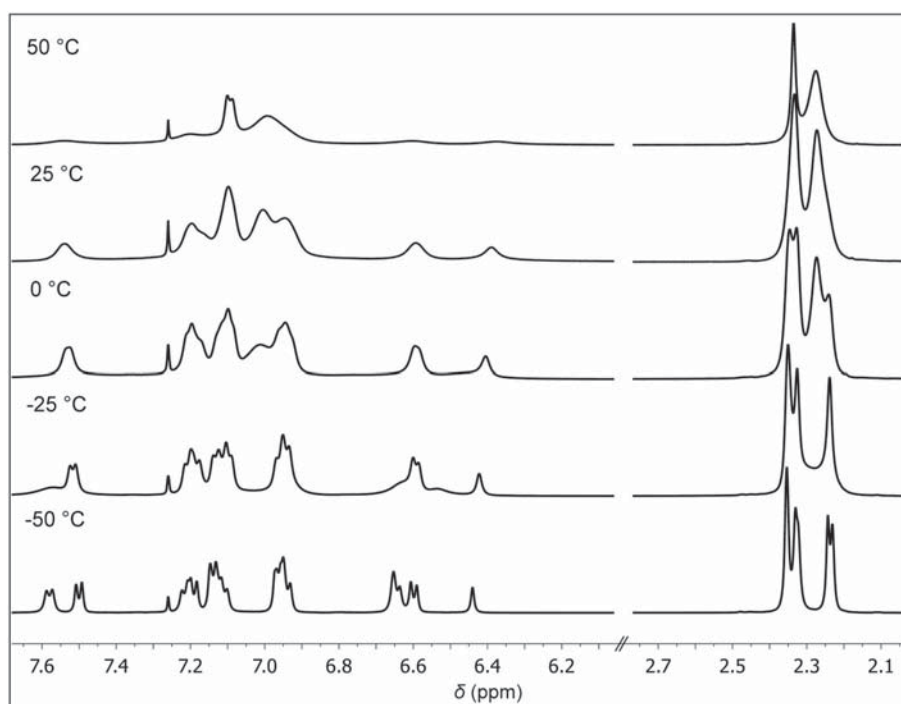


Figure 3.11. NMR spectra of **TolTolAm** in CDCl_3 at 50, 25, 0, -25 , and -50°C (top to bottom). Upon cooling the sample, the signals narrow and a second set of signals occurs.

A rather complex picture is conveyed by the NMR spectra recorded at different concentrations (Figure 3.12). Surprisingly, the spectrum of the very diluted 0.03 M **TolTolAm** solution shows at first glance only one species displaying relatively sharp signals when comparing it to the spectrum at -50°C in Figure 3.11. However, a closer look on the intensities of the signals reveals that also in the very diluted solution a second set of signals is present which features relatively broad signals. The sharp signals of the

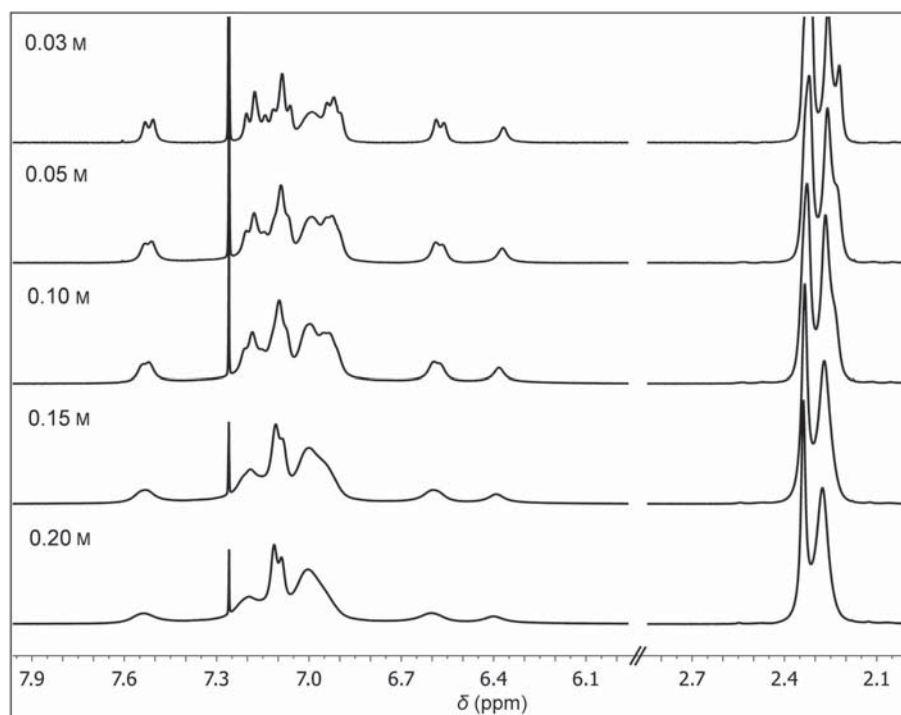


Figure 3.12. NMR spectra of TolTolAm in CDCl₃ (25 °C) at 0.03, 0.05, 0.10, 0.15 and 0.20 M concentrations (top to bottom). The signals broaden upon increasing the concentration.

first species observed in the 0.03 M solution broaden upon further increasing the concentration. This behavior points towards a molecular association phenomenon which probably also promotes the interconversion of the two isomers. At very low concentrations both isomers presumably exist more or less separated from one another in solution. Increasing the concentration then results in a rising rate of interconversion as the molecular association is favored and a broadening of signals is observed. Cooling down the solution leads to a freezing of the conversion process and hence both isomers can be observed. The importance of a properly purified NMR solvent is highlighted by a second series of concentration-dependent measurements which showed only one species featuring broad signals, irrespective of the adjusted concentration. A comparison of these spectra with the spectrum of the 0.03 M solution in Figure 3.12 is depicted in Figure 3.13. The differing appearance of the spectra points to an interference of traces of acid (or base) being present in the solution with the isomerization processes between different isomers of the amidine. Consequently, special precautions – such as stirring the NMR solvent over NaHCO₃ prior to use – were taken to avoid the interfering acid-base chemistry. An identification of the isomers involved in the processes described here follows in the next section 3.3.2.

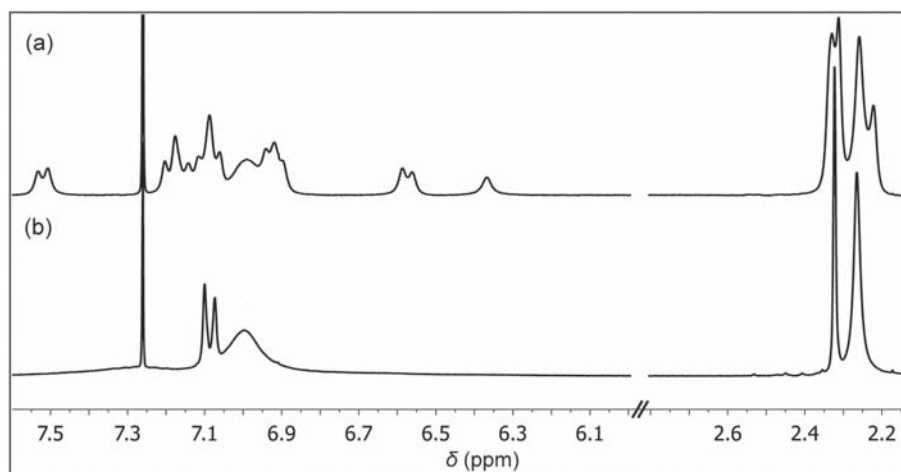


Figure 3.13. Comparison of different room temperature NMR spectra of **TolTolAm** in CDCl_3 at 0.03 M concentrations. In (b) the NMR solvent was presumably contaminated with traces of acid leading to a fast exchange of the isomers and an associated broadening of signals.

3.3.2 Identification of Isomers

As already mentioned, a powerful tool for the investigation of configuration and rotational isomerism of amidines in solution is NMR spectroscopy.^[362] This is why at this point, the results obtained by means of NOESY NMR spectroscopy will be presented which were conducted in the hope of clarifying the complex situation found in solution. In this context, the **Nuclear Overhauser Enhancement Spectroscopy** (NOESY) experiment turned out to be particularly useful as with this method spatially adjacent protons can be correlated (up to a distance of 5 – 6 Å) by looking at the dipolar relaxation between two spins through space. The cross relaxation rate is distance-related and drops with $1/r^6$.^[383] Furthermore, also exchanging protons show cross peaks in the NOESY NMR spectrum due to transfer of longitudinal magnetization, which permits a determination of exchange rates in the case of interconverting isomers (see Experimental Section 6 for details). When looking at exchange rather than NOE, the NOESY experiment is also called two-dimensional exchange spectroscopy (EXSY).^[384]

C₆F₅MesAm The NMR measurements of compound **C₆F₅MesAm** revealed a strong temperature- and concentration-dependent isomeric ratio. The fraction of the minor isomer increases as the temperature drops and as the concentration increases. In view of the fact that in the solid state a mixture of *E-syn* and *Z-anti* isomers forming a dimeric aggregate with substantial delocalization is present, it can be suggested that also in solution an equilibrium of those isomers exists. In order to prove this assumption, NOESY spectra at different temperatures were recorded. At room temperature in principle two dynamic exchange processes hampered the monitoring of the anticipated NOE signals. On the one hand, a very fast interconversion of both isomers was detected, and on

the other hand also a relatively fast interconversion between the NH- and N-aromatic rings of each isomer was present. At $-30\text{ }^{\circ}\text{C}$ the exchange of both aromatic rings within a single isomer was no longer present, but the interconversion of both isomers continued. A good evidence for this is the fact that both NH protons are still connected by cross peaks whereas the signals for the mesityl groups within a single isomer are not. At $-40\text{ }^{\circ}\text{C}$ the situation remains nearly the same, but at $-50\text{ }^{\circ}\text{C}$ – the lowest temperature possible in the applied solvent CDCl_3 – the exchange signals for the NH protons ($k_{\text{ex}} = 0.06\text{ s}^{-1}$) have almost vanished, hence at this temperature an interconversion of the two isomers does not seem to occur any longer on the NMR time scale. Instead, NOE signals which might hint at spatial proximity to the NH protons can be observed (Figure 3.14 (a)). Careful evaluation of these NOE signals not only makes an assignment of the involved isomers possible, but also suggests a formation of dimeric aggregates in solution. According to the obtained NMR data, the major isomer can be assigned to the structure of the *Z-anti* isomer and the minor isomer to the structure of the *E-syn* isomer, respectively. The hypothesis of a formation of a dimeric aggregate is supported by the fact that a NOE signal connects the NH proton of the *E-syn* isomer to the *ortho*-methyl group of the *Z-anti* isomer's N-mesityl moiety. Indeed, molecular association could also explain the extraordinary temperature and concentration dependence of the chemical shift of the *E-syn* isomer. Lowering the temperature or increasing the concentration of the amidine leads to an enhanced formation of dimeric aggregates which in turn results in an increased deshielding of the NH proton of the *E-syn* isomer. The fact that at high temperatures ($50\text{ }^{\circ}\text{C}$) only the *Z* isomer is present whereas the amount of *E* isomer increases upon lowering the temperature and/or increasing the concentration, indicates a possible stabilization of the *E-syn* isomer in the equilibrium by this molecular association. Furthermore, the structure of the dimer depicted in Figure 3.14 (a) could explain the similar chemical shifts of the *Z-anti* N- and the *E-syn* NH-mesityl protons since both aromatic rings are located in the center of the dimer. Similarly, the *Z-anti* NHMes and *E-syn* NMes aromatic rings are both "outer" arenes and are characterized by a resembling chemical environment.

However, even though the interconversion process seems to have almost entirely ceased at $-50\text{ }^{\circ}\text{C}$, when looking at the NH protons, still cross peaks connecting for example the aromatic NHMes protons of one isomer to the NMes protons of the other isomer are visible (Figure 3.14 (b), $k_{\text{ex}} = 4.45\text{ s}^{-1}$). Interestingly, the interconversion takes place in such a way that protons of the NH-aromatic ring of one isomer convert into protons of the N-aromatic ring of the other isomer and *vice versa*. Thus the isomerization reaction seems to be linked to a transfer of protons, meaning a tautomerization reaction. In this case, obviously different mechanisms exist, involving either (a) isolated isomers or (b) the transfer of protons within a molecular aggregate (Scheme 3.1). If the tautomerization reaction would only take place between the amidine and an external base/acid, the *E-syn* isomer would readily be converted into the *Z-anti* isomer and *vice versa*, and the NH protons of both isomers would show the same exchange as all other protons of the compound. The part of the external base accepting the proton and the part of

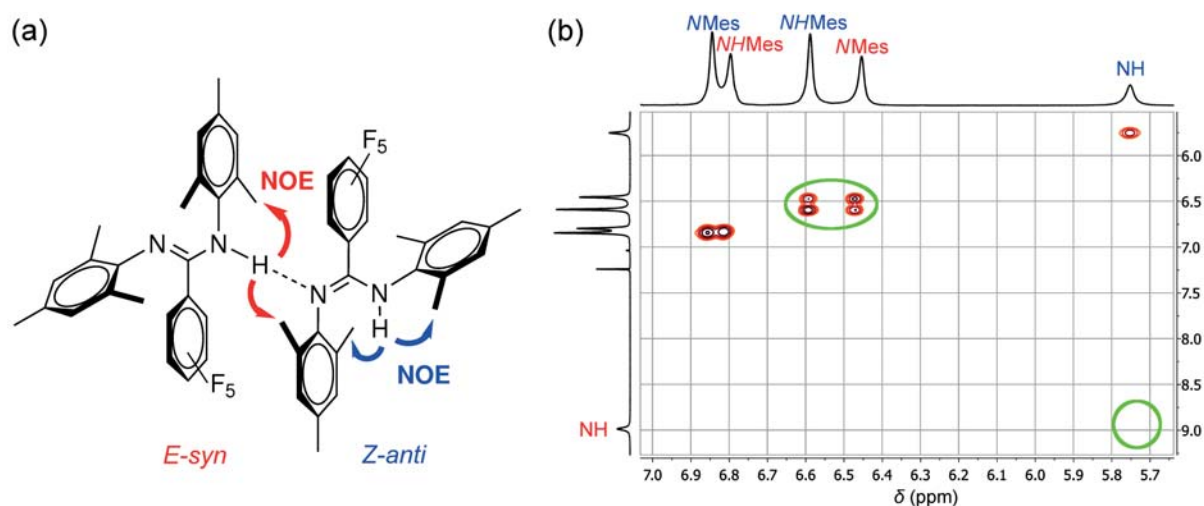
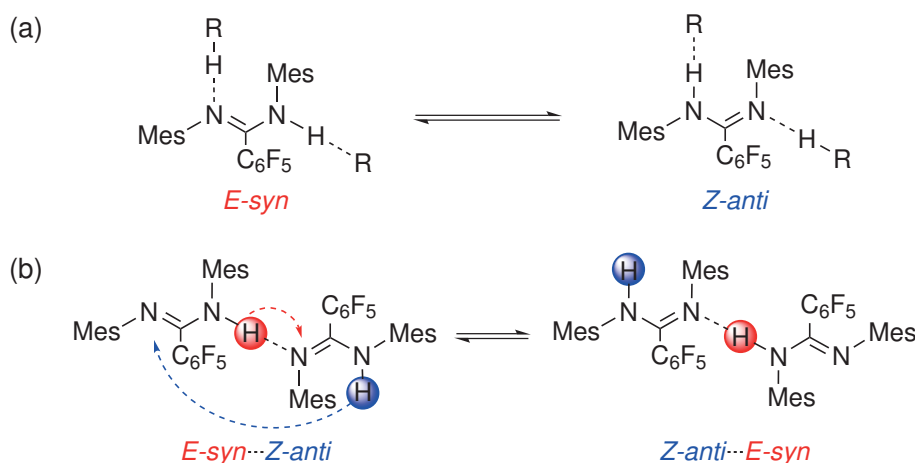


Figure 3.14. (a) NOE signals observed for amidine C_6F_5MesAm in $CDCl_3$ at $-50^\circ C$ and resulting assignment of *E-syn* and *Z-anti* isomers. (b) Low field region of the NOESY NMR spectrum ($CDCl_3$, $-50^\circ C$) indicating that the exchange of the NH protons apparently has already stopped but the exchange process between the *NHMe* and *NMe* protons still persists (exemplary evidence for this marked with green circles). Signals of the *E-syn* isomer are marked in red, those of the *Z-anti* isomer in blue.



Scheme 3.1. Possible mechanisms for the observed tautomerism in solutions of amidine C_6F_5MesAm involving isolated isomers (a) or a dimer of *E-syn* and *Z-anti* isomers (b). In (a) the external base and acid are referred to as R and RH , respectively

the external acid delivering the proton to the respective isomer in such a tautomerization reaction might be performed by other amidines or residual amounts of water or acid being present in the NMR solvent and hence could be concentration dependent (in the case of an involvement of other amidines) or independent of the amidine concentration. As becomes clear from the NOESY NMR measurements, this mechanism might be operative for amidine C_6F_5MesAm at $-40^\circ C$ and above, but at $-50^\circ C$ an

exchange between the NH protons is not observed any longer while the interconversion of protons of the NH-aromatic rings of one isomer into protons of the N-aromatic rings of the other isomer still persists. A possible explanation for this rather strange behavior is that such an exchange reaction takes place within a dimeric aggregate. In such a tautomerization reaction, for example the NH proton of the *E-syn* isomer gets transferred to the *Z-anti* isomer which thereby gets transformed into the *E-syn* isomer again (after deprotonation at the second nitrogen atom, possibly by a second dimer). Hence no exchange between the different NH protons takes place and consequently no exchange peaks between them would occur in the NOESY spectrum. The chemical environments of the NH protons of both isomers would not change, but in contrast to this the aromatic rings are variably influenced depending on the presence or absence of a proton at the nearby nitrogen atom. At this point, no statement on the actual stability or dynamic nature of the dimer can be made. On the one hand a static dimer in solution is hard to imagine, especially as DOSY measurements gave no evidence for two different species – monomer and dimer – in solution. On the other hand ESI mass spectrometry showed a peak attributable to the $[2M+H]^+$ ion with two amidines M (see Experimental Section), indicating a certain stability of the dimer.

Summing up the findings obtained so far, three different exchange processes were detected in solutions of amidine **C₆F₅MesAm** by means of NOESY NMR spectroscopy. The slowest process takes place at room temperature and involves equilibration between the NH- and N-aromatic rings within each single isomer. A second exchange is still operative at temperatures where the first process is not observed any longer ($-30\text{ }^{\circ}\text{C}$ and below). The *E-syn* isomer gets transformed into the *Z-anti* isomer and *vice versa*. A possible mechanism for this reaction might be the deprotonation and reprotonation of the isolated isomers in solution. The fastest process finally is a tautomerization reaction which presumably takes place within a dimeric aggregate consisting of an *E-syn* and a *Z-anti* isomer as could be shown by careful evaluation of NOE signals. The exchange is fast in CDCl₃ even at $-50\text{ }^{\circ}\text{C}$ and also provides a reasonable explanation for the observed concentration and temperature dependence of the recorded NMR spectra.

CF₃PhMesAm The NMR spectra of amidines **CF₃PhMesAm** and **C₆F₅MesAm** look very much alike, except for the fact that amidine **CF₃PhMesAm** exhibits almost no alteration of the isomeric ratio upon variation of temperature and concentration. Nevertheless, it can be presumed that also **CF₃PhMesAm** adopts *E-syn* and *Z-anti* conformations in solution. Evidence for this also stems from temperature-dependent NOESY NMR spectroscopy. Just like in the case of amidine **C₆F₅MesAm**, also for **CF₃PhMesAm** several exchange processes exist at room temperature in CD₂Cl₂. One of them converts one isomer into the other, whereas a second exchange process converts the signals for the NH-aromatic ring into the signals for the N-aromatic ring of each isomer. The latter of the two processes is not longer detectable at $-50\text{ }^{\circ}\text{C}$, but the exchange between both isomers persists until $-90\text{ }^{\circ}\text{C}$, where it is slow but still present. Like in the case of amidine **C₆F₅MesAm**, the exchange rate for the NH protons is lower ($k_{\text{ex}} = 0.02\text{ s}^{-1}$)

than e. g. for the aromatic mesityl protons ($k_{\text{ex}} = 0.13 \text{ s}^{-1}$) which indicates that again two different tautomeric processes are operative, one of them being related to dimer formation in solution.

At -90°C different cross peaks can be observed in the NOESY spectrum: In Figure 3.15 the NOE contacts between the NH proton of the *Z-anti* isomer and the four *ortho*-methyl groups of both mesityl moieties of the *Z-anti* isomer are highlighted with blue boxes. Furthermore, an NOE signal between the NH proton of the *E-syn* isomer and the *ortho-NHMe*s methyl groups of the *E-syn* isomer is clearly visible (red box). However, the NOE contact between the NH proton of the *E-syn* isomer and the *ortho-NMe*s methyl groups of the *Z-anti* isomer characterizing the dimer is not so evident as in the case of amidine **C₆F₅MesAm**. Nevertheless, by looking at the NOESY trace for the NH proton of the *E-syn* isomer at 7.01 ppm in Figure 3.15 (c), it becomes clear that the signal intensity of the NOE signal is significantly above the intensity of the exchange signals still present at the applied temperature and therefore also amidine **CF₃PhMesAm** should exist – although not as extensively as amidine **C₆F₅MesAm** – as molecular aggregates in solution. The weak signal at 1.91 ppm in Figure 3.15 (c) is mainly attributable to exchange processes between the two isomers, yet it remains at first glance unclear why the correlation to the *ortho-NMe*s methyl groups of the *E-syn* isomer at 1.84 ppm is relatively high compared to the signal at 1.91 ppm. The intensity of the signal should be significantly lower if it was solely attributable to the mentioned exchange process. A possible explanation could be that indeed an NOE effect is the origin of the signal. The fact that in the crystal structure of the compound a minimum distance of 4.15 Å between the NH proton and a proton of the respective methyl group can be found, seems to argue in favor of this suggestion. Besides the NOE signals highlighted in Figure 3.15, also further NOE contacts between the 4-(trifluoromethyl)phenyl groups of both isomers and different mesityl groups were recognized. All in all, these NOE contacts support the assignment of isomers already given as well as the idea of a dimeric structure in solution. In order to slow down the exchange process, also lower concentrations of the amidine were used in the NOESY NMR measurements. Indeed, at -90°C and very low concentrations, the exchange rate notably dropped further. For a 0.02 M solution of amidine **CF₃PhMesAm**, exchange peaks were not detected any longer but the NOE contact indicating dimer formation was still present, albeit not very pronounced. This suggests that dimer formation is possible even in very diluted solutions, but the actual tautomerization process may be hampered due to the absence of an external proton donor or acceptor.

Summarizing the observations made in the NMR measurements, one can state that amidine **CF₃PhMesAm** exists as *E-syn* and *Z-anti* isomers in solution, but in contrast to amidine **C₆F₅MesAm** the isomeric ratio is not altered when changing temperature or concentration. However, exchange rates are influenced by variation of those parameters. In accordance with the NOESY data obtained, an aggregation is likely to occur and could also explain the fast exchange between both isomers even at -90°C .

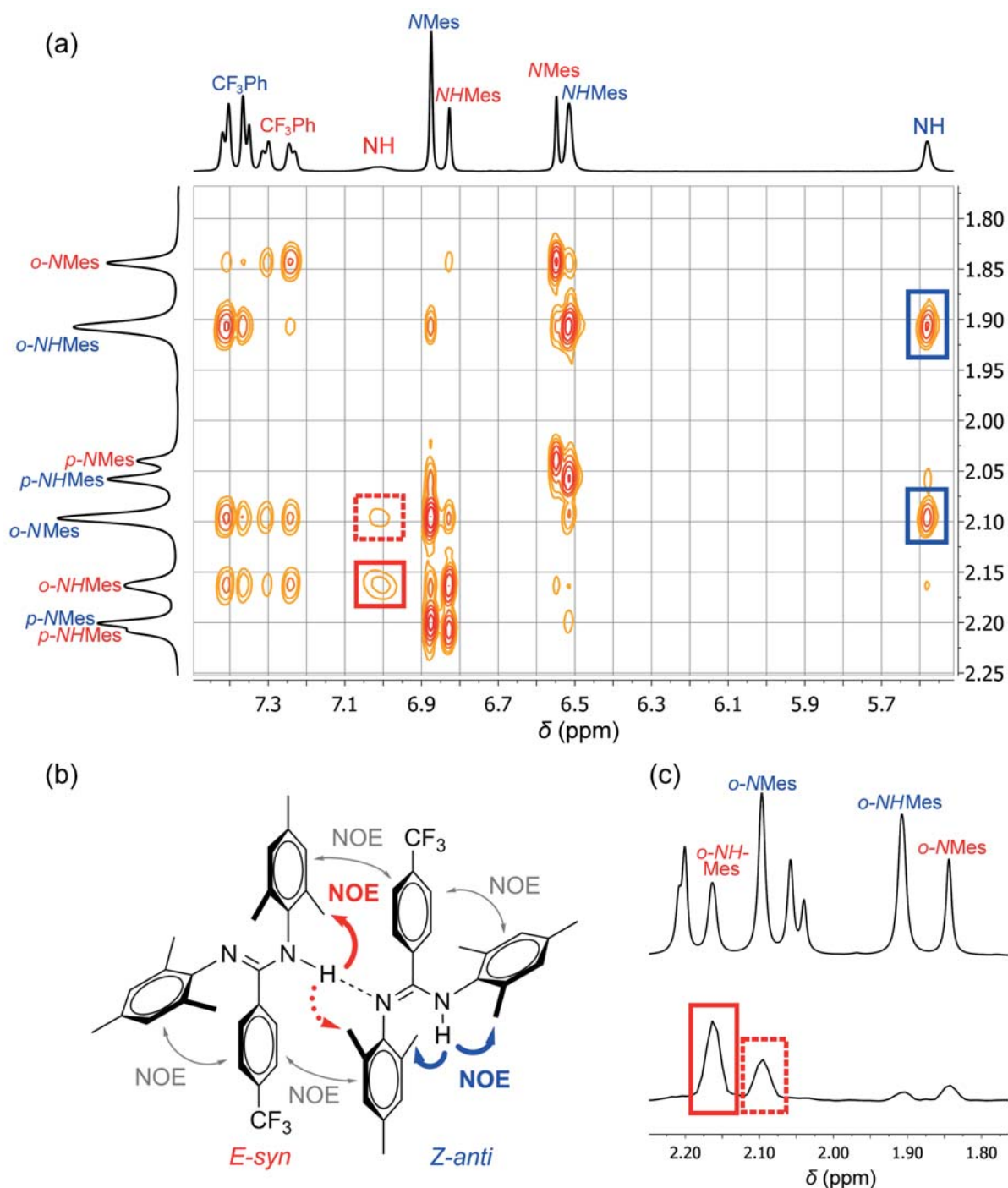


Figure 3.15. NOESY spectrum of amidine **CF₃PhMesAm** in CD₂Cl₂ at $-90\text{ }^{\circ}\text{C}$ (a) and resulting assignment of *E-syn* and *Z-anti* isomers (b). In (c) the methyl region of the ¹H NMR spectrum (top) is shown together with the NOESY trace for the NH proton of the *E-syn* isomer at 7.01 ppm (bottom). Signals for the *E-syn* isomer are always marked in red, those for the *Z-anti* isomer in blue.

TolFAm The NMR spectrum of **TolFAm** in CDCl_3 at -50°C was difficult to interpret because of overlapping of signals in the aromatic region, which especially included the NH protons of the two isomers. Furthermore, the interconversion of both isomers was still considerable at -50°C and a detection of NOE signals was therefore hampered. Nevertheless, it was possible to detect signals connecting the *meta* and *para* protons of the NH- and N-aromatic rings of the major isomer suggesting the presence of the *Z-syn* isomer (Figure 3.16).

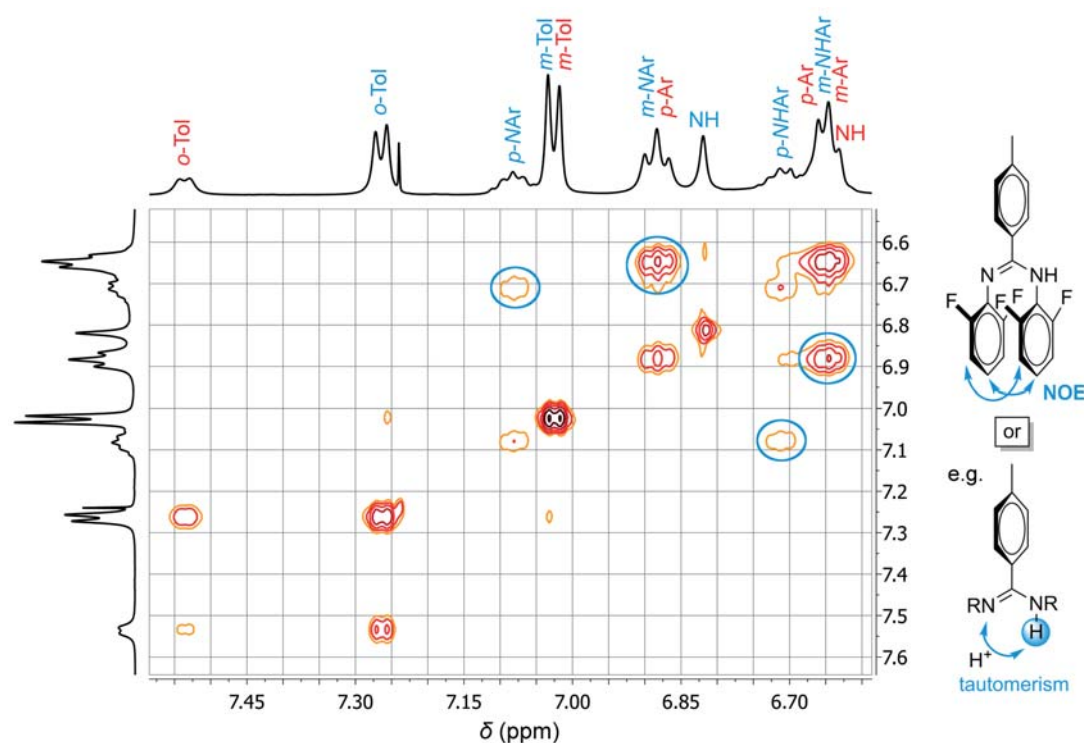


Figure 3.16. NOESY spectrum of amidine **TolFAm** in CDCl_3 at -50°C in the aromatic region and possible explanations for the observed cross peaks highlighted with blue circles.

Moreover, the *Z-syn* isomer was found in a dimer with the *E-syn* isomer in the solid state and thus it can be suspected that in solution a similar situation exists, although the presence of the *Z-syn* isomer in the crystal structure not necessarily means that this isomer is also prevailing in solution. Instead, the assignment should be regarded with caution as the available experimental NMR data do not permit a definite statement on the origin of the NOE signals highlighted in Figure 3.16. As seen in the other amidines examined before, similar signals could not only be caused by an NOE, but also by isomerization processes, probably involving tautomerism within one single isomer (in case of isomers *E-anti* or *Z-syn*) or dimers of amidines (*E-syn* and *Z-anti* isomers) which would make the N- and NH-aromatic rings indistinguishable. Especially as amidine **TolFAm** might be more acidic due to the electron-withdrawing groups, such a tautomerism cannot be excluded. Furthermore, an isomerization by rotation about

the C–N single bond is imaginable and would give the *Z-anti* isomer which has been recognized as the main isomer for the other amidines examined before.

Preliminary DFT calculations performed with the ORCA program package^[385] using the B3LYP functional, SV(P) basis set^[386] and the COSMO solvation model^[387] to simulate the influences of the solvent CHCl₃ seem to support the hypothesis that the *Z-syn* isomer might be favored in solution. However, the energy differences to the single point energies of the other isomers were very small. As represented in Figure 3.17 these differences did only account for a few kJ mol⁻¹ which hampers a reliable evaluation of the obtained results. Comparably small energy differences were also found for the other amidines discussed in this chapter, however in those cases the *Z-syn* isomer was usually the isomer with the highest energy. Furthermore, the temperature- and concentration-dependent measurements showed a low field shifting of the NH protons of both isomers contrary to the the amidines considered before, which seems to confirm that the situation found in amidine **TolFam** is distinct from the other amidines. The minor isomer presumably features *E-syn* configuration as already found in the solid state, however no experimental proof for this could be gathered by means of NOESY NMR spectroscopy as the overlapping of signals was too extensive.

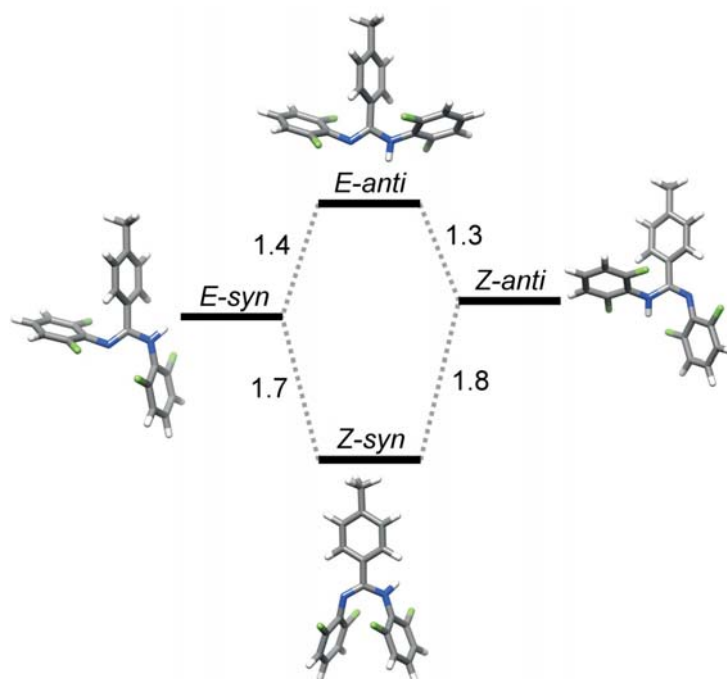


Figure 3.17. Calculated energy differences (in kJ mol⁻¹) of the isomers of amidine **TolFam** (for details see text).

TolTolAm The NMR spectrum of amidine **TolTolAm** featured significantly broader peaks at room temperature than all other amidines examined before, but at low temperatures two sets of signals were clearly distinguishable. However, different dynamic exchange processes hampered the assignment of isomers. In contrast to the other amidines discussed in this section, NOESY spectroscopy yielded no NOE signals that were helpful for answering the question which of the possible isomers exist in solution. Instead, the NOESY spectrum in Figure 3.18 illustrates that the exchange between the two isomers is fast even at $-60\text{ }^{\circ}\text{C}$ as cross peaks correlating the NH protons of both isomers exist. However, the fact that the exchange process connects the NH-aromatic protons of one isomer to the N-aromatic protons of the second isomer, suggests that, like in the case of **C₆F₅MesAm** and **CF₃PhMesAm**, an equilibrium of *E-syn* and *Z-anti* isomers exists in solution. Consequently, also in this case a tautomerization reaction involving a bimolecular mechanism can be assumed which could readily explain the observed broadening of peaks upon increasing the concentration. Due to a lack of NOE signals which could give some reliable indication of the present isomers, the isomer with the low field shift of the NH proton was tentatively assigned to the *E-syn* isomer since – as already seen for the other amidines – this proton is deshielded in the course of dimer formation in solution. Consequently, the second isomer must be the *Z-anti* isomer. The nature of the exchange processes was further elucidated by means of ^{13}C EXSY NMR spectroscopy. On the one hand, a concentration-dependent exchange between the two isomers could be detected ($k_{\text{ex}} = 3.3\text{ s}^{-1}$ at $-53\text{ }^{\circ}\text{C}$ in CDCl_3) and on the other hand also a concentration-independent exchange of the N- and NH-aromatic rings within a single isomer was observed ($k_{\text{ex}} = 1.5\text{ s}^{-1}$ at $-53\text{ }^{\circ}\text{C}$ in CDCl_3), but only for the *E-syn* isomer. From the obtained NOESY NMR data it is not clear to what extent a dimer of isomers is responsible for the observed exchange between the two isomers since even at this temperature an exchange between the NH protons of both isomers is observed. The amidine could also act as external base or acid without forming a dimer. However, when comparing the exchange rate of the NH protons in the NOESY spectrum ($k_{\text{ex}} = 2.0\text{ s}^{-1}$) with the exchange rate calculated from the ^{13}C EXSY NMR spectrum ($k_{\text{ex}} = 3.3\text{ s}^{-1}$), one notices that the exchange rate for the NH protons is smaller. As explained in detail before, this observation could be an evidence for the simultaneous action of two tautomerization mechanisms, namely protonation/reprotonation *via* isolated amidine molecules and tautomerism within a dimeric aggregate of *E-syn* and *Z-anti* isomers (Scheme 3.1). Unfortunately, the temperatures of ^1H NOESY and ^{13}C EXSY NMR measurements were not exactly identical due to problems with the temperature maintenance in the EXSY NMR measurements. Therefore the comparison of the rate constants should be regarded with care.

It is interesting to mention that according to the given assignment the *Z-anti* isomer does not show the concentration-independent exchange of the N- and NH-aromatic protons at $-60\text{ }^{\circ}\text{C}$ which was observed above for the other isomer. At the same time the *E-syn* isomer shows broader peaks in the temperature- and concentration-dependent measurements depicted in Figure 3.11 and Figure 3.12. Both observations suggest that

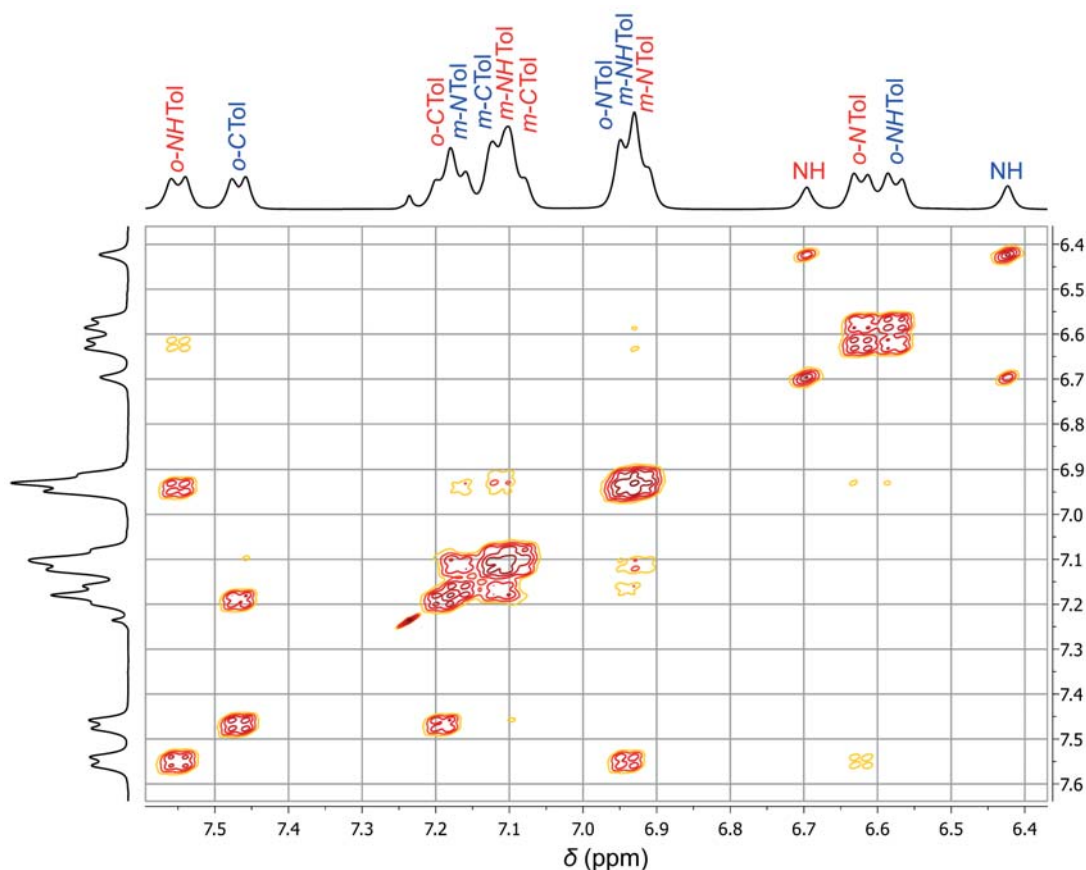


Figure 3.18. NOESY spectrum of amidine **TolTolAm** in CDCl_3 at -60°C in the aromatic region showing interconversion of *E-syn* (red) and *Z-anti* isomers (blue) and exchange of the N- and NH-aromatic rings of the *E-syn* isomer.

the respective possibilities of isomerization might in fact be quite different for the involved isomers. Obviously, the isomerization occurs easier in the *E-syn* isomer than in the *Z-anti* isomer. It is important to realize that the exchange of N- and NH-aromatic rings within a single isomer cannot be reasoned by only assuming a simple tautomerization reaction, *i. e.* the changing of position of the proton from one nitrogen atom to the other, since this would lead to an interconversion of *E-syn* and *Z-anti* isomers. A possible explanation for the observed phenomenon could be that rotation about the C–N single bond has to be considered. Whereas rotation about this bond would give the *E-anti* isomer when starting from the *E-syn* isomer, the *Z-syn* isomer is obtained when rotating about the C–N bond of the *Z-anti* isomer. Hopping of the proton should be facilitated in the *E-anti* isomer due to a more favorable interaction of the proton with both neighboring nitrogen atoms. The associated tautomerization reaction would not involve a transformation of the *E* isomer into the *Z* isomer, but it would result in an exchange of N- and NH-aromatic rings. On the contrary, a (concentration-independent) tautomerization reaction is not so easily achieved for the *Z-anti* isomer since the lone pair of the doubly bound nitrogen atom is located at that side of the molecule which is turned away from the proton which has to change its position. Thus the structure of the

isomers might provide an approach to an explanation for the differing exchange rates. However, this mechanism remains speculative as in particular no experimental proof for the presence of the *E-anti* isomer could be gathered on the basis of the available NMR data.

3.4 The Coordination Chemistry of Amidines

After examination of the chemistry of amidines in solution, the focus will now turn towards the coordination chemistry of amidines. General aspects as well as experimental and theoretical details on the synthesized silver complexes will be provided.

3.4.1 General Aspects

Amidines are an exceptionally versatile group of ligands forming metal complexes with various elements throughout the Periodic Table of the Elements. Besides the group of alkali metals^[357,358,388,389] whose well-known amidine complexes often serve as starting materials for the preparation of coordination complexes, also other main group elements,^[334,337,390–394] rare earth metals,^[331,332,395–397] and in particular transition metals as for example Ti,^[398–400] Ni,^[401] Fe,^[402–405] Ru,^[406] Cu,^[407] and many more^[355,408–410] are known to form complexes with amidine-based ligands. The possibility of variation of the substituents in the backbone of the amidine moiety as well as at the nitrogen atoms accounts for their extraordinary flexibility and allows precise tuning of steric and electronic properties.^[410] Amidines may largely coordinate as anionic^[409,410] or neutral^[351,355] ligands, but also some anion receptors have been designed where the amidinium (or the structurally related guanidinium) moiety acts as a cationic ligand.^[351,411,412] Among the diverse applications of metal complexes featuring amidine or amidinate ligands are applications as polymerization catalysts^[413,414] or in materials science for different chemical vapor deposition methods.^[410,415,416]

The structural variability of metal complexes containing amidine-based ligands is very large. A reason for this is that the amidine molecule can coordinate in different ways to the metal ion giving rise to chelating, monodentate and bridging binding modes.^[410,416] The chelating binding mode comprises symmetrically or asymmetrically coordinated complexes and also *ortho*-metallated complexes exist.^[367] Neutral amidines coordinating to metals are often engaged in additional hydrogen bonding interactions *via* the free amino NH group.^[351] Figure 3.19 shows examples for possible coordination modes of amidines in metal complexes.

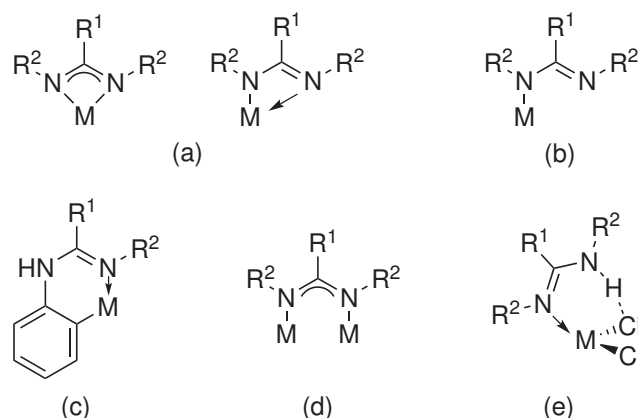


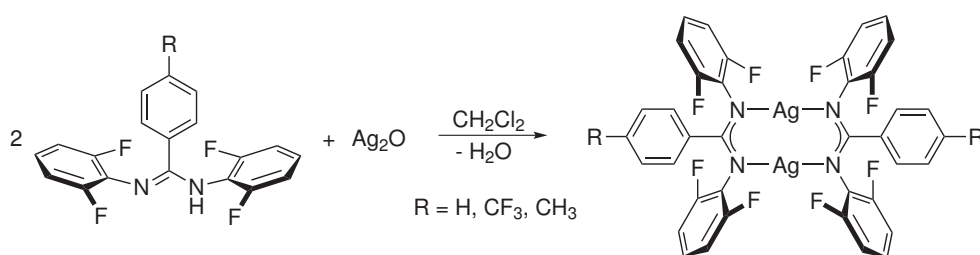
Figure 3.19. Examples for possible coordination modes of amidines in metal complexes: (a) symmetrically and asymmetrically chelating ligand, (b) monodentate ligand, (c) *ortho*-metallated complex, (d) bridging binding mode and (e) example for coordination of a neutral amidine.

3.4.2 Amidinosilver(I) Complexes

Group 11 transition metal complexes of amidines are often found to exist as dimers with the amidine ligand typically adopting a bridging binding mode (example (d) in Figure 3.19), but also trimeric and tetrameric complexes have been identified.^[409,410,417,418] In general these compounds are considered to be promising precursors for chemical vapor deposition (CVD) or atomic layer deposition (ALD) of metal films since they feature a series of beneficial properties as for example volatility, low melting points and high thermal stability. Amidinosilver(I) complexes have been reported to form trimers^[407] or a mixture of dimers and trimers^[416] in solution as well as in the solid state. For some dimeric silver(I) complexes, molecular aggregation in solution has been proposed. However, additional donating groups at the amidine moiety may prevent intermolecular interactions by coordinatively saturating the silver atoms.^[419] Other dimeric silver(I) complexes have been reported and their usually short Ag–Ag distances have been discussed controversially in terms of bonding interactions.^[419–421] In this section the synthesis and molecular structures of the amidinosilver(I) complexes synthesized in the course of this project will be described. The complexes provide interesting insights into the coordination chemistry of amidines, but they only represent a small fragment of the extraordinarily diverse chemistry of amidines.

Synthesis of Bisamidinatodisilver(I) Complexes

Amidinosilver(I) complexes were prepared before by using silver halides, silver acetate or silver nitrate as silver source producing trimeric^[407] and dimeric^[419,421,422] complexes as well as a mixture^[416] of both species. In solution, also an equilibrium of dimeric and tetrameric complexes has been detected.^[423] In this work, the scope of possible starting materials is extended to Ag_2O , providing bisamidinatodisilver(I) complexes in good to excellent yield (63 % to quantitative yield). According to the reaction in Scheme 3.2, dimeric silver(I) complexes were obtained by stirring a mixture of the respective amidine, Ag_2O and DCM at room temperature. Filtration over Celite after five days of stirring and evaporation of the solvent *in vacuo* afforded the bisamidinatodisilver(I) complexes.



Scheme 3.2. Synthesis of bisamidinatodisilver(I) complexes $\text{Ag}_2(\text{PhFam})_2$ (R = H), $\text{Ag}_2(\text{CF}_3\text{PhFam})_2$ (R = CF₃) and $\text{Ag}_2(\text{TolFam})_2$ (R = CH₃).

The method described here was found appropriate for amidines **PhFam**, **CF₃PhFam**, and **TolFam**. However, when **PhMesAm**, **CF₃PhMesAm**, **TolMesAm** or **TolTolAm** were used, no product formation was observed. Instead, only the unchanged amidines were obtained as became clear from NMR measurements of the crude products. In the case of amidine **MesFam**, the reaction yielded a mixture of products which also contained the unchanged amidine. No efforts were made to isolate and characterize the different products. The method described above gave no product for amidine **C₆F₅MesAm**, and also no starting material could be recovered from the reaction mixture. A reason for this might be that with this amidine no dimer formation takes place, but a formation of a complex of higher nuclearity which is not soluble in the applied solvent. Since the situation did not change when more polar solvents like MeCN or acetone were used, no further attempts were made to isolate and characterize the product(s) formed in the reaction. The question whether steric or electronic reasons are responsible for the failure of the reaction in the case of the mesityl-substituted amidines cannot be answered ultimately. On the one hand, larger residues at the nitrogen atoms may prevent the coordination to the silver atoms, but on the other hand also amidine **TolTolAm** – which has no substituents in the *ortho*-positions of the aromatic rings – did not show any tendency to form the desired complex either. Since the amidine has to isomerize to the *E-anti* isomer prior to formation of a dimeric complex, another reason for the hampered complex formation in the case of the mesityl-substituted amidines might be the fact that larger substituents at the nitrogen atoms tend to favor the *Z*-isomer.^[357,358]

Structural Parameters of Bisamidinatodisilver(I) Complexes

Slow evaporation of CHCl_3 or DCM solutions of the silver complexes afforded crystals suitable for X-ray crystallography. Figure 3.20 depicts the molecular structures obtained from X-ray diffraction. As anticipated, they show dimeric silver(I) complexes in which the silver atoms are coordinated almost linearly by two bridging amidinate anions. The silver atoms are slightly displaced to the outside, resulting in N–Ag–N angles which are smaller than 180° . Selected bond length and angles of the three complexes are listed in Table 3.2. Notice that for $\text{Ag}_2(\text{CF}_3\text{PhFam})_2$ and $\text{Ag}_2(\text{TotFam})_2$ the two parts of the molecule separated by a plane through both carbon atoms of the $\text{N}=\text{C}=\text{N}$ units (C^2) are symmetry-related, whereas this is not the case for $\text{Ag}_2(\text{PhFam})_2$. As a consequence, for example all four Ag–N bonds in $\text{Ag}_2(\text{PhFam})_2$ are different while for the other two complexes only two different bond lengths exist.

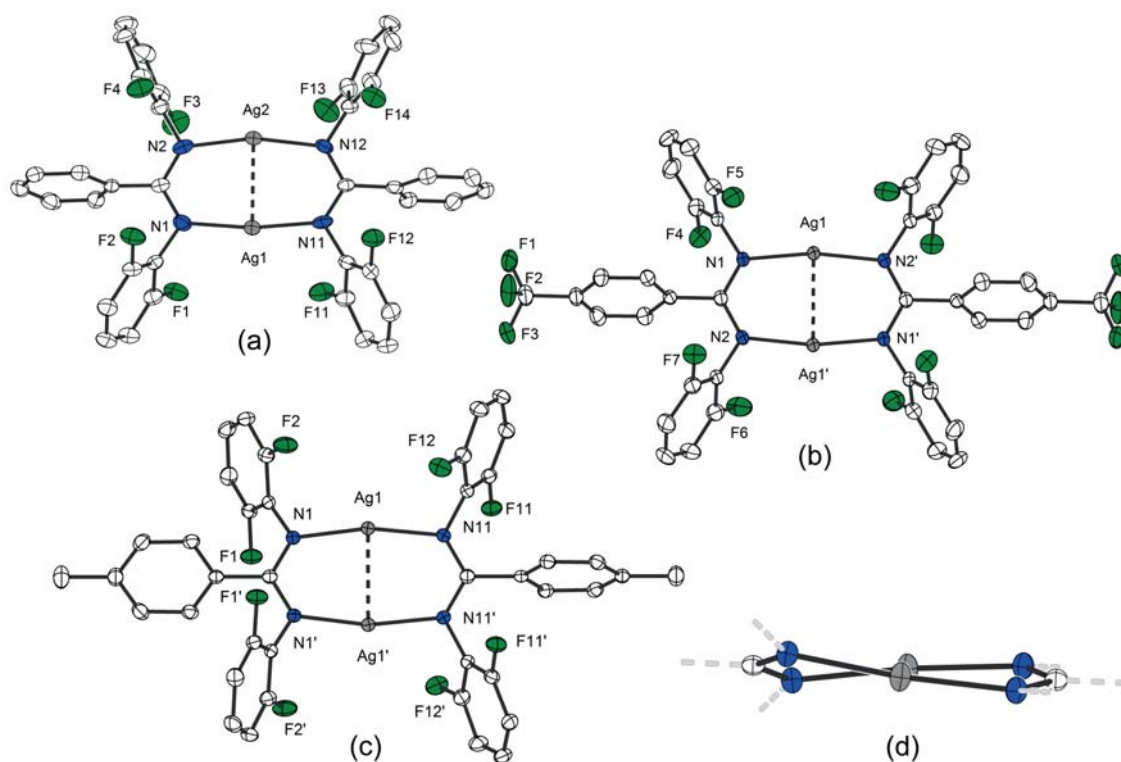


Figure 3.20. Thermal displacement ellipsoids (shown at 50 % probability) of the molecular structures of the bisamidinatodisilver(I) complexes $\text{Ag}_2(\text{PhFam})_2$ (a), $\text{Ag}_2(\text{CF}_3\text{PhFam})_2$ (b), and $\text{Ag}_2(\text{TotFam})_2$ (c); the view of the metallacycle along the Ag–Ag axis shows the puckering of the ring system of complex $\text{Ag}_2(\text{TotFam})_2$ (d). Hydrogen atoms and additional solvent molecules are omitted for clarity.

From the structural parameters shown in Table 3.2 it becomes clear that the amidinato ligands display an enhanced delocalization of electron density within the $\text{N}=\text{C}=\text{N}$ units as the bond lengths are almost equal. The difference of CN bond distances Δ_{CN} is 0.011 \AA at the most, which is significantly smaller than found for the amidines not coordinating a metal (see Table 3.1 in section 3.2). Surprisingly, only for the metallacyclic ring

Table 3.2: Selected structural parameters for the bisamidinatodisilver(I) complexes. Interatomic distances are given in [Å], angles in [°].

parameter	Ag₂(PhFam)₂	Ag₂(CF₃PhFam)₂	Ag₂(TolFam)₂
Ag...Ag	2.7108(3)	2.7175(3)	2.7033(3)
Ag–N	2.100(3)	2.105(1)	2.124(1)
	2.104(3)	2.101(1)	2.117(1)
	2.125(3)		
	2.121(3)		
C ² –N	1.326(5)	1.326(2)	1.327(2)
	1.330(5)	1.330(2)	1.328(2)
	1.330(5)		
	1.337(5)		
N–Ag–N	168.4(1)	169.1(1)	167.1(1)
	165.8(1)		
N=C–N	119.5(3)	121.7(2)	120.2(2)
	119.4(3)		

in complex **Ag₂(TolFam)₂** a significant deviation from planarity is found (Figure 3.20 (d)) whereas the other two complexes feature nearly planar metallacycles. A similar “puckering” of the ring system was recognized in dinuclear silver(I) and copper(I) selenium diimides before, and the angle Θ was introduced to quantify it.^[424] An analogous quantification for complex **Ag₂(TolFam)₂** is not justified since the twisting of the ring system is more complex. However, the distortion was found to be directly related to the metal-metal distance for the selenium diimide complexes and also in the present case the shortest Ag...Ag distance is found for the most distorted **Ag₂(TolFam)₂** complex. The reason for the puckering remains unclear in this case as the substituents at the nitrogen atoms of the amidines are identical in all three complexes and hence steric interactions can be excluded. To what extent packing forces operative in the crystal lattice are responsible for the observations made so far is not clear from the available data. In all three complexes, the distances between both silver atoms (2.711, 2.718 and 2.703 Å) are significantly shorter than twice the van der Waals radius of a silver atom^[425] (3.44 Å) and also short compared to the shortest Ag...Ag distance found in metallic silver (2.889 Å).^[426,427] Indeed, the experimentally determined covalent radius of linearly coordinated silver(I) (1.33 Å) is only slightly shorter than half of the Ag...Ag distances.^[427]

Attractive interactions between formally closed-shell d^{10} metals have fascinated scientists ever since their discovery and for gold this novel type of interactions has been coined *aurophilicity* by Schmidbaur in 1988.^[428–432] Analogous interactions – also in systems based on silver(I) or copper(I) – have been identified even before this by Hoffmann^[433,434] and Jansen.^[435] While early theoretical calculations mainly focused on the participation of s and p orbitals in order to enable bonding interactions, Pyykkö and Li later concluded that the true origin of *aurophilicity* is electron correlation strength-

ened by relativistic effects rather than hybridization effects.^[436,437] In a very simplified picture, aurophilicity is an unusually strong van der Waals-type (dispersion) interaction.^[438] For gold the energy of this kind of interactions lies within the range of typical hydrogen bonding (29 – 46 kJ mol⁻¹),^[439] but for silver and copper the effect is generally thought to be smaller.^[440,441] In fact, the analogous argentophilic and cuprophilic interactions are still under debate,^[424] primarily because ligand-unsupported examples are extremely rare^[442–445] and the influence of the ligand system has to be considered as well.^[446–448] Nevertheless, experimental and theoretical evidence has been gathered supporting the assignment of attractive interactions also in these systems^[441,449,450] and the term “metallophilicity” has been used to describe the interactions operative between closed-shell d¹⁰ metals in general.

Remarkably short Ag(I)⋯Ag(I) contacts have been observed before for other bisamidinatodisilver(I) complexes and bonding interactions have been considered as a possible reason for this.^[419–421] Cotton *et al.* found a relatively short Ag⋯Ag distance of 2.705 Å in a similar bisformamidinatodisilver(I) complex,^[420] yet no evidence for the involvement of direct metal-metal bonding was gained on the basis of theoretical calculations. According to the authors, only the ligand system is responsible for the comparably close metal-metal contacts. However, participation of metal s and p orbitals was considered essential for assigning a direct metal-metal bonding – an assumption that is controversial in light of the metallophilicity concept.^[451] In related dimeric formamidinato complexes with additional O and S donor atoms, the elongation of the Ag⋯Ag distances (2.7801 – 2.805 Å) was interpreted in terms of a possible donation of electron density in an antibonding Ag–Ag orbital.^[419] A second explanation provided by the authors was based on steric considerations involving also attractive interactions between the silver and the donor atoms.

In view of the literature collected above, the close Ag(I)⋯Ag(I) contacts observed in the synthesized complexes may be described as argentophilic. However, one should keep in mind that the ligand environment supports this arrangement. On the other hand, the tendency to establish close metal-metal contacts might be a prerequisite for the formation of such complexes.

3.5 Summary

In this chapter the amidines synthesized in the context of this project were studied more thoroughly. Crystallographic data of these compounds were collected to explore their structural parameters. As became clear from the solid state structures, all of the synthesized amidines displayed molecular association supported by hydrogen bonds. In most cases hydrogen-bonded dimers were present in the crystal structures. Furthermore, the chemistry of amidines in solution was elucidated using, as representative examples, the four amidines **C₆F₅MesAm**, **CF₃PhMesAm**, **TolFAm**, and **TolTolAm**. Extensive NMR measurements with several techniques and at variable temperatures

and concentrations suggested the presence of a dimer consisting of *E-syn* and *Z-anti* isomers. In case of the mesityl-substituted amidines **CF₃PhMesAm** and **C₆F₅MesAm**, this dimer could be directly detected by means of ¹H NOESY NMR measurements allowing for an observation of NOE effects. For amidines **TolFAm** and **TolTolAm** the presence of the dimer could not be verified directly because of fast exchange processes occurring in solution. However, the nature of the observed dynamic processes suggested a contribution of *E-syn* and *Z-anti* isomers in solutions of these amidines as well. In particular cases additional evidence for the presence of other isomers (*Z-syn* isomer and eventually also *E-anti* isomer) was obtained. In general, the performed NMR measurements suggest that the possibility of fast isomerization between *E-syn* and *Z-anti* isomers by simple deprotonation/reprotonation steps represents a general characteristic in the solution chemistry of amidines. The resulting NMR spectra are often surprisingly complex owing to the simultaneous presence of competing exchange and isomerization processes, and feature a remarkable dependency on different factors such as solvent, concentration, temperature and purity of the NMR solvent.

As has been demonstrated exemplarily for the three compounds **PhFAm**, **CF₃PhFAm**, and **TolFAm**, amidines are also versatile ligands in coordination chemistry. The corresponding amidinatosilver(I) complexes were synthesized in reactions with Ag₂O and examined more thoroughly by means of X-ray crystallography. The obtained molecular structures featured close Ag(I)⋯Ag(I) contacts which can be described as argentophilic.

4

The Transition Metal Lewis Base

Abstract In this chapter the syntheses and properties of Lewis basic metal complexes suitable for serving as proton acceptors in the heterolytic splitting reaction of dihydrogen are described. The synthetic work in this field focused on the literature-known carbonyl metalates $\text{K}[\text{CpFe}(\text{CO})_2]$ (**KFp**) and $\text{K}[\text{CpRu}(\text{CO})_2]$ (**KRp**), but alternatives were also considered. The known procedures for the synthesis of **KRp** were found to be inconsistent and hence the synthetic protocol has been revised. Reductive cleavage of the ruthenium dimer $[\text{CpRu}(\text{CO})_2]_2$ (**Rp₂**) not only produces **KRp**, but also a poorly soluble black solid (**Rs**) which has been investigated by a variety of analytical methods. The interesting properties of this material, among them also its potential to act as a Lewis base, are compiled in this chapter.

4.1 The Choice and Synthesis of a Suitable Lewis Base

In order to find an appropriate transition metal Lewis base for mimicking the reactivity of the [Fe] hydrogenase, several aspects have to be considered. On the one hand, the complex should feature a distinct Lewis basic character at the metal center to enable facile protonation of the metal complex in the heterolytic splitting reaction of dihydrogen. At the same time, the propensity to undergo other reactions than the protonation reaction should be as low as possible. An example for such an undesired reactivity could be the electron transfer associated with the oxidation of the complex. In fact, the transfer of an electron might be an important reaction pathway, especially when highly reduced metal complexes are used as Lewis bases. As already presented in the objective of this work (see chapter 1.6), efforts to synthesize transition metal Lewis bases largely focused on the carbonyl metalates $\text{K}[\text{CpFe}(\text{CO})_2]$ (**KFp**) and $\text{K}[\text{CpRu}(\text{CO})_2]$ (**KRp**). In analogy to the active site of the [Fe] hydrogenase, these complexes possess a group 8 transition metal and several CO ligands. Although the structural similarity to the FeGP cofactor is only present rudimentarily, the metalates nevertheless feature a low oxidation state (0) of the central metal atom and can thus be protonated to yield the hydride complexes $\text{HFeCp}(\text{CO})_2$ (**HFp**) and $\text{HRuCp}(\text{CO})_2$ (**HRp**), respectively. Consequently, the function of the FeGP cofactor is emulated in a simplified way. Another advantage of the presented systems is that the metal fragment bears a single negative charge and can thus form a 1:1 ion pair with the onefold positively charged imidazolium ion. The properties of **KFp** and **KRp** relevant to their envisioned role as Lewis bases in the splitting reaction of dihydrogen are presented in the following section before briefly discussing alternative metal complexes.

4.1.1 General Aspects

The preparation of the anion $[\text{CpFe}(\text{CO})_2]^-$ (**Fp**⁻) was first reported by E. O. Fischer in 1955,^[452,453] who explored reactions of cyclopentadienyl (Cp) ligated metal complexes. Since then, this organometallic reagent has been used in a vast number of chemical reactions providing access to a great variety of organic and inorganic compounds. As a tribute to this, the unique properties and reactions of this inexpensive and readily accessible reagent have been reviewed several times.^[454,455]

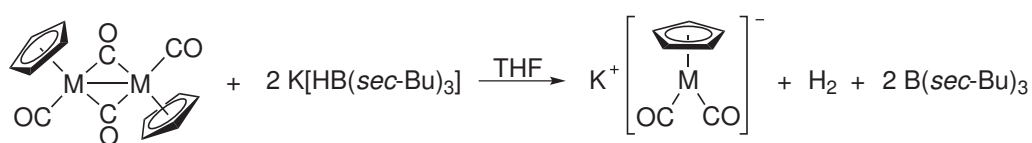
The **Fp**⁻ anion is an 18-electron complex and acts as a strongly nucleophilic Lewis base. In fact, it is one of the most nucleophilic transition metal anions and – contrasting the usual trend in a group of the Periodic Table of the Elements – even more nucleophilic than its heavier element analog $[\text{CpRu}(\text{CO})_2]^-$ (**Rp**⁻) by several orders of magnitude.^[456] Despite the many studies in this field, the reasons for the extraordinary nucleophilicity are still not entirely understood. Most probably a combination of different factors such as a high charge density at the metal center, an even coordination number in the

reaction product, and ion-pairing effects are responsible for the extremely high nucleophilicity.^[455] Despite the high tendency to undergo nucleophilic substitution reactions, the \mathbf{Fp}^- anion can also act as a base. In certain cases, this reaction path might even be favored over nucleophilic attack.^[455,457] A third possible reaction that has to be considered when working with the \mathbf{Fp}^- anion is its oxidizability. The anion is a relatively strong one-electron reductant, exhibiting an irreversible oxidation wave at a potential of approximately -1.35 V vs. the $\text{FeCp}_2/\text{FeCp}_2^+$ (Fc/Fc^+) redox couple.^[458,459]

In comparison to the iron congener, literature reports for the heavier element analog $[\text{CpRu}(\text{CO})_2]^-$ (\mathbf{Rp}^-) are much less numerous. However, experiments confirmed its lower nucleophilicity^[460] and redox activity ($E_p^{\text{ox}} = -1.06\text{ V}$ vs. Fc/Fc^+),^[458] as well as its higher basicity compared to the \mathbf{Fp}^- anion.^[461] With respect to the planned reactions with dihydrogen, these properties represent significant advantages since undesired reactions involving electron transfer or nucleophilic substitutions are less likely. Furthermore, deprotonation of the H_2 molecule should occur more easily in case of the more basic ruthenium metalate \mathbf{Rp}^- .

4.1.2 Synthesis of Carbonyl Metalates

In 1955 E. O. Fischer prepared the sodium salt of the \mathbf{Fp}^- anion by reductive cleavage of the dimer $[\text{CpFe}(\text{CO})_2]_2$ (\mathbf{Fp}_2). As a reducing agent he used sodium amalgam.^[453] Today many heterogeneous and homogeneous methods to produce the metalate are available, but all of the procedures still comprise reduction of \mathbf{Fp}_2 by chemical or electrochemical methods.^[455] In this context, trialkylborohydrides like $\text{K}[\text{HB}(\text{sec-Bu})_3]$ (K-Selectride) proved to be convenient reducing agents providing the potassium salt \mathbf{KFp} in high yields (Scheme 4.1).^[462,463] The metalate was thus synthesized by this method and recrystallized from THF/toluene yielding the compound as orange crystals.



Scheme 4.1. Synthesis of the metalates \mathbf{KFp} ($\text{M} = \text{Fe}$) and \mathbf{KRp} ($\text{M} = \text{Ru}$) by reductive cleavage of the dimers \mathbf{Fp}_2 ($\text{M} = \text{Fe}$) and \mathbf{Rp}_2 ($\text{M} = \text{Ru}$), respectively.

The first preparation of the Ru metalate \mathbf{Rp}^- was described by Wilkinson and co-workers.^[464] In comparison to the \mathbf{Fp}^- anion it was more difficult to prepare^[465] and in most cases the \mathbf{Rp}^- salt was not isolated prior to using solutions of the compound in subsequent reactions. Only very few cases are reported where \mathbf{Rp}^- salts were actually isolated, though no clear analytical proof for the purity of the compound was provided.^[466,467] As for the iron analog, commonly utilized methods for the preparation of \mathbf{Rp}^- comprise the reduction of the ruthenium dimer $[\text{CpRu}(\text{CO})_2]_2$ (\mathbf{Rp}_2) by various reagents. In this context for example sodium amalgam,^[465,468,469] NaK alloy,^[466] Na

metal,^[470] and alkyl borohydrides^[467,471,472] have been used. Owing to the good experiences made with the iron analog and realizing disadvantages of the sodium amalgam method like formation of by-products (ruthenocene and $\text{Hg}[\text{CpRu}(\text{CO})_2]_2$) and difficult handling,^[471,472] $\text{K}[\text{HB}(\text{sec-Bu})_3]$ was used also for the reductive cleavage of Rp_2 . Surprisingly, the synthesis of the potassium salt KRp did not proceed as smoothly as for the iron congener and difficulties were encountered when trying to isolate the compound as a pure material. As a consequence, the literature was carefully reinvestigated which revealed inconsistencies in the reported observations connected to the synthesis of the ruthenium metalate. Efforts to clarify these inconsistencies not only led to a revised synthetic protocol for KRp and the first determination of its molecular structure by means of X-ray crystallography, but also brought about the discovery of a novel polymeric Cp/Ru/CO compound.^[473] Experimental details on this topic are provided in section 4.2.

4.1.3 Alternative Metal Complexes

First experiences with carbonyl metalates have already been obtained in the framework of a diploma thesis focusing on the heterolytic splitting of dihydrogen with the help of certain carbonyl metalates and imidazolium salts.^[290] However, especially the metal complex $\text{K}_2[\text{Fe}(\text{CO})_4]$, whose sodium salt is also known as Collman's reagent,^[474–476] was found to easily undergo electron transfer reactions. Therefore, this highly reduced metal complex was not considered in the present work. Instead, several other alternatives were taken into account as substitutes for the above-mentioned metalate anions Fp^- and Rp^- . The neutral complexes $\text{Ni}(\text{dppe})_2$, $\text{Ni}(\text{depe})_2$ and $\text{Fe}(\text{CO})_3(\text{P}^t\text{Bu}_3)_2$ depicted in Figure 4.1 were synthesized according to existing synthetic protocols. The nickel complexes were easily obtained in ligand substitution reactions starting from bis(cyclooctadiene)nickel(0) ($\text{Ni}(\text{cod})_2$) and the respective 1,2-bisphosphinoethane.^[477] Compound $\text{Fe}(\text{CO})_3(\text{P}^t\text{Bu}_3)_2$ was obtained from triirondodecacarbonyl $\text{Fe}_3(\text{CO})_{12}$ and tri-(*tert*-butyl)phosphine.^[478]

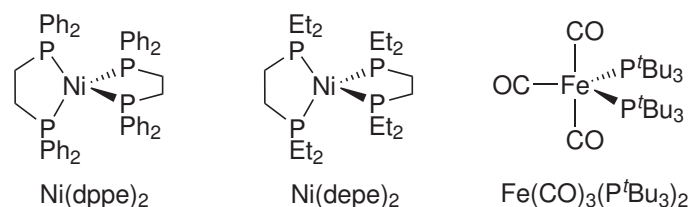


Figure 4.1. Alternative Lewis basic metal complexes (dppe = 1,2-bis(diphenylphosphino)ethane, depe = 1,2-bis(diethylphosphino)ethane).

In contrast to the carbonylates KFp and KRp , protonation of these complexes does not produce neutral metal hydrides, but positively charged metal complexes. The compounds are less reactive and hence less prone to undergo undesired side reactions.

However, the fact that the Lewis acidic imidazolium ion and the transition metal Lewis base feature differing charges, complicates the formation of the envisioned transition metal frustrated Lewis pairs (see chapter 5). Two reasons account for this: the differing solubility which hampers the search for a suitable solvent, and interactions with remaining counter ions. Indeed, solubility problems were encountered when combining the synthesized imidazolium ions with these metal complexes. Furthermore, corresponding mixtures did not react with dihydrogen. As a consequence, the alternative metal complexes shown in Figure 4.1 are not considered in the further course of this work. Nevertheless, Table 4.1, which compiles oxidation potentials of basic metal complexes (E° or E_p^{ox}) and the $\text{p}K_a$ values of the corresponding acids, includes the alternative metal complexes mentioned in this section to permit a comparison of the selected compounds.

Table 4.1: Comparison of different transition metal Lewis bases with respect to their oxidation potentials (E° or E_p^{ox}) and the $\text{p}K_a$ values of the corresponding acids. Potentials are referenced *vs.* the Fc/Fc^+ redox couple. (*) Literature values for $\text{Fe}(\text{CO})_3(\text{P}^t\text{Bu}_3)_2/[\text{HFe}(\text{CO})_3(\text{P}^t\text{Bu}_3)_2]^+$ do not exist, therefore oxidation potentials and $\text{p}K_a$ values of similar tricarbonylbis(phosphine)iron(0) complexes are given to make a rough estimation possible.

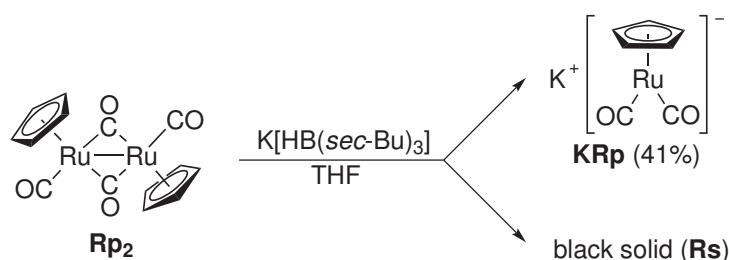
metal complex M	metal hydride M–H	E° or E_p^{ox} (M $^-$ /M)	$\text{p}K_a$ (M–H)
$\text{K}[\text{CpFe}(\text{CO})_2]$ (KFp)	$\text{CpFe}(\text{CO})_2\text{H}$ (HFp)	$-1.35 \text{ V}^{[458]}$	$27.1^{[461]}$
$\text{K}[\text{CpRu}(\text{CO})_2]$ (KRp)	$\text{CpRu}(\text{CO})_2\text{H}$ (HRp)	$-1.06 \text{ V}^{[458]}$	$28.3^{[461]}$
$\text{K}_2[\text{Fe}(\text{CO})_4]$	$\text{K}[\text{HFe}(\text{CO})_4]$	$-1.67 \text{ V}^{[479]}$	$12.7^{[480]}$
$\text{Ni}(\text{dppe})_2$	$[\text{HNi}(\text{dppe})_2]^+$	$-0.70 \text{ V}^{[481]}$	$14.2^{[481]}$
$\text{Ni}(\text{depe})_2$	$[\text{HNi}(\text{depe})_2]^+$	$-1.29 \text{ V}^{[481]}$	$23.8^{[481]}$
$\text{Fe}(\text{CO})_3(\text{P}^t\text{Bu}_3)_2$	$[\text{HFe}(\text{CO})_3(\text{P}^t\text{Bu}_3)_2]^+$	$0 \text{ to } -0.2 \text{ V}^{[482]} (*)$	$\text{ca. } 4.4^{[483]} (*)$

From the presented data it becomes clear that **KFp** and **KRp** are suitable candidates for acting as transition metal Lewis bases. The oxidation potentials are lower as for example in the case of $\text{K}_2[\text{Fe}(\text{CO})_4]$ which makes electron transfer reactions with the involvement of **KFp** and **KRp** less likely. Furthermore, the $\text{p}K_a$ values of the corresponding acids of these two metalates are relatively high. Consequently, the Lewis basicity of **KFp** and **KRp** is higher than for the other metal complexes.

4.2 Revisiting the Synthesis of $\text{K}[\text{CpRu}(\text{CO})_2]$ (KRp)

4.2.1 A Revised Synthetic Protocol

When $\text{K}[\text{HB}(\text{sec-Bu})_3]$ was added to a solution of Rp_2 in THF, a gradual darkening of the initially orange solution and the formation of a finely dispersed black precipitate (Rs) was observed.^[473] This was surprising since KRp was reported to be soluble in THF and no comparable observations were made during the synthesis of KFp . Obviously a second product was formed which suggested that the usually moderate yields (20 – 40 %, sometimes even less) encountered in the reported syntheses where solutions of KRp have been prepared for further use,^[465,471,472,484] were connected to the formation of this precipitate (Scheme 4.2).



Scheme 4.2. Reductive cleavage of Rp_2 producing two products.

The assumption that the borohydride might be involved in the formation of the second product was disproved since its formation was also observed when a potassium mirror was used to reduce the ruthenium dimer Rp_2 . However, in these reactions separation of the black material from residual amounts of potassium metal was not possible. On the contrary, the compound could be isolated from the reaction of Rp_2 and $\text{K}[\text{HB}(\text{sec-Bu})_3]$ by filtration. Addition of toluene to the filtrate produced a yellow crystalline material which could be recrystallized from THF/toluene to obtain single crystals suitable for X-ray crystallography. Structure determination by X-ray diffraction established that indeed the desired metalate KRp was synthesized. Under optimized conditions (see Experimental Section 6) 37 – 41 % of yellow crystalline KRp can be isolated from the reaction.

4.2.2 Isotope Labeling

Before focusing on the characterization of the two products obtained from the reductive cleavage of **Rp₂** by $K[HB(sec-Bu)_3]$, the synthesis of ^{13}C O-labeled **KRp** and black material will be briefly described. ^{13}C O-enriched triruthenium dodecacarbonyl $Ru_3(CO)_{12}$ was obtained according to a modified literature procedure^[485] by stirring a solution of $Ru_3(CO)_{12}$ in a mixture of THF and MeOH at 50 °C under an atmosphere of ^{13}C O gas (1 bar) and with addition of catalytic amounts of KOMe. The ^{13}C O-labeled $Ru_3(CO)_{12}$ produced by this method was directly used in the synthesis of ^{13}C O-enriched **Rp₂** which was conducted analogously to the preparation of the non-labeled compound. As expected, ^{13}C O-enriched **Rp₂** exhibits an IR spectrum distinct from the non-labeled compound (Figure 4.2).

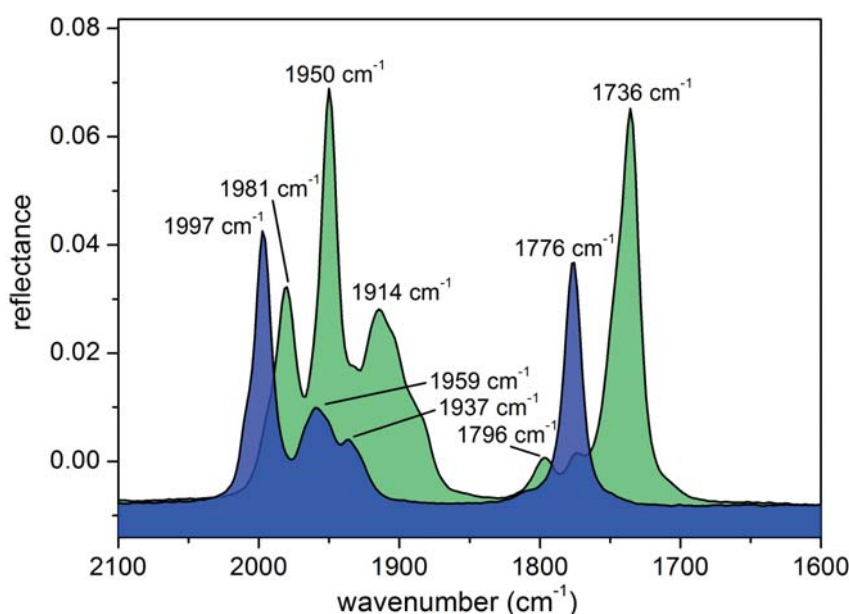


Figure 4.2. IR spectra of **Rp₂** (blue) and ^{13}C O-enriched **Rp₂** (green) in MeCN.

The IR bands attributable to the CO stretching frequencies of the ^{13}C O-enriched compound shift to lower wavenumbers compared to the IR bands of the non-labeled compound. This totally meets the expectations since the ratio of the wavenumbers complies with the following equation:^[486]

$$\frac{\tilde{\nu}_{^{13}CO}}{\tilde{\nu}_{^{12}CO}} = \sqrt{\frac{\mu_{^{12}CO}}{\mu_{^{13}CO}}} = 0.9778 \quad \text{with the reduced mass } \mu = \frac{m_1 \cdot m_2}{m_1 + m_2} \quad (4.1)$$

By applying this equation, most of the ^{13}C O bands can be calculated from the bands of the unlabeled compound. In the IR spectrum of the ^{13}C O-enriched compound additional bands are visible due to the presence of isomers with differing isotopic composition.^[487] From the ratio of the signal intensities in the ^{13}C NMR spectrum, the ^{13}C content in the CO molecules was estimated to be at least 90%. Reductive cleavage of

^{13}C -enriched Rp_2 with $\text{K}[\text{HB}(\text{sec-Bu})_3]$ analogous to the procedure described above produced ^{13}C -enriched KRp and the black solid Rs .

4.2.3 Elucidating the Structure and Further Properties of KRp

Recrystallization of the yellow material obtained by the revised synthetic protocol described above produced single crystals which enabled the the first determination of the molecular structure of KRp by means of X-ray diffraction. Caution is required when handling the compound outside a glovebox, as any exposure to air immediately destroys the crystals. The molecular structure of $\text{KRp} \cdot \text{THF}$, which crystallizes in the space group $Pbca$, is represented in Figure 4.3. Different interactions between the potassium cations and the Rp^- anions (and additional THF molecules) are clearly evident: Each potassium ion features a fourfold coordination by the oxygen atoms of two CO ligands as well as by two THF molecules. The interatomic distances are 2.754(2) and 2.737(2) Å and, respectively, 2.861(2) and 2.848(2) Å. By these interactions a threedimensional network with close $\text{K} \cdots \text{O}$ contacts is generated in which the Rp^- anions crosslink polymeric chains of alternating THF molecules and potassium ions. Furthermore, two weak interactions between the K^+ and C atoms of the carbonyl groups (3.150(2) and 3.202(2) Å) and two $\text{K} \cdots \text{Ru}$ contacts (3.607(1) and 3.981(1) Å) are observed. The resulting formal coordination number for the potassium cation is 8 or {4 + 4}. Similar interactions of alkali metal ions are common for carbonyl metalates^[485] and have also been noticed in the solid state structure of KFp .^[488]

Crystalline KRp was investigated by different methods. Elemental analysis data (Calcd.: C 32.18, H 1.93; Found: C 32.17, H 2.05) match the expected values and also IR data were found in accordance with literature values.^[466,469,484] However, the carbonyl stretching frequencies were found to be solvent-dependent (Table 4.2). This was also observed for the Fp^- anion and can likewise be attributed to competing tight, contact and solvent separated ion pairs (Figure 4.4).^[455,489] The ratio of the different species in solution and hence the exact positions of the IR bands depend on the polarity of the solvent. ^1H and ^{13}C NMR data of KRp in CD_3CN and $\text{DMSO}-d_6$ are included as well in Table 4.2. In addition to this, the table also contains ^{13}C NMR chemical shifts for the CO and Cp groups obtained from solid-state ^{13}C magic angle spinning (MAS) NMR measurements.

With the pure compound in hand, also the electrochemical properties of KRp were reinvestigated. For this purpose cyclic voltammetry measurements were conducted in a glovebox with a Metrohm Autolab PGSTAT101 potentiostat using platinum electrodes. The measurements were performed in 0.1 M NBu_4PF_6 solutions. After the measurement, decamethylferrocene was added as internal standard and the redox potentials were referenced *vs.* the $\text{FeCp}_2/\text{FeCp}_2^+$ (Fc/Fc^+) redox couple.^[342] Figure 4.5 (a) depicts the cyclic voltammogram of KRp which exhibits an irreversible oxidation at a peak potential E_p^{ox} of -1.04 V, a value very close to the literature value (-1.06 V).^[458]

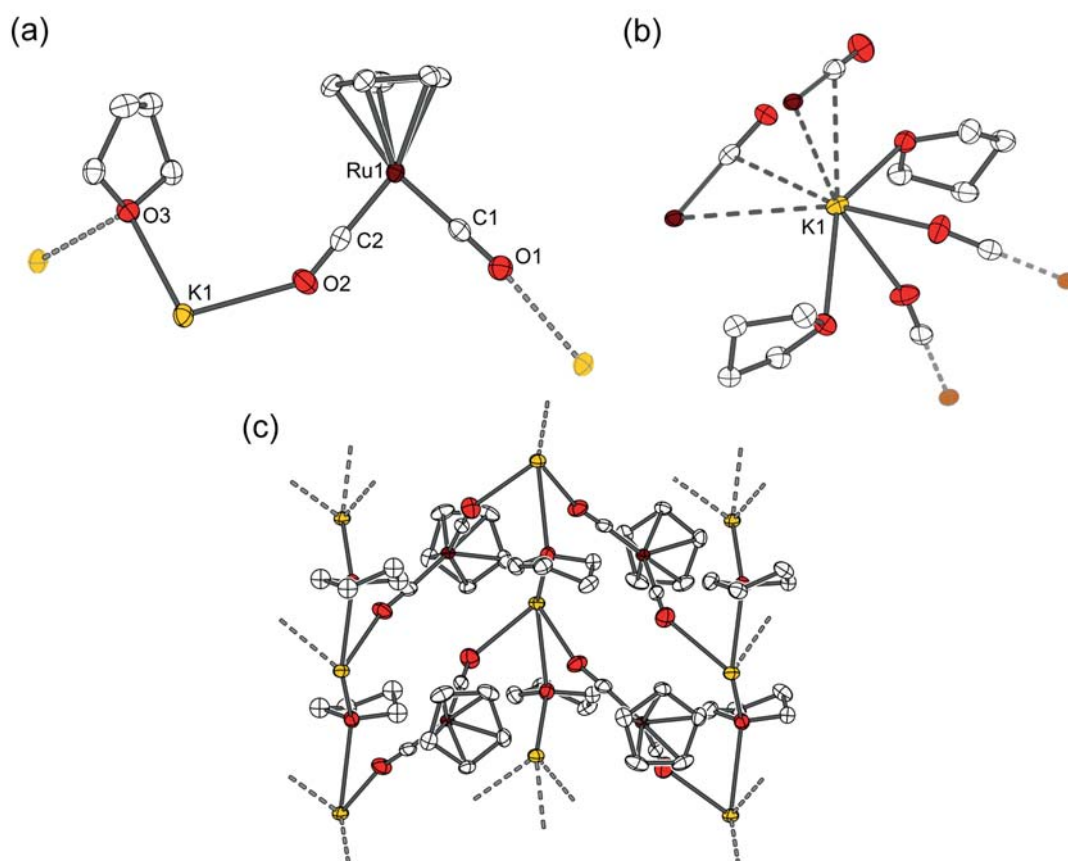


Figure 4.3. (a) Molecular structure of **KRp** · THF, (b) {4 + 4} coordination environment of the potassium ions and (c) packing diagram showing the cross-linking of the polymeric chains. Thermal displacement ellipsoids are given at 50% probability and hydrogen atoms are omitted for clarity. Selected bond length [Å] and angles [°]: Ru1–C1 1.826(2), C1–O1 1.175(3), O1–K1 2.754(2), Ru1–C2 1.818(2), C2–O2 1.179(3), O2–K1 2.737(2), K1–O3 2.861(2), O3–K1 2.848(2); K1–O1–C1 164.5(2), O1–C1–Ru1 177.3(2), C1–Ru1–C2 87.4(1), Ru1–C2–O2 179.8(2), C2–O2–K1 142.5(2), O2–K1–O3 93.97(5), K1–O3–K1 107.6(1).

Table 4.2: Spectroscopic properties of **KRp**.

method	solvent	value
IR ($\tilde{\nu}(\text{CO})$, cm^{-1})	MeCN	1888 (vs), 1803 (vs)
	THF	1895 (vs), 1812 (vs)
	DMSO	1895 (vs), 1812 (vs)
^1H NMR (δ , ppm)	CD_3CN	4.83 (Cp)
	$\text{DMSO-}d_6$	4.68 (Cp)
^{13}C NMR (δ , ppm)	CD_3CN	216 (CO), 80 (Cp)
	$\text{DMSO-}d_6$	215 (CO), 80 (Cp)
	solid	218 (CO), 87 (Cp)

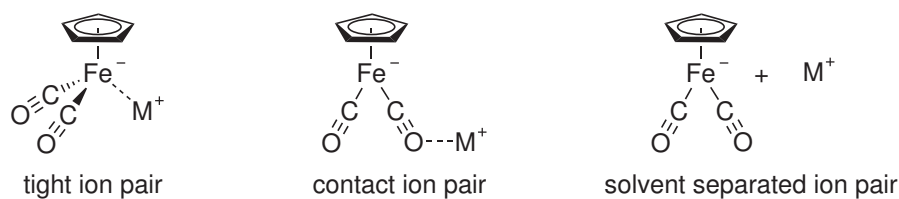


Figure 4.4. Types of ion-pairing for the Fp^- anion ($\text{M} = \text{alkali metal}$).^[455,489]

Solution state UV/Vis spectra of KRp were recorded using sealable quartz cuvettes after preparation of a THF solution of the metalate in a glovebox directly before the measurement. As the absorptions were only visible as shoulders, the spectra were transformed into energy plots and fitted with Gaussian functions using the *Fityk* program.^[490] Figure 4.5 (b) shows the recorded spectrum at a $0.7 \mu\text{M}$ concentration. Deconvolution of the spectrum gave three absorptions at 242 ($\epsilon = 3200 \text{ L mol}^{-1} \text{ cm}^{-1}$), 281 ($\epsilon = 4300 \text{ L mol}^{-1} \text{ cm}^{-1}$) and 331 nm ($\epsilon = 1200 \text{ L mol}^{-1} \text{ cm}^{-1}$).

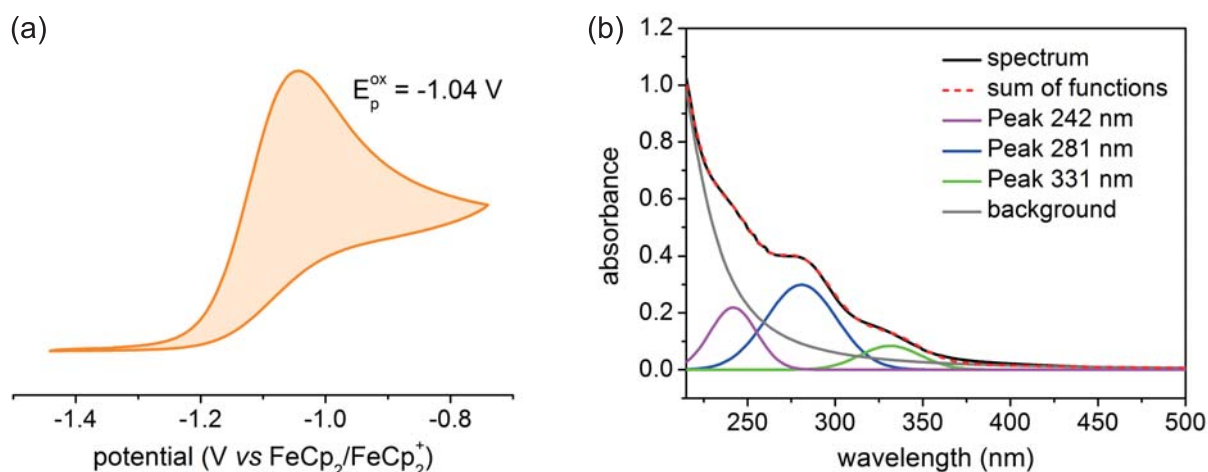


Figure 4.5. (a) Cyclic voltammogram of KRp . Measurements were performed in $0.1 \text{ M NBU}_4\text{PF}_6$ solutions (MeCN) at a scan rate of 100 mV s^{-1} and the peak potential was referenced *vs.* the Fc/Fc^+ redox couple. (b) UV/Vis spectrum of KRp in THF showing three absorptions at 242, 281 and 331 nm. Absorption bands were obtained after deconvolution with the *Fityk* program.^[490]

4.3 Rs – A Metalate with Interesting Properties

Besides yielding the metalate KRp , a typical reaction of Rp_2 and $\text{K}[\text{HB}(\text{sec-Bu})_3]$ as described above also gave a black solid (Rs).^[473] For further characterization, the unknown compound was separated by filtration, washed with THF and MeCN, and finally dried *in vacuo*. However, the chemical characterization of this second product was hampered by its insolubility in commonly used organic solvents, and even the

addition of dibenzo-18-crown-6 – regardless whether added after isolation of the compound or prior to its synthesis – could not contribute to a better solubility of **Rs**. Only when very polar solvents such as DMF or DMSO were used, partial dissolution of the compound giving black to dark purple solutions could be achieved. Despite extensive efforts, no crystals suitable for X-ray crystallography could be obtained. Crystallization attempts with various combinations of solvents solely yielded amorphous material. Only when degassed water was used to dissolve the black material, single crystals could be identified in the dark solutions. However, this turned out to be the ruthenium dimer **Rp**₂. This finding demonstrates that the “CpRu(CO)₂” unit is in some form preserved in **Rs**. Decomposition of the compound under aqueous conditions partially recovers its chemical precursor **Rp**₂, presumably after protonation of the metalate and intermediate formation of **HRp**.

4.3.1 IR Spectroscopy

The IR spectra of **Rs** dissolved in DMSO, DMF and MeOH in comparison with the spectrum of **KRp** in DMSO are depicted in Figure 4.6 (a). From these spectra it is clear that DMSO and DMF solutions of the black solid show in principle the same two CO stretching vibrations as **KRp** ($\tilde{\nu}_{\text{CO}} = 1833$ and 1795 cm⁻¹). However, the two bands protrude more or less from broad bands centered at those positions. The fact that the sharp bands are more pronounced in the more polar solvent DMSO suggests that an association phenomenon is the reason for the unusual bandshapes of the CO stretching vibrations. The degree of association strongly depends on the polarity of the solvent. When protic MeOH is used as the solvent, the black material dissolves completely and a yellow solution is obtained. The IR spectrum of this solution displays two significantly

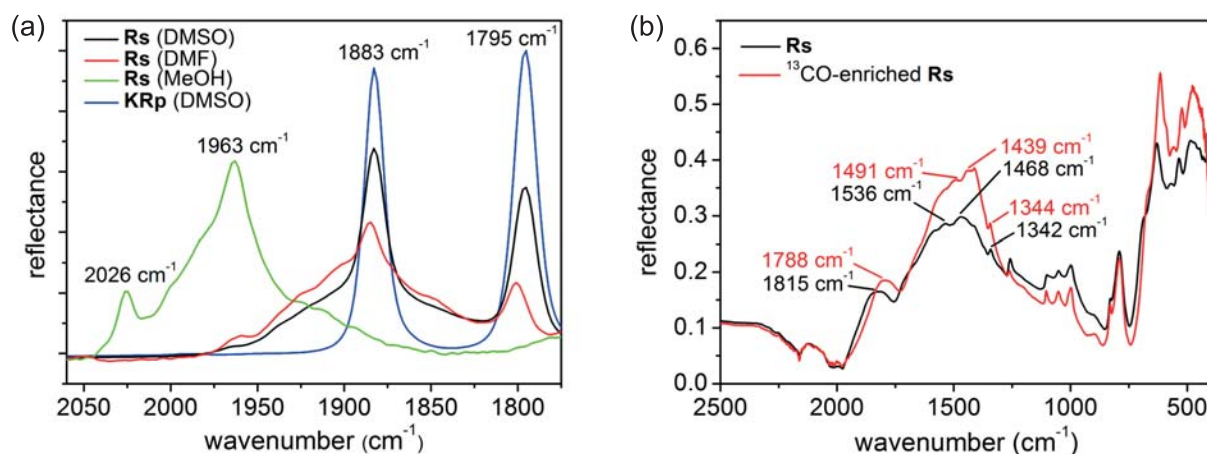


Figure 4.6. (a) Comparison of the IR spectrum of **KRp** in DMSO (blue) and the spectra of **Rs** in DMSO (black), DMF (red) and MeOH (green). Values for the measured reflectance are not comparable since a variable scaling parameter was applied. (b) ATR IR spectra of the **Rs** (black) and the ¹³CO-enriched black solid (red).

shifted IR bands at 2026 and 1963 cm^{-1} which indicates that a reaction took place. Similar bands have been observed for the ruthenium hydride **HRp**,^[461,464,491,492] but in this case the bands are highly asymmetric and especially the band at 1963 cm^{-1} has broad tails. Nevertheless, a protonation of the metalate can be assumed as a reason for the appearance of the spectrum.

Figure 4.6 (b) shows attenuated total reflectance (ATR) spectra of the black solid **Rs** and the ^{13}C O-enriched analog (preparation see section 4.2.2). Surprisingly, the spectra feature no distinct CO stretching vibrations but rather broad bands centered at 1815 and 1500 cm^{-1} . However, the fact that these broad bands are shifted to lower wavenumbers in the case of the ^{13}C O-enriched black solid indicates that they indeed have significant contributions from CO stretches. Nevertheless, the frequencies and band shapes are unusual for metal carbonyls although CO stretching frequencies as low as 1612 cm^{-1} have been reported before for a ruthenium cluster.^[493] In a special instance bands around 1445 cm^{-1} have been assigned to a ruthenium-bound $\mu_4\text{-}\eta^2\text{-CO}$ ligand.^[494] The present case of low energy stretching vibrations suggests the existence of bridging CO ligands, $\mu\text{-CO}$, $\mu_3\text{-CO}$ and/or $\eta^2\text{-bonded CO}$. Unfortunately, it was not possible to measure Raman spectra of the compound at different excitation wavelength in order to gain more information about the nature of the CO ligands. Possible reasons for this could be the unfavorable morphology of the solid sample and/or damage of the material caused by the laser irradiation.

4.3.2 Mass Spectrometry and UV/Vis Spectroscopy

The IR measurements described above suggested that **Rs** could probably be some kind of polymeric form of **KRp**. However, due to its poor solubility as well as due to ionization problems, only limited conclusions could be drawn from mass spectrometry. ESI measurements of a DMSO solution of the black solid diluted with MeCN gave no meaningful signals although the measurements were performed maintaining moisture- and oxygen-free conditions. Likewise, field desorption (FD) and matrix-assisted laser desorption/ionization (MALDI) mass spectrometry turned out to be unsuitable for the characterization of **Rs**. Electron ionization (EI) mass spectrometry performed at temperatures above 370 $^{\circ}\text{C}$ and very low pressures was also not successful in effecting the sufficient ionization of the compound. Very weak signals with isotope patterns characteristic for ruthenium could be observed around $m/z = 700$, however an assignment of the signals was not possible and even under harsh conditions most of the compound remained unaffected.

Solid-state UV/Vis spectroscopy on the other hand proved to be a valuable method to compare **KRp** and **Rs**. A dissolution of the compound was not necessary and hence a modification of the compound's structure by interactions with the solvent could be excluded. Solid-state UV/Vis spectra of **KRp** and **Rs** were recorded with a Varian Cary 5000 UV/Vis/NIR instrument equipped with a Praying Mantis sampling kit for solid

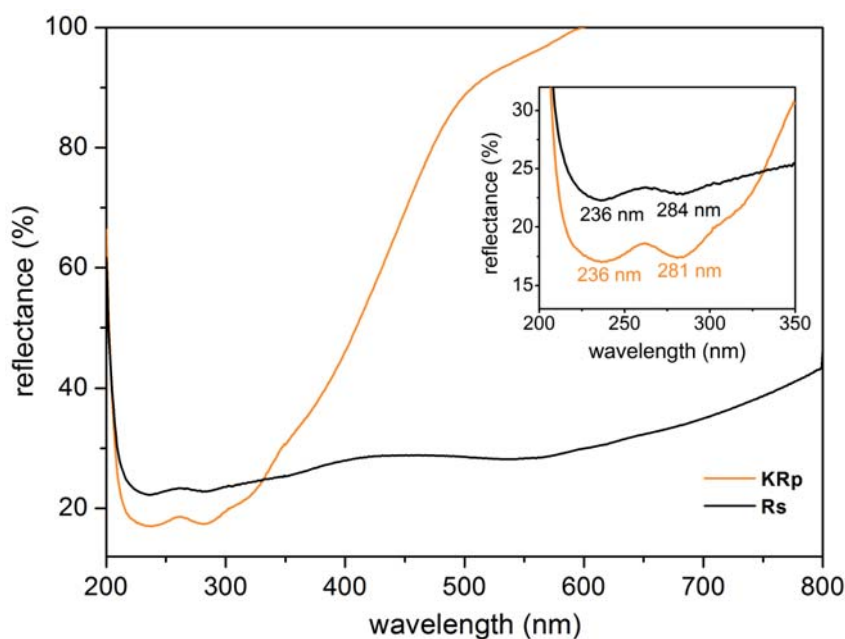


Figure 4.7. Solid-state UV/Vis spectrum of **KRp** (orange line) and the black solid **Rs** (black line). The absorptions in the UV region are similar and also comparable to the solution spectra of **KRp**.

samples. Figure 4.7 shows the solid-state UV/Vis spectrum of **KRp** and the black solid **Rs**. From the continuous absorption over a large wavelengths range, two absorptions at 236 and 284 nm are clearly discernible. These two absorptions are very similar to the absorptions found for **KRp** in the solid state (236 and 281 nm) and are similar to the absorptions at 242 and 281 nm observed in THF solution spectra of **KRp** (see part (b) of Figure 4.5). This finding demonstrates that indeed the black solid might be composed of **Rp⁻** units with UV/Vis transitions similar to the monomeric metalate.

4.3.3 Solid-State ¹³C MAS NMR Spectroscopy

Compound **Rs** was examined by means of NMR spectroscopy. However, the solution spectra in DMSO-*d*₆ provided no clear picture of the black solid's structure. In addition to the signal for the Cp ring of **KRp** ($\delta = 4.68$ ppm) only weak and partially broad signals were observed in the region between 5.35 and 4.73 ppm of the ¹H NMR spectrum. The ¹³C NMR spectrum exclusively showed signals characteristic of the carbonyl carbon atom ($\delta = 215$ ppm) and the Cp ring ($\delta = 80$ ppm) of **KRp**.

As a consequence of the limited information one could obtain from the solution-state NMR spectra of the black material, solid-state ¹³C MAS NMR spectra at different spinning rates were recorded. Unfortunately, the spectra did not permit a quantification of the signals as they were relatively broad and difficult to integrate. Nevertheless, the spectra clearly showed that at least two different kinds of CO ligands were present in the compound. In order to further examine the material, a ¹³CO-enriched sample was

prepared (see section 4.2.2) and the measurements were repeated. ^{13}C cross-polarization MAS (CP/MAS) NMR spectra at different spinning rates obtained from these measurements are depicted in Figure 4.8. As it is usually observed in solid-state NMR spectroscopy, spinning sidebands occur at both sides of a signal caused by an NMR active nucleus. The distance between the sideband and the signal is equivalent to multiples of the spinning rate of the sample. For this reason, the position of a spinning sideband in the spectrum varies at different spinning rates while the characteristic signals of a compound remain static. Consequently, the resonances induced by the carbon atoms of the black solid can be easily assigned (see Figure 4.8).

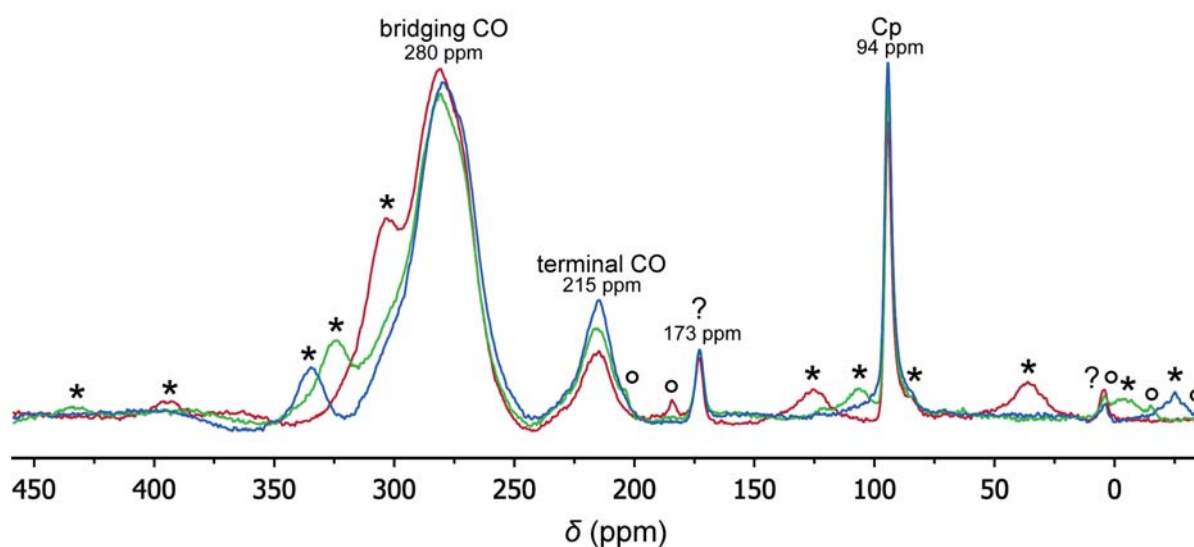


Figure 4.8. ^{13}C CP/MAS NMR spectra of ^{13}CO -enriched **Rs** at 9 kHz (red), 11 kHz (green) and 12 kHz (blue) spinning rate showing bridging (280 ppm) and terminal CO molecules (215 ppm). First and second order sidebands of the terminal CO signal are marked with an asterisk (*), first order sidebands of the Cp ring (94 ppm) with a circle (o). The two signals marked with a question mark could not yet be assigned, but are presumably due to impurities.

The spectra clearly establish that Cp rings ($\delta = 94$ ppm) as well as two different CO ligands ($\delta = 215$ and 280 ppm) are present in the compound. The signal at 215 ppm can be attributed to a terminal CO ligand, while the resonance at 280 ppm can be assigned to bridging or η_2 -bonded CO molecules. The terminal CO molecules in **Rs** show a larger chemical shift anisotropy (CSA) than the bridging molecules, and hence more intensity is distributed into the spinning sidebands of this signal. Similar observations have been made before for CO ligands in other metal complexes.^[495–499] In contrast to the observations for the bridging COs, even second-order spinning sidebands belonging to the terminal CO ligands can be identified.

In the spectra also a sharp but weak signal at 173 ppm can be observed. The origin of this signal could not be resolved, however its varying intensity in different measurements hints at an impurity – possibly residual solvent – being the source of the

signal. Nevertheless, it cannot be fully excluded that a third CO species is present in the black solid giving rise to the signal at 173 ppm. Although the upfield chemical shift is rather unusual for CO ligands, the signal exhibits a gain in intensity from the unlabeled to the ^{13}C -enriched compound. Although quantification was difficult because of problematic integration in the unlabeled compound, this gain in intensity seems to be lower than in the case of the bridging and terminal COs. Another very weak signal at 4 ppm can most likely be attributed to vacuum grease which obviously is present as an impurity as well.

In comparison with the spectra for **Rs**, the ^{13}C CP/MAS spectra of **KRp** measured at spinning rates of 9 and 11 kHz (Figure 4.9) feature only two signals at 218 and 87 ppm. The resonances can be attributed to the terminal CO ligands and the Cp ring, respectively. Interestingly, all signals in the spectra of **KRp** are significantly sharper than the signals observed for the black solid in Figure 4.8. In contrast to this, particularly the CO signals of **Rs** are extremely broad. Most probably this observation can be explained by the crystalline nature of the **KRp** sample. However, it cannot be fully excluded that the broad NMR signals in case of the black solid originate from paramagnetic impurities, anisotropic motion or incomplete scrambling of the carbonyl ligands.

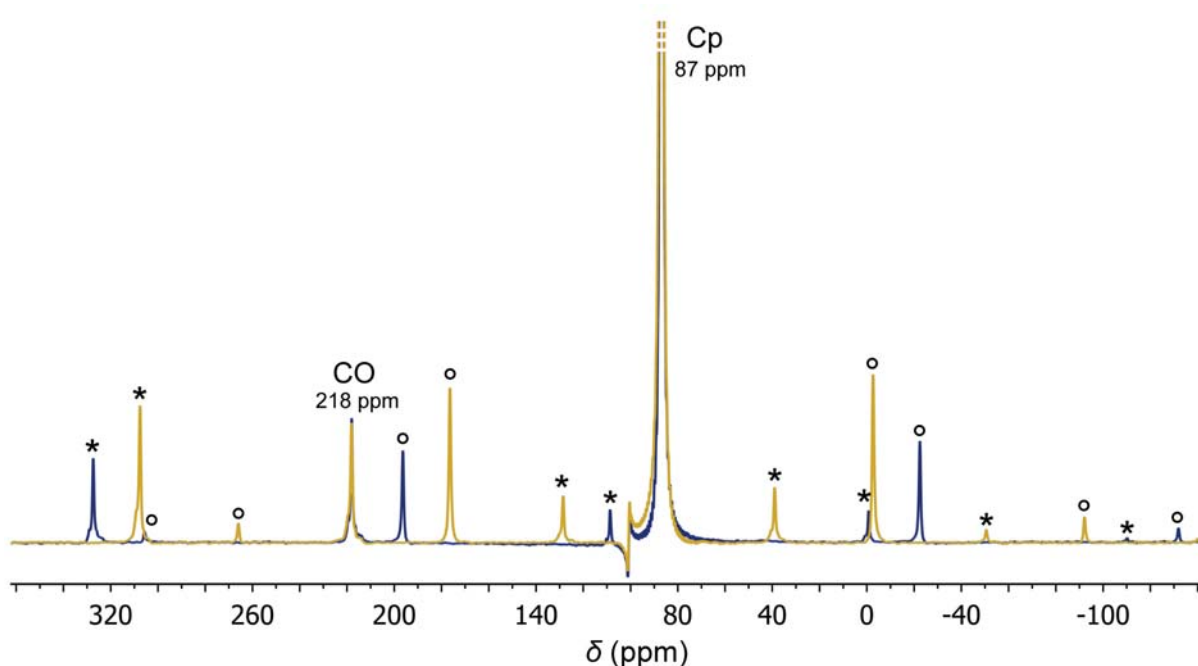


Figure 4.9. ^{13}C CP/MAS NMR spectra of crystalline **KRp** at 9 kHz (yellow) and 11 kHz (blue) spinning rate showing terminal CO molecules (218 ppm) and the Cp ring (87 ppm). Spinning sidebands of the terminal CO signal are marked with an asterisk (*), sidebands of the Cp ring with a circle (o).

The ratio between bridging and terminal CO molecules in the black solid was determined by integration of a ^{13}C MAS spectrum of the ^{13}C -enriched black solid which was acquired by a direct excitation method. The spectrum at a spinning rate of 12 kHz which is depicted in Figure 4.10 allows for integration and subsequent determination

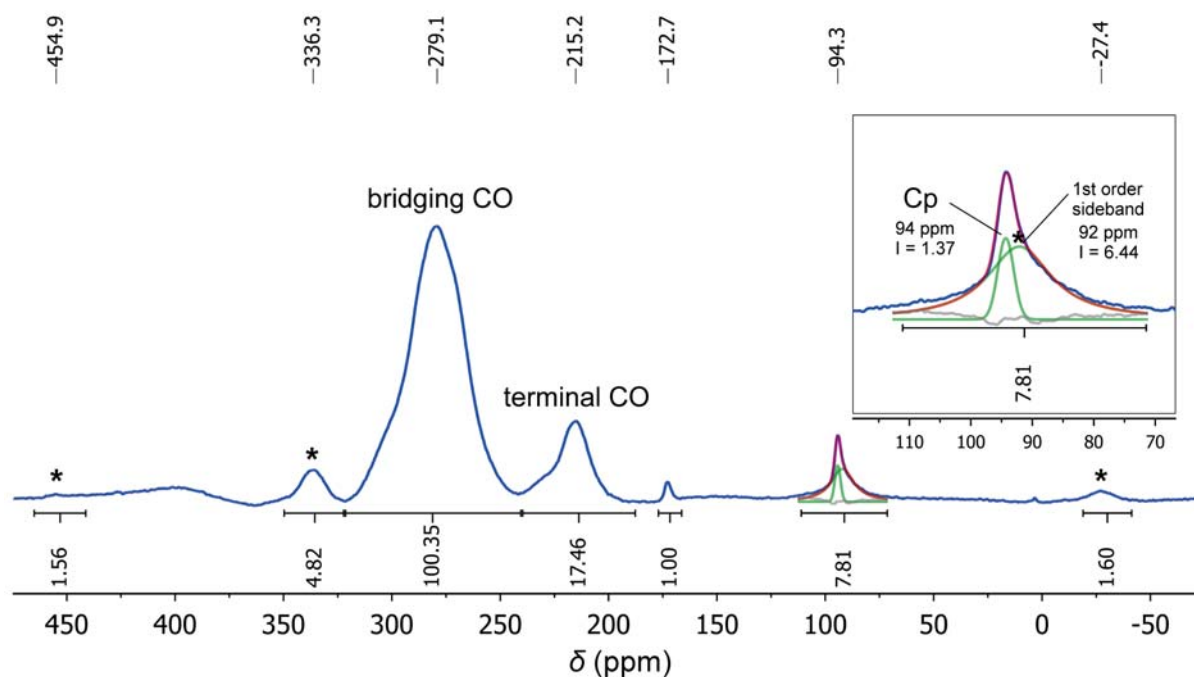


Figure 4.10. ^{13}C MAS NMR spectra of ^{13}CO -enriched **Rs** at 12 kHz spinning rate. The acquisition was performed using a direct excitation method. Fitting of the peak at 94 ppm was necessary because overlapping of the Cp signal and the first order spinning sideband of the terminal CO signal occurred. The calculated ratio of bridging and terminal COs is 3:1.

of a ratio of the CO signals as – unlike in the case of cross-polarization spectra – the intensities of the signals are independent from the chemical environment of the resonating nucleus. When integrating the signals, the intensities of the spinning sidebands of the terminal CO signal were taken into account. The integral of the upfield first order spinning sideband of the terminal CO signal overlapped considerably with the resonance for the Cp ring. Therefore it was necessary to estimate its intensity by fitting two Gaussian functions to the peak at 94 ppm (sideband and Cp signal). For **Rs**, a ratio of 3.1:1.0 for the bridging *vs.* the terminal CO molecules was calculated. Furthermore, Figure 4.10 also demonstrates that the intensity of the peaks at 173 (impurity?) and 94 ppm (Cp) decrease relative to the CO signals, hence they profit from the cross polarization method significantly more than bridging and terminal CO signals. This indicates that protons can be found in the vicinity of the respective carbon atoms.

4.3.4 Elemental Analysis and Bulk Morphology

In order to gain more insights into the composition of **Rs**, elemental analyses of the black material were performed by various methods. While the experimentally determined values for **KRp** totally confirmed the expectations (Calcd.: C 32.18, H 1.93; Found: C 32.17, H 2.05), standard CHN analysis of the black solid revealed a surprisingly low carbon content. Repeated measurements gave reproducible contents of carbon, hydrogen and nitrogen with the following mean values (%): C 23.72, H 1.54, N 0.49. The low content of nitrogen can be traced back to residual amounts of the solvent MeCN as a batch of **Rs** where the raw product was not washed with MeCN did not contain any nitrogen impurities. However, as became clear from solid-state NMR measurements, other impurities were present in this batch of the black material. The traces of MeCN could not be removed by prolonged drying of the compound *in vacuo*. The content of ruthenium was determined photometrically after pressure digestion with HNO₃ to be 42.26 %. Furthermore, ICP-OES measurements revealed a potassium content of 13.18 %.

Additional data on the elemental composition of the black material were obtained by means of a wavelength dispersive electron microprobe analysis (EMPA). By this method, detailed information on the local elemental composition can be obtained by analyzing the element specific X-rays which are emitted when a beam of accelerated electrons is focused on the surface of a solid material. Despite the difficult bulk morphology of the sample (details see below), reproducible values for the Ru, K and O content could be obtained. The measurements largely confirmed the elemental analysis data obtained before by other methods since the absolute values of Ru and K were found to be 43.2 and 13.0 %, respectively. Furthermore, an average atomic ratio Ru:K:O of 4:3:8 could be deduced based on quantification at different positions of the sample using a slightly defocussed beam of 5 μm diameter. Besides the elements Ru, K and O also a low content of Si (0.7 %) was detected in the sample. Most likely, this value can be attributed to impurities, e. g. silicon grease. Recalculating the raw data using the *CITZAF* program^[500] and assuming that the unassigned content is carbon, leads to minor deviations in the determined elemental composition. Here, the 4:3 ratio of Ru:K is even more evident than without taking carbon into account. A direct determination of the carbon content was not possible due to the inadequate surface quality of the powdered sample which did not fulfill the requirements for a quantitative light element analysis. Details on the EMPA measurements can be found in the Appendix. Taking together all experimentally determined values, 96.6 % of the elemental composition has been assigned.

In addition to performing quantitative analyses, an electron microprobe can also function like a scanning electron microscope (SEM) and obtain highly magnified secondary- and backscattered-electron images of a sample. Figure 4.11 depicts a selection of images of **Rs** acquired with the electron microprobe. The pictures show that the sample is heterogeneous and composed of different areas. Darker parts as well as lighter spots

are visible in the picture generated by the secondary electron imaging technique (SEI) in Figure 4.11 (a) and in the image obtained from the backscattered electrons (BSE, Figure 4.11 (b)). With a very focussed beam, slight differences in the composition of the different areas can be detected. The ruthenium content of the lighter domains seems to be a little higher. Furthermore, rather thin areas exist alongside with more granular structures. However, the elemental composition of these areas seems to be identical. The granular structure of the compound which can be well recognized in Figure 4.11 (c) and (d) possibly hints at a clustering of the individual molecular fragments of the compound. Obviously, aggregates of different size (a few micrometers and below) exist.

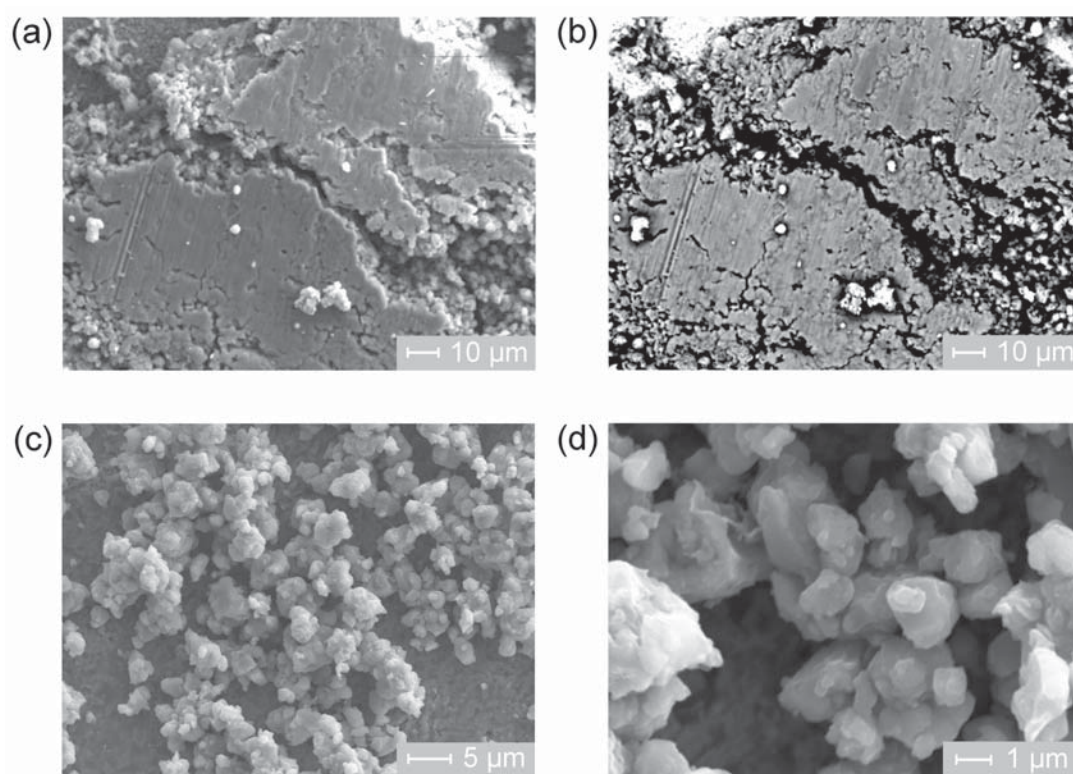


Figure 4.11. Images of R_s acquired with the electron microprobe. (a) SEI and (b) BSE images of the C-coated compound; (c) and (d): SEI images of an Au-coated sample.

4.3.5 Conclusion

It has been demonstrated that besides **KRp** a second product emerges from the reductive cleavage of **Rp₂** with $\text{K}[\text{HB}(\text{sec-Bu})_3]$. The black material **Rs** features an average atomic ratio Ru:K:O of 4:3:8 which shows that, in the black solid as well as in **KRp**, each ruthenium atom is coordinated by two CO molecules on average. As has been revealed by ^{13}C MAS NMR spectroscopy of a ^{13}C -enriched sample, these CO molecules are not only found as terminal ligands but three out of four CO molecules adopt a bridging ($\mu\text{-CO}$ or $\mu_3\text{-CO}$) and/or η^2 binding mode. Besides providing valuable information on the elemental composition of the compound, electron microprobe analysis could also show that **Rs** features a granular structure consisting of particles with variable size. This phenomenon might also offer an explanation for the unusual properties of the material. As both the ATR IR spectrum and the ^{13}C MAS NMR spectrum exhibit relatively broad signals for the CO molecules, one could assume a distribution of signals that varies with the size of the particles. Furthermore, the position and shape of the bands in the ATR IR spectrum suggest strong ion-pairing effects. The IR spectra in solution corroborate this estimation since they show a pronounced dependence on the polarity of the solvent, and hence the degree of association. In conclusion, the presented data on **Rs** suggest a polymeric or clusterlike structure in which the “ $\text{CpRu}(\text{CO})_2$ ” unit is in some form preserved. In fact, it has been noticed earlier that the accumulation of negative charge in ruthenium carbonyls might lead to a rearrangement giving bridging carbonyl ligands: Inkrott and Shore suggested that this might represent an efficient way to average the charge distribution in highly charged cluster compounds.^[501] The present case seems to argue in favor of this hypothesis, but the exact molecular structure of the obtained black solid still remains unclear. However, it is clear that a metalate has been synthesized which can be protonated and thus might possibly function as a Lewis base in the heterolytic cleavage of dihydrogen.

4.4 Summary and Outlook

In this chapter the syntheses and properties of different transition metal complexes featuring Lewis basicity have been described. Of particular interest were the carbonyl metalates **KFp** and **KRp** which possess beneficial properties for the planned reactions with H_2 like a highly Lewis basic character and moderate oxidizability. Reinvestigation of the synthesis of **KRp** brought to light a novel, presumably polymeric Cp/Ru/CO material (**Rs**) which shows interesting properties and can react as a Lewis base as well. With **KFp**, **KRp** and **Rs**, three transition metal Lewis bases are now available that could possibly work in concert with appropriate imidazolinium ions to achieve the heterolytic splitting of dihydrogen. The following chapter deals with the reactivities observed when combining the transition metal Lewis bases with the synthesized imidazolinium

ions in the hope of generating a novel type of frustrated Lewis pairs. Subsequently, reactions with dihydrogen will be discussed.

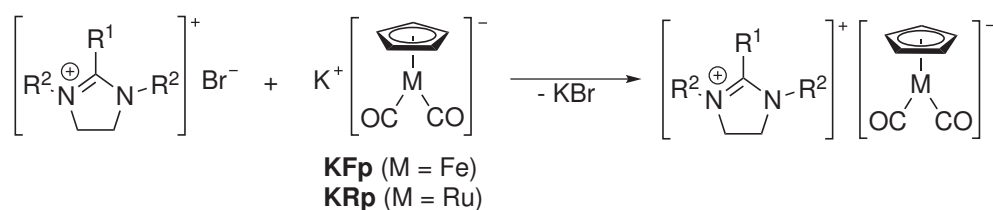
5

Transition Metal Frustrated Lewis Pairs

Abstract This chapter focuses on the attempts to combine the hydride acceptor molecules described in chapter 2 and the metal carbonylate complexes treated in chapter 4 in order to synthesize novel transition metal-based frustrated Lewis pairs. By this, it is hoped to expand the scope of frustrated Lewis pair (FLP) chemistry to also include H₂-splitting systems which resemble the active site of the naturally occurring [Fe] hydrogenase enzyme. While most of the investigated combinations of imidazolium ions and carbonyl metalates showed undesired reactivities like electron transfer and nucleophilic substitution reactions, the formation of the anticipated Lewis pairs could indeed be observed in certain cases. However, these Lewis pairs did not show FLP-type reactivities and can thus not be called “frustrated”. On the contrary, a combination involving the presumably polymeric metalate **Rs** (see chapter 4.3) was found capable of cleaving the dihydrogen molecule. The system mimics the natural enzyme [Fe] hydrogenase in terms of its reactivity and thus provides inspiration for the development of future H₂ activation catalysts.

5.1 Synthesis of Transition Metal Frustrated Lewis Pairs

The synthesis of the targeted transition metal frustrated Lewis pairs was conducted by combining the imidazolium salts with the transition metal complexes according to the following general procedure: To a mixture of the respective imidazolium salt and an appropriate solvent (usually MeCN or chlorobenzene) a stoichiometric amount of the transition metal Lewis base was added in small portions and the reaction mixture was stirred at room temperature. By this means, the carbonyl metalates **KFp** and **KRp** presented in chapter 4 should in principle yield the desired Lewis pairs *via* a salt metathesis reaction. In theory, the simultaneously formed potassium bromide can then be separated by filtration (Scheme 5.1).

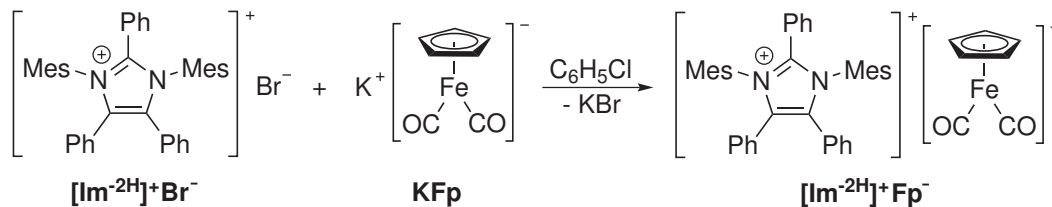


Scheme 5.1. Synthesis of transition metal Lewis pairs based on imidazolium ions and the carbonyl metalates **Fp**[−] (M = Fe) and **Rp**[−] (M = Ru).

First experiences with this relatively straightforward approach were already made in the preliminary stages of this project where it could be shown that imidazolium salt **[Im^{−2H}]⁺Br[−]** (see section 2.1.1) reacted in a salt metathesis reaction yielding the compound **[Im^{−2H}]⁺Fp[−]**. However, it was also demonstrated that the imidazolium ion was not reactive enough to achieve the activation of substrates like dihydrogen. In contrast to this, the formation of transition metal Lewis pairs turned out to be more complicated in the case of the imidazolium ions synthesized in the course of this work since undesired reactivities were encountered. The observed reactions mainly involved nucleophilic substitution and electron transfer reactions between the two components of the Lewis pair. Only in the case of imidazolium ions **PhMesIm⁺** and **TolMesIm⁺** no undesired reactions were encountered. Unfortunately, like the compound **[Im^{−2H}]⁺Fp[−]**, these Lewis pairs did also not show any reactivity towards H₂ or other substrates and can thus not be called “frustrated” in the original sense. This section will first describe – as a proof of principle for the salt metathesis reaction – the experiences made with the imidazolium-based Lewis pair **[Im^{−2H}]⁺Fp[−]** before discussing the spectroscopic properties of imidazolium-based Lewis pairs lacking the characteristic reactivities of FLPs. The following sections will then focus on matters of reactivity associated with other imidazolium ions.

5.1.1 Proof of Principle: Synthesis of $[\text{Im}^{-2\text{H}}]^+\text{Fp}^-$

The imidazolium-based Lewis pair $[\text{Im}^{-2\text{H}}]^+\text{Fp}^-$ was synthesized analogous to the procedure for imidazolium ions mentioned above by stirring a suspension of imidazolium salt $[\text{Im}^{-2\text{H}}]^+\text{Br}^-$ and KFp in chlorobenzene (Scheme 5.2). Chlorobenzene is a suitable solvent for this reaction as both starting materials are only scarcely soluble while the Lewis pair readily dissolves in this solvent. The progress of the reaction is reflected in the gradual color change of the solution from colorless to ruby-red. At the same time, precipitation of a colorless solid is observed. Since the precipitate does not exhibit any signal in the IR and NMR spectrum, it can be assumed that KBr has been formed in the reaction. Filtration of the solution and evaporation of the solvent *in vacuo* produces a solid material. NMR and IR data of this compound confirm the impression that the targeted Lewis pair was formed in the reaction. Almost no changes compared to the spectra of the starting materials are visible. Unfortunately, no crystals of the compound suitable for a structure determination *via* X-ray crystallography could be obtained by recrystallization of the material from different combinations of solvents at variable temperatures. Diffusion experiments with chlorobenzene solutions and cyclopentane carried out at $-35\text{ }^\circ\text{C}$ yielded large crystals with edge lengths of up to a few millimeters, but complicated diffraction patterns were observed due to multiple crystal twinning. Despite numerous efforts, the quality of the obtained crystallographic data was not sufficient for a determination of the compound's crystal structure.



Scheme 5.2. Synthesis of Lewis pair $[\text{Im}^{-2\text{H}}]^+\text{Fp}^-$.

The reactivity of the Lewis pair $[\text{Im}^{-2\text{H}}]^+\text{Fp}^-$ towards different substrates was explored by means of NMR spectroscopy. An NMR sample of the compound was pressurized with H_2 (1 bar) after degassing by repeated freeze-thaw cycles, but no reaction was observed in the NMR spectrum. Likewise, other substrates that are known to be activated/cleaved by FLPs such as CO_2 and $\text{THF}^{[23]}$ did not show any reactivity in mixtures with $[\text{Im}^{-2\text{H}}]^+\text{Fp}^-$.

The ruthenium-containing Rp^- salt can be prepared analogously in a reaction of the imidazolium bromide with KRp , but efforts to crystallize the Lewis pair were largely unsuccessful as well. Only in one case very few colorless crystals could be obtained from a hexane filtrate after an attempt to further purify the compound. However, this turned out to be the hydrolysis product 17. The crystal structure of this by-product which presumably is formed by nucleophilic attack of residual amounts of H_2O or OH^- at the C^2 carbon atom of the imidazolium ion and subsequent ring opening, is depicted

in Figure 5.1. While for the imidazolium-based Lewis pairs no reactivity was observed in the NMR experiments with various substrates, the crystal structure might hint at an increased reactivity compared to the imidazolium salt $[\text{Im}^{2\text{H}}]^+\text{Br}^-$ alone which is stable under aqueous conditions (see for example the workup procedure in the Experimental Section).

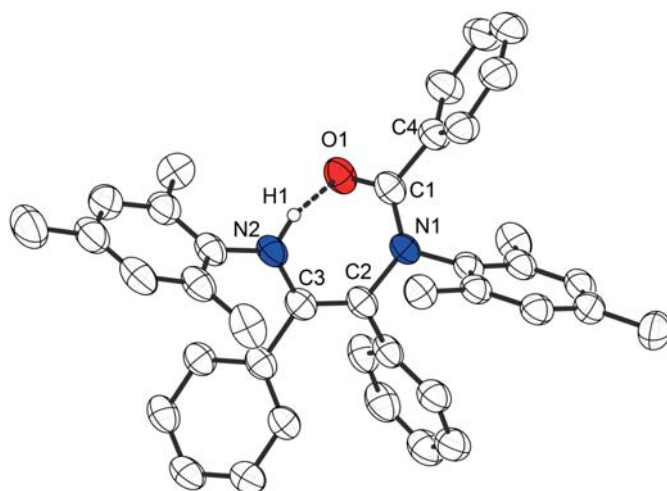


Figure 5.1. Thermal displacement ellipsoids (shown at 50 % probability) of the molecular structure of hydrolysis product **17**. Hydrogen atoms except for the NH hydrogen atom (ball-and-stick representation with a fixed radius of 0.135 Å) are omitted for clarity. Selected bond length [Å] and angles [°]: N1–C1 1.360(3), N1–C2 1.463(2), C1–C4 1.501(2), C1–O1 1.239(2), C2–C3 1.350(3), C3–N2 1.398(2); N1–C1–C2 121.5(2), O1–C1–N1 121.6(2), N2–C3–C2 121.6(2).

5.1.2 Imidazolinium-Based Lewis Pairs Lacking Frustration

As the imidazolium-based Lewis pair $[\text{Im}^{2\text{H}}]^+\text{Fp}^-$ was found to be unreactive towards H_2 and other substrates, the use of imidazolinium ions as hydride acceptor molecules was considered. Due to disruption of the aromatic system and distortion of the heterocyclic ring, a higher reactivity was anticipated for these systems. Unfortunately, most of the systems showed undesired reactions such as nucleophilic substitution and electron transfer reactions between the two components of the Lewis pair and not with the substrate. Exceptions were the combinations consisting of imidazolinium ions **PhMesIm**⁺ and **TolMesIm**⁺ and the metal carbonyl anion **Fp**⁻, as the respective solutions feature NMR and IR spectra reminiscent of the starting materials. However, mixtures of the imidazolinium bromides and **KFp** in CD_3CN showed – after stirring at room temperature and filtration – very broad signals for the imidazolinium protons in the ^1H NMR spectrum. Surprisingly, the resonance of the Cp ring was not affected by this signal broadening. Upon cooling the solution, the signals for the imidazolinium

protons become visible and sharpen as the temperature drops further. The signal broadening seems to be dependent on the solvent as for a second sample when deuterated chlorobenzene was applied as the solvent no broad signals were observed. Figure 5.2 depicts the ^1H NMR spectrum of $\text{PhMesIm}^+\text{Fp}^-$ in CD_3CN at variable temperatures. Only at low temperatures, signals for the imidazolium ion PhMesIm^+ become visible. In contrast to this, the NMR spectrum of the imidazolium bromide $\text{PhMesIm}^+\text{Br}^-$ in CD_3CN does not show an unusual signal broadening. This observation as well as the fact that the resonances of $\text{PhMesIm}^+\text{Fp}^-$ are slightly shifted to higher field ($\Delta\delta = -0.03$ ppm) compared to $\text{PhMesIm}^+\text{Br}^-$ indicate that the Fp^- metalate probably interacts with the imidazolium ion. A possible mechanism for this interaction could be similar to the formation of contact ion pairs between the Fp^- anion and an alkali metal ion (see Figure 4.4 in chapter 4) in which the oxygen atom of the CO ligand interacts with the cation. A comparable interaction of the CO molecule with the Lewis acidic C^2 carbon atom seems conceivable. However, no evidence for this type of interaction could be gathered by means of IR spectroscopy since no significant shift of the CO stretching vibrations between KFp and $\text{PhMesIm}^+\text{Fp}^-$ was observed.

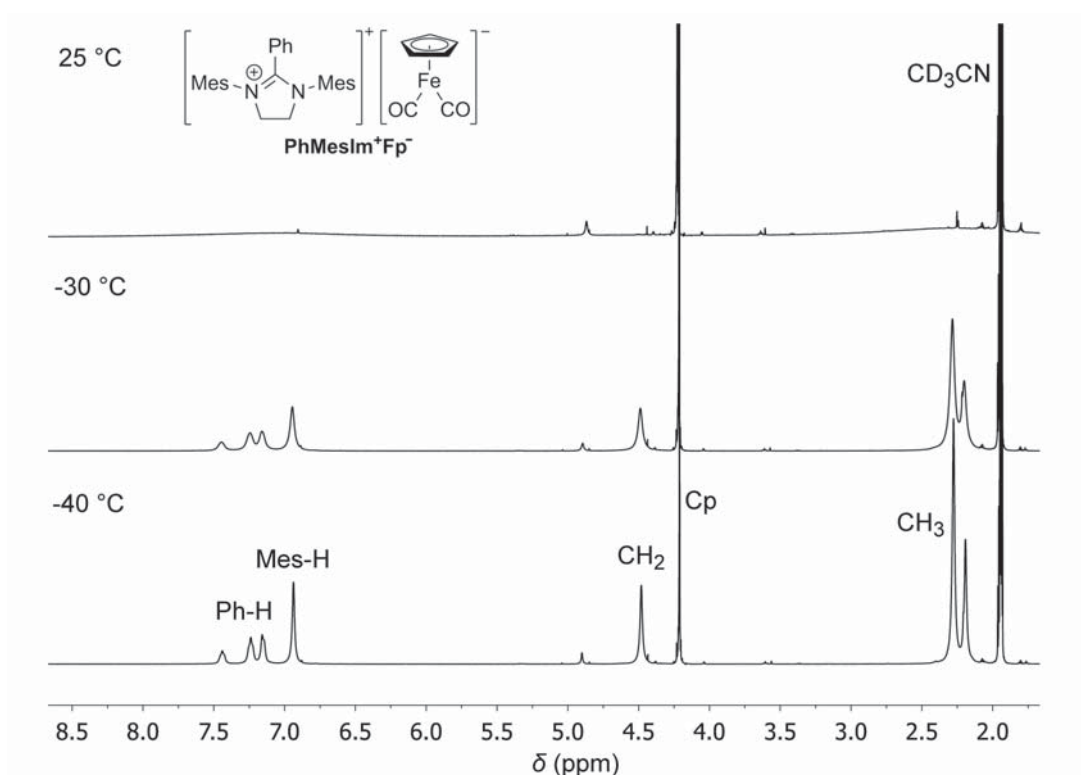


Figure 5.2. ^1H NMR spectra (500 MHz) of $\text{PhMesIm}^+\text{Fp}^-$ in CD_3CN at variable temperatures. The resonances for the imidazolium ion are very broad at room temperature but sharpen upon cooling.

An NMR sample of the compound was pressurized with H_2 (1 bar) and kept at room temperature for several hours. In the subsequently measured ^1H NMR spectrum no changes compared to the sample without dihydrogen were recognized. Likewise, no

reaction with added THF or with HSiEt_3 – a substrate which can be cleaved heterolytically as well – can be observed. Similar observations were made for combinations of the imidazolium ion ToIMesIm^+ and KFp : Also in this case signal broadening in the ^1H NMR spectrum and lacking reactivity towards H_2 (1 bar) was noticed. Despite extensive efforts to crystallize the synthesized imidazolium-based Lewis pairs no crystals suitable for X-ray crystallography could be obtained. In light of the detected dynamics in solution, the crystallization temperature seems to be crucial for obtaining crystals.

5.2 Nucleophilic Substitution Reactions

Most combinations of the synthesized imidazolium ions and carbonyl metalates led to undesired reactions between the two components. A frequently observed phenomenon was the nucleophilic substitution of fluorine atoms forming adducts of the metal carbonylate anion and the imidazolium salt, and/or coupling products. This section will first describe an example comprising the imidazolium salt $\text{C}_6\text{F}_5\text{MesIm}^+\text{Br}^-$ before briefly discussing the mechanistic details of the reaction. After this, investigations on the ruthenium adduct $[\text{Rp-TolFIm}]^+$ will be presented as a second example. Finally, the significance of the observed substitution reactions for the planned reactions with dihydrogen or other substrates will be discussed.

5.2.1 The adduct $[\text{Fp-C}_6\text{F}_4\text{MesIm}]^+$

Contrasting the observations made with imidazolium salt Im^+Fp^- and the two imidazolium salts described above ($\text{PhMesIm}^+\text{Br}^-$ and $\text{ToIMesIm}^+\text{Br}^-$), a rapid color change giving a dark green to black solution was observed when KFp was added to a mixture of imidazolium salt $\text{C}_6\text{F}_5\text{MesIm}^+\text{Br}^-$ and chlorobenzene at -35°C . This already indicated that a reaction took place between the two components since solutions containing the Fp^- anion were mostly red. After stirring at room temperature for 1 h, the mixture was filtered and an IR spectrum of the filtrate was acquired. Compared to the starting material KFp ($\tilde{\nu}(\text{CO}) = 1861$ and 1787 cm^{-1}), a shift of the CO stretching frequencies was recognized. Two bands at 2046 and 1999 cm^{-1} were found characteristic of the reaction product. Besides this, minor amounts of the dimer Fp_2 ($\tilde{\nu}(\text{CO}) = 1997, 1954$ and 1781 cm^{-1} in chlorobenzene) were detected in solution. The product could be isolated by the addition of Et_2O to the solution which induced precipitation of a red solid. An ESI mass spectrum of this compound measured in MeCN under oxygen- and moisture-free conditions (Figure 5.3) revealed that the identity of the product is consistent with the structure of the *para*-substituted imidazolium ion $[\text{Fp-C}_6\text{F}_4\text{MesIm}]^+\text{Br}^-$ (Scheme 5.3).

NMR measurements confirmed the proposed structure, especially as the ^{19}F NMR spectrum featured only two signals at -103 and -135 ppm , respectively. This indicated that

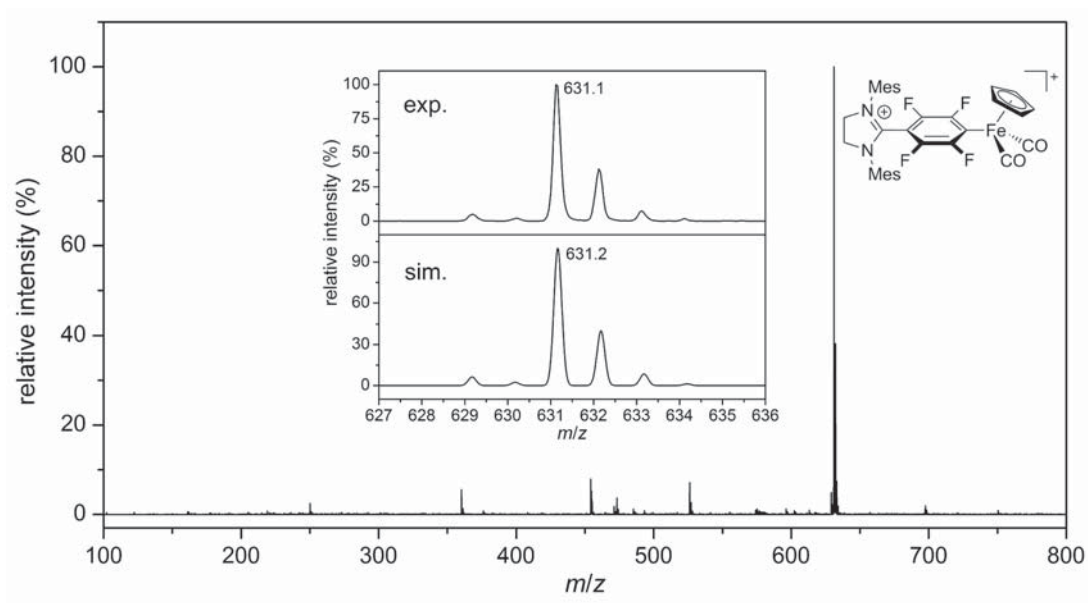
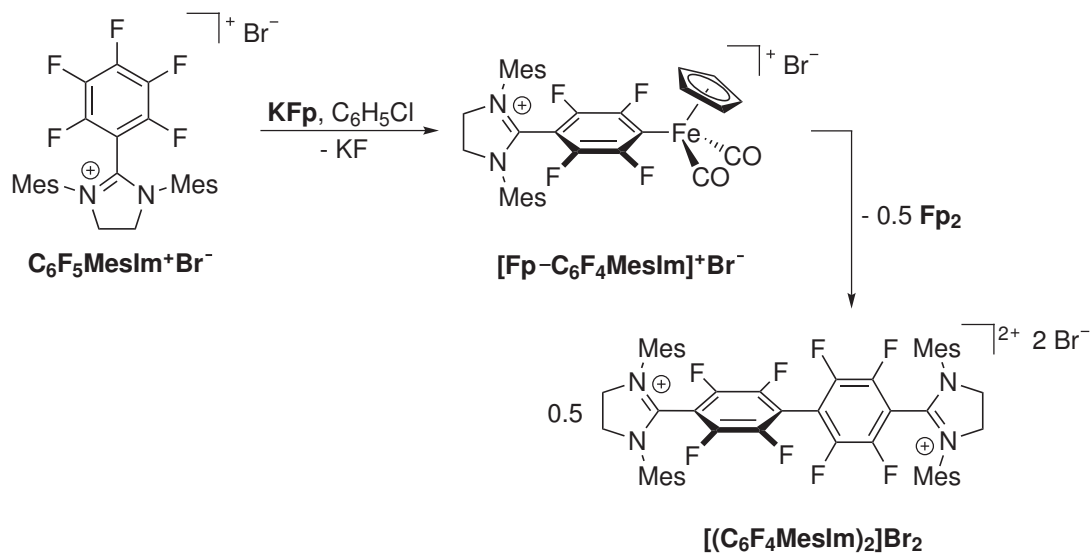


Figure 5.3. Mass spectrum (ESI⁺, MeCN) of the adduct [Fp-C₆F₄MesIm]⁺Br⁻ in the $m/z = 100 - 800$ region. A good correlation between simulated and experimental isotopic distribution patterns (see inset) is found.



Scheme 5.3. Synthesis of substitution product [Fp-C₆F₄MesIm]⁺Br⁻ and consecutive reaction yielding the dimer [(C₆F₄MesIm)₂]Br₂.

the *para*-fluorine atom of the aromatic ring was not present in the product any longer. Unfortunately, no crystals suitable for X-ray crystallography could be obtained by crystallization attempts at variable temperatures. A possible reason for this could be that the adduct is not stable in solution over longer periods of time. This assumption is supported by the fact that precipitation of a slightly reddish compound was observed after some time from solutions of the adduct. The solid was separated by filtration, dissolved in MeCN, and stirred over an excess of KBPh_4 in order to exchange the bromide counterion for BPh_4^- . Et_2O diffusion experiments with MeCN solutions of this compound at room temperature finally produced crystalline material. Structure determination of the crystals by means of X-ray crystallography could confirm that a coupling reaction producing the dication $[(\text{C}_6\text{F}_4\text{MesIm})_2]^{2+}$ took place (Scheme 5.3). However, the quality of the single crystals was insufficient for an accurate refinement and therefore a more thorough interpretation of the crystallographic data was not carried out. Attempts to obtain crystals of better quality were unsuccessful, but NMR and ESI-MS data are in accordance with the proposed structure.

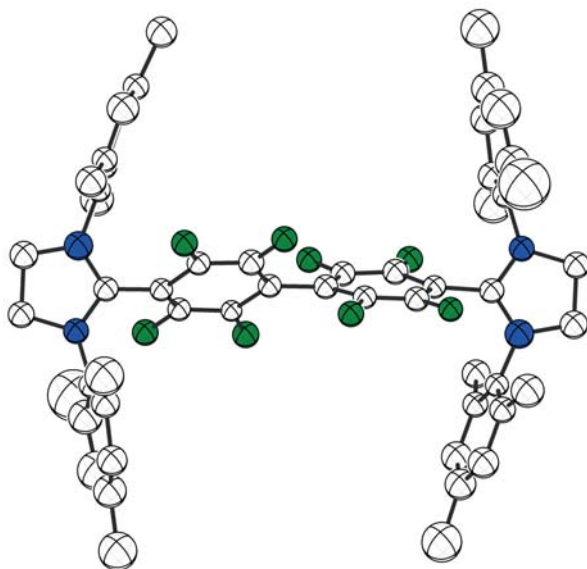
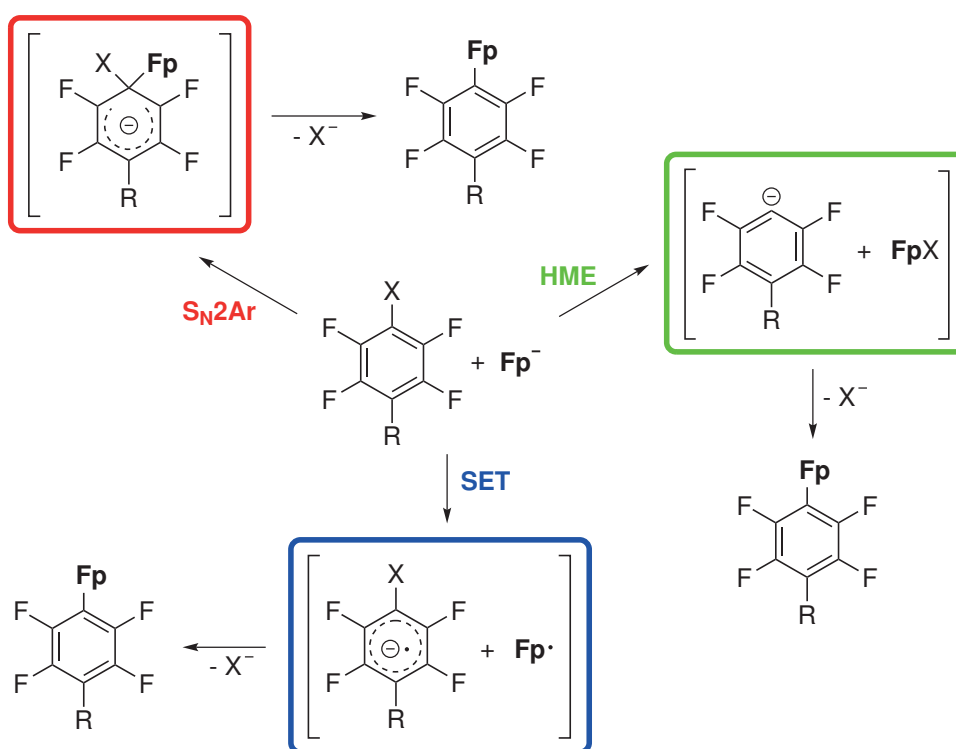


Figure 5.4. Representation with isotropic temperature factors of the molecular structure of the dimer $[(\text{C}_6\text{F}_4\text{MesIm})_2]^{2+}$. The BPh_4^- counteranions as well as hydrogen atoms are omitted for clarity. **Note:** The qualities of the single crystals and collected crystallographic data were insufficient for an accurate refinement. Therefore only a picture is shown as an “educated guess” for the molecular structure of the coupling product. Further interpretation or analysis is inappropriate.

5.2.2 Mechanistic Details

In general, there are three possible reaction pathways that have to be considered when dealing with reactions of metalates and fluorinated/halogenated aromatic compounds (Scheme 5.4). The “classical” mechanism is the nucleophilic aromatic substitution following a bimolecular addition–elimination mechanism (S_N2Ar). Most of the frequently used nucleophiles react with fluorocarbons according to this mechanism.^[502] After addition of a metal-centered nucleophile like the Fp^- anion to the carbon atom and formation of a Meisenheimer complex, the halide is eliminated giving the substitution product. Similar reactions have been observed for the Fp^- nucleophile and other metalates before.^[503,504]



Scheme 5.4. Possible reaction pathways of the Fp^- nucleophile with aromatic fluorocarbons (X = F, Cl, Br, I).

The second possibility is the halogen–metal exchange (HME). Here, attack of the metalate does not occur at the carbon atom but directly at the halogen atom. The intermediary formed aromatic carbanion has been detected in reactions of KFp with chloropentafluorobenzene by anion scavenging experiments.^[505] However, $FpCl$ could not be identified in solution and it was speculated that this unstable intermediate might also decompose in a side-reaction to yield the dimer Fp_2 . The fact that different reactions are possible for the carbanion could explain the often complicated mixtures of different products encountered in nucleophilic substitution reactions where a HME mechanism can be assumed.^[505,506] In general, the reactivity is highest for iodine-substituted fluorocarbons

and decreases when ascending the group of the periodic table. This trend is exactly reverse to the normal leaving group effect encountered in classical S_N2Ar reactions.

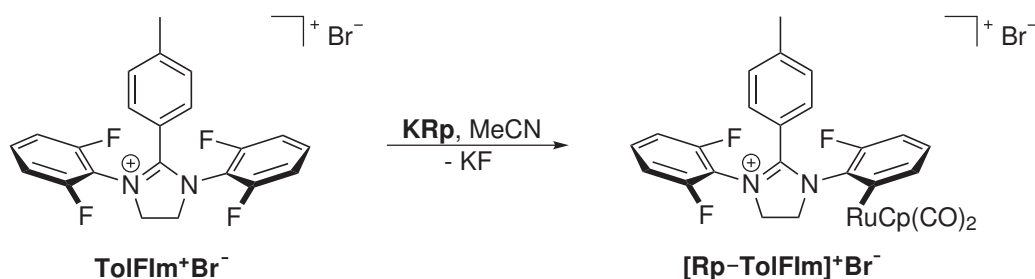
The third possible reaction mechanism is a single electron transfer (SET) reaction in which the metalate initially reduces the aromatic fluorocarbon before dissociation of the halide and recombination (possibly within a solvent cage).^[507] Indeed, radicals have been detected in reactions of certain metalate anions with alkyl halides.^[508] Although metal-centered nucleophiles often have a high reducing power, an outer-sphere electron transfer was not considered feasible in the case of aromatic fluorocarbons, and experiments with radical traps could not confirm the presence of any radicals in reactions with **KFp**.^[505]

To conclude, one can say that the reaction of imidazolium salt **C₆F₅MesIm⁺Br⁻** and **KFp** most likely occurs *via* an S_N2Ar mechanism, especially as the HME mechanism usually is not observed for fluoride leaving groups and an SET mechanism has not been found for reactions of aromatic fluorocarbons and the **Fp⁻** anion before. The *para*-fluorine atom is substituted for the **Fp⁻** unit giving rise to the adduct [**Fp-C₆F₄MesIm**]⁺. The fact that no other reaction products (apart from minor amounts of **Fp₂** which is also a decomposition product of the starting material **KFp**) were detected, accounts for this estimation. In a second step, the adduct decomposes – possibly in a metathesis-like reaction – to yield the coupling product and the dimer **Fp₂**.

5.2.3 A Second Example: Ruthenium Adduct [**Rp-TolFIm**]⁺

Nucleophilic substitution reactions were not only observed for the iron metalate **KFp**, but also mixtures of imidazolium salts and the ruthenium metalate **KRp** underwent this reaction type. When **KRp** was added to a solution of imidazolium salt **C₆F₅MesIm⁺Br⁻**, a rapid color change analogous to the reaction of metalate **KFp** described above was recognized. This suggests that in principle similar reactions can be expected for the two metalates. However, for imidazolium salt **TolFIm⁺Br⁻** this turned out to be not the case as different reactivities were found for **KFp** and **KRp**, respectively. While reactions with the iron metalate **KFp** involved electron transfer reactions (see section 5.3), a nucleophilic substitution reaction was found for the ruthenium anion.^[345] As depicted in Scheme 5.5, the adduct [**Rp-TolFIm**]⁺ is formed after nucleophilic attack of the **Rp⁻** anion at the *ortho*-position of the N-aromatic ring and substitution of the fluorine atom. As in the case of adduct [**Fp-C₆F₄MesIm**]⁺, an S_N2Ar mechanism can be assumed for this reaction.

The structure of the reaction product was confirmed by ESI mass spectrometry. As can be seen in Figure 5.5, the peak at $m/z = 589.1$ corresponds to the molecular ion peak of the adduct. A good correlation between simulated and experimentally determined isotopic distribution patterns is observed. Also NMR data were found in accordance with the proposed structure as the compound features three different resonances in the ¹⁹F NMR spectrum at roughly -118, -119 and -120 ppm. This indicates that rotation



Scheme 5.5. Formation of adduct $[\mathbf{R}p\text{-TolFIm}]^+\mathbf{Br}^-$ by nucleophilic attack of the $\mathbf{R}p^-$ nucleophile at the *ortho*-position of the N-aromatic ring.

of the fluorine-containing aromatic rings is hindered in the adduct $[\mathbf{R}p\text{-TolFIm}]^+\mathbf{Br}^-$ due to interactions with the $\mathbf{R}p^-$ moiety. Ultimate proof for the structure of the adduct comes from X-ray crystallography. Layering a few milliliters of toluene with the MeCN solution of the compound produced – upon standing at room temperature – pale yellow crystals suitable for X-ray crystallography. The obtained molecular structure is depicted in Figure 5.6.

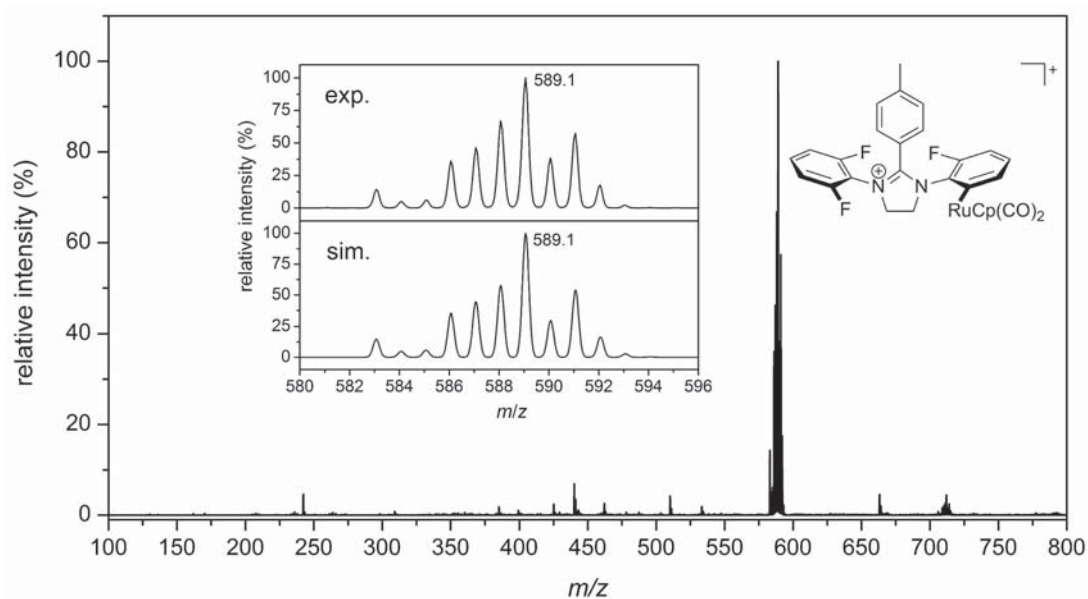


Figure 5.5. Mass spectrum (ESI^+ , MeCN) of the adduct $[\mathbf{R}p\text{-TolFIm}]^+\mathbf{Br}^-$ in the $m/z = 100\text{--}800$ region. A good correlation between simulated and experimental isotopic distribution patterns (see inset) is found.

The reaction between imidazolium salt $\mathbf{TolFIm}^+\mathbf{Br}^-$ and $\mathbf{KR}p$ was monitored by means of IR spectroscopy with a Cary 630 FTIR spectrometer (Agilent) placed in a glovebox. Upon mixing of the two compounds in MeCN, a gradual decrease of the CO bands of the $\mathbf{R}p^-$ anion at 1887 and 1802 cm^{-1} and a concomitant rise of new bands at 2034 and 1971 cm^{-1} was observed. Besides this, also small amounts of the dimer $\mathbf{R}p_2$ ($\tilde{\nu} = 1996$ and 1775 cm^{-1}) were detected. The change of the appearance of the spectrum in the carbonyl region is depicted in Figure 5.7 (a). Kinetic analysis of the reaction by

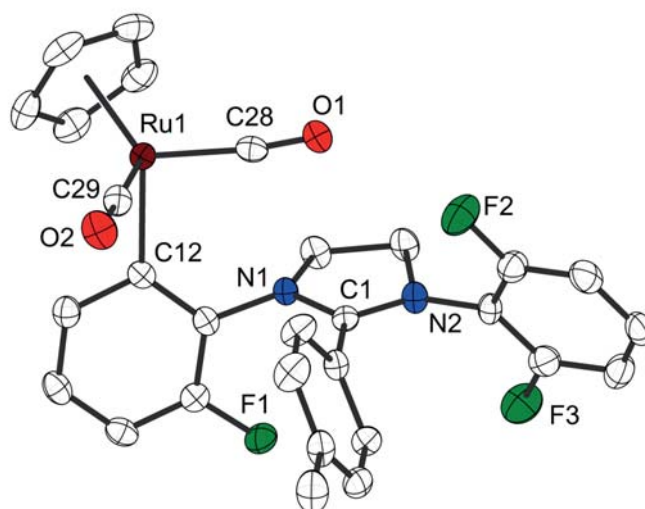


Figure 5.6. Thermal displacement ellipsoids (shown at 50% probability) of the molecular structure of adduct $[\text{Rp-TolFIm}]^+ \text{Br}^-$. Hydrogen atoms, the bromide counterion as well as an additional MeCN molecule per unit cell are omitted for clarity. Selected bond length [\AA] and angles [$^\circ$]: Ru1–C12 2.107(2), Ru1–C28 1.879(3), Ru1–C29 1.884(3), C28–O1 1.146(3), C29–O2 1.138(3), N1–C1 1.324(3), N2–C1 1.323(3); Ru1–C28–O1 173.0(2), Ru1–C29–O2 176.2(2), C29–Ru1–C28 94.5(1), C29–Ru1–C12 84.1(1), C28–Ru1–C12 97.4(1), N1–C1–N2 111.9(2).

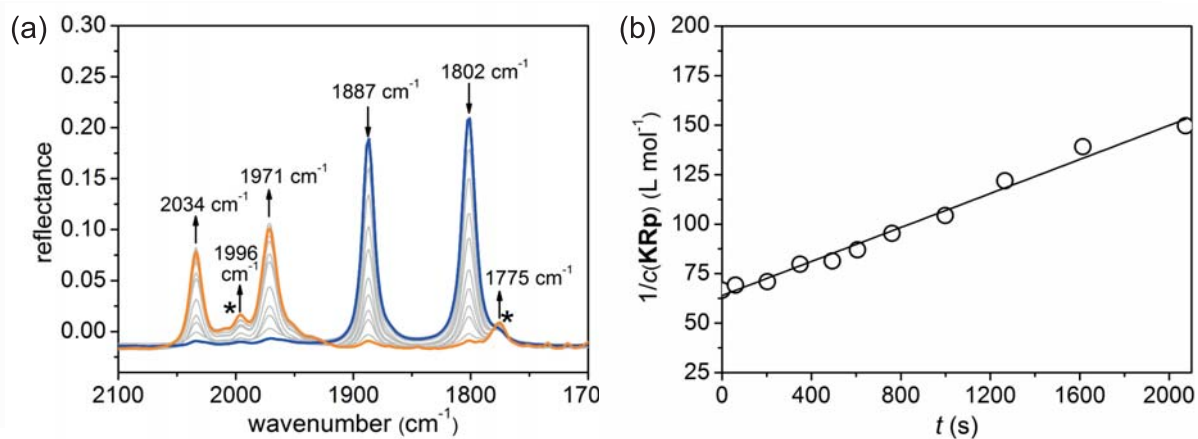


Figure 5.7. (a) Superposition of different IR spectra in the carbonyl region of the reaction between imidazolium salt $\text{TolFIm}^+ \text{Br}^-$ and KRp acquired after certain periods of time (bands of the dimer Rp_2 are marked with an asterisk); (b) linear fit of the $1/c(\text{KRp})$ vs. reaction time plot.

quantifying the area beneath the peak at 1887 cm^{-1} and plotting the inverse concentration of the starting material **KRp** vs. the reaction time gave the graph shown in Figure 5.7 (b). From the slope of the linear fit, a rate constant of $k = 4 \times 10^{-2}\text{ L mol}^{-1}\text{ s}^{-1}$ in the initial stages of the bimolecular reaction could be deduced. Integration of the other peak areas was hampered by overlapping bands of the dimer **Rp₂** and therefore only the peak at 1887 cm^{-1} was considered in the kinetic analysis.

5.2.4 Consequences for Reactions with H₂ and Other Substrates

The substitution reactions described in this section were not anticipated when designing the hydride acceptor molecules and complicated the envisioned reactions with dihydrogen. Especially the reactions of imidazolium salt **C₆F₅MesIm⁺Br⁻** with **KFp** and **KRp** were very fast even at low temperatures. Therefore, a reactivity towards H₂ was not observed. In contrast to this, reactions of **KRp** with imidazolium salt **TolFIm⁺Br⁻** were considerably slower, as full conversion usually was reached not before a few hours. Consequently, experiments were carried out in which the components were mixed directly in an NMR tube, immediately frozen, subjected to an atmosphere of dihydrogen (10 bar), and warmed to room temperature. However, instead of observing a reaction with dihydrogen, NMR measurements confirmed the formation of the adduct **[Rp–TolFIm]⁺** as shown above. No differences to the direct mixing of the salts in the absence of H₂ were recognized. Obviously, the nucleophilic substitution reaction is preferred and the desired heterolytic splitting of dihydrogen does not take place. Further substrates which usually are more prone to undergo heterolytic splitting reactions like for example triethyl silane and phenylacetylene were added to mixtures of the imidazolium salt and the metal carbonyl anion. Also in these cases no reactions with the substrates were observed and only adduct formation took place.

To conclude, one can say that the observed nucleophilic substitution reactions hampered the reactions with small molecules like H₂. The metalate anion (**Fp⁻** or **Rp⁻**) reacted with the imidazolium ions in a nucleophilic substitution reaction following an S_N2Ar mechanism. In these reactions, fluoride ions were eliminated and the resulting adducts were found unable to activate small molecules. Hence, the reactivity which otherwise might probably be used for bond activation is quenched. In this respect an analogy to the formation of classical Lewis acid–base adducts exists.

5.3 Electron Transfer Reactions

Nucleophilic substitution reactions were not the only reactions observed in the context of attempting to synthesize novel transition metal frustrated Lewis pairs. As it turned out, a second reaction pathway was the electron transfer (ET) from the metalate to the imidazolinium ion. This section focuses on the theoretical and experimental background of the electron transfer reactions which were encountered when mixing imidazolinium salts and carbonyl metalates.

5.3.1 General Considerations

A prerequisite for a spontaneous transfer of electrons between an electron donor and an acceptor is that the standard potentials of the reaction partners E° are compatible. The Gibbs energy of the reaction is proportional to the difference of the standard potentials ΔE° and corresponds to the following equation:

$$\Delta G = -nF \cdot \Delta E^\circ \quad (5.1)$$

with the number of transferred electrons n and the Faraday constant F . ΔE° is the difference of reductive and oxidative half reactions. As the Gibbs energy is negative for a spontaneous reaction, ΔE° has to be positive. Consequently, the potential of the reductive part of the reaction has to be less negative or more positive than the potential of the oxidative half reaction. This means that the potential of the electron donor has to be lower than the potential of the electron acceptor in order to observe a transfer of electrons.

Figure 5.8 summarizes again the experimentally determined standard potentials E° of the synthesized imidazolinium ions presented in section 2.3.2. Furthermore, the potentials for the irreversible oxidation waves of the metalate ions \mathbf{Fp}^- and \mathbf{Rp}^- are given. The values are referenced *vs.* the $\text{FeCp}_2/\text{FeCp}_2^+$ (Fc/Fc^+) redox couple.

As becomes clear from the figure, the potentials of the metal carbonyl anions are more positive than the potentials found for the imidazolinium ions. Therefore, from a theoretical point of view, electron transfer reactions between the two components should not be possible at all. Nevertheless, electron transfer reactions with the iron metalate \mathbf{KFp} were found as will be discussed in more detail in the following sections. An explanation for this observation could be related to the fact that only irreversible oxidation waves were measured which is indicative of additional reactions taking place at the electrode surfaces. Indeed, rapid follow-up reactions are expected for the metal-centered radicals produced by one-electron oxidation of the \mathbf{Fp}^- and \mathbf{Rp}^- anions since recombination of these radicals gives the thermodynamically very stable dimers \mathbf{Fp}_2 and \mathbf{Rp}_2 . However, the shift resulting from these reactions consuming the electrode-generated species is expected to occur to lower/more negative potentials for oxidation processes.^[458] This

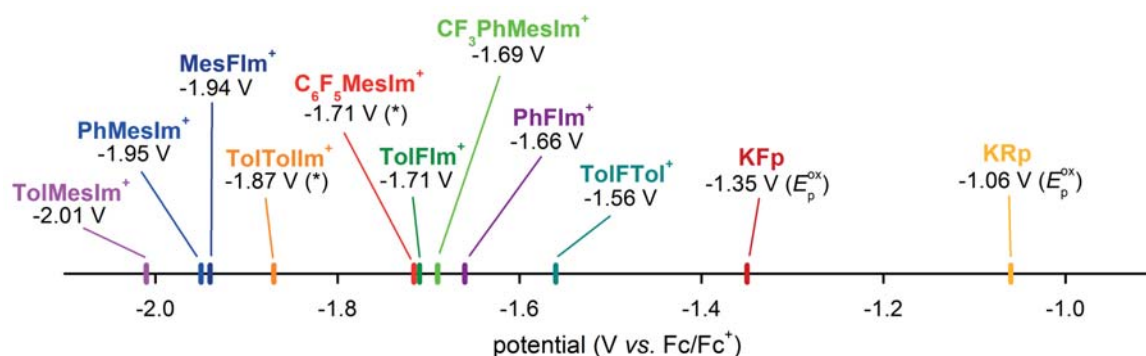


Figure 5.8. Standard potentials E° and estimated standard potentials (marked with an asterisk, see section 2.3.2 for details) of the synthesized imidazolium ions, and irreversible peak potentials E_p^{ox} of the metalates **KFp** and **KRp**^[458] referenced *vs.* the Fc/Fc^+ redox couple.

would mean that the reversible potential for the oxidation of the metalates is expected at even higher potentials than the potentials given in Figure 5.8. On the other hand, the situation seems to be still a little different in solutions containing appropriate oxidation agents. T. J. Meyer *et al.* found a potential of -1.81 V for **KFp** by means of elegant redox equilibration studies^[459] and similar values have been reported elsewhere.^[509] This might offer an explanation for the observed reactions since such an oxidation potential would be in the region of the reduction potentials of some of the synthesized imidazolium ions. It seems like the redox chemistry of the metalates used in the framework of this thesis is rather complex and has to be examined for each specific case.

5.3.2 Electron Transfer between $\text{TolFlm}^+\text{Br}^-$ and **KFp**

When the metalate **KFp** was added to a solution of the imidazolium salt $\text{TolFlm}^+\text{Br}^-$ in the hope of creating a novel transition metal frustrated Lewis pair, a rapid color change from a slightly yellow to a dark red solution was observed. This already indicated a fast reaction of the two components. As could be shown by NMR spectroscopy, the reaction solution contained different products, among them the iron dimer **Fp**₂ and the imidazolidine **HTolFlm**. The ratio of these compounds and also the presence of other reaction products varied with the solvent. In chlorobenzene the reactions were cleaner and a 1:1 ratio of **HTolFlm** and **Fp**₂ was recognized, whereas in MeCN the reaction solutions generally contained several other products and higher amounts of the dimer. These observations already suggested a reaction type involving the formation of radicals and further measures were taken to prove this assumption.

Figure 5.9 (a) shows the EPR spectrum of a 14 mM MeCN solution of a mixture of the imidazolium salt and the metalate at 133 K. As can be seen in the spectrum, only a single resonance is observed which does not exhibit a hyperfine splitting pattern. The g -factor amounts to 2.006 which is close to the g -factor of the free electron ($g_e = 2.002$).

This accounts for the presence of a carbon-centered radical. The unpaired electron has to be mostly localized at the carbon atom – presumably the C² carbon atom of the central nitrogen heterocycle – as no interactions with the nuclear spins of other atoms could be resolved. Also at higher temperatures (188 K) this picture does not change.

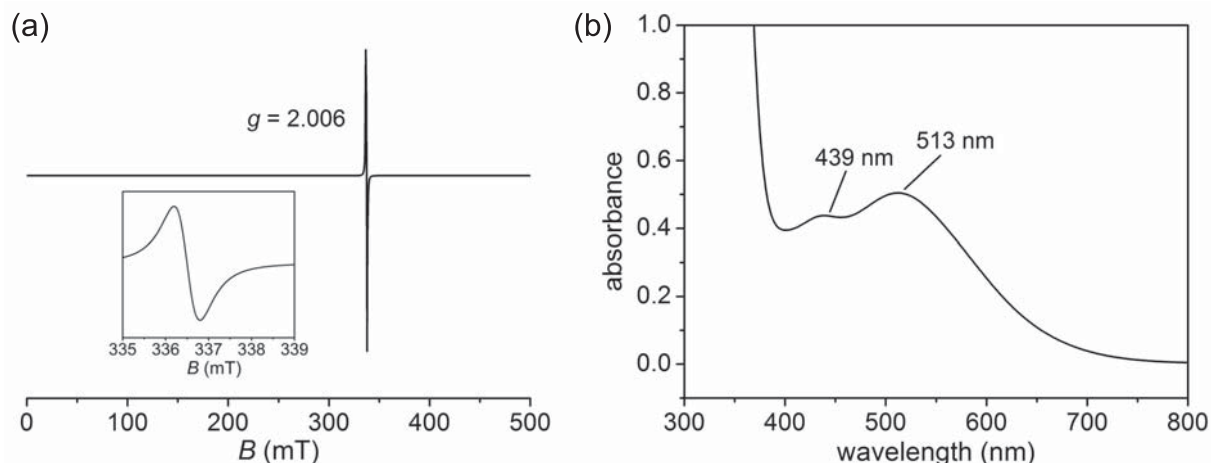


Figure 5.9. (a) EPR spectrum (MeCN, 133 K) of the reaction mixture containing **TolFIm⁺Br⁻** and **KFp**. The inset shows the magnified signal region; (b) UV/Vis spectrum of the mixture at a 0.2 mM concentration.

The color change taking place upon mixing the two components was examined by means of UV/Vis spectroscopy. Figure 5.9 (b) depicts the UV/Vis spectrum of the mixture recorded at a 0.2 mM concentration. While solutions of the imidazolium salt show almost no characteristic absorptions, the mixture exhibits relatively intense absorption bands at 439 ($\epsilon = 1900 \text{ L mol}^{-1} \text{ cm}^{-1}$) and 513 nm ($\epsilon = 2200 \text{ L mol}^{-1} \text{ cm}^{-1}$).

The characteristic features of the observed EPR and UV/Vis spectra of the reaction mixture could be reproduced by measuring samples which have been produced by electrochemical reduction of the imidazolium salt **TolFIm⁺Br⁻**. For the EPR measurements, bulk electrolysis of a 20 mM MeCN solution of the imidazolium salt was carried out at -30°C with a VersaSTAT 3 potentiostat (Princeton Applied Research) using a platinum net electrode, a silver quasi-reference electrode, and a platinum counter electrode. As electrolyte $0.1 \text{ mol L}^{-1} \text{ NBu}_4\text{PF}_6$ was added. During electrochemical reduction at a potential of roughly -1.00 V vs. Ag ($-1.73 \text{ V vs. Fc/Fc}^+$), a gradual color change from a slightly yellow to a dark red solution was observed. The EPR sample was then prepared maintaining oxygen- and moisture-free conditions. Analogous to the reaction mixture of the imidazolium salt and **KFp**, the EPR spectrum of the electrochemically reduced species recorded at 133 K features again a signal that lacks a hyperfine splitting pattern (Figure 5.10 (a)). The g -factor of the signal is 2.008, a value that is comparable to the g -factor measured for the mixture of imidazolium salt and **KFp**.

In a second experiment, a 10 mM MeCN solution of **TolFIm⁺Br⁻** was reduced electrochemically at room temperature directly in a UV/Vis cuvette analogously to the

procedure described above for the preparation of the EPR sample. The UV/Vis spectra recorded simultaneously to reduction of the imidazolinium salt are shown in Figure 5.10 (b). The absorption bands that rapidly emerge in the spectrum after starting the reduction are comparable to the bands observed before in the mixture of imidazolinium salt and metalate. However, a determination of absorption coefficients was not carried out because a relatively fast decay of the bands was observed. The concentration of the radical could therefore not be assigned reliably. A reason for the observed decay is the inadequate setup of the experiment. Although the cuvette was constantly provided with a flow of argon gas, it could obviously not be excluded that the radical species got exposed to air. Most likely the contact to dioxygen resulted in the degradation of the radical giving again a slightly yellow to nearly colorless solution. Attempts to reduce this reaction product again by electrochemical methods were not successful.

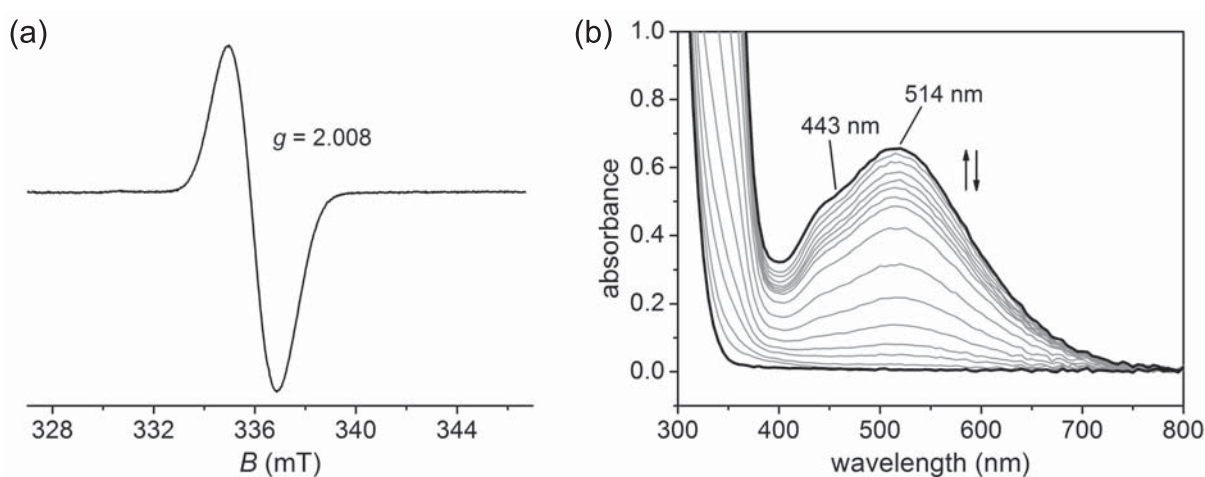


Figure 5.10. (a) EPR spectrum (MeCN, 133 K) of the electrochemically reduced imidazolinium salt $\text{ToIFIm}^+\text{Br}^-$; (b) UV/Vis spectra of an analogously prepared sample.

5.3.3 Structure of the Radical ToIFIm

The structure of the radical (**ToIFIm**) resulting from the electron transfer reaction between the Fp^- anion and the imidazolinium ion was further examined by means of theoretical calculations performed with the *ORCA* program^[385] using the B3LYP functional and the TZVP basis set.^[386] The calculations predict a Mulliken spin density of 53 % localized at the C^2 carbon atom and only 4 % on average at the neighboring nitrogen atoms. The remaining fraction of the spin density is mostly found in the aromatic ring connected to the C^2 carbon atom. These results largely confirm the structure of a carbon-centered radical proposed on the basis of the experimentally obtained EPR data. However, the results also indicate that more than 40 % of the spin density is located in the C^2 aromatic ring which could not be confirmed by the EPR measurements as no

coupling to the nuclear spins of the adjacent protons was observed. Also in EPR measurements at higher temperatures no hyperfine splitting patterns were found. Further calculations using other basis sets and the COSMO solvation model^[387] to simulate the influences of the solvent MeCN do not change the general picture of the radical **TolFIm** but merely show slightly lower spin densities at the C² carbon atom. Probably the insufficient description of the experimental conditions by the preconditions of the theoretical calculations is responsible for this discrepancy.

Figure 5.11 depicts the calculated molecular structure of the radical **TolFIm** including also a plot of the spin density. From the representations it is clear that the heterocycle adopts a distorted, non-planar structure which is similar to the structure found for the imidazolidine **HTolFIm** (Figure 2.8 in chapter 2.3.3).

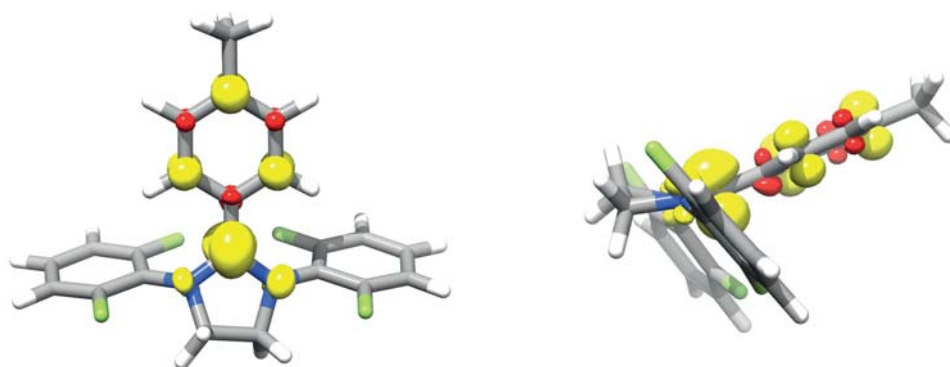
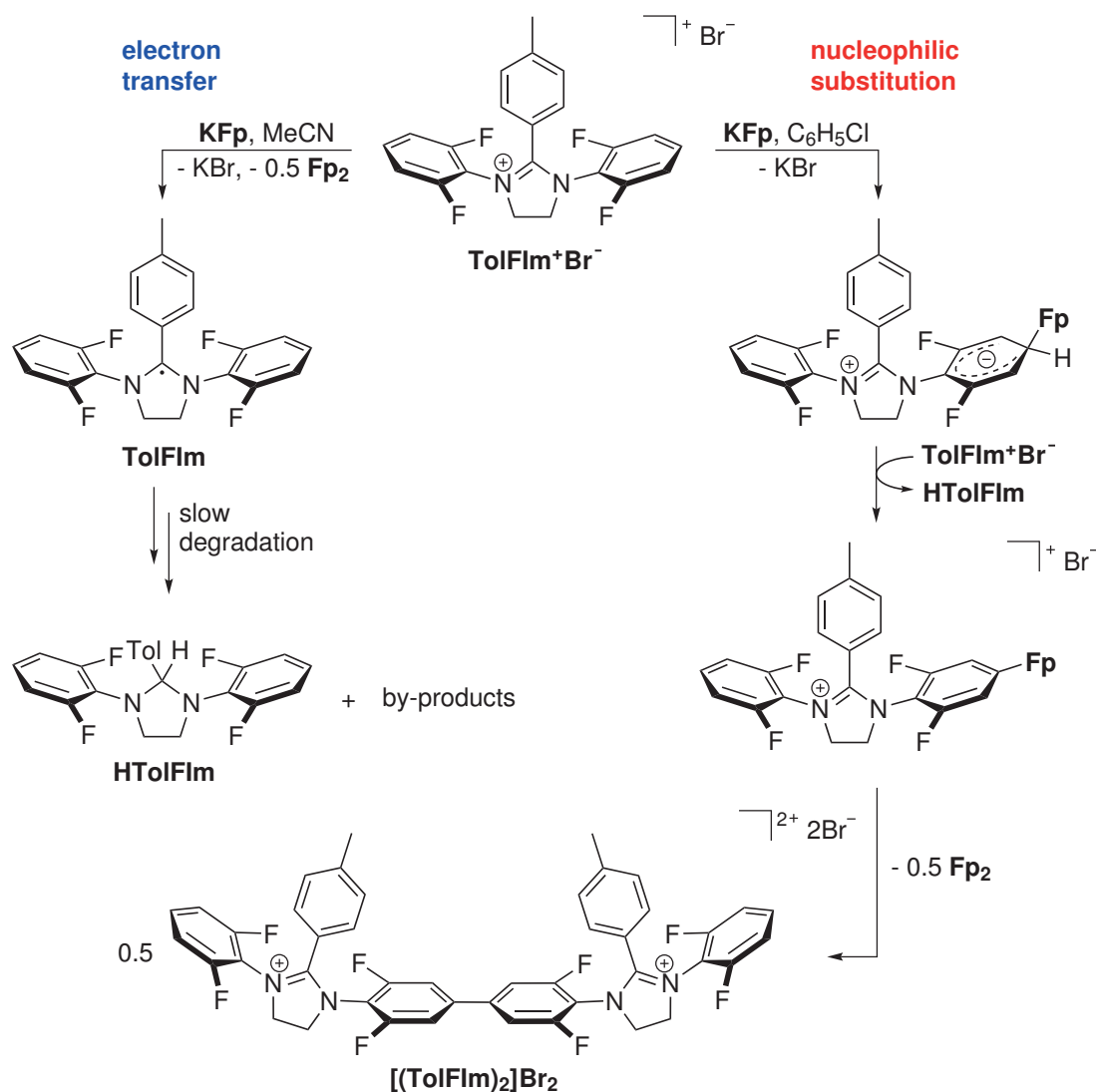


Figure 5.11. Calculated molecular structure of the radical **TolFIm** in different views showing also a plot of the spin density.

5.3.4 Competing ET and Nucleophilic Substitution Reactions

As already briefly mentioned, different products were detected in reactions of the imidazolium salt **TolFIm**⁺**Br**⁻ and the metalate **KFp** by NMR spectroscopy. The data suggest that the ratio of these products is strongly dependent on the chosen solvent. While the radical **TolFIm** seems to be relatively stable in MeCN solutions even at room temperature, it most probably is – if present at all – only a transient species in chlorobenzene solutions. An indication for this is the fact that EPR and UV/Vis measurements of the radical species were possible in MeCN. Furthermore, NMR spectra of CD₃CN solutions of the mixture featured many different signals, among them those characteristic of the imidazolidine **HTolFIm** and the dimer **Fp**₂. The slow degradation of the **TolFIm** radical – presumably by proton abstraction from more or less random sites of imidazolium ions or solvent – could explain the variety of the formed products. The formation of the dimer **Fp**₂ can also be easily rationalized by recombination of two metal-centered radicals which are formed by one-electron oxidation of the metalate anion. The generally low intensity of the NMR spectra might offer additional evidence for the presence of significant amounts of the paramagnetic radical **TolFIm**.

On the contrary, reactions of **TolFlm**⁺**Br**⁻ and **KFp** were much cleaner when chlorobenzene was chosen as the solvent. Apart from the already mentioned products **HTolFlm** and **Fp**₂ only one additional product was present in solution. This species exhibits two signals in the ¹⁹F NMR spectrum at -116.3 and -128.1 ppm showing a 1:1 ratio, indicative of nonequivalent fluorine-containing aromatic rings. The obtained NMR and ESI-MS data are in accordance with the dimeric structure **[(TolFlm)₂]²⁺** in which two imidazolium ions are joint at the *para*-positions of their fluoro-substituted aromatic rings (Scheme 5.6).



Scheme 5.6. Radical and nucleophilic substitution mechanisms of the reaction between imidazolium salt **TolFlm**⁺**Br**⁻ and the metalate **KFp**.

A possible explanation for the formation of the dimer comprises nucleophilic attack of the **Fp**⁻ anion at the *para*-position of the aromatic ring. Subsequently, the metalate adduct is formed before the final coupling reaction, involving the formation of **Fp**₂, occurs (Scheme 5.6). The intermediary formed Meisenheimer complex eliminates

a hydride ion which is then accepted by an imidazolium ion. This could explain the formation of the imidazolidine **HTolFIIm** and the observed 2:1:1 ratio of **HTolFIIm**, **Fp₂**, and **[(TolFIIm)₂]Br₂**. The formation of the products by a radical mechanism is rather unlikely because a marked selectivity for the formation of **HTolFIIm** and **[(TolFIIm)₂]²⁺** was observed. If a radical reaction would be the reason for the formation of those compounds, several by-products originating from reactions at other positions or with the solvent could be expected. As this is not the case, a radical mechanism is not feasible. Nevertheless, it is still surprising that the metalate exclusively attacks the *para*-position of the aromatic ring, especially as the ruthenium analog **KRp** was found to attack the *ortho*-positions (see section 5.2.3).

In summary, two different reaction paths for the reaction between **TolFIIm⁺Br⁻** and **KFp** exist, namely electron transfer from the metalate anion to the imidazolium ion and nucleophilic substitution at the *para*-position of the aromatic ring by the **Fp⁻** nucleophile. Obviously, the system represents a borderline case between the two reactions. A change of the solvent might influence the redox-potentials of the reaction partners and thus determine the outcome of the reaction.

5.3.5 Dihydrogen Splitting Despite Other Reactivities?

Although different reactions between the imidazolium salt **TolFIIm⁺Br⁻** and the metalate **KFp** were found, it was nevertheless attempted to achieve a reaction of the mixture with dihydrogen. For this purpose, both compounds were added to a Schlenk tube and cooled to $-30\text{ }^{\circ}\text{C}$ before addition of the precooled deuterated chlorobenzene, $\text{C}_6\text{D}_5\text{Cl}$. H_2 (0.8 bar) was then added and the mixture was allowed to warm to room temperature overnight with stirring. After this, the solution was filtered (Sartorius PTFE syringe filter, $0.45\text{ }\mu\text{m}$) and filled into a J. Young NMR tube. The ^1H and ^{19}F NMR spectra of this solution were distinct from the NMR spectra of the mixture of the two compounds measured without addition of H_2 . Contrary to what was observed before, no formation of the dimer **[(TolFIIm)₂]Br₂** could be detected. Instead, several other products were observed, among them also the imidazolidine **HTolFIIm**. Figure 5.12 shows a comparison of the ^{19}F NMR spectra of the mixture of **KFp** and the imidazolium salt in chlorobenzene, the pure imidazolidine **HTolFIIm**, the mixture after addition of H_2 and D_2 , and the mixture in CD_3CN without addition of any gas.

From the presented NMR data it becomes clear that imidazolidine **HTolFIIm** is present in the ^{19}F NMR spectrum regardless whether H_2 was added to the mixture of **TolFIIm⁺Br⁻** and **KFp** or not. However, the mechanism of its formation seems to differ. As discussed earlier, the origin of the imidazolidine in the mixture of **TolFIIm⁺Br⁻** and **KFp** most probably is the nucleophilic attack of the **Fp⁻** anion at the *para*-position of the aromatic ring and concomitant elimination of a hydride ion. The liberated H^- ion then adds to the C^2 carbon atom of the imidazolium ion, thereby forming the imidazolidine. On the contrary, **HTolFIIm** seems to be the product of a radical reaction when H_2 is added

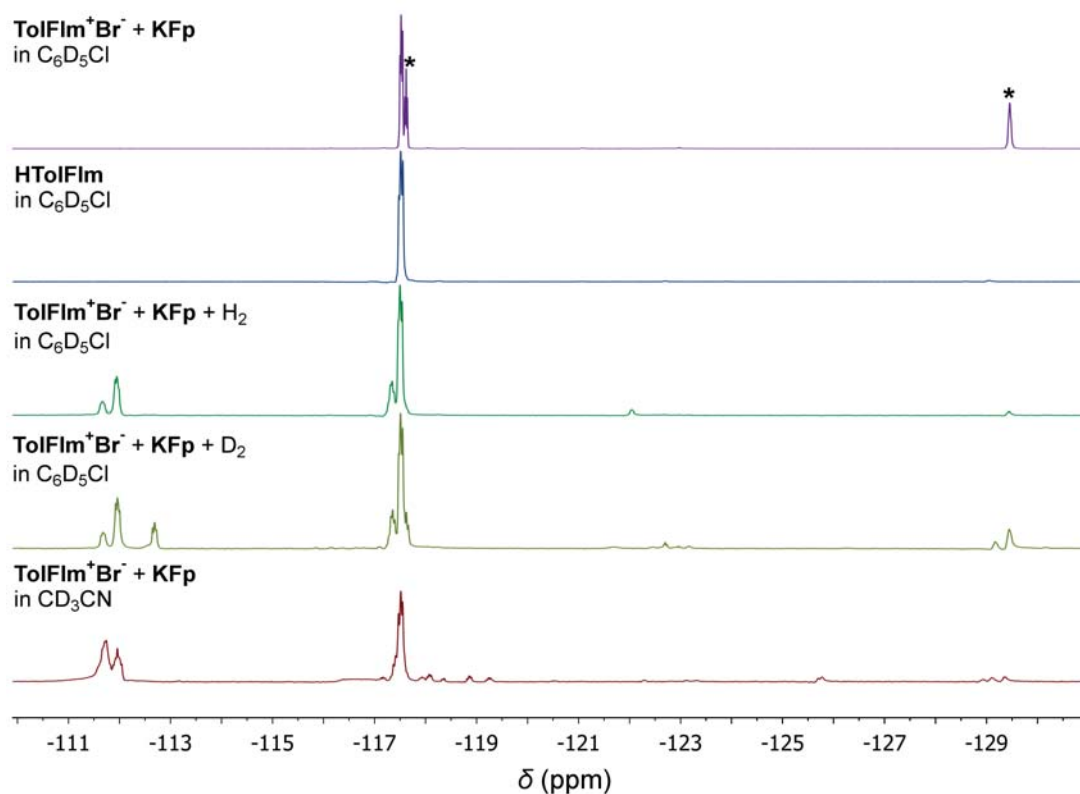


Figure 5.12. ^{19}F NMR spectra of different reaction mixtures containing the imidazolium salt $\text{TolFlm}^+\text{Br}^-$ and the metalate KFp . For comparison also the ^{19}F NMR spectrum of the pure imidazolidine HTolFlm is given. The two signals belonging to the dimer $[(\text{TolFlm})_2]\text{Br}_2$ are marked with an asterisk.

to the reaction mixture. An indication for this is the fact that the respective NMR spectrum show similarities to the NMR spectrum of the mixture in MeCN for which the formation of the radical species TolFlm has been verified by other methods. Hydrogen atom abstraction by this radical would also yield the imidazolidine HTolFlm . Mixtures with added H_2 contained almost no dimer $[(\text{TolFlm})_2]\text{Br}_2$, like the reaction mixture of the two components in MeCN.

Nevertheless, a third possibility for the formation of HTolFlm could still be the reaction with dihydrogen giving the imidazolidine and the hydride complex $\text{HFeCp}(\text{CO})_2$ (HFp). The ^1H NMR spectrum did not show a signal for the metal hydride which is expected to exhibit a signal at approximately -12 ppm.^[510] However, this not necessarily excludes the possibility of a heterolytic splitting of H_2 since the complex HFp is reported to be rather unstable and decomposition yielding H_2 and the dimer Fp_2 is a known issue.^[461] In order to investigate this reaction more thoroughly, a reaction with D_2 was conducted under the same conditions as the reaction with H_2 . The ^{19}F NMR spectrum (Figure 5.12) is almost identical to the spectrum acquired after addition of H_2 but shows an additional signal at -112.7 ppm which seems to confirm that H_2 and D_2 are involved in the reaction. Yet the identity of the product giving rise to this resonance remains unclear. In case of a heterolytic splitting of D_2 , one would expect the

formation of the deuterated imidazolidine **DTolFIm**. As has been verified by reference measurements, this compound would exhibit almost the same isomeric shift for the fluorine atoms of the aromatic rings as the “normal” imidazolidine **HTolFIm**. Hence it is difficult to distinguish **HTolFIm** and **DTolFIm** in the ^{19}F NMR spectrum presented in Figure 5.12. However, the ^1H NMR spectra after addition of H_2 and D_2 are almost identical which seems to suggest that **HTolFIm** is also the main product in the reaction when D_2 is added to the mixture of the imidazolinium salt **TolFIm** $^+\text{Br}^-$ and the metalate **KFp**.

Summing up the experiences made in the reactions with dihydrogen, one can say that a heterolytic splitting of the H_2 molecule by the mixture of imidazolinium salt **TolFIm** $^+\text{Br}^-$ and the metalate **KFp** could not be proved unequivocally. On the one hand, a reactivity distinct from the reaction of the two components without the addition of any gas was noticed. On the other hand, the observed distribution of products resembles the reactivity pattern of mixtures of **TolFIm** $^+\text{Br}^-$ and **KFp** in MeCN solutions. Obviously competing reaction pathways – electron transfer and nucleophilic substitution reactions – exist and which of them prevails depends on subtle changes of the underlying conditions.

5.4 Further Examples and Unclear Reactions

In addition to the already described combinations of imidazolinium salts and transition metal Lewis bases, also other imidazolinium salts and metal complexes were tested to finally achieve the formation of a transition metal frustrated Lewis pair that is active in the heterolytic splitting reaction of dihydrogen. Before presenting such a system in the next section, this part will briefly summarize some further examples where undesired reactivities comprising the two components were observed. Not in every case the reaction products could be unambiguously identified.

$\text{CF}_3\text{PhMesIm}^+\text{Br}^-$

When carbonyl metalate **KFp** was combined with **$\text{CF}_3\text{PhMesIm}^+\text{Br}^-$** in chlorobenzene and stirred at room temperature, a color change giving a dark green to black solution was observed. This already indicated a reaction between the two compounds. Filtration of the suspension and crystallization attempts with mixtures of chlorobenzene and cyclopentane finally produced small amounts of green to blue crystals. Unfortunately, the molecular structure of the compound could not be determined by means of X-ray crystallography as the quality of the obtained crystallographic data was insufficient for an accurate refinement. Nevertheless, the data proposed that possibly a coupling reaction between the CF_3 groups of two molecules has taken place. NMR spectroscopy showed only broad signals which suggests the presence of a paramagnetic species. As the redox potential of the imidazolinium salt is higher than that of **$\text{TolFIm}^+\text{Br}^-$** (for which electron transfer reactions have already been found, see chapter 5.3.4), an electron

transfer reaction is indeed feasible. Unfortunately, no final proof for the identity of the reaction product(s) could be obtained.

PhFIm⁺Br⁻

Upon stirring a mixture of imidazolium salt **PhFIm⁺Br⁻** and metalate **KFp** in chlorobenzene at room temperature, the color of the solution turned dark red. While ESI-MS measurements of the reaction mixture only showed the unchanged **PhFIm⁺** cation, NMR measurements indicated that the product was not symmetric any longer. As a consequence, the resonance characteristic for the CH₂ groups was not a singlet, but instead two multiplets appeared in the spectrum. Besides this, also the dimer **Fp₂** could be detected in solution. A possible explanation for this could be an electron transfer reaction from the metalate anion to the imidazolium ion which is associated with a distortion of the planar structure of the heterocycle. The relatively high redox potential of the imidazolium ion would support this assumption. However, the imidazolidine **HPhFIm** could not be unambiguously detected in solution which hints either at a good stability of the radical or alternative decomposition or rearrangement paths.

TolFTolIm⁺Br⁻

In the case of imidazolium salt **TolFTolIm⁺Br⁻** and **KFp** an electron transfer reaction analogous to the reaction of **TolFIm⁺Br⁻** and **KFp** in chlorobenzene was observed. This can be readily explained since the reduction potential of the **TolFTolIm⁺** ion is the highest potential of all synthesized imidazolium ions and therefore an ET is more likely to happen. NMR spectra of the mixture in CD₃CN showed many different signals of relatively low intensities. Besides this, the dimer **Fp₂** could be detected in solution. The presence of a radical **TolFTolIm** could be verified by means of EPR spectroscopy since the EPR spectrum of a frozen MeCN solution at -133 K showed a signal lacking a hyperfine splitting pattern with a *g*-factor of 2.006 which is identical to the value observed for the radical **TolFIm**.

TolTolIm⁺Br⁻

¹H NMR spectra of mixtures containing the imidazolium salt **TolTolIm⁺Br⁻** and **KFp** were very complex and many different signals were observed, especially in the CH₂ and CH₃ regions of the spectrum. However, an electron transfer reaction/the formation of radicals is rather unlikely as the origin for the complicated NMR spectra because the estimated standard potential of the imidazolium ion is found at relatively low/cathodic potentials ($E^\circ \approx -1.87$ V *vs.* Fc/Fc⁺, for details see section 2.3.2). In addition to this, similar reactions took place with the metalate **KRp** for which electron transfer reactions with imidazolium ions have not yet been observed. Unfortunately, the structure of the reaction product(s) could also not be clarified by ESI-MS measurements and crystallization attempts were unsuccessful as well.

5.5 TolFIm⁺Br⁻ and **Rs**: A Novel H₂ Splitting System

As has already been shown in the course of this chapter, different reactivities of imidazolinium salt TolFIm⁺Br⁻ and the two metalates **KFp** and **KRp** have been observed. While mixtures of TolFIm⁺Br⁻ and the **Fp**⁻ anion were found to exhibit – depending on the reaction conditions – both electron transfer and nucleophilic substitution reactions, only nucleophilic substitution of a fluoride substituent was noticed in reactions between the imidazolinium ion and the **Rp**⁻ anion. The adduct [**Rp**–TolFIm]⁺Br⁻ could be identified as main product in those reactions.^[345] Unfortunately, formation of the adduct was also observed when dihydrogen or other substrates were added to the reaction mixture.

This section now focuses on the metalate **Rs** (see chapter 4.3) and its mixtures with the imidazolinium salt TolFIm⁺Br⁻ for which reactions with dihydrogen have been observed.^[345] In order to get some background information on the thermodynamics of the dihydrogen splitting process, the results of some initially performed theoretical calculations will be provided before discussing the experimental details of the reaction.

5.5.1 DFT Calculations

The experimental findings described in chapter 4.3 indicate that the metalate **Rs** features a polymeric or clusterlike structure in which the “CpRu(CO)₂” unit is in some form preserved. In order to set a starting point for the computational investigation of the reaction with H₂, the presence of a free **Rp**⁻ anion in solution was assumed. However, the true nature of the used metalate **Rs** remains uncertain (see chapter 4.3 for details). What is sure is that **KRp** preferably reacts with the imidazolinium ion TolFIm⁺ to yield the nucleophilic substitution product [**Rp**–TolFIm]⁺. This reaction is not observed with the metalate **Rs**. The calculations are expected to give some insights into the H₂ splitting reaction, the reactive species, and possible intermediates. Furthermore, an evaluation of the stability of the reaction products **HRp** and **HTolFIm** with respect to H₂ formation is possible.

The theoretical calculations were performed in cooperation with the group of Jun.-Prof. Dr. Ricardo Mata at the Institute of Physical Chemistry of the Georg-August-University Göttingen. The **Rp**⁻ anion as well as the imidazolinium ion TolFIm⁺ were optimized at the B3LYP-D3/def2-TZVP level of theory. In order to obtain the Lewis pair, the compounds were placed in close contact. The ruthenium complex was then rotated about the axis of contact to obtain starting structures for geometry optimization. The Gibbs free energy was computed for each resulting local minimum. The final electronic energy was computed at the B3LYP-D3/def2-QZVPP level, including a COSMO correction from single point calculations with the def2-TZVP basis set to simulate the influence of the surrounding solvent MeCN. This procedure was followed in all other stationary points of the reaction path. In order to follow the hydrogen dissociation at the site,

to the final products should then readily be observed in solution. It should, however, be mentioned that a reoptimization at the B3LYP-D3/def2-TZVP level of theory – as performed for the RC and PC structures – was not possible for the transition state (TS). The reaction path therefore contains the constrained structure with the highest energy as an approximation. The value for the Gibbs free energy is approximated on the basis of the energy difference to the PC and RC states.

Further calculations on this reaction path, including also a correction for the typical overestimation of entropic factors in solution along a pathway in which the number of molecular units is changing, can be found in the recent publication of Kalz and co-workers.^[345] According to these results, the formation of the Lewis pair has a free energy penalty of only 55.5 kJ mol⁻¹ and the dihydrogen complex RC is stable relative to the Lewis pair by about 10.3 kJ mol⁻¹. The actual reaction barrier remains unchanged. Summarizing the obtained results, one can say that the major obstacle for achieving the heterolytic splitting of dihydrogen is the formation of the frustrated Lewis pair consisting of the **Rp⁻** and **TolFIm⁺** ions. However, once the pair is formed, reaction with dihydrogen should proceed smoothly as a relatively low activation barrier has been found. The products of the reaction, **HRp** and **HTolFIm**, are energetically favored accounting for an overall exothermic course of the reaction. In which way the polymeric structure of the actual reaction partner **Rs** affects the free energy profile, cannot be judged on the basis of the presented calculations. Nevertheless, major effects on the association of the two components can be expected while the overall reaction profile should be similar to what was obtained for the **Rp⁻** anion.

5.5.2 Advantages of **Rs** and H/D Exchange Reactions

In contrast to what was found for the metalates **KFp** and **KRp**, no reaction was observed by means of NMR spectroscopy when imidazolinium salt **TolFIm⁺Br⁻** was combined with the metalate **Rs** in CD₃CN. The initially broad signals – which presumably were caused by the undissolved particles – sharpened after a short time and only signals characteristic for the imidazolinium ion were recorded. No changes occurred over a period of four days at room temperature. When the sample was heated to 50 °C for 1 d, still only minor changes in the spectrum in the form of small additional signals were noticed. Only when the NMR sample was heated to 70 °C for 7 d, considerable amounts of (decomposition) products were formed. The ¹⁹F NMR spectrum recorded after this time featured several signals that could not be assigned, apart from the resonance attributable to the imidazolinium ion. Compared to the other two metalates, this experimental finding represents a major advantage for the envisioned reaction with dihydrogen. Presumably due to the polymeric structure of the metalate **Rs** and its poor solubility in the applied solvent MeCN/CD₃CN, the metalate and the imidazolinium ion are not (or only to a small fraction) present simultaneously in solution. A reaction of the two components is therefore hampered.

Despite its lacking reactivity in mixtures with imidazolium salt **TolFIm⁺Br⁻**, the metalate **Rs** was found to be active in a H/D exchange reaction. Suspensions of **Rs** in CD₃CN in a high pressure NMR tube showed – after degassing the solvent and pressurization with H₂ (8 bar) – the gradual formation of HD. A clear evidence for this is the fact that the H₂ signal ($\delta = 4.57$ ppm) recedes while a triplet at 4.53 ppm becomes more and more intense. The measured ¹J(H,D) coupling constant of HD is 43 Hz which is in agreement with literature values.^[511] H/D exchange was observed over the course of 47 d, after which the H₂:HD ratio is 1:6. Furthermore, the overall decreasing intensity of the signals points to the formation of D₂. In addition to the ¹H NMR signals for H₂ and HD also a third species with a resonance at 4.86 ppm becomes visible after some time. The chemical shift of this signal is similar to the chemical shift of the Cp ring of **KRp** ($\delta = 4.83$ ppm) and probably hints at the liberation of **Rp⁻** anions as time passes. The H/D exchange reaction was also observed when the experiment was repeated in MeCN with D₂ gas. In the ²H NMR spectrum the formed HD exhibits a doublet at 4.56 ppm (¹J(D,H) = 43 Hz).

The most probable explanation for the observed H/D exchange reactions is an interaction of the metalate **Rs** with the solvent. An indication for this assumption is the fact that the intensity of the CHD₂CN resonance increases over time (relative to residual amounts of silicon grease) in the ¹H NMR spectrum of a CD₃CN reaction mixture pressurized with H₂. Obviously, the compound activates the C–D/C–H bonds of the solvent CD₃CN/MeCN so that exchange reactions with H₂/D₂ are possible. However, the exact mechanism of this interaction remains unclear.

5.5.3 Heterolytic Splitting of Dihydrogen

As already demonstrated, mixtures of the imidazolium salt **TolFIm⁺Br⁻** and the metalate **Rs** in CD₃CN did not give any indication of a reaction between the two compounds at room temperature. However, when the mixture was exposed to dihydrogen, heterolytic splitting of the H₂ molecule was observed.^[345] The splitting of dihydrogen was noticed already with moderate pressures of H₂ (1.5 bar), however the reactions were cleaner (fewer by-products were formed) when higher pressures were applied. Figure 5.14 depicts several ¹H NMR spectra recorded at selected times after combining **TolFIm⁺Br⁻**, **Rs**, and H₂ (8 bar) in CD₃CN at room temperature. The spectra demonstrate that the imidazolium ion is consumed while the imidazolidine **HTolFIm** is formed.

A more detailed inspection of the presented NMR data reveals that a new signal at 6.06 ppm arises which can be attributed to the CH proton of the product **HTolFIm**. Furthermore, the resonance for the CH₂ groups of the starting material at 4.64 ppm decreases and at the same time two multiplets at 4.05 – 4.00 and 3.60 – 3.55 ppm become more intense. The multiplets correspond to the diastereotopic CH₂ protons of the imidazolidine. Furthermore, a resonance at –11.05 ppm arises which is characteristic

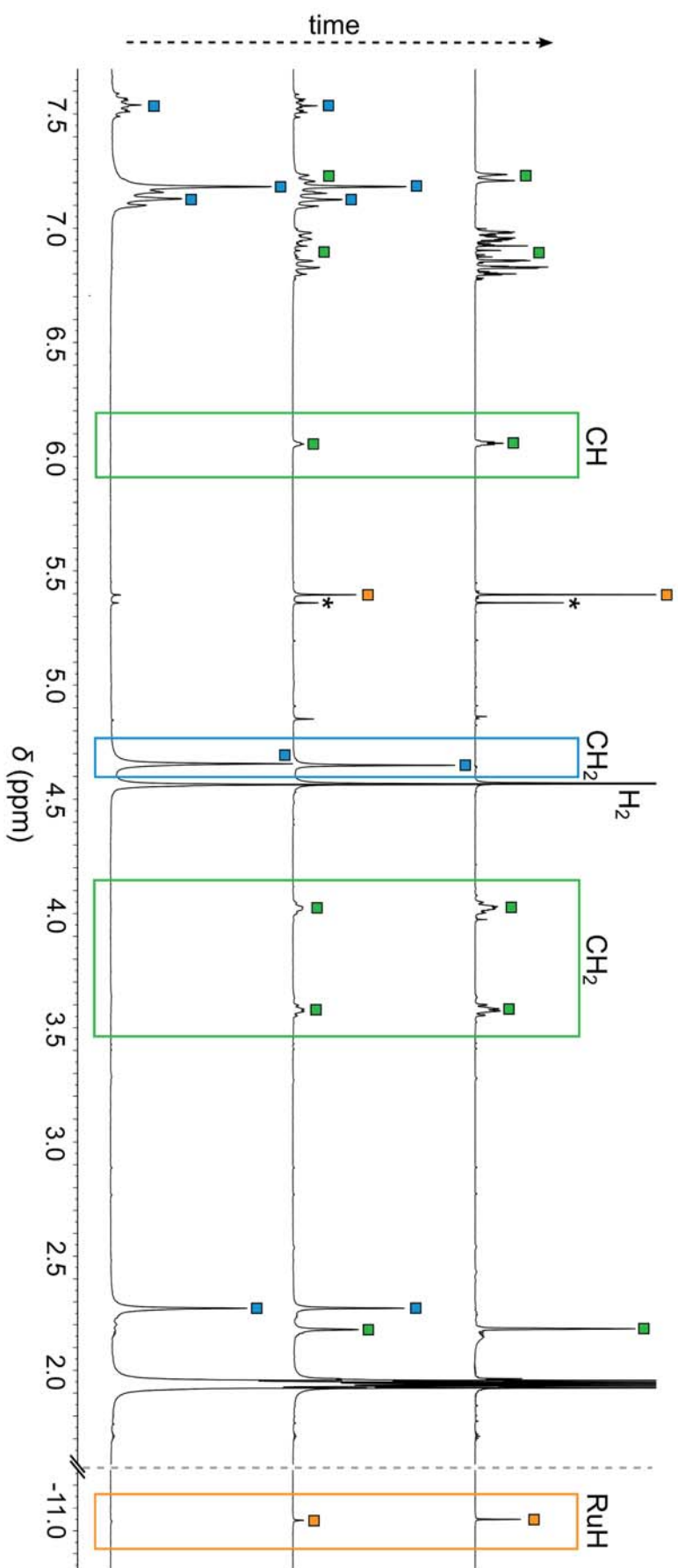


Figure 5.14. ^1H NMR spectra (300 MHz) of the mixture of $\text{TolFlm}^+\text{Br}^-$, R_s and H_2 (8 bar) in CD_3CN at rt after 6 minutes, 1 h and 3 d (bottom to top). Signals that can be assigned to $\text{TolFlm}^+\text{Br}^-$ (blue), H_2 (green), R_s (orange) are marked with colors; CH, CH₂ and hydride regions are highlighted by frames. The resonance attributable to the Cp rings of R_p is marked with an asterisk. Detailed views of the time-dependent evolution of the different signals are provided in the Appendix.

of the metal hydride HRuCp(CO)₂ (**HRp**).^[491] The observed signals clearly originate from the uptake of a hydride ion at the C² position of the imidazolium ion and from protonation of the metalate. Hence a heterolytic splitting of H₂ has taken place. In the spectra no signals for the polymeric black material **Rs** are present because of its poor solubility under the applied conditions.

For the products **HTolFIm** and **HRp** formed in this reaction, a ratio of 1:1 is expected. However, integration of the CH signal of **HTolFIm** and the Ru-H signal does not confirm this expectation, but the concentration of the metal hydride **HRp** seems to be constantly too low. A possible explanation for this could be the partial decomposition of the formed **HRp** to dimeric **Rp**₂ (which is also present in the ¹H NMR spectrum, see Figure 5.14). Furthermore, the influence of the structure of the starting material **Rs** is not entirely clear. After the reaction, still a solid material can be recognized in the reaction mixture. This is expected since one would assume that – analogous to the reaction with **KRp** – considerable amounts of KBr are formed during the reaction. To what extent parts of the formed product **HRp** are still associated with this solid material cannot be judged on the basis of the obtained experimental data. ATR IR measurements of the solid residue could, however, not prove the presence of **HRp**. On the contrary, the presence of the reaction product **HRp** in solution could be further confirmed by its reactivity with triphenylphosphine. Since it is known that **HRp** readily reacts with this reagent to produce the ruthenium hydride complex CpRu(CO)(PPh₃)H,^[491] the phosphine was added to the reaction mixture after completion of the H₂ reaction. Heating of the NMR sample to 45 °C for 3 d indeed caused the gradual conversion of **HRp** to the phosphine complex CpRu(CO)(PPh₃)H. An evidence for this is the appearance of a doublet at -11.69 ppm (²J(H,P) = 32 Hz) in the ¹H NMR spectrum and a doublet at 66.6 ppm (²J(P,H) = 31 Hz) in the ³¹P NMR spectrum.

The fact that the hydride acceptor molecule features fluorine atoms in its aromatic rings represents an important advantage since ¹⁹F NMR spectroscopy can be used as an additional probe to examine the reaction with dihydrogen. Consequently, the time dependence of the reaction with H₂ was followed by ¹⁹F NMR spectroscopy. The measurements showed the gradual decrease of the signal for the starting material **TolFIm**⁺**Br**⁻ at -118.5 ppm while the intensity of the resonance for the imidazolidine **HTolFIm** at -119.3 ppm increased over time. The progress of the reaction is visible in Figure 5.15. From the ratio of the integrals it becomes clear that, under the specific reaction conditions, the reaction is almost complete after 1 d (96 % conversion). A kinetic analysis of the reaction was not performed because of the heterogeneous character of the sample. It should, however, be mentioned that thorough mixing of the reaction mixture was required to prevent the formation of a by-product. In the experiment this was realized by placing the NMR sample in an ultrasonic bath equipped with a timer (2 min on, 12 min off). By this method, an undesired heating of the bath is avoided and room temperature is maintained throughout the reaction. The by-product exhibits chemical shifts similar to those observed for the dimer [(**TolFIm**)₂]**Br**₂ which was identified in reactions of the imidazolium salt with **KFp** (for details see section 5.3.4). However, the exact reasons for its formation could not be resolved.

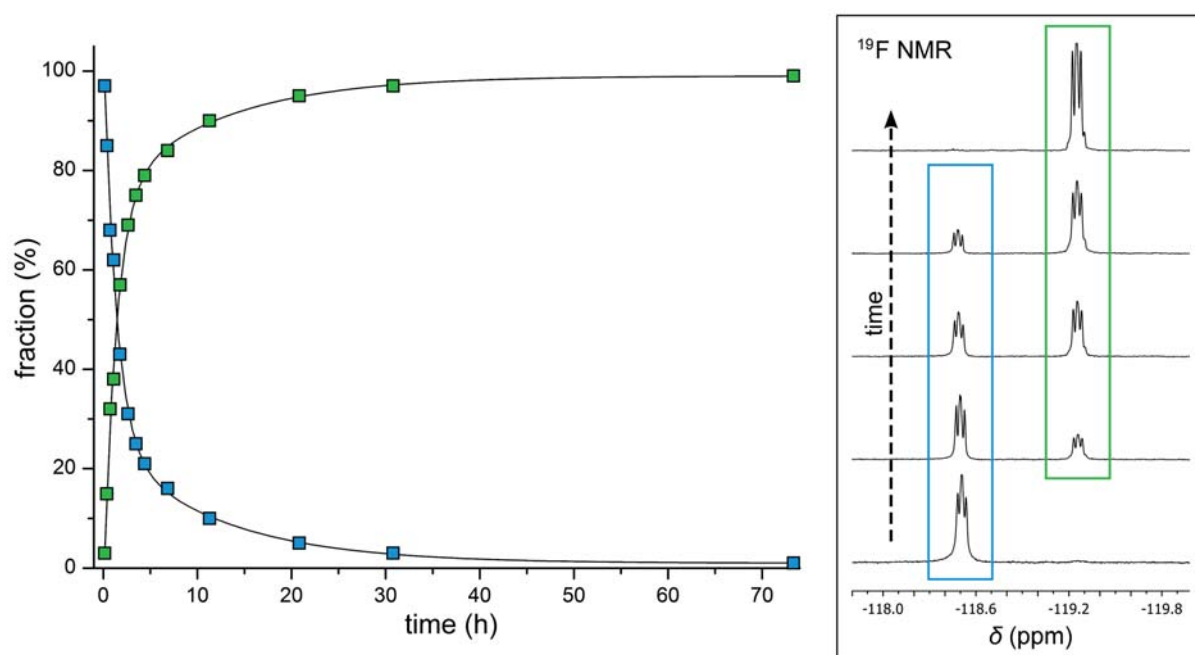


Figure 5.15. Time dependence of the composition of the reaction mixture of TolFIm⁺Br⁻, **Rs** and H₂ (8 bar) in CD₃CN at rt. The signal for TolFIm⁺Br⁻ (blue) decreases while the signal for HTolFIm (green) increases over time.

In order to confirm that the identified reaction products **HRp** and **HTolFIm** indeed originate from the heterolytic splitting of dihydrogen, analogous experiments with D₂ were conducted. Figure 5.16 depicts the ²H NMR spectrum of a reaction mixture consisting of the imidazolinium salt, the metalate, and D₂ (8 bar) in MeCN, acquired after 3 d. Signals for the deuterated products **DTolFIm** (6.05 ppm) and **DRp** (-10.97 ppm) are present. Furthermore, resonances for D₂ (4.58 ppm), HD (4.63 ppm, d, ¹J(D,H) = 43 Hz) and CDH₂CN (1.94 ppm, t, ²J(D,H) = 2.5 Hz) can be observed. The peak at 2.15 ppm can probably be attributed to D₂O which presumably originates from residual water present in the imidazolinium salt. Extensive efforts to remove the water (e.g. by prolonged heating of the compound to 120 °C *in vacuo* and stirring a MeCN solution of the salt over molecular sieves) were undertaken, however the water could not be removed entirely. The implications for the actual H₂/D₂ splitting process are not yet entirely clear. In general one would expect that (deuterated) water reacts with the metalate **Rs** to produce the metal hydride complexes **HRp/DRp**. However, this is obviously not the case since an excess of **HTolFIm/DTolFIm** has been formed in the heterolytic splitting reactions. In a control experiment, degassed water was added to a mixture of TolFIm⁺Br⁻ and **Rs**. After sonication like in the reactions with H₂/D₂, the mixture mainly contained the decomposition product already detected as a by-product before. Only trace amounts of the imidazolidine **HTolFIm** could be verified by means of NMR spectroscopy. The origin of these trace amounts of imidazolidine formed in the absence of H₂/D₂, could not be finally clarified.

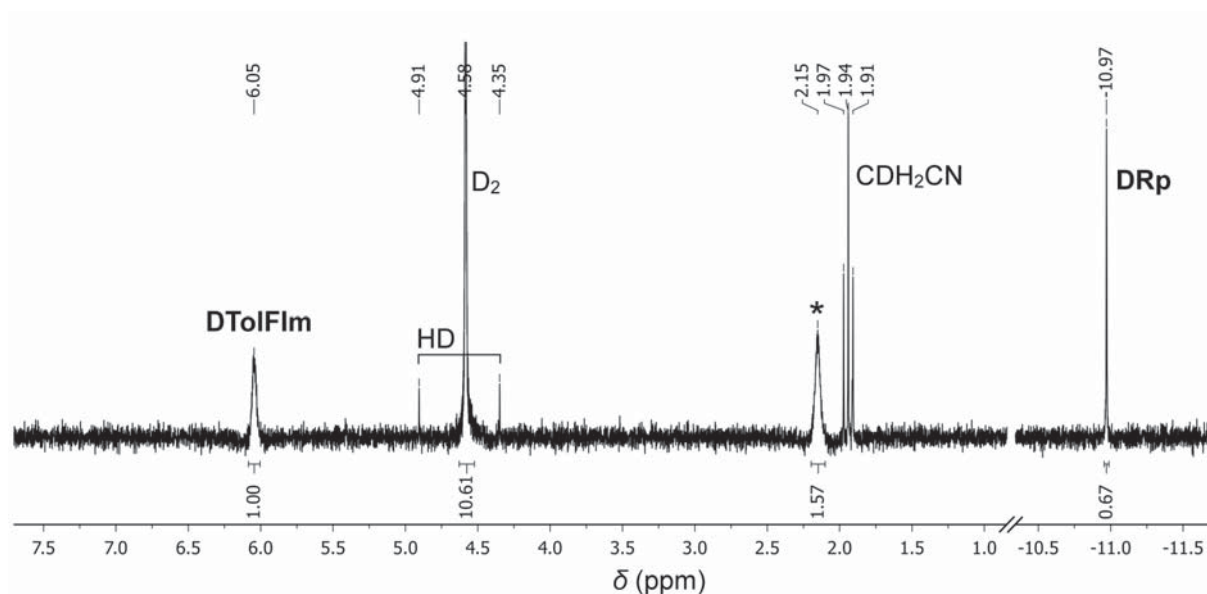


Figure 5.16. ²H NMR spectrum of the reaction mixture of **TolFIm**⁺**Br**⁻, **Rs** and D₂ (8 bar) in MeCN at rt acquired after 3 d. The signal marked with an asterisk presumably can be assigned to D₂O.

The H₂ splitting reaction was further examined by means of IR spectroscopy in solution. Figure 5.17 shows an IR spectrum of the reaction mixture after full conversion of the imidazolium salt **TolFIm**⁺**Br**⁻ to the imidazolidine **HTolFIm**. Furthermore, also IR spectra of **HTolFIm** (synthesized independently by reduction of **TolFIm**⁺**Br**⁻ with NaBD₄, see Experimental Section), **TolFIm**⁺**Br**⁻, and **Rp**₂ are included in the figure for comparison.

As becomes clear when comparing the different IR spectra, the reaction mixture contains the imidazolidine **HTolFIm** and not the starting material **TolFIm**⁺**Br**⁻. Also minor amounts of ruthenium dimer **Rp**₂ are present in the reaction mixture, a finding that has already been made in the NMR measurements. The remaining very intensive bands at 2025 and 1960 cm⁻¹ are characteristic CO stretching vibrations for the ruthenium hydride **HRp**.^[461,464,512] The two bands are highly asymmetric and especially the band at 1960 cm⁻¹ has broad tails. This has also been observed for the reaction of **Rs** with protic MeOH yielding a similar IR spectrum, and association effects have been proposed as a possible explanation for this (see section 4.3). The differing intensity of the two bands is expected since the ratio of the intensities of symmetric and asymmetric CO stretching vibrations is a function of the angle (2θ) between the two CO ligands.^[513–516] In a simplified picture, equation 5.2 can be used to calculate the angle between the CO molecules:

$$\frac{I_{\text{asym}}}{I_{\text{sym}}} = \tan^2 \theta \quad (5.2)$$

For 2θ = 90°, equal IR intensities of symmetric and asymmetric stretching vibrations are expected. With an increasing angle between the two CO ligands, the intensity of the symmetric stretching vibration recedes. In case of a linear arrangement (2θ = 180°),

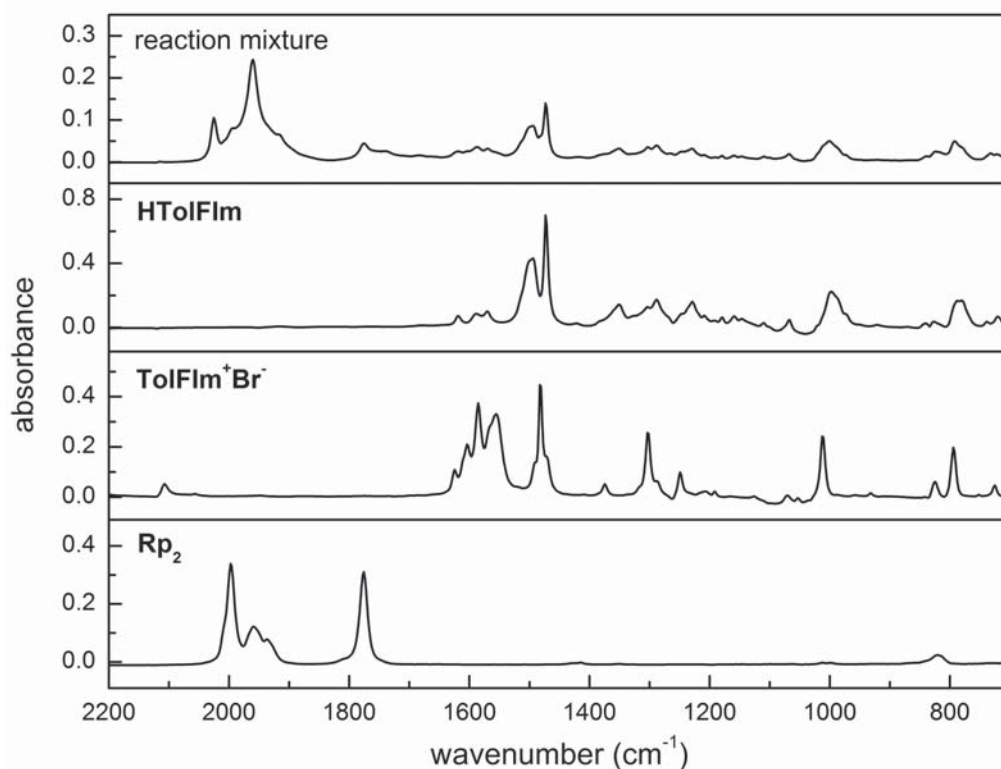


Figure 5.17. IR spectrum of the reaction mixture of **TolFIm**⁺**Br**⁻, **Rs**, and H₂ (8 bar) after completion of the reaction. For comparison, also IR spectra of **HTolFIm**, **TolFIm**⁺**Br**⁻, and **Rp**₂ are shown. All measurements were performed in CD₃CN

only the asymmetric stretching vibration can be observed. The symmetric stretching vibration is IR inactive for a linear geometry since the dipole moment does not change for this vibration. Unfortunately, a determination of the angle between the two CO ligands was not possible for the IR spectrum of the reaction mixture presented in Figure 5.17 because of the unfavorable bandshape of the signals and the overlapping bands of the impurity **Rp**₂. However, the fact that the intensity of the asymmetric CO stretching vibration is significantly larger than the intensity of the symmetric stretching vibration makes clear that the angle between the two CO ligands in the reaction product is larger than 90°.

In conclusion, also the IR data confirm the presence of **HTolFIm** and **HRp** in the reaction mixture and thus provide further arguments in favor of a heterolytic splitting of dihydrogen.

5.6 Summary and Conclusion

In summary, it has been demonstrated that the reactions occurring after mixing of the synthesized hydride acceptor molecules and carbonyl metalates are manifold. While imidazolium salt $[\text{Im}^{2\text{H}}]^+\text{Br}^-$ and imidazolinium salts $\text{PhMesIm}^+\text{Br}^-$ and $\text{TolMesIm}^+\text{Br}^-$ did not show any reactivity in combination with the metalates KFp and KRp – neither upon mixing with the metalate, nor after addition of H_2 or other substrates – differing reaction pathways have been identified for other imidazolinium ions. The reactions that have been observed after addition of the metal carbonyl anions comprise nucleophilic substitution and electron transfer reactions. Which of the two competing pathways is taken depends *inter alia* on the metalate and the chosen solvent.

With imidazolinium ion TolFIm^+ and the metalate Rs a combination of organic Lewis acid and transition metal Lewis base has been found that can cleave H_2 to produce the imidazolidine HTolFIm and the ruthenium hydride complex HRp . Theoretical investigations on the heterolytic splitting of dihydrogen mediated by the frustrated Lewis pair $\text{TolFIm}^+\text{Rp}^-$ by means of DFT calculations showed that in principle a relatively low activation barrier can be expected once the FLP is formed. However, the formation of the FLP is crucial for the overall process and less likely to occur in solutions of the free ions. The effects of the polymeric nature of Rs on this process could not be resolved. In a variety of experiments, NMR and IR spectroscopy were used to confirm the identity of the formed products and to establish essential characteristics of the reaction. Although not containing Fe but its heavier congener Ru, the system represents the first functional model system for the [Fe] hydrogenase active site because it correctly emulates the heterolytic splitting of H_2 through the cooperative action of a Lewis acidic imidazolinium ion and a Lewis basic metal complex. In the H_2 splitting reaction, the imidazolinium ion serves as a hydride acceptor similar to methenyl- H_4MPT^+ and the metal complex accepts the proton. This finding permits a new view on the H_2 activation performed by hydrogenases since it suggests that the metal ion might also act as a proton acceptor and gets formally oxidized in the natural systems. This possibility has only rarely been considered since it was mostly proposed that a ligand in the coordination sphere of the Fe ion (cysteine thiolato-S or pyridinol-O) takes up the proton while the metal ion itself acts as a Lewis acid.^[219,247–249] Furthermore, the presented work demonstrates that superelectrophilic activation by protonation as has been proposed for methenyl- H_4MPT^+ to increase its Lewis acidity (see also chapter 1.4.2),^[245,246] is not necessarily required for an imidazolinium ion to serve as a hydride acceptor. This work might therefore contribute to a better understanding of the [Fe] hydrogenase and stimulate the development of novel H_2 activation catalysts with exciting properties.

6

Experimental Section

6.1 General Considerations

All manipulations of air- and moisture-sensitive compounds were carried out under an atmosphere of purified argon (dried over phosphorus pentoxide on solid support [Sicapent[®], Merck] and liberated from traces of oxygen by a heated copper catalyst) using standard Schlenk techniques or in a glovebox (MBRAUN LABmaster) under a nitrogen atmosphere. Solvents were dried over sodium benzophenone ketyl (Et₂O, *n*-pentane, *n*-heptane, DME), potassium benzophenone ketyl (THF, toluene, *n*-hexane), CaH₂ (DMSO, chlorobenzene, DMF, MeCN, EtCN, DCM, CHCl₃) or Mg (EtOH, MeOH) and distilled as well as degassed before use. Deuterated solvents were dried analogously. Alternatively, DCM, *n*-hexane and toluene were dried using a solvent purification system (MB-SPS). Commercially available chemicals were purchased from Aldrich, Acros, Merck, Fluka, Deutero, Euriso-Top or ABCR and used without further purification unless stated otherwise. Hydrogen gas was purchased from Messer, deuterium gas was provided by Linde. ¹³C-enriched CO gas (99 % ¹³C) was obtained from Euriso-Top. 2,3,5,6-Tetrafluoro-4-methylaniline,^[517] [CpFe(CO)₂]₂ (**Fp**₂),^[518] Ni(dppe)₂,^[477] and Fe(CO)₃(^tBu)₂^[478] were synthesized according to published procedures. Ni(depe)₂ was prepared analogously to Ni(dppe)₂.^[477]

NMR spectra were recorded on Bruker Avance 200, 300, 400 or 500 instruments at 25 °C if not noted otherwise. Chemical shifts (δ) are given in ppm and are referenced to the solvent residual signals.^[519] The peaks are labeled according to their splitting patterns with s (singlet), d (doublet), t (triplet), q (quartet), quin (quintet) or m (multiplet). ¹⁹F NMR spectra were referenced externally relative to CFCl₃. If necessary, 2D NMR measurements were performed in order to assure a correct assignment of the observed resonances. Exchange rates were determined from NOESY spectra using the program *EXSYCalc*.^[520] Reactions which required high pressures of H₂ or D₂ were performed in Wilmad-LabGlass high pressure NMR tubes (medium wall, 524-PV-7). Solid-state NMR experiments were carried out on a Bruker Avance 400 spectrometer equipped with a

(^1H , X, Y) triple resonance 4 mm MAS probe. The ^{13}C chemical shifts were referenced externally to adamantane. Typical 90° pulse lengths were $3\ \mu\text{s}$ for proton and $5\ \mu\text{s}$ for carbon. In carbon direct excitation experiments, interscan delays were set to 240 s to avoid saturation. The ^1H – ^{13}C cross polarization contact time was 1.3 ms. The interscan delay in CP experiments was set to 2.5 s. In all solid-state NMR experiments, the ^1H decoupling field strength was 80 kHz during acquisition.

Standard CHN elemental analyses were performed on an Elementar 4.1 vario EL 3 element analyzer. Ruthenium contents were determined photometrically by a Perkin-Elmer Lambda 2 UV/Vis spectrometer after pressure digestion with HNO_3 and potassium was quantified using a Thermo Scientific IRIS Intrepid II instrument (ICP-OES). Wavelength dispersive electron microprobe analysis (EMPA) was conducted using a JEOL JXA8900 RL instrument. The beam conditions were set to an accelerating voltage of 15 kV, a beam current of 15 nA and a slightly defocused beam of $5\ \mu\text{m}$. The standards MgO (synthetic), sanidine (KAlSi_3O_8), wollastonite (CaSiO_3) and Ru metal were chosen to calibrate O, K, Si and Ru, respectively. Matrix correction was performed using the $\Phi\rho z$ method (CITZAF program) after Armstrong.^[500]

Cyclic voltammetry measurements were conducted either at a PerkinElmer 263A potentiostat using a glassy carbon working electrode, a silver quasi-reference electrode and a platinum counter electrode or in a glovebox (MBRAUN UNIlab, argon atmosphere) with a Metrohm Autolab PGSTAT101 potentiostat using platinum electrodes. All measurements were performed in 0.1 M solutions of NBu_4PF_6 in MeCN at room temperature. Decamethylferrocene (FcCp_2^*) was added as internal standard and the redox potentials were referenced *vs.* the $\text{FcCp}_2/\text{FcCp}_2^+$ (Fc/Fc^+) redox couple ($\text{FcCp}_2^*/\text{FcCp}_2^{*+}$ *vs.* Fc/Fc^+ : 0.510 V in MeCN).^[342] Electrochemical reductions were performed with a VersaSTAT 3 potentiostat from Princeton Applied Research using a platinum net electrode, a silver quasi-reference electrode, and a platinum counter electrode.

X-ray data were collected on a STOE IPDS II diffractometer with an area detector (graphite-monochromated Mo- K_α radiation, $\lambda = 0.71073\ \text{\AA}$) by use of ω scans at 133 K. The structures were solved by direct methods and refined against F^2 using all reflections with *SHELX-97* or *SHELX-2013*.^[521] Most non-hydrogen atoms were refined anisotropically. Most hydrogen atoms were placed in calculated positions and assigned to an isotropic displacement parameter of 1.2/1.5 $U_{\text{eq}}(\text{C})$. Face-indexed absorption corrections were performed numerically with the program *X-RED*.^[522] Crystal structure data for **TolFIm** $^+\text{Br}^- \cdot \text{H}_2\text{O}$ (CCDC-944125), **HTolFIm** (CCDC-944126), **KRp** \cdot THF (CCDC-983836), and **[Rp–TolFIm] $^+\text{Br}^- \cdot \text{MeCN}$** (CCDC-1007089) have been deposited at The Cambridge Crystallographic Data Centre CCDC and can be obtained free of charge *via* the Internet at http://www.ccdc.cam.ac.uk/data_request/cif.

Mass spectrometry was performed on an Applied Biosystems API 2000 device or on a Bruker HCTultra instrument. Mass spectrometry samples sensitive to oxygen or moisture were prepared in a glovebox (MBRAUN UNIlab) under an argon atmosphere and injected into the Bruker HCTultra instrument *via* a direct Peek[™] tubing connection.

IR spectra were recorded using either an Excalibur FTS 3000, a Bruker VERTEX 70 or a Cary 630 FTIR spectrometer equipped with DialPath and Diamond ATR acces-

sory (Agilent) placed in a glovebox (MBRAUN UNIlab, argon atmosphere). IR bands were labeled according to their relative intensities with vs (very strong), s (strong), m (medium), w (weak), vw (very weak) and sh (shoulder).

UV/Vis/NIR spectra were recorded with a Varian Cary 50 Bio or Varian Cary 5000 instrument using quartz cuvettes for solutions or a Praying Mantis™ sampling kit for solid samples. UV/Vis spectra at low temperature were measured with a quartz immersion probe (1 mm path length, Hellma Analytics). If necessary, the obtained spectra were transformed into energy plots and fitted with Gaussian functions using the *Fityk* program.^[490]

X-band EPR derivative spectra were recorded on a Bruker ELEXSYS E500 spectrometer equipped with the Bruker standard cavity (ER4102ST) and a helium flow cryostat (Oxford Instruments ESR 910). Microwave frequencies were calibrated with a Hewlett-Packard frequency counter (HP5352B), and the field control was calibrated with a Bruker NMR field probe (ER035M).

Melting points were determined in glass capillary tubes on a Stanford Research Systems OptiMelt MPA 100 device, the values given are uncorrected.

6.2 Synthesis of Amidines

The amidines synthesized in the framework of this thesis were prepared according to modified existing protocols.^[328,332] One of the following two general working procedures was applied:

General procedure 1 Diphosphorus pentoxide (21.3 g, 75.0 mmol, 6.0 eq), hexamethyldisiloxane (26.0 g, 34.2 mL, 160 mmol, 13 eq) and dichloromethane (30 mL) were heated to reflux for 1 h. All volatile compounds were removed by distillation at 165 °C. To the obtained viscous syrup, the benzoic acid derivative (12.5 mmol, 1.0 eq) and the corresponding aniline (30.0 mmol, 2.4 eq) were added, and the mixture was heated to 165 °C for 44 h. The hot reaction mixture was poured into aqueous KOH solution (0.5 M, 400 mL), stirred for 30 min and extracted with DCM (3 × 200 mL). The combined organic extracts were dried over Na₂SO₄, concentrated *in vacuo* and filtered over neutral aluminium oxide. The raw product obtained after removal of the solvent was recrystallized from H₂O/EtOH, washed with water and dried *in vacuo*.

General procedure 2 The synthesis parallels procedure 1, the workup was conducted as follows: The hot reaction mixture was poured into aqueous KOH solution (0.5 M, 400 mL), stirred for 30 min and extracted with DCM (3 × 200 mL). The combined organic extracts were dried over Na₂SO₄, concentrated *in vacuo* and filtered over neutral aluminium oxide. *N*-pentane was then added to the solution

and the mixture was kept at $-26\text{ }^{\circ}\text{C}$ to induce crystallization. Filtration, washing the product with *n*-pentane and drying *in vacuo* afforded the amidine.

***N,N'*-Bis-(2,4,6-trimethylphenyl)benzamidine (PhMesAm)**

PhMesAm was prepared according to general procedure 1. The product was obtained as yellowish crystals with a yield of 82 %.

$^1\text{H NMR}$ (500 MHz, CDCl_3 , $-45\text{ }^{\circ}\text{C}$): $\delta_{\text{major isomer}}$ (ppm) = 7.47 (d, $^3J(\text{H,H}) = 8\text{ Hz}$, 2 H; *o*-Ph-H), 7.32 (t, $^3J(\text{H,H}) = 8\text{ Hz}$, 1 H; *p*-Ph-H), 7.24 (t, $^3J(\text{H,H}) = 8\text{ Hz}$, 2 H; *m*-Ph-H), 6.97 (s, 2 H; *N*Mes-H), 6.68 (s, 2 H; *NH*Mes-H), 5.68 (s, 1 H; NH), 2.33 (s, 6 H; *o*-*N*Mes- CH_3), 2.30 (s, 3 H; *p*-*N*Mes- CH_3), 2.17 (s, 3 H; *p*-*NH*Mes- CH_3), 2.07 (s, 6 H; *o*-*NH*Mes- CH_3). $\delta_{\text{minor isomer}}$ (ppm) = 7.36 – 7.28 (m, 5 H, *o*-Ph-H, *p*-Ph-H, *m*-Ph-H), 6.98 (s, 2 H; Mes-H), 6.59 (s, 2 H; Mes-H), 5.76 (s, 1 H; NH), 2.42 (s, 6 H; *o*-Mes- CH_3), 2.29 (s, 3 H; *p*-Mes- CH_3), 2.11 (s, 3 H; *p*-Mes- CH_3), 2.01 (s, 6 H; *o*-Mes- CH_3).

$^{13}\text{C}\{^1\text{H}\}$ NMR (75 MHz, CDCl_3): $\delta_{\text{major isomer}}$ (ppm) = 154.4 (N=C–N), 143.4 (*ipso*-*N*Mes-C), 136.2 (*p*-*NH*Mes-C), 135.6 (*ipso*-Ph-C), 134.7 (*o*-*NH*Mes-C), 134.6 (*ipso*-*NH*Mes-C), 132.1 (*p*-*N*Mes-C), 129.5 (*p*-Ph-C), 129.3 (*m*-*N*Mes-C, *m*-*NH*Mes-C), 128.9 (*o*-*N*Mes-C), 128.3 (*o*-Ph-C), 127.8 (*m*-Ph-C), 20.9 (*p*-*NH*Mes- CH_3), 20.9 (*p*-*N*Mes- CH_3), 19.1 (*o*-*NH*Mes- CH_3), 18.1 (*o*-*N*Mes- CH_3). The intensity of the signals belonging to the minor isomer was generally too low for an accurate assignment.

MS (ESI⁺, MeCN): m/z (%) = 357.1 (100) [$\text{M}+\text{H}$]⁺.

IR (KBr): $\tilde{\nu}$ (cm^{-1}) = 3356 (m), 3289 (w), 3000 (m), 2965 (m), 2915 (m), 2855 (m), 2728 (w), 1634 (s), 1623 (s), 1600 (s), 1575 (m), 1470 (s), 1365 (s), 1312 (w), 1281 (w), 1243 (w), 1213 (m), 1151 (w), 1092 (m), 1073 (m), 1029 (m), 914 (w), 891 (w), 857 (m), 809 (m), 768 (m), 697 (s), 598 (w), 557 (w), 510 (w), 478 (w).

Elemental Analysis: Calcd. (%) for $\text{C}_{25}\text{H}_{28}\text{N}_2$: C 84.23, H 7.92, N 7.86. Found: C 83.39, H 7.62, N 7.85.

***N,N'*-Bis-(2,4,6-trimethylphenyl)pentafluorobenzamidine ($\text{C}_6\text{F}_5\text{MesAm}$)**

$\text{C}_6\text{F}_5\text{MesAm}$ was prepared according to general procedure 1. The product was obtained as yellowish crystals with a yield of 87 %.

$^1\text{H NMR}$ (500 MHz, CDCl_3): $\delta_{\text{major isomer}}$ (ppm) = 6.93 (s, 2 H; *N*Mes-H), 6.69 (s, 2 H; *NH*Mes-H), 5.86 (s_{br} , 1 H; NH), 2.30 (s, 6 H; *o*-*N*Mes- CH_3), 2.29 (s, 3 H; *p*-*N*Mes- CH_3), 2.15 (s, 3 H; *p*-*NH*Mes- CH_3), 2.10 (s, 6 H; *o*-*NH*Mes- CH_3). $\delta_{\text{minor isomer}}$ (ppm) = 8.10 (s_{br} , 1 H; NH), 6.85 (s_{br} , 2 H; *NH*Mes-H), 6.52 (s_{br} , 2 H; *N*Mes-H), 2.36 (s_{br} , 6 H; *o*-*NH*Mes- CH_3), 2.27 (s_{br} , 3 H; *p*-*NH*Mes- CH_3), 2.06 (s_{br} , 3 H; *p*-*N*Mes- CH_3), 1.95 (s_{br} , 6 H; *o*-*N*Mes- CH_3).

$^{13}\text{C}\{^1\text{H}\}$ NMR (126 MHz, CDCl_3): $\delta_{\text{major isomer}}$ (ppm) = 145.6 (*ipso*-NMe_s-C), 137.3 (*p*-NHMe_s-C), 135.9 (*o*-NHMe_s-C), 133.6 (*p*-NMe_s-C), 131.6 (*ipso*-NHMe_s-C), 129.5 (*m*-NMe_s-C), 129.3 (*m*-NHMe_s-C), 128.5 (*o*-NMe_s-C), 20.9 (*p*-NHMe_s-CH₃), 20.8 (*p*-NMe_s-CH₃), 18.2 (*o*-NHMe_s-CH₃), 17.8 (*o*-NMe_s-CH₃). The carbon atoms of the pentafluorophenyl ring as well as the N=C–N carbon atom could not be assigned due to their very low intensity caused by coupling to the ^{19}F nuclei. The intensity of the signals belonging to the minor isomer was generally too low for an accurate assignment.

$^{19}\text{F}\{^1\text{H}\}$ NMR (282 MHz, CDCl_3): $\delta_{\text{major isomer}}$ (ppm) = –137.9 – (–138.0) (m, 2 F; *o*-F), –152.0 (t, $^3J(\text{F},\text{F}) = 20$ Hz, 1 F; *p*-F), –161.0 – (–161.1) (m, 2 F; *m*-F). $\delta_{\text{minor isomer}}$ (ppm) = –136.9 – (–136.9) (m, 2 F; *o*-F), –151.4 (t, $^3J(\text{F},\text{F}) = 20$ Hz, 1 F; *p*-F), –160.6 – (–160.7) (m, 2 F; *m*-F).

MS (ESI⁺, MeCN): m/z (%) = 447.1 (100) [M+H]⁺, 469.1 (8) [M+Na]⁺, 485.1 (10) [M+K]⁺, 893.2 (48) [2M+H]⁺, 915.2 (6) [2M+Na]⁺, 955.2 (8) [2M+Cu]⁺.

IR (KBr): $\tilde{\nu}$ (cm^{–1}) = 3359 (m), 3194 (m), 2985 (m), 2922 (m), 2858 (m), 2731 (w), 1624 (s), 1520 (s), 1495 (s), 1439 (m), 1362 (m), 1327 (m), 1277 (m), 1204 (m), 1150 (m), 1092 (m), 988 (s), 856 (s), 802 (m), 654 (w), 592 (w), 556 (w), 505 (w), 478 (w).

Elemental Analysis: Calcd. (%) for C₂₅H₂₃F₅N₂: C 67.26, H 5.19, N 6.27. Found: C 66.83, H 5.43, N 6.29.

***N,N'*-Bis-(2,4,6-trimethylphenyl)-4-trifluoromethylbenzamidine (CF₃PhMesAm)**

CF₃PhMesAm was prepared according to general procedure 1. The product was obtained as yellowish crystals with a yield of 87 %.

^1H NMR (500 MHz, CD₂Cl₂, –75 °C): $\delta_{\text{major isomer}}$ (ppm) = 7.47 (d, $^3J(\text{H},\text{H}) = 8$ Hz, 2 H; *o*-Ar-H), 7.40 (d, $^3J(\text{H},\text{H}) = 8$ Hz, 2 H; *m*-Ar-H), 6.89 (s, 2 H; NMe_s-H), 6.61 (s, 2 H; NHMe_s-H), 5.67 (s, 1 H; NH), 2.21 (s, 3 H; *p*-NMe_s-CH₃), 2.15 (s, 6 H; *o*-NMe_s-CH₃), 2.06 (s, 3 H; *p*-NHMe_s-CH₃), 1.97 (s, 6 H; *o*-NHMe_s-CH₃). $\delta_{\text{minor isomer}}$ (ppm) = 7.38 (d, $^3J(\text{H},\text{H}) = 8$ Hz, 2 H; *m*-Ar-H), 7.32 (d, $^3J(\text{H},\text{H}) = 8$ Hz, 2 H; *o*-Ar-H), 5.67 (s_{br}, 1 H; NH), 6.88 (s, 2 H; NHMe_s-H), 6.57 (s, 2 H; NMe_s-H), 2.23 (s, 9 H; *o*-NHMe_s-CH₃, *p*-NHMe_s-CH₃), 2.06 (s, 3 H; *p*-NMe_s-CH₃), 1.87 (s, 6 H; *o*-NMe_s-CH₃).

$^{13}\text{C}\{^1\text{H}\}$ NMR (126 MHz, CD₂Cl₂, –75 °C): $\delta_{\text{major isomer}}$ (ppm) = 152.7 (N=C–N), 142.3 (*ipso*-NMe_s-C), 138.3 (*ipso*-Ar-C), 136.2 (*p*-NHMe_s-C), 134.4 (*o*-NHMe_s-C), 133.4 (*ipso*-NHMe_s-C), 131.8 (*p*-NMe_s-C), 129.9 (q, $^2J(\text{C},\text{F}) = 32$ Hz; *p*-Ar-C), 128.7 (*m*-NHMe_s-C), 128.6 (*m*-NMe_s-C), 128.2 (*o*-NMe_s-C), 128.2 (*o*-Ar-C), 124.2 (q, $^4J(\text{C},\text{F}) = 3$ Hz; *m*-Ar-C), 123.5 (q, $^2J(\text{C},\text{F}) = 272$ Hz; CF₃), 20.4 (*p*-NHMe_s-CH₃), 20.3 (*p*-NMe_s-CH₃), 18.8 (*o*-NHMe_s-CH₃), 17.6 (*o*-NMe_s-CH₃). $\delta_{\text{minor isomer}}$ (ppm) = 153.2 (N=C–N), 144.5 (*ipso*-NMe_s-C), 138.5 (*ipso*-Ar-C), 136.5 (*o*-NHMe_s-C), 136.4 (*p*-NHMe_s-C), 133.5 (*ipso*-NHMe_s-C), 129.9 (*p*-NMe_s-C), 129.8 (q, $^2J(\text{C},\text{F}) = 32$ Hz; *p*-Ar-C), 128.2 (*m*-NHMe_s-C), 127.7 (*m*-NMe_s-C), 127.6 (*o*-NMe_s-C), 127.5 (*o*-Ar-C), 124.6 (m; *m*-Ar-C), 123.3 (q,

$^2J(\text{C},\text{F}) = 272 \text{ Hz}$; CF_3), 20.6 (*p*-NHMe-CH₃), 20.2 (*p*-NMe-CH₃), 18.9 (*o*-NMe-CH₃), 17.9 (*o*-NHMe-CH₃).

$^{19}\text{F}\{^1\text{H}\}$ NMR (282 MHz, CDCl_3): $\delta_{\text{major isomer}}$ (ppm) = -62.8 (3 F; CF_3). $\delta_{\text{minor isomer}}$ (ppm) = -62.8 (3 F; CF_3).

MS (ESI⁺, MeCN): m/z (%) = 425.0 (100) [M+H]⁺.

IR (KBr): $\tilde{\nu}$ (cm⁻¹) = 3331 (m), 2987 (w), 2952 (w), 2918 (m), 2863 (w), 2730 (vw), 1644 (m), 1623 (s), 1573 (m), 1516 (w), 1475 (m), 1407 (m), 1375 (m), 1322 (vs), 1234 (w), 1216 (m), 1172 (s), 1128 (s), 1110 (m), 1063 (s), 1017 (m), 890 (w), 849 (s), 798 (m), 747 (w), 700 (m), 690 (m), 647 (w), 610 (w), 561 (w), 505 (w).

Elemental Analysis: Calcd. (%) for C₂₆H₂₇F₃N₂: C 73.56, H 6.41, N 6.60. Found: C 73.43, H 6.23, N 6.58.

***N,N'*-Bis-(2,4,6-trimethylphenyl)-4-toluamidine (TolMesAm)**

TolMesAm was prepared according to general procedure 1. The product was obtained as yellowish needles with a yield of 74 %.

^1H NMR (300 MHz, CDCl_3): $\delta_{\text{major isomer}}$ (ppm) = 7.37 (d, $^3J(\text{H},\text{H}) = 7 \text{ Hz}$, 2 H; *o*-Tol-H), 7.02 (d, $^3J(\text{H},\text{H}) = 8 \text{ Hz}$, 2 H; *m*-Tol-H), 6.94 (s, 2 H; NMe-H), 6.72 (s, 2 H; NHMe-H), 5.67 (s, 1 H; NH), 2.33 (s, 6 H; *o*-NMe-CH₃), 2.30 (s, 6 H; *p*-NMe-CH₃, *p*-Tol-CH₃), 2.19 (s, 3 H; *p*-NHMe-CH₃), 2.10 (s, 6 H; *o*-NHMe-CH₃). The intensity of the signals belonging to the minor isomer was generally too low for an accurate assignment.

$^{13}\text{C}\{^1\text{H}\}$ NMR (75 MHz, CDCl_3): $\delta_{\text{major isomer}}$ (ppm) = 154.4 (N=C-N), 143.5 (*ipso*-NMe-C), 139.5 (*p*-Tol-C), 136.1 (*p*-NHMe-C), 134.8 (*o*-NHMe-C, *ipso*-NHMe-C), 132.8 (*ipso*-Tol-C), 132.0 (*p*-NMe-C), 129.2 (*m*-NMe-C, *m*-NHMe-C), 129.0 (*o*-NMe-C), 128.5 (*m*-Tol-C), 128.2 (*o*-Tol-C), 21.4 (*p*-Tol-CH₃), 20.9 (*p*-NHMe-CH₃, *p*-NMe-CH₃), 19.1 (*o*-NHMe-CH₃), 18.1 (*o*-NMe-CH₃). The intensity of the signals belonging to the minor isomer was generally too low for an accurate assignment.

MS (ESI⁺, MeCN): m/z (%) = 371 (100) [M+H]⁺.

IR (KBr): $\tilde{\nu}$ (cm⁻¹) = 3334 (m), 3212 (w), 2947 (m), 2918 (m), 2857 (w), 2728 (w), 1622 (s), 1603 (s), 1570 (m), 1515 (s), 1497 (s), 1477 (s), 1405 (w), 1368 (m), 1322 (w), 1297 (w), 1281 (w), 1246 (w), 1224 (m), 1213 (m), 1181 (w), 1151 (w), 1115 (w), 1096 (w), 1024 (w), 1021 (w), 1011 (w), 894 (w), 852 (m), 834 (m), 804 (w), 791 (m), 726 (w), 694 (w), 677 (w), 639 (w), 623 (w), 552 (w), 533 (w), 497 (w), 486 (w).

Elemental Analysis: Calcd. (%) for C₂₆H₃₀N₂: C 84.28, H 8.16, N 7.56. Found: C 83.14, H 8.48, N 7.33.

***N,N'*-Bis-(2,6-difluorophenyl)benzamidine (PhFam)**

PhFam was prepared according to general procedure 2. The product was obtained as colorless crystals with a yield of 90 %.

¹H NMR (500 MHz, CDCl₃, -50 °C): δ_{major isomer} (ppm) = 7.42 (d, ³J(H,H) = 8 Hz, 2 H; *o*-Ph-H), 7.40 – 7.34 (m, 1 H; *p*-Ph-H), 7.31 (t, ³J(H,H) = 7 Hz, 2 H; *m*-Ph-H), 7.19 – 7.14 (m, 1 H; *p*-NAr-H), 6.98 (dd, ³J(H,F) = 8 Hz, ³J(H,H) = 8 Hz, 2 H; *m*-NAr-H), 6.78 – 6.67 (m, 3 H; *p*-NHAr-H, *m*-NHAr-H), 6.52 (s, 1 H; NH). δ_{minor isomer} (ppm) = 7.72 (d, ³J(H,H) = 7 Hz, 2 H; *o*-Ph-H), 7.45 – 7.42 (m, 1 H; *p*-Ph-H), 7.39 – 7.34 (m, 2 H; *m*-Ph-H), 6.99 – 6.96 (m, 1 H; *p*-Ar-H), 6.83 (s_{br}, 1 H; NH), 6.78 – 6.67 (m, 5 H; *p*-Ar-H, *m*-NAr-H, *m*-NHAr-H).

¹³C{¹H} NMR (126 MHz, CDCl₃, -50 °C): δ_{major isomer} (ppm) = 158.7 (N=C–N), 156.6 (dd, ¹J(C,F) = 284 Hz, ³J(C,F) = 6 Hz; *o*-NAr-C), 154.7 (dd, ¹J(C,F) = 278 Hz, ³J(C,F) = 6 Hz; *o*-NHAr-C), 133.4 (*ipso*-Ph-C), 130.6 (*p*-Ph-C), 128.5 (*m*-Ph-C), 127.9 (*o*-Ph-C), 127.7 (t, ²J(C,F) = 16 Hz; *ipso*-NHAr-C), 126.5 (t, ³J(C,F) = 9 Hz; *p*-NAr-C), 122.1 (t, ³J(C,F) = 9 Hz; *p*-NHAr-C), 115.5 (t, ²J(C,F) = 16 Hz; *ipso*-NAr-C), 111.9 (dd, ²J(C,F) = 19 Hz, ⁴J(C,F) = 3 Hz; *m*-NAr-C), 111.1 (dd, ²J(C,F) = 18 Hz, ⁴J(C,F) = 6 Hz; *m*-NHAr-C). The intensity of the signals belonging to the minor isomer was generally too low for an accurate assignment.

¹⁹F{¹H} NMR (282 MHz, CDCl₃): δ_{major isomer} (ppm) = -120.4 (s_{br}, 4 F; *o*-Ar-F). δ_{minor isomer} (ppm) = -119.4 (t, ⁸J(F,F) = 4 Hz, 2 F; *o*-NAr-F), -121.6 (t, ⁸J(F,F) = 4 Hz, 2 F; *o*-NHAr-F). MS (ESI⁺, MeCN): *m/z* (%) = 345.1 (100) [M+H]⁺, 367.0 (15) [M+Na]⁺, 383.0 (20) [M+K]⁺, 711.1 (4) [2M+Na]⁺.

IR (KBr): $\tilde{\nu}$ (cm⁻¹) = 3437 (m), 3213 (w), 1917 (w), 1896 (w), 1829 (w), 1750 (w), 1634 (s), 1618 (s), 1600 (s), 1516 (s), 1462 (s), 1322 (s), 1290 (s), 1274 (s), 1242 (s), 1232 (s), 1150 (m), 1105 (m), 1075 (m), 1059 (m), 1011 (s), 998 (s), 927 (m), 914 (m), 877 (m), 845 (w), 768 (s), 743 (s), 700 (s), 612 (m), 588 (m), 569 (m), 530 (m), 501 (m), 453 (m).

Elemental Analysis: Calcd. (%) for C₁₉H₁₂F₄N₂: C 66.28, H 3.51, N 8.14. Found: C 65.86, H 3.52, N 8.08.

***N,N'*-Bis-(2,6-difluorophenyl)-4-trifluoromethylbenzamidine (CF₃PhFam)**

CF₃PhFam was prepared according to general procedure 2. The product was obtained as colorless crystals with a yield of 79 %.

¹H NMR (300 MHz, CDCl₃): δ_{major isomer} (ppm) = 7.61 – 7.55 (m, 4 H; *o*-CF₃Ph-H, *m*-CF₃Ph-H), 7.02 – 6.70 (m, 6 H; *p*-NAr-H, *m*-NAr-H), *p*-NHAr-H, *m*-NHAr-H), 6.18 (s, 1 H; NH). δ_{minor isomer} (ppm) = 7.84 (d, ³J(H,H) = 7 Hz, 2 H; *o*-Ph-H), 7.61 – 7.55 (m, 2 H; *m*-CF₃Ph-H), 7.02 – 6.70 (m, 6 H; *p*-NAr-H, *m*-NAr-H), *p*-NHAr-H, *m*-NHAr-H), 6.18 (s_{br}, 1 H; NH).

$^{13}\text{C}\{^1\text{H}\}$ NMR (75 MHz, CDCl_3): $\delta_{\text{major isomer}}$ (ppm) = 157.7 (N=C–N), 156.9 (dm, $^1\text{J}(\text{C},\text{F}) = 245$ Hz; *o*-NAr-C), 156.9 (dm, $^1\text{J}(\text{C},\text{F}) = 245$ Hz; *o*-NHAr-C), 137.3 (*ipso*- CF_3 Ph-C), 132.2 (q, $^2\text{J}(\text{C},\text{F}) = 33$ Hz; *p*- CF_3 Ph-C), 128.3 (*o*- CF_3 Ph-C), 127.3 (t, $^3\text{J}(\text{C},\text{F}) = 9$ Hz; *p*-NAr-C), 125.6 (q, $^3\text{J}(\text{C},\text{F}) = 4$ Hz; *m*- CF_3 Ph-C), 125.5 – 125.2 (m; *ipso*-NHAr-C), 123.9 (t, $^3\text{J}(\text{C},\text{F}) = 9$ Hz; *p*-NHAr-C), 116.6 (t, $^2\text{J}(\text{C},\text{F}) = 15$ Hz; *ipso*-NAr-C), 111.8 – 111.5 (m; *m*-NAr-C, *m*-NHAr-C). The chemical shift for the CF_3 moiety could not be determined due to overlapping with other signals. The quartet is expected to appear at 123 – 124 ppm. The intensity of the signals belonging to the minor isomer was in most cases too low for an accurate assignment.

$^{19}\text{F}\{^1\text{H}\}$ NMR (282 MHz, CDCl_3): $\delta_{\text{major isomer}}$ (ppm) = –63.0 (s, 3 F; CF_3), –119.5 (s_{br} , 2 F; *o*-NAr-F), –121.4 (s_{br} , 2 F; *o*-NHAr-F).

MS (ESI⁺, MeCN): m/z (%) = 413.0 (100) [M+H]⁺, 435.0 (8) [M+Na]⁺.

IR (KBr): $\tilde{\nu}$ (cm^{-1}) = 3385 (s), 3209 (m), 3145 (m), 3020 (m), 2994 (m), 2885 (w), 1632 (s), 1580 (m), 1544 (s), 1507 (s), 1469 (vs), 1436 (m), 1410 (s), 1375 (s), 1323 (vs), 1277 (s), 1240 (s), 1216 (m), 1154 (s), 1131 (vs), 1109 (s), 1066 (s), 1008 (vs), 998 (s), 924 (m), 866 (m), 834 (m), 781 (s), 774 (s), 766 (s), 757 (m), 734 (m), 727 (m), 701 (m), 689 (m), 637 (w), 607 (w), 591 (w), 569 (w), 527 (w), 504 (w), 485 (w).

Elemental Analysis: Calcd. (%) for $\text{C}_{20}\text{H}_{11}\text{F}_7\text{N}_2$: C 58.26, H 2.69, N 6.79. Found: C 57.82, H 2.55, N 6.77.

***N,N'*-Bis-(2,6-difluorophenyl)-4-toluidine (TolFam)**

TolFam was prepared according to general procedure 2. The product was obtained as colorless crystals with a yield of 86 %.

^1H NMR (500 MHz, CDCl_3 , –50 °C): $\delta_{\text{major isomer}}$ (ppm) = 7.31 (d, $^3\text{J}(\text{H},\text{H}) = 8$ Hz, 2 H; *o*-Tol-H), 7.16 – 7.07 (m, 3 H; *p*-NAr-H, *m*-Tol-H), 6.94 (dd, $^3\text{J}(\text{H},\text{F}) = 9$ Hz, $^3\text{J}(\text{H},\text{H}) = 7$ Hz, 2 H; *m*-NAr-H), 6.78 – 6.67 (m, 3 H; *p*-NHAr-H, *m*-NHAr-H), 6.64 (s, 1 H; NH), 2.28 (s, 3 H; CH_3). $\delta_{\text{minor isomer}}$ (ppm) = 7.58 (d, $^3\text{J}(\text{H},\text{H}) = 8$ Hz, 2 H; *o*-Tol-H), 7.16 – 7.07 (m, 3 H; *m*-Tol-H), 6.94 (m, 1 H; *p*-Ar-H), 6.78 – 6.67 (m, 5 H; *m*-Ar-H, *p*-Ar-H, *m*-Ar-H), 6.64 (s, 1 H; NH), 2.30 (s, 3 H; CH_3).

$^{13}\text{C}\{^1\text{H}\}$ NMR (126 MHz, CDCl_3 , –50 °C): $\delta_{\text{major isomer}}$ (ppm) = 156.7 (N=C–N), 156.7 (dd, $^1\text{J}(\text{C},\text{F}) = 265$ Hz; $^3\text{J}(\text{C},\text{F}) = 6$ Hz; *o*-NAr-C), 154.6 (dd, $^1\text{J}(\text{C},\text{F}) = 260$ Hz, $^3\text{J}(\text{C},\text{F}) = 6$ Hz; *o*-NHAr-C), 140.8 (*p*-Tol-C), 130.4 (*ipso*-Tol-C), 129.0 (*m*-Tol-C), 127.9 (t, $^2\text{J}(\text{C},\text{F}) = 16$ Hz; *ipso*-NHAr-C), 127.9 (*o*-Tol-C), 126.2 (t, $^3\text{J}(\text{C},\text{F}) = 9$ Hz; *p*-NAr-C), 121.9 (t, $^3\text{J}(\text{C},\text{F}) = 9$ Hz; *p*-NHAr-C), 115.6 (t, $^2\text{J}(\text{C},\text{F}) = 16$ Hz; *ipso*-NAr-C), 111.9 (dd, $^2\text{J}(\text{C},\text{F}) = 20$ Hz, $^4\text{J}(\text{C},\text{F}) = 3$ Hz; *m*-NAr-C), 111.1 (dd, $^2\text{J}(\text{C},\text{F}) = 18$ Hz, $^4\text{J}(\text{C},\text{F}) = 5$ Hz; *m*-NHAr-C), 21.6 (CH_3). The intensity of the signals belonging to the minor isomer was generally too low for an accurate assignment.

$^{19}\text{F}\{^1\text{H}\}$ NMR (282 MHz, CDCl_3): $\delta_{\text{major isomer}}$ (ppm) = –120.6 (s_{br} , 4 F; *o*-Ar-F). $\delta_{\text{minor isomer}}$ (ppm) = –119.5 (s, 2 F; *o*-NAr-F), –121.6 (s, 2 F; *o*-NHAr-F).

MS (ESI⁺, MeCN): m/z (%) = 359.1 (100) [M+H]⁺.

IR (KBr): $\tilde{\nu}$ (cm⁻¹) = 3409 (m), 3192 (w), 2954 (w), 2913 (w), 2363 (w), 1643 (s), 1607 (s), 1524 (m), 1509 (m), 1468 (s), 1385 (w), 1328 (m), 1312 (m), 1288 (m), 1274 (m), 1240 (m), 1183 (w), 1150 (w), 1105 (w), 1058 (w), 1005 (s), 948 (w), 928 (w), 862 (w), 816 (m), 781 (m), 734 (m), 722 (m), 686 (w), 654 (w), 630 (w), 590 (w), 568 (w), 530 (w), 505 (w), 486 (m).

Elemental Analysis: Calcd. (%) for C₂₀H₁₄F₄N₂: C 67.04, H 3.94, N 7.82. Found: C 66.56, H 3.87, N 7.87.

***N,N'*-Bis-(2,6-difluorophenyl)-2,4,6-trimethylbenzamidine (MesFAM)**

MesFAM was prepared according to general procedure 2. The product was obtained as colorless crystals with a yield of 77%.

¹H NMR (500 MHz, CDCl₃, -50 °C): $\delta_{\text{major isomer}}$ (ppm) = 7.27 – 7.21 (m, 1 H; *p*-NAr-H), 7.04 (dd, ³*J*(H,H) = 8 Hz, ³*J*(H,F) = 8 Hz, 2 H; *m*-NAr-H), 6.79 (s, 2 H; *m*-Mes-H), 6.77 – 6.70 (m, 1 H; *p*-NHAr-H), 6.67 (dd, ³*J*(H,H) = 8 Hz, ³*J*(H,F) = 8 Hz, 2 H; *m*-NHAr-H), 6.08 (s, 1 H; NH), 2.36 (s, 6 H; *o*-Mes-CH₃), 2.21 (s, 3 H; *p*-Mes-CH₃). At -50 °C the intensity of the signals belonging to the minor isomer was generally too low for an accurate assignment.

¹³C{¹H} NMR (126 MHz, CDCl₃, -50 °C): $\delta_{\text{major isomer}}$ (ppm) = 157.8 (N=C-N), 157.8 (dd, ¹*J*(C,F) = 250 Hz; ³*J*(C,F) = 6 Hz; *o*-NAr-C), 155.0 (dd, ¹*J*(C,F) = 245 Hz, ³*J*(C,F) = 6 Hz; *o*-NHAr-C), 138.8 (*p*-Mes-C), 136.0 (*o*-Mes-C), 130.8 (*ipso*-Mes-C), 128.1 (*m*-Mes-C), 127.4 (t, ³*J*(C,F) = 9 Hz; *p*-NAr-C), 126.3 (t, ²*J*(C,F) = 16 Hz; *ipso*-NHAr-C), 122.3 (t, ³*J*(C,F) = 10 Hz; *p*-NHAr-C), 114.8 (t, ²*J*(C,F) = 16 Hz; *ipso*-NAr-C), 112.0 (dd, ²*J*(C,F) = 19 Hz, ⁴*J*(C,F) = 4 Hz; *m*-NAr-C), 111.1 (dd, ²*J*(C,F) = 19 Hz, ⁴*J*(C,F) = 6 Hz; *m*-NHAr-C), 21.3 (*p*-Mes-CH₃), 19.5 (t, ⁷*J*(C,F) = 3 Hz; *o*-Mes-CH₃). The intensity of the signals belonging to the minor isomer was generally too low for an accurate assignment.

¹⁹F{¹H} NMR (282 MHz, CDCl₃): $\delta_{\text{major isomer}}$ (ppm) = -116.8 (s, 2 F; *o*-NAr-F), -121.0 (s, 2 F; *o*-NHAr-F). $\delta_{\text{minor isomer}}$ (ppm) = -117.7 (s, 2 F; *o*-NAr-F), -121.1 (s, 2 F; *o*-NHAr-F).

MS (ESI⁺, MeCN): m/z (%) = 387.1 (100) [M+H]⁺.

IR (KBr): $\tilde{\nu}$ (cm⁻¹) = 3436 (w), 3373 (m), 3196 (w), 2923 (m), 2856 (w), 1631 (vs), 1502 (s), 1469 (vs), 1323 (s), 1273 (s), 1240 (s), 1209 (m), 1150 (w), 1091 (m), 1058 (m), 1005 (vs), 855 (m), 778 (s), 730 (m), 694 (m), 580 (w), 501 (m), 443 (w).

Elemental Analysis: Calcd. (%) for C₂₂H₁₈F₄N₂: C 68.39, H 4.70, N 7.25. Found: C 67.98, H 4.60, N 7.35.

***N,N'*-Bis-(2,3,5,6-tetrafluoro-4-tolyl)-4-toluamidine (TolFTolAm)**

TolFTolAm was prepared according to general procedure 2. The product was obtained as a colorless solid with a yield of 58 %. As the starting material 2,3,5,6-tetrafluoro-4-methylaniline was not available free of regioisomers, also amidine **TolFTolAm** contained small amounts of differently substituted isomers as impurities which could not be removed by crystallization or column chromatography.

¹H NMR (300 MHz, CDCl₃): $\delta_{\text{major isomer}}$ (ppm) = 7.30 (d, $^3J(\text{H,H}) = 7$ Hz, 2 H; *o*-Tol-H), 7.13 (d, $^3J(\text{H,F}) = 9$ Hz, 2 H; *m*-Tol-H), 5.69 (s_{br}, 1 H; NH), 2.33 (s, 3 H; Tol-CH₃), 2.19 (s, 6 H; FTol-CH₃). The intensity of the signals belonging to the minor isomer was generally too low for an accurate assignment.

¹³C{¹H} NMR (75 MHz, CDCl₃): $\delta_{\text{major isomer}}$ (ppm) = 159.9 – 159.6 (m; N=C–N), 145.2 (dm, $^1J(\text{C,F}) = 247$ Hz; *o*-FTol-C, *m*-FTol-C), 141.6 (*p*-Tol-C), 130.1 (*ipso*-Tol-C), 129.5 (*m*-Tol-C), 127.7 (*o*-Tol-C), 111.3 (m; *p*-FTol-C), 21.5 (Tol-CH₃), 7.31 (FTol-CH₃). Due to enhanced delocalization of the NH proton, no separate signals for *N* and *NH* aromatic rings could be recorded. The *ipso*-FTol carbon atoms were not observed, presumably because of extensive coupling to the fluorine atoms. The intensity of the signals belonging to the minor isomer was generally too low for an accurate assignment.

¹⁹F NMR (282 MHz, CDCl₃, –30 °C): $\delta_{\text{major isomer}}$ (ppm) = –143.8 (dd, $^3J(\text{F,F}) = 23$ Hz, $^5J(\text{F,F}) = 10$ Hz, 2 F; *m*-NFTol-F), –145.9 (dd, $^3J(\text{F,F}) = 23$ Hz, $^5J(\text{F,F}) = 10$ Hz, 2 F; *m*-NHFTol-F), –146.3 – (–146.4) (m; *o*-NFTol-F), –153.9 (dd, $^3J(\text{F,F}) = 22$ Hz, $^5J(\text{F,F}) = 10$ Hz, 2 F; *o*-NHFTol-F). The intensity of the signals belonging to the minor isomer was generally too low for an accurate assignment.

MS (ESI⁺, MeCN): m/z (%) = 459.0 (100) [M+H]⁺, 979.2 (13) [2M+Cu]⁺.

IR (KBr): $\tilde{\nu}$ (cm^{–1}) = 3433 (w), 3194 (w), 3125 (w), 3039 (w), 2987 (w), 2936 (w), 2867 (w), 2809 (w), 1617 (s), 1542 (s), 1486 (s), 1330 (m), 1301 (m), 1186 (w), 1125 (m), 1070 (m), 982 (m), 929 (s), 824 (m), 658 (w), 617 (w), 600 (w), 580 (w), 536 (w), 476 (w).

Elemental Analysis: Calcd. (%) for C₂₂H₁₄F₈N₂: C 57.65, H 3.08, N 6.11. Found: C 57.53, H 3.54, N 6.05.

***N,N'*-Bis-(4-methylphenyl)-4-toluamidine (TolTolAm)**

TolTolAm was prepared according to general procedure 2. The product was obtained as colorless crystals with a yield of 62 %.

¹H NMR (400 MHz, CDCl₃, –60 °C): $\delta_{\text{isomer 1}}$ (ppm) = 7.57 (d, $^3J(\text{H,H}) = 8$ Hz, 2 H; *o*-NHTol-H), 7.22 – 7.18 (m, 2 H; *o*-CTol-H), 7.15 – 7.10 (m, 4 H; *m*-NHTol-H, *m*-CTol-H), 6.97 – 6.94 (m, 2 H; *m*-NTol-H), 6.73 (s, 1 H; NH), 6.65 (d, $^3J(\text{H,H}) = 8$ Hz, 2 H; *o*-NTol-H), 2.33 (s, 6 H; CTol-CH₃, NHTol-CH₃), 2.23 (s, 3 H; NTol-CH₃). $\delta_{\text{isomer 2}}$ (ppm) = 7.49 (d, $^3J(\text{H,H}) = 8$ Hz, 2 H; *o*-CTol-H), 7.22 – 7.18 (m, 2 H; *m*-NTol-H), 7.15 – 7.10 (m, 2 H; *m*-CTol-H), 6.97 – 6.94 (m, 4 H; *o*-NTol-H, *m*-NHTol-H), 6.60 (d, $^3J(\text{H,H}) = 8$ Hz,

2 H; *o*-NHTol-H), 6.45 (s, 1 H; NH), 2.35 (s, 6 H; CTol-CH₃, NTol-CH₃), 2.24 (s, 3 H; NHTol-CH₃).

¹³C{¹H} NMR (101 MHz, CDCl₃, -60 °C): δ_{isomer 1} (ppm) = 154.3 (N=C-N), 147.4 (*ipso*-NTol-C), 139.6 (*p*-CTol-C), 137.3 (*ipso*-NHTol-C), 132.1 (*p*-NHTol-C), 131.7 (*ipso*-CTol-C), 130.6 (*p*-NTol-C), 129.4 (*m*-NHTol-C), 129.1 (*m*-NTol-C, *m*-CTol-C), 128.7 (*o*-CTol-C), 122.3 (*o*-NTol-C), 118.9 (*o*-NHTol-C), 21.6 (CTol-CH₃), 21.0 (NHTol-CH₃), 20.9 (NTol-CH₃). δ_{isomer 2} (ppm) = 155.0 (N=C-N), 145.8 (*ipso*-NTol-C), 140.3 (*p*-CTol-C), 137.9 (*ipso*-NHTol-C), 133.0 (*p*-NTol-C), 132.6 (*p*-NHTol-C), 131.5 (*ipso*-CTol-C), 130.2 (*m*-NTol-C), 129.3 (*m*-NHTol-C), 129.0 (*m*-CTol-C), 128.9 (*o*-CTol-C), 121.7 (*o*-NHTol-C), 121.6 (*o*-NTol-C), 21.7 (CTol-CH₃), 21.1 (NTol-CH₃), 20.9 (NHTol-CH₃).

MS (ESI⁺, MeCN): *m/z* (%) = 315.1 (100) [M+H]⁺, 651.3 (6) [2M+Na]⁺.

IR (KBr): $\tilde{\nu}$ (cm⁻¹) = 3273 (m), 3019 (m), 2918 (m), 2860 (w), 1623 (s), 1592 (vs), 1530 (vs), 1514 (vs), 1503 (vs), 1404 (m), 1336 (s), 1222 (m), 1101 (m), 1018 (w), 933 (w), 920 (w), 861 (w), 816 (s), 760 (w), 641 (w), 617 (w), 571 (w), 528 (w), 512 (m), 485 (w).

Elemental Analysis: Calcd. (%) for C₂₂H₂₂N₂: C 84.04, H 7.05, N 8.91. Found: C 84.01, H 7.18, N 8.88.

6.3 Synthesis of Bisamidinatodisilver(I) Complexes

General procedure Ag₂O (0.21 g, 0.9 mmol, 1.5 eq), DCM (20 mL) and the respective amidine (0.6 mmol, 1.0 eq) were added to a flask, protected against light by aluminum foil, and the mixture was stirred at room temperature for 5 d. Activated carbon was then added to the reaction flask before stirring was continued for another 5 min. Subsequently, the mixture was filtrated over celite. The desired amidinatodisilver(I) complex was obtained after concentrating the filtrate *in vacuo*.

Ag₂(PhFam)₂

Silver amidinato complex Ag₂(PhFam)₂ was obtained in a quantitative yield as a colorless solid. Slow evaporation of a CHCl₃ solution of the compound gave crystals suitable for X-ray crystallography.

¹H NMR (300 MHz, CD₂Cl₂): δ (ppm) = 7.10 – 7.03 (m, 4 H; *o*-Ph-H), 6.98 – 6.94 (m, 6 H; *m*-Ph-H, *p*-Ph-H), 6.80 – 6.70 (m, 4 H; *p*-Ar-H), 6.66 – 6.55 (m, 8 H; *m*-Ar-H).

¹³C{¹H} NMR (75 MHz, CD₂Cl₂): δ (ppm) = 175.2 (N=C-N), 157.6 (dd, ¹J(C,F) = 244 Hz, ³J(C,F) = 5 Hz; *o*-Ar-C), 136.3 (*ipso*-Ph-C), 129.3 (t, ²J(C,F) = 16 Hz; *ipso*-Ar-C), 128.5 (*p*-Ph-C), 127.4 (*m*-Ph-C), 127.3 (*o*-Ph-C), 124.1 (t, ³J(C,F) = 10 Hz; *p*-Ar-C), 111.4 – 111.1 (m; *m*-Ar-C).

¹⁹F{¹H} NMR (282 MHz, CD₂Cl₂): δ (ppm) = -119.7 (s, 8 F; *o*-Ar-F).

MS (ESI⁺, MeCN): *m/z* (%) = 797.1 (80) [2M+Ag]⁺, 751.2 (45) [2M+Cu]⁺, 727.2 (6) [2M+K]⁺, 711.2 (35) [2M+Na]⁺, 383.1 (20) [M+K]⁺, 367.1 (15) [M+Na]⁺, 345.1 (100) [M]⁺ with M = PhFam.

IR (KBr): $\tilde{\nu}$ (cm⁻¹) = 3029 (w), 2062 (w), 1897 (w), 1616 (w), 1584 (m), 1562 (w), 1496 (s), 1471 (s), 1441 (m), 1417 (m), 1278 (m), 1259 (m), 1237 (m), 1211 (m), 1180 (w), 1148 (w), 1130 (w), 1077 (w), 1059 (m), 1027 (w), 1005 (s), 944 (w), 929 (w), 872 (w), 809 (m), 783 (m), 772 (m), 760 (m), 740 (m), 704 (m), 615 (w), 571 (w), 558 (w), 538 (w), 500 (w).

Elemental Analysis: Calcd. (%) for C₃₈H₂₂Ag₂F₈N₄: C 50.58, H 2.46, N 6.21. Found: C 50.04, H 2.75, N 5.83.

Ag₂(CF₃PhFam)₂

Silver amidinato complex **Ag₂(CF₃PhFam)₂** was obtained in a quantitative yield as a colorless solid. Slow evaporation of a DCM solution of the compound gave crystals suitable for X-ray crystallography.

¹H NMR (500 MHz, CD₂Cl₂): δ (ppm) = 7.27 – 7.17 (m, 8 H; *o*-CF₃Ph-H, *m*-CF₃Ph-H), 6.82 – 6.73 (m, 4 H; *p*-Ar-H), 6.66 – 6.58 (m, 8 H; *m*-Ar-H).

¹³C{¹H} NMR (126 MHz, CD₂Cl₂): δ (ppm) = 173.6 (N=C–N), 157.5 (dd, ¹J(C,F) = 245 Hz, ³J(C,F) = 4 Hz; *o*-Ar-C), 140.3 (*ipso*-CF₃Ph-C), 130.2 (q, ²J(C,F) = 32 Hz; *p*-CF₃Ph-C), 128.7 (t, ²J(C,F) = 15 Hz; *ipso*-Ar-C), 127.8 (*o*-CF₃Ph-C), 124.6 (t, ³J(C,F) = 9 Hz; *p*-Ar-C), 124.4 (q, ³J(C,F) = 4 Hz; *m*-CF₃Ph-C), 124.2 (q, ¹J(C,F) = 273 Hz; CF₃), 111.6 – 111.4 (m; *m*-Ar-C).

¹⁹F{¹H} NMR (282 MHz, CD₂Cl₂): δ (ppm) = –63.3 (s, 6 F; CF₃), –119.8 (s, 8 F, *o*-Ar-F).

IR (KBr): $\tilde{\nu}$ (cm⁻¹) = 3075 (w), 2471 (w), 1911 (w), 1619 (w), 1584 (m), 1562 (w), 1511 (s), 1472 (s), 1407 (m), 1325 (s), 1280 (m), 1238 (m), 1222 (w), 1210 (w), 1169 (m), 1152 (w), 1134 (m), 1108 (m), 1066 (m), 1019 (m), 1006 (s), 943 (w), 881 (w), 866 (w), 837 (m), 798 (w), 777 (m), 770 (m), 760 (w), 739 (w), 726 (w), 707 (w), 697 (w), 662 (w), 652 (w), 611 (w), 597 (w), 570 (w), 559 (w), 537 (w), 503 (w).

Elemental Analysis: Calcd. (%) for C₄₀H₂₀Ag₂F₁₄N₄: C 46.27, H 1.94, N 5.40. Found: C 46.04, H 2.11, N 5.24.

Ag₂(TolFam)₂

Silver amidinato complex **Ag₂(TolFam)₂** was obtained in a yield of 63 % as a colorless solid. Slow evaporation of a DCM solution of the compound gave crystals suitable for X-ray crystallography.

¹H NMR (500 MHz, CD₂Cl₂): δ (ppm) = 6.95 – 6.88 (m, 4 H; *o*-Tol-H), 6.79 – 6.69 (m, 8 H; *m*-Tol-H, *p*-Ar-H), 6.64 – 6.57 (m, 8 H; *m*-Ar-H), 2.08 (s, 6 H, CH₃).

¹³C{¹H} NMR (75 MHz, CD₂Cl₂): δ (ppm) = 175.4 (N=C–N), 157.6 (dd, ¹J(C,F) = 245 Hz, ³J(C,F) = 4 Hz; *o*-Ar-C), 138.5 (*ipso*-Tol-C), 133.2 (*p*-Tol-C), 129.4 (t, ²J(C,F) = 15 Hz; *ipso*-Ar-C), 128.0 (*m*-Ph-C), 127.4 (*o*-Ph-C), 123.9 (t, ³J(C,F) = 9 Hz; *p*-Ar-C), 111.4 – 111.1 (m; *m*-Ar-C).

¹⁹F{¹H} NMR (282 MHz, CD₂Cl₂): δ (ppm) = -119.9 (s, 8 F, *o*-Ar-F).

IR (KBr): $\tilde{\nu}$ (cm⁻¹) = 3037 (w), 2921 (w), 1897 (w), 1807 (w), 1728 (w), 1700 (w), 1616 (w), 1584 (m), 1562 (w), 1495 (s), 1471 (s), 1406 (m), 1278 (m), 1253 (w), 1237 (m), 1211 (m), 1183 (w), 1149 (w), 1131 (w), 1113 (w), 1060 (w), 1020 (w), 1004 (s), 944 (w), 856 (w), 842 (w), 824 (m), 789 (m), 773 (m), 758 (w), 745 (w), 734 (w), 725 (m), 715 (w), 694 (w), 630 (w), 575 (w), 560 (w), 540 (w), 503 (w), 484 (w), 461 (w).

Elemental Analysis: Calcd. (%) for C₄₀H₂₆Ag₂F₈N₄: C 51.64, H 2.82, N 6.02. Found: C 51.02, H 2.89, N 5.77.

6.4 Synthesis of Imidazolium Salt [$\text{Im}^{-2\text{H}}$]⁺ Br⁻

2-Bromo-2-phenylacetophenone (1)

Compound **1** was synthesized according to modified existing protocols.^[291,292] 2-Phenylacetophenone (5.9 g, 30 mmol, 1.0 eq) and *p*-toluenesulfonic acid (0.57 g, 3.0 mmol, 0.1 eq) were dissolved in DCM (15 mL) and cooled to 0 °C before adding NBS (5.3 g, 30 mmol, 1.0 eq) in small portions to the reaction mixture. The solution was warmed to room temperature and stirred for a further 23 h. Pentane (40 mL) was added and the precipitating solid was separated by filtration and washed with pentane (3 × 10 mL). After this, the filtrate was washed with a saturated Na₂S₂O₅ solution (40 mL) and a half-saturated NaHCO₃ solution (40 mL), and dried over MgSO₄. Removal of the solvent *in vacuo* afforded the title compound as a white solid (6.9 g, 25 mmol, 83 %).

¹H NMR (300 MHz, CDCl₃): δ (ppm) = 8.01 – 7.98 (m, 2 H; *o*-COPh-H), 7.59 – 7.52 (m, 3 H; *p*-COPh-H, *o*-BrPh-H), 7.48 – 7.42 (m, 2 H; *m*-COPh-H), 7.41 – 7.32 (m, 3 H; *m*-BrPh-H, *p*-BrPh-H), 6.38 (s, 1 H; CH).

¹³C{¹H} NMR (75 MHz, CDCl₃): δ (ppm) = 191.2 (CO), 136.1 (*ipso*-BrPh-C), 134.4 (*ipso*-COPh-C), 133.8 (*p*-COPh-C), 129.3 (*p*-BrPh-C, *o*-COPh-C, *o*-BrPh-C), 129.2 (*m*-BrPh-C), 129.0 (*m*-COPh-C), 51.2 (CH).

1,3-Bis-(2,4,6-trimethylphenyl)-2,4,5-phenylimidazolium bromide ([$\text{Im}^{-2\text{H}}$]⁺ Br⁻)

Imidazolium salt [$\text{Im}^{-2\text{H}}$]⁺ Br⁻ was synthesized according to a modified literature procedure.^[291] To a mixture of amidine **PhMesAm** (4.19 g, 11.8 mmol, 1.0 eq), ethyldiisopropylamine (1.82 g, 2.39 mL, 14.1 mmol, 1.2 eq), and MeCN (20 mL) a solution of 2-bromo-2-phenylacetophenone **1** (6.47 g, 23.5 mmol, 2.0 eq) in MeCN (15 mL) was slowly added, and the mixture was heated to reflux for 7 d. The solvent was removed *in vacuo* before adding toluene, acetic anhydride (3.61 g, 3.35 mL, 35.4 mmol, 3.0 eq) and HBr (48 % in water, 2.98 g, 17.7 mmol, 1.5 eq). The mixture was stirred for 10 d at 90 °C before

pouring it into water (80 mL) and extraction with DCM (3×80 mL). The combined organic extracts were washed with a saturated NaHCO_3 solution (100 mL) and concentrated *in vacuo* to approximately 10 mL. Addition of Et_2O led to precipitation of the raw product which can be recrystallized by layering a DCM solution of the compound with Et_2O . By this procedure, the title compound can be obtained as cube-shaped slightly orange crystals (3.47 g, 5.65 mmol, 48 %). The Br^- counterion can be easily exchanged for PF_6^- by stirring a DCM solution over KPF_6 for 5 h. Filtration over silica, removal of the solvent *in vacuo* and recrystallization from a mixture of chlorobenzene and *n*-pentane yielded crystals suitable for X-ray crystallography.

^1H NMR (300 MHz, CD_2Cl_2): δ (ppm) = 7.49 (tt, $^3J(\text{H,H}) = 8$ Hz, $^4J(\text{H,H}) = 1$ Hz, 1 H; *p*- $\text{C}^2\text{Ph-H}$), 7.39 (tt, $^3J(\text{H,H}) = 8$ Hz, $^4J(\text{H,H}) = 1$ Hz, 2 H; *p*-Ph-H), 7.33 – 7.23 (m, 6 H; *m*- $\text{C}^2\text{Ph-H}$, *m*-Ph-H), 7.03 – 6.98 (m, 6 H; *o*- $\text{C}^2\text{Ph-H}$, *o*-Ph-H), 6.95 (s, 4 H; *m*-Mes-H), 2.29 (s, 6 H; *p*-Mes- CH_3), 2.04 (s, 12 H; *o*-Mes- CH_3).

$^{13}\text{C}\{^1\text{H}\}$ NMR (75 MHz, CD_2Cl_2): δ (ppm) = 144.5 (C^2), 142.4 (*p*-Mes-C), 134.8 (*o*-Mes-C), 133.3 (C^4 , C^5), 133.2 (*p*- $\text{C}^2\text{Ph-C}$), 130.8 (*p*-Ph-C), 130.5 (*m*-Mes-C), 130.4 (*o*-Ph-C), 129.6 (*m*- $\text{C}^2\text{Ph-C}$), 129.5 (*o*- $\text{C}^2\text{Ph-C}$), 129.4 (*m*-Ph-C), 128.7 (*ipso*-Mes-C), 124.8 (*ipso*-Ph-C), 121.1 (*ipso*- $\text{C}^2\text{Ph-C}$), 21.2 (*p*-Mes- CH_3), 18.3 (*o*-Mes- CH_3).

MS (ESI⁺, MeCN): m/z (%) = 533.3 (100) $[\text{M}]^+$; (ESI⁻, MeCN): m/z (%) = 78.8 (100) $[\text{Br}]^-$.

Elemental Analysis: Calcd. (%) for $\text{C}_{39}\text{H}_{37}\text{BrN}_2 \cdot \text{H}_2\text{O}$: C 74.16, H 6.22, N 4.43. Found: C 72.28, H 5.97, N 4.28.

Melting Point: 202 °C.

6.5 Synthesis of Imidazolinium Salts

The syntheses of imidazolinium salts presented in the following paragraphs are inspired by existing protocols for the synthesis of imidazolinium ions and larger heterocyclic ring systems lacking a C^2 substituent.^[302,309] The reactions were found highly dependent on the utilized amidine and consequently no general procedure for the preparation of imidazolinium ions can be given here. In general, a relatively large variance of the yield was noticed and hence each synthesis was optimized as effectively as possible.

1,3-Bis-(2,4,6-trimethylphenyl)-2-phenylimidazolinium bromide (PhMesIm⁺Br⁻)

Amidine **PhMesAm** (0.25 g, 0.70 mmol, 1.0 eq) was dissolved in 1,2-dibromoethane (5 mL) and ethyldiisopropylamine (0.10 g, 0.13 mL, 0.77 mmol, 1.1 eq) was added to the reaction mixture prior to heating to reflux for 4 h. After cooling to room temperature, the solvent was evaporated *in vacuo* and the remaining solid was washed with acetone. Recrystallization from a mixture of acetone and DCM gave the desired imidazolinium salt in crystalline form. The product **PhMesIm⁺Br⁻** was obtained as colorless cube-shaped crystals (0.28 g, 0.60 mmol, 85 %).

¹H NMR (300 MHz, CDCl₃): δ (ppm) = 7.40 (tt, ³J(H,H) = 8 Hz, ⁴J(H,H) = 1 Hz, 1 H; *p*-Ph-H), 7.18 (t, ³J(H,H) = 8 Hz, 2 H; *m*-Ph-H), 7.00 (dd, ³J(H,H) = 8 Hz, ⁴J(H,H) = 1 Hz, 2 H; *o*-Ph-H), 6.84 (s, 4 H; Mes-H), 4.83 (s, 4 H; CH₂), 2.31 (s, 12 H; *o*-Mes-CH₃), 2.21 (s, 6 H; *p*-Mes-CH₃); (300 MHz, CD₃CN): δ (ppm) = 7.46 (tt, ³J(H,H) = 8 Hz, ⁴J(H,H) = 1 Hz, 1 H; *p*-Ph-H), 7.26 (t, ³J(H,H) = 8 Hz, 2 H; *m*-Ph-H), 7.17 (dd, ³J(H,H) = 8 Hz, ⁴J(H,H) = 1 Hz, 2 H; *o*-Ph-H), 6.96 (s, 4 H; Mes-H), 4.51 (s, 4 H; CH₂), 2.31 (s, 12 H; *o*-Mes-CH₃), 2.22 (s, 6 H; *p*-Mes-CH₃).

¹³C{¹H} NMR (75 MHz, CDCl₃): δ (ppm) = 165.6 (C²), 140.4 (*p*-Mes-C), 134.8 (*o*-Mes-C), 133.9 (*p*-Ph-C), 131.4 (*ipso*-Mes-C), 130.4 (*m*-Mes-C), 129.1 (*m*-Ph-C), 128.3 (*o*-Ph-C), 121.8 (*ipso*-Ph-C), 52.3 (CH₂), 21.1 (*p*-Mes-CH₃), 18.3 (*o*-Mes-CH₃); (75 MHz, CD₃CN): δ (ppm) = 167.4 (C²), 141.4 (*p*-Mes-C), 136.2 (*o*-Mes-C), 134.7 (*p*-Ph-C), 132.2 (*ipso*-Mes-C), 130.9 (*m*-Mes-C), 129.9 (*m*-Ph-C), 129.3 (*o*-Ph-C), 125.5 (*ipso*-Ph-C), 51.9 (CH₂), 20.9 (*p*-Mes-CH₃), 18.1 (*o*-Mes-CH₃).

MS (ESI⁺, MeCN): *m/z* (%) = 383.1 (100) [M]⁺; (ESI⁻, MeCN): *m/z* (%) = 78.8 (100) [Br]⁻.

IR (KBr): $\tilde{\nu}$ (cm⁻¹) = 2949 (w), 2919 (m), 2762 (w), 1812 (w), 1605 (s), 1584 (s), 1548 (vs), 1485 (s), 1454 (s), 1393 (m), 1360 (m), 1282 (s), 1219 (m), 1191 (m), 1154 (m), 1098 (m), 1026 (m), 950 (w), 926 (w), 907 (w), 868 (m), 805 (w), 779 (s), 701 (m), 578 (m), 521 (w), 424 (w), 340 (w), 370(w).

Elemental Analysis: Calcd. (%) for C₂₇H₃₁BrN₂: C 69.97, H 6.74, N 6.04. Found: C 69.74, H 6.85, N 6.08.

Melting Point: decomposition at *T* > 363 °C.

1,3-Bis-(2,4,6-trimethylphenyl)-2-pentafluorophenylimidazolinium bromide (C₆F₅MesIm⁺Br⁻)

Amidine **C₆F₅MesAm** (5.0 g, 11 mmol, 1.0 eq) was dissolved in a mixture of 1,2-dibromoethane (30 mL) and MeCN (30 mL) before Cs₂CO₃ (2.9 g, 9.0 mmol, 0.8 eq) was added. The reaction mixture was stirred for 64 h at 110 °C. After this, the solvent was evaporated *in vacuo* and the raw product was dissolved in DCM (50 mL), washed

with saturated NaHCO₃ (50 mL), and dried over Na₂SO₄. The DCM solution was concentrated to approximately 20 mL and diethylether (60 mL) was added to the solution. Upon standing at room temperature, the product crystallized as slightly orange needles (2.3 g, 4.2 mmol, 38 %).

¹H NMR (300 MHz, CDCl₃): δ (ppm) = 6.89 (s, 4 H; Mes-H), 5.07 (s, 4 H; CH₂), 2.36 (s, 12 H; *o*-Mes-CH₃), 2.24 (s, 6 H; *p*-Mes-CH₃).

¹³C{¹H} NMR (75 MHz, CDCl₃): δ (ppm) = 157.8 (C²), 141.2 (*p*-Mes-C), 135.2 (*o*-Mes-C), 130.5 (*m*-Mes-C), 129.3 (*ipso*-Mes-C), 54.0 (CH₂), 21.1 (*p*-Mes-CH₃), 18.0 – 17.9 (m, *o*-Mes-CH₃). The carbon atoms of the pentafluorophenyl ring could not be assigned due to their very low intensity caused by coupling to the ¹⁹F nuclei. The C² carbon atom was identified by its coupling to the CH₂ groups in the ¹H, ¹³C HMBC NMR spectrum.

¹⁹F{¹H} NMR (282 MHz, CDCl₃): δ (ppm) = -130.6 – (-130.8) (m, 2 F; *o*-F), -139.8 (tt, ³J(F,F) = 22 Hz, ⁴J(F,F) = 7 Hz, 1 F; *p*-F), -155.3 – (-155.5) (m, 2 F; *m*-F).

MS (ESI⁺, MeCN): *m/z* (%) = 373.1 (100) [M]⁺; (ESI⁻, MeCN): *m/z* (%) = 78.8 (100) [Br]⁻.

IR (KBr): $\tilde{\nu}$ (cm⁻¹) = 2964 (m), 2924 (m), 2177 (w), 1732 (w), 1642 (m), 1610 (s), 1578 (vs), 1499 (vs), 1383 (m), 1289 (s), 1210 (m), 1119 (m), 1088 (m), 999 (vs), 924 (m), 856 (m), 802 (m), 728 (m), 675 (w), 637 (w), 571 (m), 412 (w).

Elemental Analysis: Calcd. (%) for C₂₇H₂₆BrF₅N₂: C 58.60, H 4.74, N 5.06. Found: C 58.49, H 4.80, N 4.77.

Melting Point: decomposition at *T* > 245 °C.

1,3-Bis-(2,4,6-trimethylphenyl)-2-(4-trifluoromethylphenyl)imidazolium bromide (CF₃PhMesIm⁺Br⁻)

Amidine CF₃PhMesAm (1.0 g, 2.4 mmol, 1.0 eq) was dissolved in 1,2-dibromoethane (4 mL) and ethyldiisopropylamine (0.33 g, 0.44 mL, 2.6 mmol, 1.1 eq) was added to the reaction mixture prior to heating to reflux for 3 h. The solvent was evaporated *in vacuo* and the raw product was washed with boiling toluene. The title compound was obtained after recrystallization from a mixture of DCM and Et₂O as colorless needles (0.49 g, 0.92 mmol, 39 %).

¹H NMR (300 MHz, CDCl₃): δ (ppm) = 7.47 (d, ³J(H,H) = 8 Hz, 2 H; *m*-CF₃Ph-H), 7.19 (d, ³J(H,H) = 8 Hz, 2 H; *o*-CF₃Ph-H), 6.88 (s, 4 H; Mes-H), 4.94 (s, 4 H; CH₂), 2.36 (s, 12 H; *o*-Mes-CH₃), 2.25 (s, 6 H; *p*-Mes-CH₃).

¹³C{¹H} NMR (75 MHz, CDCl₃): δ (ppm) = 164.4 (C²), 140.9 (*p*-Mes-C), 135.1 (q, ²J(C,F) = 34 Hz; *p*-CF₃Ph-C), 134.8 (*o*-Mes-C), 130.8 (*ipso*-Mes-C), 130.5 (*m*-Mes-C), 128.9 (*o*-CF₃Ph-C), 126.1 (q, ³J(C,F) = 4 Hz; *m*-CF₃Ph-C), 125.4 (q, ⁵J(C,F) = 1 Hz; *ipso*-CF₃Ph-C), 123.2 (q, ¹J(C,F) = 274 Hz; CF₃), 52.6 (CH₂), 21.1 (*p*-Mes-CH₃), 18.4 (*o*-Mes-CH₃).

¹⁹F{¹H} NMR (282 MHz, CDCl₃): δ (ppm) = -63.6 (s, 3 F; CF₃).

MS (ESI⁺, MeCN): *m/z* (%) = 451.2 (100) [M]⁺; (ESI⁻, MeCN): *m/z* (%) = 78.8 (100) [Br]⁻.

IR (KBr): $\tilde{\nu}$ (cm⁻¹) = 3343 (w), 2970 (w), 2956 (w), 2938 (w), 1611 (m), 1588 (m), 1564 (s),

1464 (w), 1406 (w), 1384 (w), 1324 (vs), 1287 (m), 1168 (m), 1131 (s), 1115 (m), 1067 (s), 1016 (w), 855 (m), 840 (m), 695 (m), 600 (w), 575 (w).

Elemental Analysis: Calcd. (%) for $C_{28}H_{30}BrF_3N_2$: C 63.28, H 5.69, N 5.27. Found: C 62.35, H 5.52, N 5.12.

Melting Point: decomposition at $T > 303^\circ\text{C}$.

1,3-Bis-(2,4,6-trimethylphenyl)-2-(4-tolyl)imidazolinium bromide (TolMesIm⁺Br⁻)

TolMesAm (1.0 g, 2.7 mmol, 1.0 eq) was dissolved in 1,2-dibromoethane (10 mL) and ethyldiisopropylamine (0.38 g, 0.5 mL, 3.0 mmol, 1.1 eq) was added. The reaction mixture was stirred for 17 h at reflux temperature. After this, the solvent was evaporated *in vacuo* and the raw product was dissolved in DCM (100 mL), washed with saturated NaHCO_3 (100 mL), and dried over Na_2SO_4 . The DCM solution was concentrated to approximately 20 mL and layered with Et_2O (60 mL). Upon standing at room temperature, the product precipitated as colorless crystals (0.85 g, 1.8 mmol, 66 %).

^1H NMR (300 MHz, CDCl_3): δ (ppm) = 6.97 (d, $^3J(\text{H,H}) = 8$ Hz, 2 H; *m*-Tol-H), 6.89 (d, $^3J(\text{H,H}) = 8$ Hz 2 H; *o*-Tol-H), 6.86 (s, 4 H; Mes-H), 4.81 (s, 4 H; CH_2), 2.31 (s, 12 H; *o*-Mes- CH_3), 2.23 (s, 9 H; *p*-Mes- CH_3 , Tol- CH_3).

$^{13}\text{C}\{^1\text{H}\}$ NMR (75 MHz, CDCl_3): δ (ppm) = 165.6 (C^2), 145.1 (*p*-Tol-C), 140.4 (*p*-Mes-C), 134.9 (*o*-Mes-C), 131.6 (*ipso*-Mes-C), 130.4 (*m*-Mes-C), 129.8 (*m*-Tol-C), 128.3 (*o*-Tol-C), 118.8 (*ipso*-Tol-C), 52.3 (CH_2), 21.8 (Tol- CH_3), 21.1 (*p*-Mes- CH_3), 18.3 (*o*-Mes- CH_3).

MS (ESI⁺, MeCN): m/z (%) = 397.1 (100) [$\text{M}]^+$; (ESI⁻, MeCN): m/z (%) = 78.8 (100) [$\text{Br}]^-$.

IR (KBr): $\tilde{\nu}$ (cm^{-1}) = 2967 (m), 2919 (m), 2860 (w), 1609 (vs), 1581 (vs), 1546 (vs), 1499 (m), 1482 (s), 1470 (s), 1405 (w), 1382 (m), 1362 (m), 1308 (w), 1292 (vs), 1216 (m), 1190 (m), 1158 (w), 1122 (w), 1035 (m), 1020 (m), 985 (w), 951 (w), 855 (m), 818 (s), 724 (m), 693 (w), 639 (w), 620 (w), 570 (m), 529 (w), 472 (w).

Elemental Analysis: Calcd. (%) for $C_{28}H_{33}BrN_2 \cdot 0.5\text{H}_2\text{O}$: C 69.13, H 7.04, N 5.76. Found: C 68.96, H 7.17, N 5.71.

Melting Point: decomposition at $T > 317^\circ\text{C}$.

1,3-Bis-(2,6-difluorophenyl)-2-phenylimidazolinium bromide (PhFI^{m+}Br⁻)

Amidine PhFAM (2.0 g, 5.8 mmol, 1.0 eq) was dissolved in 1,2-dibromoethane (4 mL) and ethyldiisopropylamine (0.83 g, 1.1 mL, 6.4 mmol, 1.1 eq) was added to the reaction mixture prior to heating to reflux for 6 h. After cooling to room temperature, the solvent was evaporated *in vacuo* and the remaining solid was washed with acetone. Recrystallization from a mixture of acetone and DCM gave the desired imidazolinium salt as colorless crystals (0.74 g, 1.6 mmol, 28 %).

¹H NMR (300 MHz, CDCl₃): δ (ppm) = 7.53 – 7.41 (m, 3 H; *p*-Ph-H, *p*-Ar-H), 7.31 (t, ³J(H,H) = 8 Hz, 2 H; *m*-Ph-H), 7.16 (d, ³J(H,H) = 8 Hz, 2 H; *o*-Ph-H), 7.03 – 6.97 (m, 4 H; *m*-Ar-H), 5.02 (s, 4 H; CH₂).

¹³C{¹H} NMR (75 MHz, CDCl₃): δ (ppm) = 169.6 (C²), 157.6 (dd, ¹J(C,F) = 256 Hz, ³J(C,F) = 3 Hz; *o*-Ar-C), 134.8 (*p*-Ph-C), 133.2 (t, ³J(C,F) = 10 Hz; *p*-Ar-C), 129.7 (*m*-Ph-C), 127.6 (*o*-Ph-C), 120.2 (*ipso*-Ph-C), 113.1 (t, ²J(C,F) = 16 Hz; *ipso*-Ar-C), 113.1 (dd, ²J(C,F) = 19 Hz, ⁴J(C,F) = 4 Hz; *m*-Ar-C), 53.8 (CH₂).

¹⁹F{¹H} NMR (282 MHz, CDCl₃): δ (ppm) = -117.1 (s, 4 F; *o*-Ar-F).

MS (ESI⁺, MeCN): *m/z* (%) = 371.0 (100) [M]⁺; (ESI⁻, MeCN): *m/z* (%) = 78.8 (100) [Br]⁻.

IR (KBr): $\tilde{\nu}$ (cm⁻¹) = 3057 (w), 2977 (w), 2891 (w), 1622 (s), 1590 (vs), 1557 (vs), 1474 (vs), 1442 (m), 1366 (w), 1293 (s), 1233 (m), 1190 (s), 1062 (m), 1028 (m), 1005 (vs), 930 (m), 810 (s), 797 (vs), 775 (vs), 699 (s), 627 (m), 562 (m), 503 (m), 411 (w), 348 (w).

Elemental Analysis: Calcd. (%) for C₂₁H₁₅BrF₄N₂: C 55.89, H 3.35, N 6.21. Found: C 55.67, H 3.09, N 6.34.

Melting Point: 358 °C.

1,3-Bis-(2,6-difluorophenyl)-2-(4-tolyl)imidazolinium bromide (ToIFIm⁺Br⁻)

Imidazolinium salt ToIFIm⁺Br⁻ can be prepared by two different methods. Method 1 does not require a base since the amidine can also act as a base in the reaction. Consequently, the maximum yield in such a reaction is 50%. After precipitation of the product, the organic phase still contains protonated ToIFAM, which can be reused for additional runs of the reaction after deprotonation. If an additional base is used to deprotonate the amidine prior to reacting it with 1,2-dibromoethane (method 2), column chromatography is required as a further purification step.

Method 1 Amidine ToIFAM (5.7 g, 16 mmol) and 1,2-dibromoethane (20 mL) were heated to reflux for 63 h. The solvent was removed *in vacuo* and the crude product was dissolved in DCM (100 mL). After washing with a saturated NaHCO₃ solution (100 mL) and drying over Na₂SO₄, the organic phase was concentrated.

Upon addition of Et₂O, the product precipitated as a beige solid which can be recrystallized from DCM/Et₂O to yield colorless crystals (2.9 g, 6.1 mmol, 39 %).

Method 2 Amidine TolFAm (4.7 g, 13 mmol, 1.0 eq) and KO^tBu (1.6 g, 14 mmol, 1.1 eq) were dissolved in MeCN (15 mL) and stirred at room temperature for 1 h. The solvent was evaporated *in vacuo* and 1,2-dibromoethane (10 mL) was added before heating the mixture to reflux for 71 h. The solution was concentrated and the crude product was purified by column chromatography (silica, DCM/MeOH 12:1, *R_f*(DCM/MeOH 9:1) = 0.36) and subsequent crystallization from DCM/Et₂O to yield the desired product (3.1 g, 6.7 mmol, 52 %).

¹H NMR (300 MHz, CDCl₃): δ (ppm) = 7.52 – 7.42 (m, 2 H; *p*-Ar-H), 7.09 – 6.97 (m, 8 H; *o*-Tol-H, *m*-Tol-H, *m*-Ar-H), 4.98 (s, 4 H; CH₂), 2.26 (s, 3 H; CH₃); (300 MHz, CD₃CN): δ (ppm) = 7.60 – 7.50 (m, 2 H; *p*-Ar-H), 7.21 – 7.10 (m, 8 H; *o*-Tol-H, *m*-Tol-H, *m*-Ar-H), 4.67 (s, 4 H; CH₂), 2.27 (s, 3 H; CH₃).

¹³C{¹H} NMR (75 MHz, CDCl₃): δ (ppm) = 169.6 (C²), 157.6 (dd, ¹J(C,F) = 255 Hz, ³J(C,F) = 3 Hz; *o*-Ar-C), 146.3 (*p*-Tol-C), 133.1 (t, ³J(C,F) = 10 Hz; *p*-Ar-C), 130.4 (*m*-Tol-C), 127.7 (*o*-Tol-C), 117.1 (*ipso*-Tol-C), 113.4 (t, ²J(C,F) = 16 Hz; *ipso*-Ar-C), 113.1 (dd, ²J(C,F) = 19 Hz, ⁴J(C,F) = 4 Hz; *m*-Ar-C), 53.7 (CH₂), 21.9 (CH₃); (75 MHz, CD₃CN): δ (ppm) = 170.2 (C²), 158.7 (dd, ¹J(C,F) = 254 Hz, ³J(C,F) = 3 Hz; *o*-Ar-C), 147.3 (*p*-Tol-C), 134.1 (t, ³J(C,F) = 10 Hz; *p*-Ar-C), 131.0 (*m*-Tol-C), 129.2 (*o*-Tol-C), 118.3 (*ipso*-Tol-C), 114.3 (t, ²J(C,F) = 16 Hz; *ipso*-Ar-C), 113.9 (dd, ²J(C,F) = 19 Hz, ⁴J(C,F) = 4 Hz; *m*-Ar-C), 53.2 (CH₂), 21.7 (CH₃).

¹⁹F{¹H} NMR (282 MHz, CDCl₃): δ (ppm) = -117.2 (s, 4 F; *o*-Ar-F); (282 MHz, CD₃CN): δ (ppm) = -118.5 (s, 4 F; *o*-Ar-F).

MS (ESI⁺, MeCN): *m/z* (%) = 385.0 (100) [M]⁺; (ESI⁻, MeCN): *m/z* (%) = 78.8 (100) [Br]⁻.

IR (KBr): $\tilde{\nu}$ (cm⁻¹) = 3057 (w), 2907 (vw), 2051 (vw), 1603 (m), 1582 (s), 1544 (s), 1475 (s), 1369 (w), 1295 (m), 1236 (m), 1190 (m), 1050 (m), 1004 (s), 804 (m), 789 (s), 723 (w), 561 (m), 517 (m); (MeCN): $\tilde{\nu}$ (cm⁻¹) = 2230 (w), 2107 (w), 1625 (w), 1605 (m), 1586 (s), 1556 (s), 1484 (vs), 1376 (w), 1305 (m), 1251 (w), 1015 (m), 827 (w), 797 (m), 728 (w).

Elemental Analysis: Calcd. (%) for C₂₂H₁₇BrF₄N₂ · 0.5 H₂O: C 55.71, H 3.83, N 5.91. Found: C 55.41, H 4.01, N 5.85.

Melting Point: 330 °C.

1,3-Bis-(2,6-difluorophenyl)-2-(2,4,6-trimethylphenyl)imidazolinium bromide (MesFIm⁺Br⁻)

Amidine MesFAm (0.50 g, 1.3 mmol, 1.0 eq) was dissolved in 1,2-dibromoethane (10 mL) and ethyldiisopropylamine (0.18 g, 0.24 mL, 1.4 mmol, 1.1 eq) was added to the reaction mixture prior to heating to reflux for 26 h. After cooling to room temperature, the solvent was evaporated *in vacuo* and the remaining solid was dissolved in DCM

(100 mL), washed with a saturated NaHCO₃ solution (100 mL), and concentrated. Addition of Et₂O precipitated the raw product. Recrystallization by layering a DCM solution with Et₂O gave the desired imidazolium salt as brownish crystals (0.39 g, 0.79 mmol, 60 %).

¹H NMR (300 MHz, CDCl₃): δ (ppm) = 7.46 – 7.36 (m, 2 H; *p*-Ar-H), 7.02 – 6.95 (m, 4 H; *m*-Ar-H), 6.74 (s, 2 H; *m*-Mes-H), 5.16 (s, 4 H; CH₂), 2.19 (s_{br}, 6 H; *o*-Mes-CH₃), 2.17 (s, 3 H; *p*-Mes-CH₃).

¹³C{¹H} NMR (75 MHz, CDCl₃): δ (ppm) = 170.1 (C²), 157.5 (dd, ¹J(C,F) = 256 Hz, ³J(C,F) = 3 Hz; *o*-Ar-C), 143.6 (*o*-Mes-C), 137.9 (*p*-Mes-C), 132.6 (t, ³J(C,F) = 10 Hz; *p*-Ar-C), 129.5 (*m*-Mes-C), 116.4 (*ipso*-Mes-C), 113.1 (dd, ²J(C,F) = 20 Hz, ⁴J(C,F) = 4 Hz; *m*-Ar-C), 112.9 (t, ²J(C,F) = 15 Hz; *ipso*-Ar-C), 53.4 (CH₂), 21.4 (*p*-Mes-CH₃), 19.3 (t, ³J(C,H) = 6 Hz; *o*-Mes-CH₃).

¹⁹F{¹H} NMR (282 MHz, CDCl₃): δ (ppm) = –114.3 (s, 4 F; *o*-Ar-F).

MS (ESI⁺, MeCN): *m/z* (%) = 413.0 (100) [M]⁺; (ESI[–], MeCN): *m/z* (%) = 78.8 (100) [Br][–].

IR (KBr): $\tilde{\nu}$ (cm^{–1}) = 3016 (m), 2956 (m), 1974 (vw), 1596 (s), 1551 (vs), 1480 (s), 1383 (m), 1299 (s), 1201 (m), 1072 (m), 1003 (s), 913 (w), 858 (m), 802 (s), 727 (m), 631 (m), 564 (s), 507 (m), 374 (m).

Elemental Analysis: Calcd. (%) for C₂₄H₂₁BrF₄N₂: C 58.43, H 4.29, N 5.68. Found: C 58.37, H 4.06, N 5.58.

Melting Point: 343 °C.

1,3-Bis-(2,3,5,6-tetrafluoro-4-tolyl)-2-(4-tolyl)imidazolium bromide (TolFTollm⁺Br[–])

Amidine TolFTolAm (1.0 g, 2.2 mmol) and 1,2-dibromoethane (10 mL) were heated to reflux for 7 d. The solvent was removed *in vacuo* and the crude product was dissolved in DCM (100 mL). After washing with a saturated NaHCO₃ solution (100 mL) and drying over Na₂SO₄, the organic phase was concentrated. After precipitation by addition of Et₂O, the raw product was further purified by column chromatography (silica, DCM/MeOH 9:1, *R_f*(DCM/MeOH 9:1) = 0.30) and subsequent recrystallization from DCM/Et₂O. The title compound was obtained as colorless needles (0.48 g, 0.84 mmol, 39 %). As in the synthesis of TolFIm⁺Br[–] (method 1), the amidine also acts as a base in this reaction. Therefore, the maximum yield is 50 %. Since amidine TolFTolAm was contaminated with traces of regioisomers (see above), also TolFTollm⁺Br[–] contained small amounts of differently substituted isomers as impurities which could not be removed by crystallization or column chromatography.

¹H NMR (300 MHz, CDCl₃): δ (ppm) = 7.21 (d, ³J(H,H) = 8 Hz, 2 H; *m*-Tol-H), 7.10 (d, ³J(H,H) = 8 Hz, 2 H; *o*-Tol-H), 5.12 (s, 4 H; CH₂), 2.35 (s, 3 H; Tol-CH₃), 2.26 (t, ⁴J(H,F) = 2 Hz, 6 H; FTol-CH₃).

$^{13}\text{C}\{^1\text{H}\}$ NMR (75 MHz, CDCl_3): δ (ppm) = 169.9 (C^2), 147.3 (*p*-Tol-C), 147.1 – 140.5 (m; *m*-FTol-C, *o*-FTol-C), 131.0 (*m*-Tol-C), 127.8 (*o*-Tol-C), 120.6 (t, $^2J(\text{C},\text{F}) = 19$ Hz; *p*-Tol-C), 116.6 (*ipso*-Tol-C), 112.7 (tt, $^2J(\text{C},\text{F}) = 14$ Hz, $^3J(\text{C},\text{F}) = 3$ Hz; *ipso*-FTol-C), 54.1 (CH_2), 22.1 (Tol- CH_3), 8.17 (s_{br} ; FTol- CH_3).

$^{19}\text{F}\{^1\text{H}\}$ NMR (282 MHz, CDCl_3): δ (ppm) = -138.7 – (-138.8) (m, 2 F; *o*-F), -145.3 – (-145.4) (m, 2 F; *m*-F).

MS (ESI⁺, MeCN): m/z (%) = 484.9 (100) $[\text{M}]^+$; (ESI⁻, MeCN): m/z (%) = 78.8 (100) $[\text{Br}]^-$.

IR (KBr): $\tilde{\nu}$ (cm^{-1}) = 2984 (vw), 1609 (w), 1583 (m), 1549 (s), 1506 (vs), 1470 (m), 1435 (w), 1282 (m), 1076 (m), 956 (w), 943 (w), 929 (m), 821 (m), 730 (w), 718 (w), 625 (w), 587 (w), 474 (vw).

Elemental Analysis: Calcd. (%) for $\text{C}_{24}\text{H}_{17}\text{BrF}_8\text{N}_2$: C 50.99, H 3.03, N 4.96. Found: C 48.73, H 2.94, N 4.68.

Melting Point: 266 °C.

1,2,3-Tris-(4-tolyl)imidazolinium bromide (TolTollm⁺Br⁻)

Amidine **TolTolAm** (0.50 g, 1.6 mmol, 1.0 eq) was dissolved in 1,2-dibromoethane (5 mL) and ethyldiisopropylamine (0.23 g, 0.30 mL, 1.7 mmol, 1.1 eq) was added. The reaction mixture was stirred for 24 h at reflux temperature. After this, the solvent was evaporated *in vacuo* and the residue was dissolved in DCM (100 mL), washed with saturated NaHCO_3 (100 mL), and dried over Na_2SO_4 . The DCM solution was concentrated before adding Et_2O to precipitate the raw product which was again recrystallized from DCM/ Et_2O . The product was obtained as slightly brownish crystals (0.48 g, 1.1 mmol, 71 %).

^1H NMR (300 MHz, CDCl_3): δ (ppm) = 7.32 (d, $^3J(\text{H},\text{H}) = 8$ Hz, 4 H; *o*-NTol-H), 7.26 (d, $^3J(\text{H},\text{H}) = 8$ Hz, 2 H; *o*-Tol-H), 7.02 (d, $^3J(\text{H},\text{H}) = 8$ Hz, 4 H; *m*-NTol-H), 6.94 (d, $^3J(\text{H},\text{H}) = 8$ Hz, 2 H; *m*-Tol-H), 4.79 (s, 4 H; CH_2), 2.24 (s, 6 H; NTol- CH_3), 2.20 (s, 3 H; Tol- CH_3).

$^{13}\text{C}\{^1\text{H}\}$ NMR (75 MHz, CDCl_3): δ (ppm) = 164.5 (C^2), 143.1 (*p*-Tol-C), 139.0 (*p*-NTol-C), 134.3 (*ipso*-NTol-C), 130.3 (*m*-NTol-C), 130.1 (*o*-Tol-C), 129.5 (*m*-Tol-C), 126.3 (*o*-NTol-C), 119.3 (*ipso*-Tol-C), 53.3 (CH_2), 21.7 (Tol- CH_3), 21.2 (NTol- CH_3).

MS (ESI⁺, MeCN): m/z (%) = 341.4 (100) $[\text{M}]^+$; (ESI⁻, MeCN): m/z (%) = 78.8 (100) $[\text{Br}]^-$.

IR (KBr): $\tilde{\nu}$ (cm^{-1}) = 3025 (w), 2915 (w), 2880 (w), 1612 (m), 1576 (s), 1564 (s), 1547 (vs), 1509 (s), 1498 (s), 1377 (m), 1304 (vs), 1210 (m), 1185 (m), 1112 (w), 1040 (w), 1022 (m), 990 (w), 972 (w), 938 (w), 821 (vs), 723 (m), 694 (w), 650 (w), 626 (m), 619 (w), 563 (m), 525 (s), 472 (m).

Elemental Analysis: Calcd. (%) for $\text{C}_{24}\text{H}_{25}\text{BrN}_2$: C 68.41, H 5.98, N 6.65. Found: C 66.80, H 5.82, N 6.32. **Melting Point:** 271 °C.

6.6 Synthesis of Imidazolidines

Imidazolidines were synthesized as precursors for imidazolinium ions in the synthetic route described in section 2.2.4. Furthermore, a variety of imidazolidines was obtained in reactions of a hydride donor reagent (NaBH_4) with imidazolinium ions which were performed in order to demonstrate their hydride acceptor properties.

General procedure To a solution of the imidazolinium salt (0.13 mmol, 1.0 eq) in EtOH (10 mL), NaBH_4 (7.2 mg, 0.19 mmol, 1.5 eq) was added in small portions and the mixture was stirred at room temperature for 2 h. The solvent was removed *in vacuo* and after addition of CHCl_3 , the resulting suspension was filtered (Sartorius PTFE syringe filter, 0.45 μm) and again concentrated to yield the respective imidazolidine.

N,N'-Di-(*tert*-butyl)oxamide (8)

N,N'-Di-(*tert*-butyl)oxamide (8) was synthesized according to a modified literature procedure.^[338] Diethyl oxalate (14.6 g, 13.6 mL, 100 mmol, 1.0 eq) was mixed with *tert*-butylamine (21.9 g, 31.8 mL, 300 mmol, 3.0 eq) in EtOH (15 mL) and the mixture was stirred at room temperature for 3 d. The solid material was collected by filtration and washed with EtOH (10 mL). The filtrate was concentrated *in vacuo* and the remaining solid was washed with EtOH (5 mL) to produce a second portion of the product. After drying under reduced pressure, the title compound was obtained as a white solid (18.8 g, 93.8 mmol, 94 %).

^1H NMR (300 MHz, CDCl_3): δ (ppm) = 7.40 (s_{br}, 2 H; NH), 1.37 (s, 18 H; CH_3).

$^{13}\text{C}\{^1\text{H}\}$ NMR (75 MHz, CDCl_3): δ (ppm) = 159.7 (C=O), 51.4 (*tert*Bu-C), 28.3 (CH_3).

N,N'-Di-*tert*-butyl-1,2-ethylenediamine (9)

N,N'-Di-*tert*-butyl-1,2-ethylenediamine (9) was synthesized according to a modified literature procedure.^[338] *N,N'*-Di-(*tert*-butyl)oxamide (8) (10.0 g, 50 mmol, 1.0 eq) was added as a THF suspension (50 mL) dropwise to a mixture of LiAlH_4 (11.4 g, 300 mmol, 6.0 eq) and THF (40 mL). After this, the mixture was heated to reflux for 19 h before careful addition of water at 0 °C. The solid material was separated by filtration and washed with Et_2O (180 mL). The layers of the filtrate were separated and the aqueous phase was extracted with Et_2O (3 \times 40 mL). The organic layers were combined, dried with MgSO_4 and concentrated *in vacuo*. Distillation under reduced pressure (78 °C, 24 mbar) gave the title compound as a colorless liquid (5.96 g, 35 mmol, 69 %).

^1H NMR (300 MHz, CDCl_3): δ (ppm) = 2.67 (s, 4 H; CH_2), 1.62 (s_{br} , 2 H; NH), 1.10 (s, 18 H; CH_3).

$^{13}\text{C}\{^1\text{H}\}$ NMR (75 MHz, CDCl_3): δ (ppm) = 50.5 ($^{\text{tert}}\text{Bu-C}$), 43.3 (CH_2), 29.2 (CH_3).

1,3-Di-*tert*-butyl-2-(4-trifluoromethylphenyl)imidazolidine (10)

N,N'-Di-*tert*-butyl-1,2-ethylenediamine (9) (2.0 g, 12 mmol, 1.2 eq), 4-(trifluoromethyl)benzaldehyde (1.7 g, 1.3 mL, 9.7 mmol, 1.0 eq) and toluene (20 mL) were heated to reflux at a distilling trap for 67 h. The solvent was removed *in vacuo* and the crude product was purified by Kugelrohr distillation under reduced pressure. By this procedure, imidazolidine 10 was obtained as a white solid (2.0 g, 6.2 mmol, 64 %).

^1H NMR (300 MHz, CDCl_3): δ (ppm) = 7.57 (d, $^3J(\text{H,H}) = 8$ Hz, 2 H; *o*- $\text{CF}_3\text{Ph-H}$), 7.49 (d, $^3J(\text{H,H}) = 8$ Hz, 2 H; *m*- $\text{CF}_3\text{Ph-H}$), 4.80 (s, 1 H; CH), 3.20 – 3.12 (m, 2 H; CH_2), 3.04 – 2.96 (m, 2 H; CH_2), 0.99 (s, 18 H; CH_3).

$^{13}\text{C}\{^1\text{H}\}$ NMR (75 MHz, CDCl_3): δ (ppm) = 155.7 (*ipso*- $\text{CF}_3\text{Ph-C}$), 128.5 (q, $^2J(\text{C,F}) = 32$ Hz; *p*- $\text{CF}_3\text{Ph-C}$), 128.4 (*o*- $\text{CF}_3\text{Ph-C}$), 124.7 (q, $^3J(\text{C,F}) = 4$ Hz; *m*- $\text{CF}_3\text{Ph-C}$), 124.7 (q, $^1J(\text{C,F}) = 272$ Hz; CF_3), 76.1 (CH_2), 54.1 ($^{\text{tert}}\text{Bu-C}$), 46.7 (CH_2), 28.2 (CH_3).

$^{19}\text{F}\{^1\text{H}\}$ NMR (282 MHz, CDCl_3): δ (ppm) = -62.1 (s, 3 F; CF_3).

1,3-Bis-(2,6-difluorophenyl)-2-phenylimidazolidine (HPhFIIm)

Imidazolidine HPhFIIm was prepared according to the general procedure by reaction of PhFIIm $^+\text{Br}^-$ with NaBH_4 in EtOH. The product was obtained in a quantitative yield.

^1H NMR (300 MHz, CDCl_3): δ (ppm) = 7.37 – 7.34 (m, 2 H; *o*-Ph-H), 7.18 – 7.11 (m, 3 H; *p*-Ph-H, *m*-Ph-H), 6.89 – 6.69 (m, 6 H; *p*-Ar-H, *m*-Ar-H), 6.12 (s, 1 H; CH), 4.13 – 4.02 (m, 2 H; CH_2), 3.68 – 3.57 (m, 2 H; CH_2).

$^{13}\text{C}\{^1\text{H}\}$ NMR (75 MHz, CDCl_3): δ (ppm) = 159.0 (dd, $^1J(\text{C,F}) = 248$ Hz, $^3J(\text{C,F}) = 7$ Hz; *o*-Ar-C), 140.7 (*ipso*-Ph-C), 128.2 (*p*-Ph-C), 128.0 (*m*-Ph-C), 127.9 (*o*-Ph-C), 123.5 (t, $^3J(\text{C,F}) = 10$ Hz; *p*-Ar-C), 123.3 (t, $^2J(\text{C,F}) = 14$ Hz; *ipso*-Ar-C), 112.0 (dd, $^2J(\text{C,F}) = 17$ Hz, $^4J(\text{C,F}) = 8$ Hz; *m*-Ar-C), 79.7 (quin, $^4J(\text{C,F}) = 4$ Hz; CH), 50.6 (t, $^4J(\text{C,F}) = 4$ Hz; CH_2).

$^{19}\text{F}\{^1\text{H}\}$ NMR (282 MHz, CDCl_3): δ (ppm) = -118.1 (s, 4 F; *o*-Ar-F).

1,3-Bis-(2,6-difluorophenyl)-2-(4-tolyl)imidazolidine (HTolFIIm)

Imidazolidine **HTolFIIm** was prepared according to the general procedure by reaction of **TolFIIm**⁺**Br**⁻ with NaBH₄ in EtOH. The product was obtained quantitatively and crystals were grown by slow evaporation of a CHCl₃ solution.

¹H NMR (300 MHz, CD₃CN): δ (ppm) = 7.23 (d, ³J(H,H) = 8 Hz, 2 H; *o*-Tol-H), 7.00 – 6.78 (m, 8 H; Ar-H, *p*-Tol-H), 6.07 (quin, ⁵J(H,F) = 2 Hz, 1 H; CH), 4.09 – 3.97 (m, 2 H; CH₂), 3.64 – 3.52 (m, 2 H; CH₂), 2.18 (s, 3 H; CH₃).

¹³C{¹H} NMR (75 MHz, CD₃CN): δ (ppm) = 159.9 (dd, ¹J(C,F) = 247 Hz, ³J(C,F) = 7 Hz; *o*-Ar-C), 139.3 (*p*-Tol-C), 138.7 (*ipso*-Tol-C), 129.5 (*m*-Tol-C), 128.9 (*o*-Tol-C), 125.1 (t, ³J(C,F) = 10 Hz; *p*-Ar-C), 123.8 (t, ²J(C,F) = 14 Hz; *ipso*-Ar-C), 113.0 (dd, ²J(C,F) = 17 Hz, ⁴J(C,F) = 8 Hz; *m*-Ar-C), 80.0 (quin, ⁴J(C,F) = 4 Hz; CH), 51.3 (t, ⁴J(C,F) = 3 Hz; CH₂), 21.1 (CH₃).

¹⁹F{¹H} NMR (282 MHz, CD₃CN): δ (ppm) = -120.3 (s, 4 F; *o*-Ar-F).

IR (CD₃CN): $\tilde{\nu}$ (cm⁻¹) = 1619 (w), 1590 (w), 1571 (w), 1495 (s), 1474 (s), 1351 (m), 1305 (w), 1290 (m), 1230 (m), 1180 (w), 1162 (w), 1068 (w), 1000 (m), 843 (w), 828 (w), 782 (m), 722 (w).

1,3-Bis-(2,6-difluorophenyl)-2-(4-tolyl)-(2-²H)-imidazolidine (DTolFIIm)

Imidazolidine **DTolFIIm** was prepared starting from **TolFIIm**⁺**Br**⁻ according to the general procedure, but with NaBD₄ (8.1 mg, 0.19 mmol, 1.5 eq) instead of NaBH₄. The product was obtained in a quantitative yield.

¹H NMR (300 MHz, CD₃CN): δ (ppm) = 7.23 (d, ³J(H,H) = 8 Hz, 2 H; *o*-Tol-H), 6.99 – 6.78 (m, 8 H; Ar-H, *p*-Tol-H), 4.09 – 3.98 (m, 2 H; CH₂), 3.63 – 3.52 (m, 2 H; CH₂), 2.18 (s, 3 H; CH₃).

¹³C{¹H} NMR (75 MHz, CD₃CN): δ (ppm) = 159.9 (dd, ¹J(C,F) = 247 Hz, ³J(C,F) = 8 Hz; *o*-Ar-C), 139.3 (*p*-Tol-C), 138.6 (*ipso*-Tol-C), 129.5 (*m*-Tol-C), 128.9 (*o*-Tol-C), 125.0 (t, ³J(C,F) = 10 Hz; *p*-Ar-C), 123.8 (t, ²J(C,F) = 14 Hz; *ipso*-Ar-C), 113.0 (dd, ²J(C,F) = 17 Hz, ⁴J(C,F) = 8 Hz; *m*-Ar-C), 80.1 – 79.2 (m; CD), 51.3 (t, ⁴J(C,F) = 3 Hz; CH₂), 21.1 (CH₃).

¹⁹F{¹H} NMR (282 MHz, CD₃CN): δ (ppm) = -120.4 (s, 4 F; *o*-Ar-F).

²H NMR (77 MHz, MeCN): δ (ppm) = 5.98 (s, CD).

IR (CD₃CN): $\tilde{\nu}$ (cm⁻¹) = 1571 (w), 1619 (w), 1586 (w), 1497 (s), 1474 (s), 1344 (m), 1290 (m), 1232 (m), 1160 (w), 1147 (w), 1085 (w), 1003 (m), 977 (w), 828 (w), 784 (m), 722 (w).

1,3-Bis-(2,3,5,6-tetrafluoro-4-tolyl)-2-(4-tolyl)imidazolidine (HTolFTolIm)

Imidazolidine **HTolFTolIm** was prepared according to the general procedure by reaction of **TolFTolIm**⁺**Br**[−] with NaBH₄ in EtOH. The product was obtained in a quantitative yield, however, since imidazolium salt **TolFTolIm**⁺**Br**[−] was contaminated with traces of regioisomers (see above), also **HTolFTolIm** contained small amounts of differently substituted isomers as impurities which could not be removed by crystallization or column chromatography.

¹H NMR (300 MHz, CD₃CN): δ (ppm) = 7.24 (d, ³J(H,H) = 8 Hz, 2 H; *o*-Tol-H), 7.02 (d, ³J(H,H) = 8 Hz, 2 H; *m*-Tol-H), 6.10 (quin, ⁵J(H,F) = 2 Hz, 1 H; CH), 4.13 – 4.01 (m, 2 H; CH₂), 3.69 – 3.58 (m, 2 H; CH₂), 2.20 (s, 3 H; Tol-CH₃), 2.12 (t, ⁴J(H,H) = 2 Hz, 6 H; FTol-CH₃).

¹³C{¹H} NMR (75 MHz, CD₃CN): δ (ppm) = 146.4 (dm, ¹J(C,F) = 241 Hz; *m*-FTol-C), 143.9 (dm, ¹J(C,F) = 244 Hz; *o*-FTol-C), 139.9 (*p*-Tol-C), 137.6 (*ipso*-Tol-C), 129.8 (*m*-Tol-C), 128.8 (*o*-Tol-C), 123.6 (tt, ²J(C,F) = 12 Hz, ³J(C,F) = 2 Hz; *ipso*-FTol-C), 111.0 (t, ²J(C,F) = 20 Hz; *p*-FTol-C), 79.9 (quin, ⁴J(C,F) = 4 Hz; CH), 51.2 (t, ⁴J(C,F) = 4 Hz; CH₂), 21.1 (Tol-CH₃), 7.24 – 7.00 (m, FTol-CH₃).

¹⁹F{¹H} NMR (282 MHz, CD₃CN): δ (ppm) = −147.0 – (−147.1) (m, 2 F; *o*-F), −150.9 – (−151.0) (m, 2 F; *m*-F).

6.7 Synthesis of Carbonyl Metalates

Potassium Cyclopentadienyldicarbonylferrate K[CpFe(CO)₂] (KFp)

KFp was synthesized according to a modified literature procedure.^[463] [CpFe(CO)₂]₂ (4.1 g, 12 mmol, 1.0 eq) was added to a THF solution of K[HB(sec-Bu)₃] (1.0 M, 25 mL, 25 mmol, 2.2 eq). The reaction mixture was heated to reflux for 3 h before cooling to 0 °C overnight. After this, the precipitate was separated by filtration and washed with THF. The orange filtrate was layered with toluene and kept at −20 °C to induce crystallization. The orange crystals were collected, washed with toluene and dried *in vacuo* to afford the title compound (3.8 g, 18 mmol, 74 %).

¹H NMR (300 MHz, CD₃CN): δ (ppm) = 4.24 (s, 5 H; Cp).

¹³C{¹H} NMR (75 MHz, CD₃CN): δ (ppm) = 229.3 (CO), 76.9 (Cp).

IR (MeCN): $\tilde{\nu}$ (CO, cm^{−1}) = 1866 (s), 1790 (s); (THF): $\tilde{\nu}$ (CO, cm^{−1}) = 1870 (s), 1793 (sh), 1774 (s); (DMF): $\tilde{\nu}$ (CO, cm^{−1}) = 1865 (s), 1790 (s); (C₆H₅Cl): $\tilde{\nu}$ (CO, cm^{−1}) = 1861 (s), 1787 (s); (ATR): $\tilde{\nu}$ (CO, cm^{−1}) = 1860 (m), 1727 (s); (KBr): $\tilde{\nu}$ (CO, cm^{−1}) = 1886 (m), 1744 (s).

Bis(cyclopentadienylruthenium dicarbonyl) [CpRu(CO)₂]₂ (Rp₂)

The ruthenium dimer **Rp₂** was synthesized according to a slightly modified literature procedure.^[523] Triruthenium dodecacarbonyl Ru₃(CO)₁₂ (1.7 g, 2.7 mmol, 1.0 eq), dry and deoxygenated *n*-heptane (80 mL) and freshly distilled cyclopentadiene (4.1 g, 5.3 mL, 62 mmol, 23 eq) were heated for 2 h at reflux in a two-necked round-bottomed flask under an argon atmosphere. The glass stopper was then removed and the volume of solvent was reduced to roughly 10 mL under a brisk flow of argon before adding again a volume of 110 mL of unpurified *n*-heptane directly from the reagent bottle. The solution was heated for a further 3 h. Upon standing overnight, the product crystallized from the reaction mixture. In order to complete crystallization, an additional amount of 30 mL of unpurified *n*-heptane was added to the reaction mixture and the flask was kept at 0 °C for 1 d. Decantation, washing the crystals with *n*-pentane and drying *in vacuo* afforded the product as orange needles (1.3 g, 3.0 mmol, 74 %).

¹H NMR (300 MHz, CD₃CN): δ (ppm) = 5.36 (s, 5 H; Cp).

¹³C{¹H} NMR (75 MHz, CD₃CN): δ (ppm) = 220.8 (CO), 90.7 (Cp).

IR (MeCN): $\tilde{\nu}$ (CO, cm⁻¹) = 1997 (s), 1959 (m), 1937 (sh), 1776 (s); (KBr): $\tilde{\nu}$ (CO, cm⁻¹) = 1948 (s), 1771 (s).

Potassium Cyclopentadienyldicarbonylruthenate K[CpRu(CO)₂] (KRp) and Black Solid (Rs)

To a solution of **Rp₂** (0.50 g, 1.1 mmol, 1.0 eq) in THF (20 mL), K[HB(*sec*-Bu)₃] (1 M in THF, 6.7 mL, 6.7 mmol, 6.1 eq) was added and the resulting mixture was heated to 40 °C for 6 h. After a short time the initially orange solution darkened and precipitation of a finely dispersed black solid was observed. Stirring of the mixture was continued overnight and the precipitate was isolated by filtration and subsequent washing with THF (2 × 5 mL) and MeCN (2 × 10 mL). Exhaustive drying of the solid *in vacuo* afforded a black material (**Rs**, 0.10 g). Toluene (60 mL) was added to the filtrate and after 1 d the resulting crystals were collected by decantation, washed with toluene, and dried *in vacuo*. By this method, **KRp** was obtained as yellow crystals (0.24 g, 0.90 mmol, 41 %). Crystals suitable for X-ray diffraction were obtained by layering a THF solution of the compound with toluene. Caution is required when handling the compound outside a glovebox as any exposure to air immediately destroys the crystals.

Analytical data of **KRp**:

¹H NMR (300 MHz, CD₃CN): δ (ppm) = 4.83 (s, 5 H; Cp); (300 MHz, DMSO-*d*₆): δ (ppm) = 4.68 (s, 5 H; Cp).

¹³C{¹H} NMR (75 MHz, CD₃CN): δ (ppm) = 216 (CO), 80 (Cp); (75 MHz, DMSO-*d*₆): δ (ppm) = 215 (CO), 80 (Cp); (101 MHz, solid): δ (ppm) = 218 (CO), 87 (Cp).

IR (MeCN): $\tilde{\nu}$ (CO, cm^{-1}) = 1888 (s), 1803 (s); (THF): $\tilde{\nu}$ (CO, cm^{-1}) = 1895 (s), 1812 (s); (DMSO): $\tilde{\nu}$ (CO, cm^{-1}) = 1882 (s), 1796 (s); (ATR): $\tilde{\nu}$ (CO, cm^{-1}) = 1889 (s), 1785 (s).

UV/Vis (THF): λ_{max} [nm] (ϵ [$\text{L mol}^{-1} \text{cm}^{-1}$]) = 242 (3200), 281 (4300), 331 (1200); (MeCN): λ_{max} [nm] (ϵ [$\text{L mol}^{-1} \text{cm}^{-1}$]) = 218 (7660), 258 (4440), 319 (1970); (solid): λ_{max} [nm] = 281, 236.

Elemental Analysis: Calcd. (%) for $\text{C}_7\text{H}_5\text{KO}_2\text{Ru}$ (the THF found in the crystal structure is lost upon drying under reduced pressure): C 32.18, H 1.93. Found: C 32.17, H 2.05.

Analytical data of **Rs** (for details see chapter 4.3):

$^{13}\text{C}\{^1\text{H}\}$ NMR (101 MHz, solid): δ (ppm) = 280 (CO), 215 (CO), 94 (Cp).

IR (DMSO): $\tilde{\nu}$ (CO, cm^{-1}) = 1882 (s), 1795 (s); (DMF): $\tilde{\nu}$ (CO, cm^{-1}) = 1885 (s), 1801 (s); (ATR): $\tilde{\nu}$ (CO, cm^{-1}) = 1815 (m, br), 1500 (s, br).

UV/Vis (solid): λ_{max} [nm] = 284, 236.

Elemental Analysis: Found: C 23.72, H 1.54, N 0.49, K 13.18, Ru 42.26.

^{13}CO -Labeled Compounds

^{13}CO -enriched triruthenium dodecacarbonyl was obtained according to a modified literature procedure from Darensbourg and co-workers.^[485] Commercially available $\text{Ru}_3(\text{CO})_{12}$ (1.0 g, 1.6 mmol) dissolved in a mixture of THF (90 mL) and MeOH (50 mL) and catalytic amounts of KOMe (0.1 M in MeCN/toluene, 0.2 mL, 0.02 mmol) were placed in a 500 mL Schlenk flask and the mixture was degassed by repeated freeze-thaw cycles. The flask was charged with an atmosphere of ^{13}CO gas (1 bar) and the mixture was stirred for 3 h at 50 °C. Stirring was continued overnight. After this, the atmosphere of ^{13}CO was renewed and the mixture was stirred for another 5 h at 50 °C. The solvent was removed *in vacuo* and the raw product was extracted with warm *n*-hexane. Filtration and removal of the solvent afforded ^{13}CO -enriched $\text{Ru}_3(\text{CO})_{12}$ which was directly used in the synthesis of ^{13}CO -enriched **Rp₂** analogously to the preparation of the non-labeled compound. From NMR spectroscopy of ^{13}CO -enriched **Rp₂** in comparison with the unlabeled compound, the ^{13}C content in the CO molecules was estimated to be at least 90%. Subsequent reductive cleavage according to the method described above gave the ^{13}CO -enriched metalate and the ^{13}CO -enriched black solid **Rs**.

6.8 Attempted Syntheses of Transition Metal FLPs

General procedure To a solution/suspension of the imidazolium salt (0.10 mmol, 1.0 eq) in an appropriate solvent (usually MeCN or chlorobenzene), the carbonyl metalate (**KFp** or **KRp**) (0.10 mmol, 1.0 eq) was added in small portions and the mixture was stirred at room temperature for 1 – 3 h. Filtration (Sartorius PTFE syringe filter, 0.45 μm) and removal of the solvent *in vacuo* or precipitation with an apolar solvent (e. g. cyclopentane) gave the reaction product as solid material.

Lewis Pair [**Im**^{-2H}]⁺**Fp**⁻

A mixture consisting of imidazolium salt [**Im**^{-2H}]⁺**Br**⁻ (0.13 g, 0.20 mmol, 1.0 eq), **KFp** (0.05 g, 0.22 mmol, 1.1 eq) and chlorobenzene (5 mL) was stirred at room temperature for 1 h. The dark red solution was then filtered (Sartorius PTFE syringe filter, 0.45 μm) and concentrated *in vacuo*. Crystals of the compound can be obtained from a chlorobenzene solution by diffusion with cyclopentane at $-35\text{ }^\circ\text{C}$. The synthesis of the **Rp**⁻ salt can be conducted analogously.

¹**H NMR** (500 MHz, C₆D₅Cl, $-35\text{ }^\circ\text{C}$): δ (ppm) = 7.18 (d, ³*J*(H,H) = 7 Hz, 4 H; *o*-Ph-H), 7.13 (d, ³*J*(H,H) = 7 Hz, 2 H; *o*-C²Ph-H), 7.04 – 6.84 (m, 9 H; Ph-H), 6.42 (s, 4 H; Mes-H), 4.77 (s, 5 H; Cp), 2.11 (s, 12 H; *o*-Mes-CH₃), 1.83 (s, 6 H; *p*-Mes-CH₃); (200 MHz, CD₃CN): δ (ppm) = 7.50 (tt, ³*J*(H,H) = 8 Hz, ⁴*J*(H,H) = 1 Hz, 1 H; *p*-Ph-H), 7.43 – 7.13 (m, 14 H; Ph-H), 6.96 (s, 4 H; Mes-H), 4.23 (s, 5 H; Cp), 2.23 (s, 6 H; *p*-Mes-CH₃), 2.09 (s, 12 H; *o*-Mes-CH₃).

¹³**C**{¹**H**} NMR (126 MHz, C₆D₅Cl, $-35\text{ }^\circ\text{C}$): δ (ppm) = 229.4 (CO), 143.9 (C²), 141.6 (*p*-Mes-C), 135.1 (*o*-Mes-C), 133.2 (C⁴, C⁵), 132.7 (*p*-C²Ph-C), 130.9 (*p*-Ph-C), 130.4 (*m*-Mes-C), 130.0 (*o*-Ph-C), 129.8 (*m*-C²Ph-C), 129.6 (*o*-C²Ph-C), 129.2 (*m*-Ph-C), 128.8 (*ipso*-Mes-C), 125.1 (*ipso*-Ph-C), 121.4 (*ipso*-C²Ph-C), 77.4 (Cp), 21.2 (*p*-Mes-CH₃), 18.9 (*o*-Mes-CH₃). **IR** (C₆H₅Cl): $\tilde{\nu}$ (CO, cm⁻¹) = 1859 (s), 1782 (s); (THF): $\tilde{\nu}$ (CO, cm⁻¹) = 1863 (s), 1789 (s); (toluene): $\tilde{\nu}$ (CO, cm⁻¹) = 1858 (s), 1780 (s).

Lewis Pair PhMesIm⁺Fp⁻

Imidazolinium salt **PhMesIm⁺Br⁻** (15 mg, 0.03 mmol, 1.0 eq) and **KFp** (8 mg, 0.04 mmol, 1.2 eq) were stirred at room temperature in MeCN (0.7 mL) for 1 h. After cooling to -35 °C for 10 min, the dark red solution was filtered (Sartorius PTFE syringe filter, 0.45 μm). The compound was not isolated as solid material.

¹H NMR (500 MHz, CD₃CN, -50 °C): δ (ppm) = 7.44 (s_{br}, 1 H; *p*-Ph-H), 7.24 (s_{br}, 2 H; Ph-H), 7.16 (s_{br}, 2 H; Ph-H), 4.48 (s_{br}, 4 H; CH₂), 4.21 (s, 5 H; Cp), 2.28 (s_{br}, 12 H; *o*-Mes-CH₃), 2.21 (s_{br}, 6 H; *p*-Mes-CH₃).

IR (MeCN): $\tilde{\nu}$ (CO, cm⁻¹) = 1863 (s), 1788 (s).

Lewis Pair TolMesIm⁺Fp⁻

The synthesis of Lewis pair **TolMesIm⁺Fp⁻** was performed in MeCN according to the general procedure. The imidazolinium NMR resonances of the compound are extremely broad at room temperature but narrow upon cooling. The synthesis of the **Rp⁻** salt can be conducted analogously.

¹H NMR (300 MHz, CD₃CN, -30 °C): δ (ppm) = 7.03 (s, 4 H; Ph-H), 6.95 (s, 4 H; Mes-H), 4.43 (s, 4 H; CH₂), 4.21 (s, 5 H; Cp), 2.26 (s, 12 H; *o*-Mes-CH₃), 2.21 (s, 6 H; *p*-Mes-CH₃).

Adduct [Fp-C₆F₄MesIm]⁺Br⁻

C₆F₅MesIm⁺Br⁻ (0.11 g, 0.2 mmol, 1.0 eq) was dissolved in chlorobenzene and cooled to -35 °C. **KFp** (0.04 g, 0.2 mmol, 1.0 eq) was then added in small portions and the mixture was stirred at room temperature for 1 h. The solution was filtered (Sartorius PTFE syringe filter, 0.45 μm) before adding diethyl ether to precipitate the title compound.

¹H NMR (300 MHz, C₆D₅Cl): δ (ppm) = 6.45 (s, 4 H; Mes-H), 5.36 (s_{br}, 4 H; CH₂), 4.21 (s, 5 H; Cp), 2.44 (s_{br}, 12 H; *o*-Mes-CH₃), 1.81 (s, 6 H; *p*-Mes-CH₃).

¹⁹F{¹H} NMR (282 MHz, C₆D₅Cl): δ (ppm) = -102.8 – (-102.9) (m, 2 F; Ar-F), -135.2 – (-135.4) (m, 2 F; Ar-F).

MS (ESI⁺, MeCN): m/z (%) = 631.1 (100) [M]⁺.

IR (C₆H₅Cl): $\tilde{\nu}$ (CO, cm⁻¹) = 2046 (s), 1999 (s); (MeOH): $\tilde{\nu}$ (CO, cm⁻¹) = 2044 (s), 1997 (s).

Dimer [(C₆F₄MesIm)₂](BPh₄)₂

Upon standing, solutions of the adduct [Fp–C₆F₄MesIm]⁺Br[–] (preparation see above) slowly decompose to yield the coupling product [(C₆F₄MesIm)₂]²⁺ and the dimer Fp₂. In order to obtain crystalline material, the bromide counterion was exchanged for BPh₄[–] by stirring a MeCN solution of the compound over an excess of KBPh₄ for 4 h. Filtration of the solution and Et₂O diffusion at room temperature produced crystals of the title compound.

¹H NMR (500 MHz, CD₃CN): δ (ppm) = 7.29 – 7.25 (m, 16 H; *o*-Ph-H), 7.00 – 6.97 (m, 24 H; *m*-Ph-H, Mes-H), 6.84 (t, ³J(H,H) = 7 Hz, 8 H; *p*-Ph-H), 4.60 (s, 8 H; CH₂), 2.29 (s, 24 H; *o*-Mes-CH₃), 2.23 (s, 12 H; *p*-Mes-CH₃).

¹³C{¹H} NMR (126 MHz, CD₃CN): δ (ppm) = 164.8 (q, ¹J(C,B) = 49 Hz; *ipso*-Ph-C), 158.9 (C²), 142.1 (*p*-Mes-C), 136.7 (q, ³J(C,B) = 1 Hz; *m*-Ph-C), 136.5 (*o*-Mes-C), 131.1 (*m*-Mes-C), 130.2 (*ipso*-Mes-C), 126.5 (q, ²J(C,B) = 3 Hz; *o*-Ph-C), 122.7 (*p*-Ph-C), 53.5 (CH₂), 21.0 (*p*-Mes-CH₃), 17.8 – 17.7 (m, *o*-Mes-CH₃). The carbon atoms of the pentafluorophenyl ring could not be assigned due to their very low intensity caused by coupling to the ¹⁹F nuclei.

¹⁹F{¹H} NMR (188 MHz, CD₃CN): δ (ppm) = –131.9 (s, 4 F; *m*-F), –133.0 (s, 4 F; *o*-F).

MS (ESI⁺, MeCN): *m/z* (%) = 454.1 (100) [M]²⁺, 491.1 (14) [M+Et₂O]²⁺; (ESI[–], MeCN): *m/z* (%) = 319.0 (100) [BPh₄][–].

Adduct [Rp–TolFIm]⁺Br[–]

TolFIm⁺Br[–] (70 mg, 0.15 mmol, 1.0 eq) and KRp (39 mg, 0.15 mmol, 1.0 eq) were dissolved in MeCN (10 mL) and stirred at room temperature. The reaction was largely complete after 5 h as determined by IR spectroscopy. Besides traces of the dimer Rp₂ ($\tilde{\nu}(\text{CO}) = 1996, 1775 \text{ cm}^{-1}$) only the adduct [Rp–TolFIm]⁺Br[–] was detected in solution. The resulting suspension was filtered (Sartorius PTFE syringe filter, 0.45 μm) and the solvent was removed under reduced pressure. The remaining solid was then washed with small amounts of THF and toluene and dissolved in MeCN. Layering toluene with the MeCN solution produced – upon standing at room temperature – crystals suitable for X-ray crystallography confirming the identity of the adduct [Rp–TolFIm]⁺Br[–].

¹H NMR (500 MHz, CD₃CN): δ (ppm) = 7.55 – 7.49 (m, 1 H; *p*-FAr-H), 7.35 (ddd, ³J(H,H) = 8 Hz, ⁴J(H,H) = 1 Hz, ⁵J(H,F) = 1 Hz, 1 H; *m*-RpAr-H), 7.25 – 7.12 (m, 5 H; *m*-FAr-H, Tol-H), 7.05 – 7.01 (m, 1 H; *m*-FAr-H), 6.94 (td, ³J(H,H) = 8 Hz, ⁴J(H,F) = 6 Hz, 1 H; *p*-RpAr-H), 6.72 (ddd, ³J(H,F) = 10 Hz, ³J(H,H) = 8 Hz, ⁴J(H,H) = 1 Hz, 1 H; *m*-RpAr-H), 5.54 (s, 5 H; Cp), 4.87 – 4.81 (m, 1 H; CH₂), 4.72 – 4.66 (m, 1 H; CH₂), 4.60 – 4.53 (m, 1 H; CH₂), 4.40 – 4.33 (m, 1 H; CH₂), 2.24 (s, 3 H; CH₃).

¹³C{¹H} NMR (126 MHz, CD₃CN): δ (ppm) = 202.6 (CO), 201.0 (CO), 169.9 (C²), 159.3 (dd, ¹J(C,F) = 254 Hz, ³J(C,F) = 3 Hz; *o*-FAr-C), 158.6 (d, ¹J(C,F) = 252 Hz; *o*-RpAr-C),

158.3 (dd, $^1J(\text{C},\text{F}) = 254 \text{ Hz}$, $^3J(\text{C},\text{F}) = 3 \text{ Hz}$; *o*-FAr-C), 146.6 (*p*-Tol-C), 145.2 (s_{br} ; *o*-RpAr-C), 144.1 (d, $^4J(\text{C},\text{F}) = 4 \text{ Hz}$; *m*-RpAr-C), 134.6 (d, $^2J(\text{C},\text{F}) = 9 \text{ Hz}$; *ipso*-RpAr-C), 133.7 (t, $^3J(\text{C},\text{F}) = 10 \text{ Hz}$; *p*-FAr-C), 130.6 (*m*-Tol-C), 129.5 (*o*-Tol-C), 129.0 (d, $^3J(\text{C},\text{F}) = 8 \text{ Hz}$; *p*-RpAr-C), 119.1 (*ipso*-Tol-C), 114.7 (t, $^2J(\text{C},\text{F}) = 16 \text{ Hz}$; *ipso*-FAr-C), 113.9 (t, $^2J(\text{C},\text{F}) = 20 \text{ Hz}$; *m*-FAr-C), 113.8 (t, $^2J(\text{C},\text{F}) = 20 \text{ Hz}$; *m*-FAr-C), 112.1 (d, $^2J(\text{C},\text{F}) = 20 \text{ Hz}$; *m*-RpAr-C), 91.0 (Cp), 53.8 (CH₂), 52.6 (CH₂), 21.6 (CH₃).

^{19}F NMR (471 MHz, CD₃CN): δ (ppm) = -118.4 – (-118.5) (m, 1 F; *o*-FAr-F), -118.9 – (-118.9) (m, 1 F; *o*-FAr-F), -119.5 – (-119.5) (m, 1 F; *o*-RpAr-F).

MS (ESI⁺, MeCN): m/z (%) = 589.1 (100) [M]⁺.

IR (MeCN): $\tilde{\nu}$ (CO, cm⁻¹) = 2034 (s), 1971 (s).

Imidazolidine Radical TolFIm

Mixtures of imidazolinium salt **TolFIm**⁺**Br**⁻ and **KFp** in MeCN prepared according to the general procedure mentioned above contained the imidazolidine radical **TolFIm** as evidenced by EPR and UV/Vis spectroscopy and the dimer **Fp**₂ as deduced from NMR spectra (δ (Cp) = 4.88 ppm in CD₃CN). The radical is relatively stable under oxygen-free conditions at room temperature, but small amounts of imidazolidine **HTolFIm** (see section 6.6) and other decomposition products can be detected in the NMR spectrum. Alternatively, the radical can be prepared electrochemically by reduction of **TolFIm**⁺**Br**⁻ (0.1 M NBu₄PF₆ solution in MeCN) at a platinum net electrode. The reaction is very sensitive to changes of reaction conditions. If e. g. chlorobenzene is used as the solvent, larger amounts of the imidazolidine **HTolFIm** and the coupling product [(**TolFIm**)₂]²⁺ can be detected in solution (see below).

UV/Vis (MeCN): λ_{max} [nm] (ϵ [L mol⁻¹ cm⁻¹]) = 439 (1900), 513 (2200).

EPR (MeCN, 133 K): $g = 2.006$.

Dimer [(TolFIm)₂]Br₂

Mixtures of imidazolinium salt **TolFIm**⁺**Br**⁻ and **KFp** in chlorobenzene prepared according to the general procedure mentioned above mainly contained imidazolidine **HTolFIm** (see section 6.6) and the dimer [(**TolFIm**)₂]²⁺ in a 2:1 ratio as deduced from NMR spectroscopy. Furthermore, the iron dimer **Fp**₂ (δ (Cp) = 4.44 ppm in C₆D₅Cl) could be detected in solution. Unfortunately, attempts to isolate the pure title compound failed.

^1H NMR (500 MHz, C₆D₅Cl): δ (ppm) = 7.41 – 7.35 (m, 4 H; *o*-Tol-H), 6.78 – 6.74 (m, 4 H; *m*-Tol-H), 6.67 – 6.28 (m, 10 H; *m*-FPh-H, *p*-FPh-H), 4.04 – 3.97 (m, 4 H; CH₂), 3.57 – 3.55 (m, 4 H; CH₂), 1.92 (s, 3 H; CH₃).

$^{13}\text{C}\{^1\text{H}\}$ NMR (126 MHz, C₆D₅Cl): δ (ppm) = 172.0 (C²), 158.6 (d, $^1J(\text{C},\text{F}) = 251 \text{ Hz}$; *o*-FPh-C), 153.6 (dd, $^1J(\text{C},\text{F}) = 241 \text{ Hz}$, $^3J(\text{C},\text{F}) = 8 \text{ Hz}$; *o*-FPh-C), 140.6 (*ipso*-Tol-C), 128.5

(*m*-Tol-C), 127.9 (*o*-Tol-C), 123.4 (t, $^2J(\text{C},\text{F}) = 14$ Hz; *ipso*-FPh-C), 116.6 (t, $^3J(\text{C},\text{F}) = 9$ Hz; *p*-FPh-C), 111.5 (dd, $^2J(\text{C},\text{F}) = 18$ Hz, $^4J(\text{C},\text{F}) = 7$ Hz; *m*-FPh-C), 49.2 (CH₂), 45.2 (CH₂), 21.0 (CH₃).

$^{19}\text{F}\{^1\text{H}\}$ NMR (282 MHz, C₆D₅Cl): δ (ppm) = -116.3 (t, $^7J(\text{F},\text{F}) = 1$ Hz, 4 F; *o*-FPh-F), -128.1 (s, 4 F; *o*-FPh-F).

MS (ESI⁺, MeCN): m/z (%) = 425.1 (29) [$^{1/2}\text{M} + \text{MeCN}$]⁺, 827.2 (100) [$\text{M} + \text{CH}_3\text{COO}$]⁺.

Imidazolidine Radical TolFTolIm

Mixtures of imidazolinium salt **TolFTolIm**⁺**Br**⁻ and **KFp** in MeCN prepared according to the general procedure mentioned above contained the imidazolidine radical **TolFTolIm** as evidenced by EPR spectroscopy and the dimer **Fp**₂ as deduced from ¹H NMR spectra (δ (Cp) = 4.88 ppm in CD₃CN). The radical is relatively stable under oxygen-free conditions at room temperature, but small amounts of imidazolidine **HTolFTolIm** (see section 6.6) and other decomposition products can be detected in the NMR spectrum.

EPR (MeCN, 133 K): $g = 2.006$.

Reaction between TolFIm⁺Br⁻ and Rs

Mixtures of imidazolinium salt **TolFIm**⁺**Br**⁻ and **Rs** in (deuterated) MeCN prepared according to the general procedure described above mainly contained signals of the unchanged imidazolinium salt. Due to the insufficient solubility of **Rs**, no signals can be attributed to the metalate. The observed ¹H and ¹⁹F NMR signals are relatively broad in the beginning, but sharpen after a while. Heating the sample to 70 °C for a few days leads to the formation of several decomposition products, however the major part of the imidazolinium ions remains unchanged.

6.9 Reactions with H₂ or D₂

General procedure for NMR experiments NMR experiments that required the addition of H₂ or D₂ were conducted either in J. Young NMR tubes (for pressures up to 1.5 bar) or in Wilmad-LabGlass high pressure NMR tubes (for higher pressures). The NMR tubes were filled with the respective compound(s) and NMR solvent in a glovebox (the preparation of transition metal Lewis pairs was conducted analogous to section 6.8), and degassed by repeated freeze-thaw cycles. After this, the gas was added to the NMR tube.

Alternatively, the compounds were filled into a Schlenk tube and cooled to -30 °C before addition of the precooled NMR solvent. H₂ or D₂ was then added to

the flask and the mixtures were allowed to slowly warm to room temperature overnight with stirring. After this, the solutions were filtered (Sartorius PTFE syringe filter, 0.45 μm) and filled in J. Young NMR tubes for the measurements.

Rs-Catalyzed H/D Isotope Exchange Reaction

A high pressure NMR tube was loaded with **Rs** (11 mg) and MeCN (0.6 mL). Pressurization with D₂ (8 bar) as described above, mixing by using an ultrasonic bath, and keeping the sample at room temperature leads to a gradual H/D-exchange of D₂ over several days. The reaction can be followed by ²H NMR spectroscopy. Mixtures of **Rs** and CD₃CN catalyze the analogous exchange reaction of H₂.

²H NMR (46 MHz, MeCN): δ (ppm) = 4.56 (d, ¹J(D,H) = 43 Hz; HD), 4.52 (s; D₂).

¹H NMR (500 MHz, CD₃CN): δ (ppm) = 4.57 (s; H₂), 4.53 (t, ¹J(H,D) = 43 Hz; HD).

Reactions of TolFIm⁺Br⁻ and Rs with H₂/D₂

The black solid **Rs** (11 mg, equivalent to 0.04 mmol/1.4 eq **KRp**^a) was transferred to a high pressure NMR tube in the glovebox. After addition of TolFIm⁺Br⁻ (14 mg, 0.030 mmol, 1.0 eq) dissolved in CD₃CN/CH₃CN (0.6 mL), the sample was immediately frozen in liquid nitrogen and degassed by repeated freeze-thaw cycles. Addition of H₂/D₂ (8 bar) was followed by warming to room temperature. In order to guarantee a sufficient mixing of the heterogeneous solution, the sample was placed in an ultrasonic bath equipped with a timer (2 min on, 12 min off). By this method, an undesired heating of the bath is avoided and room temperature is maintained throughout the reaction. Besides the imidazolidines **HTolFIm** and **DTolFIm** (for experimental data see section 6.6), the reaction mixtures contained NMR signals that could be assigned to the metal hydrides **HRp**/**DRp**:

Experimental data for **HRp**:

¹H NMR (500 MHz, CD₃CN): δ (ppm) = 5.39 (s, 5 H; Cp), -11.06 (s, 1 H; RuH).

¹³C{¹H} NMR (126 MHz, CD₃CN): δ (ppm) = 202.5 (CO), 86.6 (Cp).

IR (CD₃CN): $\tilde{\nu}$ (CO, cm⁻¹) = 2025 (m), 1960 (s).

Experimental data for **DRp**:

²H NMR (77 MHz, MeCN): δ (ppm) = -10.97 (s; RuD).

IR (MeCN): $\tilde{\nu}$ (CO, cm⁻¹) = 2024 (m), 1960 (s).

^aThe exact structure and formula weight of **Rs** are unclear. Nevertheless, the equivalents were calculated for **KRp** to get a rough impression of the required amount of black material. The transfer of the powder to the NMR tube was always associated with a substantial loss of compound and therefore an excess of the metalate was used.

Ruthenium Hydride $\text{CpRu}(\text{CO})(\text{PPh}_3)\text{H}$

The ruthenium hydride complex $\text{CpRu}(\text{CO})(\text{PPh}_3)\text{H}$ can be prepared from HRp produced in the splitting reaction of H_2 . For this purpose, PPh_3 (8 mg, 0.03 mmol, 1.0 eq) was added to the reaction mixture of $\text{ToIFIm}^+\text{Br}^-$, Rs , and H_2 after the reaction was performed as described above. The NMR sample was heated to 45°C for 3 d. During this time, the gradual conversion of HRp into $\text{CpRu}(\text{CO})(\text{PPh}_3)\text{H}$ can be observed by means of NMR spectroscopy.

^1H NMR (500 MHz, CD_3CN): δ (ppm) = 7.49 – 7.29 (m, 15 H; Ph-H), 4.95 (s, 5 H; Cp), –11.69 (d, $^2J(\text{H},\text{P}) = 32$ Hz, 1 H; RuH).

$^{13}\text{C}\{^1\text{H}\}$ NMR (126 MHz, CD_3CN): δ (ppm) = 207.6 (d, $^2J(\text{C},\text{P}) = 19$ Hz; CO), 85.0 (d, $^2J(\text{C},\text{P}) = 2$ Hz; Cp).

^{31}P NMR (202 MHz, CD_3CN): δ (ppm) = 66.6 (d, $^2J(\text{P},\text{H}) = 31$ Hz; PPh_3).

6.10 Reactions with Other Substrates

General procedure To a solution/suspension of the imidazolium salt (0.04 mmol, 1.0 eq) in CD_3CN or $\text{C}_6\text{D}_5\text{Cl}$, the substrate (e. g. phenylacetylene, triethylsilane or propylene oxide; 0.04 mmol, 1.0 eq) and the carbonyl metalate (KFp or KRp) (0.04 mmol, 1.0 eq) were added in small portions and the mixture was stirred at room temperature for 1 – 3 h. After filtration (Sartorius PTFE syringe filter, $0.45\ \mu\text{m}$) the solution was transferred into a J. Young NMR tube.

6.11 DFT Calculations

Calculations on the Reaction Path for Dihydrogen Splitting

Calculations concerning the mechanism of dihydrogen splitting by the FLP $\text{ToIFIm}^+\text{Rp}^-$ in chapter 5.5.1 were carried out in cooperation with the group of Jun.-Prof. Dr. Ricardo Mata at the Institute of Physical Chemistry of the Georg-August-University Göttingen with the *ORCA* program package.^[385] The B3LYP functional^[524] was used including dispersion corrections as proposed by Grimme *et al.*,^[525] with Becke-Johnson damping.^[526] The basis sets used were the def2-SVP, def2-TZVP and def2-QZVPP sets,^[527] in combination with the respective Stuttgart/Dresden effective core potential ECP.^[528] The RIJCOSX approximation was used throughout in order to accelerate the calculation of two-electron integrals.^[529] All structure optimizations were carried out in the gas phase. The thermodynamic corrections used to derive the Gibbs free energies (as well as the zero point energy) were based on harmonic frequency calculations considering a temperature of 298.15 K. In order to correct for solution effects, single points with

the COSMO continuum model were performed with standard defaults for MeCN ($\epsilon = 36.6$).^[530]

Other Calculations

Calculations on the amidine isomers (chapter 3.3.2) were performed with the *ORCA* program package^[385] using the B3LYP functional,^[524] SV(P) basis set^[386] and the COSMO solvation model^[387] to simulate the influences of the solvent CHCl₃. Before the geometry optimizations, atom coordinates for the different isomers were obtained from first guess structures drawn with ChemDraw3D.

Calculations concerning the structure of the radical **TolFIm** (see chapter 5.3.3) were carried out with the *ORCA* program package as well.^[385] The B3LYP functional^[524] with SV(P), TZVP or def2-TZVPP^[386,527] basis sets was used for geometry optimization. In some of the performed calculations the RIJCOSX approximation^[529] and the COSMO correction^[387] for MeCN were used. Spin densities are based on the Mulliken population analysis.

Bibliography

- [1] N. S. Lewis, D. G. Nocera, *PNAS* **2006**, *103*, 15729–15735.
- [2] J. Barber, P. D. Tran, *J. R. Soc. Interface* **2013**, *10*, 20120984.
- [3] S. Bensaid, G. Centi, E. Garrone, S. Perathoner, G. Saracco, *ChemSusChem* **2012**, *5*, 500–521.
- [4] D. G. Nocera, *Acc. Chem. Res.* **2012**, *45*, 767–776.
- [5] K. S. Joya, Y. F. Joya, K. Ocakoglu, R. van de Krol, *Angew. Chem. Int. Ed.* **2013**, *52*, 10426–10437.
- [6] J. O. Bockris, *Science* **1972**, *176*, 1323.
- [7] J. A. Turner, *Science* **2004**, *305*, 972–974.
- [8] J. Andrews, B. Shabani, *Procedia Eng.* **2012**, *49*, 15–25.
- [9] L. Schlapbach, A. Züttel, *Nature* **2001**, *414*, 353–358.
- [10] U. Sahaym, M. G. Norton, *J. Mater. Sci.* **2008**, *43*, 5395–5429.
- [11] G. J. Kubas, *J. Organomet. Chem.* **2009**, *694*, 2648–2653.
- [12] F. A. Armstrong, N. A. Belsey, J. A. Cracknell, G. Goldet, A. Parkin, E. Reisner, K. A. Vincent, A. F. Wait, *Chem. Soc. Rev.* **2009**, *38*, 36–51.
- [13] R. M. Navarro, M. A. Peña, J. L. G. Fierro, *Chem. Rev.* **2007**, *107*, 3952–3991.
- [14] A. L. Kenward, W. E. Piers, *Angew. Chem. Int. Ed.* **2008**, *47*, 38–41.
- [15] G. J. Kubas, R. R. Ryan, B. I. Swanson, P. J. Vergamini, H. J. Wasserman, *J. Am. Chem. Soc.* **1984**, *106*, 451–452.
- [16] G. J. Kubas, *J. Organomet. Chem.* **2001**, *635*, 37–68.
- [17] R. Crabtree, *Angew. Chem. Int. Ed.* **1993**, *32*, 789–805.
- [18] G. J. Kubas, *Chem. Rev.* **2007**, *107*, 4152–4205.
- [19] O. Eisenstein, R. H. Crabtree, *New J. Chem.* **2013**, *37*, 21–27.
- [20] J. G. de Vries, C. J. Elsevier (Eds.), *Handbook of Homogeneous Hydrogenation*, Wiley VCH Verlag GmbH & Co. KGaA, Weinheim, **2007**.
- [21] R. Noyori, *Angew. Chem. Int. Ed.* **2002**, *41*, 2008–2022.

- [22] G. D. Frey, V. Lavallo, B. Donnadiou, W. W. Schoeller, G. Bertrand, *Science* **2007**, *316*, 439–441.
- [23] D. W. Stephan, G. Erker, *Angew. Chem. Int. Ed.* **2010**, *49*, 46–76.
- [24] G. Erker, D. W. Stephan (Eds.), *Top. Curr. Chem.* **2013**, *332*, 1–350.
- [25] G. Erker, D. W. Stephan (Eds.), *Top. Curr. Chem.* **2013**, *334*, 1–317.
- [26] G. C. Welch, L. Cabrera, P. a. Chase, E. Hollink, J. D. Masuda, P. Wei, D. W. Stephan, *Dalton Trans.* **2007**, 3407–3414.
- [27] D. W. Stephan, *Top. Curr. Chem.* **2013**, *332*, 1–44.
- [28] G. C. Welch, R. R. San Juan, J. D. Masuda, D. W. Stephan, *Science* **2006**, *314*, 1124–1126.
- [29] G. C. Welch, D. W. Stephan, *J. Am. Chem. Soc.* **2007**, *129*, 1880–1881.
- [30] P. Spies, G. Erker, G. Kehr, K. Bergander, R. Fröhlich, S. Grimme, D. W. Stephan, *Chem. Commun.* **2007**, 5072–5074.
- [31] B. G. Janesko, *J. Phys. Chem. C* **2012**, *116*, 16467–16472.
- [32] G. Kehr, S. Schwendemann, G. Erker, *Top. Curr. Chem.* **2013**, *332*, 45–83.
- [33] T. A. Rokob, A. Hamza, I. Pápai, *J. Am. Chem. Soc.* **2009**, *131*, 10701–10710.
- [34] T. A. Rokob, I. Pápai, *Top. Curr. Chem.* **2013**, *332*, 157–211.
- [35] M. Sajid, G. Kehr, T. Wiegand, H. Eckert, C. Schwickert, R. Pöttgen, A. J. P. Cardenas, T. H. Warren, R. Fröhlich, C. G. Daniliuc, G. Erker, *J. Am. Chem. Soc.* **2013**, *135*, 8882–8895.
- [36] D. W. Stephan, *Org. Biomol. Chem.* **2008**, *6*, 1535–1539.
- [37] D. W. Stephan, *Dalton Trans.* **2009**, 3129–3136.
- [38] D. W. Stephan, *Chem. Commun.* **2010**, *46*, 8526–8533.
- [39] P. A. Chase, T. Jurca, D. W. Stephan, *Chem. Commun.* **2008**, 1701–1703.
- [40] D. Holschumacher, T. Bannenberg, C. G. Hrib, P. G. Jones, M. Tamm, *Angew. Chem. Int. Ed.* **2008**, *47*, 7428–7432.
- [41] P. A. Chase, D. W. Stephan, *Angew. Chem. Int. Ed.* **2008**, *47*, 7433–7437.
- [42] P. A. Chase, A. L. Gille, T. M. Gilbert, D. W. Stephan, *Dalton Trans.* **2009**, 7179–7188.
- [43] E. L. Kolychev, T. Bannenberg, M. Freytag, C. G. Daniliuc, P. G. Jones, M. Tamm, *Chem. Eur. J.* **2012**, *18*, 16938–16946.
- [44] E. L. Kolychev, E. Theuergarten, M. Tamm, *Top. Curr. Chem.* **2013**, *334*, 121–155.
- [45] P. Eisenberger, A. M. Bailey, C. M. Crudden, *J. Am. Chem. Soc.* **2012**, *134*, 17384–17387.
- [46] E. R. Clark, A. Del Grosso, M. J. Ingleson, *Chem. Eur. J.* **2013**, *19*, 2462–2466.

- [47] M. Erdmann, C. Rösener, T. Holtrichter-Rößmann, C. G. Daniliuc, R. Fröhlich, W. Uhl, E.-U. Würthwein, G. Kehr, G. Erker, *Dalton Trans.* **2013**, *42*, 709–718.
- [48] B. Inés, S. Holle, R. Goddard, M. Alcarazo, *Angew. Chem. Int. Ed.* **2010**, *49*, 8389–8391.
- [49] G. R. Whittell, E. I. Balmond, A. P. M. Robertson, S. K. Patra, M. F. Haddow, I. Manners, *Eur. J. Inorg. Chem.* **2010**, 3967–3975.
- [50] A. Schäfer, M. Reissmann, A. Schäfer, W. Saak, D. Haase, T. Müller, *Angew. Chem. Int. Ed.* **2011**, *50*, 12636–12638.
- [51] D. Palomas, S. Holle, B. Inés, H. Bruns, R. Goddard, M. Alcarazo, *Dalton Trans.* **2012**, *41*, 9073–9082.
- [52] H. Li, A. J. A. Aquino, D. B. Cordes, F. Hung-Low, W. L. Hase, C. Krempner, *J. Am. Chem. Soc.* **2013**, *135*, 16066–16069.
- [53] C. Appelt, H. Westenberg, F. Bertini, A. W. Ehlers, J. C. Slootweg, K. Lammertsma, W. Uhl, *Angew. Chem. Int. Ed.* **2011**, *50*, 3925–3928.
- [54] C. Appelt, J. C. Slootweg, K. Lammertsma, W. Uhl, *Angew. Chem. Int. Ed.* **2012**, *51*, 5911–5914.
- [55] C. Appelt, J. C. Slootweg, K. Lammertsma, W. Uhl, *Angew. Chem. Int. Ed.* **2013**, *52*, 4256–4259.
- [56] W. Uhl, E.-U. Würthwein, *Top. Curr. Chem.* **2013**, *334*, 101–119.
- [57] G. Ménard, D. W. Stephan, *Angew. Chem. Int. Ed.* **2011**, *50*, 8396–8399.
- [58] G. Ménard, D. W. Stephan, *Angew. Chem. Int. Ed.* **2012**, *51*, 4409–4412.
- [59] G. Ménard, D. W. Stephan, *Angew. Chem. Int. Ed.* **2012**, *51*, 8272–8275.
- [60] G. Ménard, L. Tran, J. S. J. McCahill, A. J. Lough, D. W. Stephan, *Organometallics* **2013**, *32*, 6759–6763.
- [61] G. Ménard, J. A. Hatnean, H. J. Cowley, A. J. Lough, J. M. Rawson, D. W. Stephan, *J. Am. Chem. Soc.* **2013**, *135*, 6446–6449.
- [62] G. Ménard, L. Tran, D. W. Stephan, *Dalton Trans.* **2013**, *42*, 13685–13691.
- [63] S. Roters, C. Appelt, H. Westenberg, A. Hepp, J. C. Slootweg, K. Lammertsma, W. Uhl, *Dalton Trans.* **2012**, *41*, 9033–9045.
- [64] Y. Zhang, G. M. Miyake, E. Y.-X. Chen, *Angew. Chem. Int. Ed.* **2010**, *49*, 10158–10162.
- [65] G. Erós, H. Mehdi, I. Pápai, T. A. Rokob, P. Király, G. Tárkányi, T. Soós, *Angew. Chem. Int. Ed.* **2010**, *49*, 6559–6563.
- [66] G. Erós, K. Nagy, H. Mehdi, I. Pápai, P. Nagy, P. Király, G. Tárkányi, T. Soós, *Chem. Eur. J.* **2012**, *18*, 574–585.
- [67] L. Greb, C.-G. Daniliuc, K. Bergander, J. Paradies, *Angew. Chem. Int. Ed.* **2013**, *52*, 5876–5879.

- [68] L. Greb, S. Tussing, B. Schirmer, P. Oña-Burgos, K. Kaupmees, M. Lökov, I. Leito, S. Grimme, J. Paradies, *Chem. Sci.* **2013**, *4*, 2788–2796.
- [69] C. M. Mömning, E. Otten, G. Kehr, R. Fröhlich, S. Grimme, D. W. Stephan, G. Erker, *Angew. Chem. Int. Ed.* **2009**, *48*, 6643–6646.
- [70] A. Berkefeld, W. E. Piers, M. Parvez, *J. Am. Chem. Soc.* **2010**, *132*, 10660–10661.
- [71] C.-H. Lim, A. M. Holder, J. T. Hynes, C. B. Musgrave, *Inorg. Chem.* **2013**, *52*, 10062–10066.
- [72] M. J. Sgro, J. Dömer, D. W. Stephan, *Chem. Commun.* **2012**, *48*, 7253–7255.
- [73] A. E. Ashley, D. O'Hare, *Top. Curr. Chem.* **2013**, *334*, 191–217.
- [74] E. Theuergarten, T. Bannenber, M. D. Walter, D. Holschumacher, M. Freytag, C. G. Daniliuc, P. G. Jones, M. Tamm, *Dalton Trans.* **2014**, *43*, 1651–1662.
- [75] T. Sakakura, J.-C. Choi, H. Yasuda, *Chem. Rev.* **2007**, *107*, 2365–2387.
- [76] M. Sajid, L.-M. Elmer, C. Rosorius, C. G. Daniliuc, S. Grimme, G. Kehr, G. Erker, *Angew. Chem. Int. Ed.* **2013**, *52*, 2243–2246.
- [77] M. Sajid, A. Lawzer, W. Dong, C. Rosorius, W. Sander, B. Schirmer, S. Grimme, C. G. Daniliuc, G. Kehr, G. Erker, *J. Am. Chem. Soc.* **2013**, *135*, 18567–18574.
- [78] M. Sajid, G. Kehr, C. G. Daniliuc, G. Erker, *Angew. Chem. Int. Ed.* **2013**, *53*, 1118–1121.
- [79] J. S. J. McCahill, G. C. Welch, D. W. Stephan, *Angew. Chem. Int. Ed.* **2007**, *46*, 4968–4971.
- [80] M. A. Dureen, D. W. Stephan, *J. Am. Chem. Soc.* **2009**, *131*, 8396–8397.
- [81] W. Nie, H. F. T. Klare, M. Oestreich, R. Fröhlich, G. Kehr, G. Erker, *Z. Naturforsch.* **2012**, *67b*, 987–994.
- [82] S. Frömel, R. Fröhlich, C. G. Daniliuc, G. Kehr, G. Erker, *Eur. J. Inorg. Chem.* **2012**, 3774–3779.
- [83] E. Otten, R. C. Neu, D. W. Stephan, *J. Am. Chem. Soc.* **2009**, *131*, 9918–9919.
- [84] R. C. Neu, E. Otten, A. Lough, D. W. Stephan, *Chem. Sci.* **2011**, *2*, 170–176.
- [85] M. J. Kelly, J. Gilbert, R. Tirfoin, S. Aldridge, *Angew. Chem. Int. Ed.* **2013**, *52*, 14094–14097.
- [86] J. C. M. Pereira, M. Sajid, G. Kehr, A. M. Wright, B. Schirmer, Z.-W. Qu, S. Grimme, G. Erker, P. C. Ford, *J. Am. Chem. Soc.* **2014**, *136*, 513–519.
- [87] A. J. P. Cardenas, B. J. Culotta, T. H. Warren, S. Grimme, A. Stute, R. Fröhlich, G. Kehr, G. Erker, *Angew. Chem. Int. Ed.* **2011**, *50*, 7567–7571.
- [88] M. Sajid, A. Stute, A. J. P. Cardenas, B. J. Culotta, J. a. M. Hepperle, T. H. Warren, B. Schirmer, S. Grimme, A. Studer, C. G. Daniliuc, R. Fröhlich, J. L. Petersen, G. Kehr, G. Erker, *J. Am. Chem. Soc.* **2012**, *134*, 10156–10168.

- [89] M. Sajid, A. Klose, B. Birkmann, L. Liang, B. Schirmer, T. Wiegand, H. Eckert, A. J. Lough, R. Fröhlich, C. G. Daniliuc, S. Grimme, D. W. Stephan, G. Kehr, G. Erker, *Chem. Sci.* **2013**, *4*, 213–219.
- [90] E. Y.-X. Chen, *Top. Curr. Chem.* **2013**, *334*, 239–260.
- [91] T. Xu, E. Y.-X. Chen, *J. Am. Chem. Soc.* **2014**, *136*, 1774–1777.
- [92] P. A. Chase, G. C. Welch, T. Jurca, D. W. Stephan, *Angew. Chem.* **2007**, *119*, 8196–8199.
- [93] L. Greb, P. Oña-Burgos, B. Schirmer, S. Grimme, D. W. Stephan, J. Paradies, *Angew. Chem. Int. Ed.* **2012**, *51*, 10164–10168.
- [94] B. Inés, D. Palomas, S. Holle, S. Steinberg, J. A. Nicasio, M. Alcarazo, *Angew. Chem. Int. Ed.* **2012**, *51*, 12367–12369.
- [95] K. Chernichenko, A. Madarász, I. Pápai, M. Nieger, M. Leskelä, T. Repo, *Nat. Chem.* **2013**, *5*, 718–723.
- [96] T. Mahdi, J. N. del Castillo, D. W. Stephan, *Organometallics* **2013**, *32*, 1971–1978.
- [97] L. J. Hounjet, C. Bannwarth, C. N. Garon, C. B. Caputo, S. Grimme, D. W. Stephan, *Angew. Chem. Int. Ed.* **2013**, *52*, 7492–7495.
- [98] Y. Liu, H. Du, *J. Am. Chem. Soc.* **2013**, *135*, 6810–6813.
- [99] D. W. Stephan, *Org. Biomol. Chem.* **2012**, *10*, 5740–5746.
- [100] D. W. Stephan, G. Erker, *Top. Curr. Chem.* **2013**, *332*, 85–110.
- [101] L. J. Hounjet, D. W. Stephan, *Org. Process Res. Dev.* **2014**, *18*, 385–391.
- [102] T. A. Rokob, A. Hamza, A. Stirling, T. Soós, I. Pápai, *Angew. Chem. Int. Ed.* **2008**, *47*, 2435–2438.
- [103] Y. Guo, S. Li, *Inorg. Chem.* **2008**, *47*, 6212–6219.
- [104] A. Moroz, R. L. Sweany, S. L. Whittenburg, *J. Phys. Chem.* **1990**, *94*, 1352–1357.
- [105] W. E. Piers, A. J. V. Marwitz, L. G. Mercier, *Inorg. Chem.* **2011**, *50*, 12252–12262.
- [106] P. Spies, R. Fröhlich, G. Kehr, G. Erker, S. Grimme, *Chem. Eur. J.* **2008**, *14*, 333–343.
- [107] I. Bakó, A. Stirling, S. Bálint, I. Pápai, *Dalton Trans.* **2012**, *41*, 9023–9025.
- [108] L. Rocchigiani, G. Ciancaleoni, C. Zuccaccia, A. Macchioni, *J. Am. Chem. Soc.* **2014**, *136*, 112–115.
- [109] A. Hamza, A. Stirling, T. András Rokob, I. Pápai, *Int. J. Quantum. Chem.* **2009**, *109*, 2416–2425.
- [110] L. L. Zeonjuk, N. Vankova, A. Mavrandonakis, T. Heine, G.-V. Rösenthaller, J. Eicher, *Chem. Eur. J.* **2013**, *19*, 17413–17424.
- [111] H. Zaher, A. E. Ashley, M. Irwin, A. L. Thompson, M. J. Gutmann, T. Krämer, D. O'Hare, *Chem. Commun.* **2013**, *49*, 9755–9757.

- [112] S. Grimme, H. Kruse, L. Goerigk, G. Erker, *Angew. Chem. Int. Ed.* **2010**, *49*, 1402–1405.
- [113] D. M. Camaioni, B. Ginovska-Pangovska, G. K. Schenter, S. M. Kathmann, T. Autrey, *J. Phys. Chem. A* **2012**, *116*, 7228–7237.
- [114] R. Ponec, P. Beran, *J. Phys. Chem. A* **2013**, *117*, 2656–2663.
- [115] T. A. Rokob, I. Bakó, A. Stirling, A. Hamza, I. Pápai, *J. Am. Chem. Soc.* **2013**, *135*, 4425–4437.
- [116] D. F. Wass, A. M. Chapman, *Top. Curr. Chem.* **2013**, *334*, 261–280.
- [117] A. M. Chapman, M. F. Haddow, D. F. Wass, *J. Am. Chem. Soc.* **2011**, *133*, 8826–8829.
- [118] A. M. Chapman, M. F. Haddow, D. F. Wass, *J. Am. Chem. Soc.* **2011**, *133*, 18463–18478.
- [119] A. M. Chapman, D. F. Wass, *Dalton Trans.* **2012**, *41*, 9067–9072.
- [120] A. M. Chapman, M. F. Haddow, D. F. Wass, *Eur. J. Inorg. Chem.* **2012**, 1546–1554.
- [121] S. R. Flynn, D. F. Wass, *ACS Catal.* **2013**, *3*, 2574–2581.
- [122] A. Berkefeld, W. E. Piers, M. Parvez, L. Castro, L. Maron, O. Eisenstein, *J. Am. Chem. Soc.* **2012**, *134*, 10843–10851.
- [123] A. Berkefeld, W. E. Piers, M. Parvez, L. Castro, L. Maron, O. Eisenstein, *Chem. Sci.* **2013**, *4*, 2152–2162.
- [124] P. L. Arnold, I. A. Marr, S. Zlatogorsky, R. Bellabarba, R. P. Tooze, *Dalton Trans.* **2014**, *43*, 34–37.
- [125] S. Frömel, G. Kehr, R. Fröhlich, C. G. Daniliuc, G. Erker, *Dalton Trans.* **2013**, *42*, 14531–14536.
- [126] X. Xu, G. Kehr, C. G. Daniliuc, G. Erker, *J. Am. Chem. Soc.* **2013**, *135*, 6465–6476.
- [127] X. Xu, G. Kehr, C. G. Daniliuc, G. Erker, *Angew. Chem. Int. Ed.* **2013**, *52*, 13629–13632.
- [128] X. Xu, G. Kehr, C. G. Daniliuc, G. Erker, *Organometallics* **2013**, *32*, 7306–7311.
- [129] M. J. Sgro, D. W. Stephan, *Chem. Commun.* **2013**, *49*, 2610–2612.
- [130] M. J. Sgro, D. W. Stephan, *Angew. Chem. Int. Ed.* **2012**, *51*, 11343–11345.
- [131] J. C. DeMott, N. Bhuvanesh, O. V. Ozerov, *Chem. Sci.* **2013**, *4*, 642–649.
- [132] P. Jochmann, D. W. Stephan, *Angew. Chem. Int. Ed.* **2013**, *52*, 9831–9835.
- [133] M. P. Boone, D. W. Stephan, *J. Am. Chem. Soc.* **2013**, *135*, 8508–8511.
- [134] M. P. Boone, D. W. Stephan, *Organometallics* **2014**, *33*, 387–393.
- [135] G. Erker, *Dalton Trans.* **2011**, *40*, 7475–7483.
- [136] J. Bauer, H. Braunschweig, R. D. Dewhurst, *Chem. Rev.* **2012**, *112*, 4329–4346.

- [137] J. Bauer, H. Braunschweig, R. D. Dewhurst, K. Radacki, *Chem. Eur. J.* **2013**, *19*, 8797–8805.
- [138] Y. Jiang, O. Blacque, T. Fox, H. Berke, *J. Am. Chem. Soc.* **2013**, *135*, 7751–7760.
- [139] G. R. Owen, *Chem. Soc. Rev.* **2012**, *41*, 3535–3546.
- [140] W. H. Harman, J. C. Peters, *J. Am. Chem. Soc.* **2012**, *134*, 5080–5082.
- [141] S. K. Podiyanachari, R. Fröhlich, C. G. Daniliuc, J. L. Petersen, C. Mück-Lichtenfeld, G. Kehr, G. Erker, *Angew. Chem. Int. Ed.* **2012**, *51*, 8830–8833.
- [142] S. K. Podiyanachari, G. Kehr, C. Mück-Lichtenfeld, C. G. Daniliuc, G. Erker, *J. Am. Chem. Soc.* **2013**, *135*, 17444–17456.
- [143] R. K. Thauer, *Eur. J. Inorg. Chem.* **2011**, 919–921.
- [144] M. Adams, *Biochim. Biophys. Acta Bioenerg.* **1990**, *1020*, 115–145.
- [145] P. M. Vignais, B. Billoud, *Chem. Rev.* **2007**, *107*, 4206–4272.
- [146] W. Lubitz, E. Reijerse, M. van Gestel, *Chem. Rev.* **2007**, *107*, 4331–4365.
- [147] J. C. Fontecilla-Camps, P. Amara, C. Cavazza, Y. Nicolet, A. Volbeda, *Nature* **2009**, *460*, 814–822.
- [148] A. I. Krasna, *Enzyme Microb. Technol.* **1979**, *1*, 165–172.
- [149] C. Tard, C. J. Pickett, *Chem. Rev.* **2009**, *109*, 2245–2274.
- [150] A. L. De Lacey, V. M. Fernandez, M. Rousset, R. Cammack, *Chem. Rev.* **2007**, *107*, 4304–4330.
- [151] J. C. Gordon, G. J. Kubas, *Organometallics* **2010**, *29*, 4682–4701.
- [152] A. J. M. Stams, C. M. Plugge, *Nat. Rev. Microbiol.* **2009**, *7*, 568–577.
- [153] J. Alper, *Science* **2003**, *299*, 1686–1687.
- [154] J. Y. Yang, R. M. Bullock, M. R. DuBois, D. L. DuBois, *MRS Bulletin* **2011**, *36*, 39–47.
- [155] M. Frey, *ChemBioChem* **2002**, *3*, 153–160.
- [156] J. C. Fontecilla-Camps, A. Volbeda, C. Cavazza, Y. Nicolet, *Chem. Rev.* **2007**, *107*, 4273–303.
- [157] T. Yagi, Y. Higuchi, *Proc. Jpn. Acad. Ser. B* **2013**, *89*, 16–33.
- [158] P. M. Vignais, B. Billoud, J. Meyer, *FEMS Microbiol. Rev.* **2001**, *25*, 455–501.
- [159] R. K. Thauer, A.-K. Kaster, M. Goenrich, M. Schick, T. Hiromoto, S. Shima, *Annu. Rev. Biochem.* **2010**, *79*, 507–536.
- [160] M. Darensbourg, E. Lyon, J. Smee, *Coord. Chem. Rev.* **2000**, *206-207*, 533–561.
- [161] D. J. Evans, C. J. Pickett, *Chem. Soc. Rev.* **2003**, *32*, 268–275.
- [162] F. Gloaguen, T. B. Rauchfuss, *Chem. Soc. Rev.* **2009**, *38*, 100–108.
- [163] T. R. Simmons, G. Berggren, M. Bacchi, M. Fontecave, V. Artero, *Coord. Chem. Rev.* **2014**, *270-271*, 127–150.

- [164] P. E. M. Siegbahn, J. W. Tye, M. B. Hall, *Chem. Rev.* **2007**, *107*, 4414–4435.
- [165] M. T. Stiebritz, M. Reiher, *Chem. Sci.* **2012**, *3*, 1739–1751.
- [166] J. Fritsch, O. Lenz, B. Friedrich, *Nat. Rev. Microbiol.* **2013**, *11*, 106–114.
- [167] S. E. McGlynn, D. W. Mulder, E. M. Shepard, J. B. Broderick, J. W. Peters, *Dalton Trans.* **2009**, 4274–4285.
- [168] K. A. Vincent, A. Parkin, F. A. Armstrong, *Chem. Rev.* **2007**, *107*, 4366–4413.
- [169] P. D. Tran, J. Barber, *Phys. Chem. Chem. Phys.* **2012**, *14*, 13772–13784.
- [170] W. Lubitz, H. Ogata, O. Rüdiger, E. Reijerse, *Chem. Rev.* **2014**, *114*, 4081–4148.
- [171] M. Stephenson, L. H. Stickland, *Biochem. J.* **1931**, *25*, 205–214.
- [172] J. W. Peters, *Science* **1998**, *282*, 1853–1858.
- [173] Y. Nicolet, C. Piras, P. Legrand, C. E. Hatchikian, J. C. Fontecilla-Camps, *Structure* **1999**, *7*, 13–23.
- [174] A. Volbeda, M.-H. Charon, C. Piras, E. C. Hatchikian, M. Frey, J. C. Fontecilla-Camps, *Nature* **1995**, *373*, 580–587.
- [175] R. Cammack, *Nature* **1999**, *397*, 214–215.
- [176] E. C. Hatchikian, N. Forget, V. M. Fernandez, R. Williams, R. Cammack, *Eur. J. Biochem.* **1992**, *209*, 357–365.
- [177] K. A. Bagley, E. C. Duin, W. Roseboom, S. P. J. Albracht, W. H. Woodruff, *Biochemistry* **1995**, *34*, 5527–5535.
- [178] A. Silakov, B. Wenk, E. Reijerse, W. Lubitz, *Phys. Chem. Chem. Phys.* **2009**, *11*, 6592–6599.
- [179] U. Ryde, C. Greco, L. De Gioia, *J. Am. Chem. Soc.* **2010**, *132*, 4512–4513.
- [180] O. F. Erdem, L. Schwartz, M. Stein, A. Silakov, S. Kaur-Ghumaan, P. Huang, S. Ott, E. J. Reijerse, W. Lubitz, *Angew. Chem. Int. Ed.* **2011**, *50*, 1439–1443.
- [181] G. Berggren, A. Adamska, C. Lambertz, T. R. Simmons, J. Esselborn, M. Atta, S. Gambarelli, J.-M. Mouesca, E. Reijerse, W. Lubitz, T. Happe, V. Artero, M. Fontecave, *Nature* **2013**, *499*, 66–69.
- [182] A. Silakov, C. Kamp, E. Reijerse, T. Happe, W. Lubitz, *Biochemistry* **2009**, *48*, 7780–7786.
- [183] A. Adamska, A. Silakov, C. Lambertz, O. Rüdiger, T. Happe, E. Reijerse, W. Lubitz, *Angew. Chem. Int. Ed.* **2012**, *51*, 11458–11462.
- [184] J. M. Camara, T. B. Rauchfuss, *Nat. Chem.* **2012**, *4*, 26–30.
- [185] Y. Nicolet, C. Cavazza, J. C. Fontecilla-Camps, *J. Inorg. Biochem.* **2002**, *91*, 1–8.
- [186] X. Liu, S. Ibrahim, C. Tard, C. Pickett, *Coord. Chem. Rev.* **2005**, *249*, 1641–1652.
- [187] D. Das, T. Dutta, K. Nath, S. Kotay, A. K. Das, T. N. Veziroglu, *Curr. Sci.* **2006**, *90*, 1627–1637.

- [188] J.-F. Capon, F. Gloaguen, F. Y. Pétilion, P. Schollhammer, J. Talarmin, *Eur. J. Inorg. Chem.* **2008**, 4671–4681.
- [189] S. Tschierlei, S. Ott, R. Lomoth, *Energy Environ. Sci.* **2011**, *4*, 2340–2352.
- [190] Y. Montet, P. Amara, A. Volbeda, X. Vernede, E. C. Hatchikian, M. J. Field, M. Frey, J. C. Fontecilla-Camps, *Nat. Struct. Biol.* **1997**, *4*, 523–526.
- [191] J. Fritsch, P. Scheerer, S. Frielingsdorf, S. Kroschinsky, B. Friedrich, O. Lenz, C. M. T. Spahn, *Nature* **2011**, *479*, 249–252.
- [192] Y. Shomura, K.-S. Yoon, H. Nishihara, Y. Higuchi, *Nature* **2011**, *479*, 253–256.
- [193] A. Volbeda, P. Amara, C. Darnault, J.-M. Mouesca, A. Parkin, M. M. Roessler, F. A. Armstrong, J. C. Fontecilla-Camps, *PNAS* **2012**, *109*, 5305–5310.
- [194] K. Grubel, P. L. Holland, *Angew. Chem. Int. Ed.* **2012**, *51*, 3308–3310.
- [195] A. Parkin, F. Sargent, *Curr. Opin. Chem. Biol.* **2012**, *16*, 26–34.
- [196] M.-E. Pandelia, D. Bykov, R. Izsak, P. Infossi, M.-T. Giudici-Ortoni, E. Bill, F. Neese, W. Lubitz, *PNAS* **2013**, *110*, 483–488.
- [197] J.-M. Mouesca, J. C. Fontecilla-Camps, P. Amara, *Angew. Chem. Int. Ed.* **2013**, *52*, 2002–2006.
- [198] L. Lauterbach, O. Lenz, *J. Am. Chem. Soc.* **2013**, *135*, 17897–17905.
- [199] C. S. A. Baltazar, M. C. Marques, C. M. Soares, A. M. DeLacey, I. A. C. Pereira, P. M. Matias, *Eur. J. Inorg. Chem.* **2011**, 948–962.
- [200] H. Ogata, W. Lubitz, Y. Higuchi, *Dalton Trans.* **2009**, 9226, 7577–7587.
- [201] S. Ogo, K. Ichikawa, T. Kishima, T. Matsumoto, H. Nakai, K. Kusaka, T. Ohhara, *Science* **2013**, *339*, 682–684.
- [202] A. Marr, D. Spencer, M. Schröder, *Coord. Chem. Rev.* **2001**, *219-221*, 1055–1074.
- [203] E. Bouwman, J. Reedijk, *Coord. Chem. Rev.* **2005**, *249*, 1555–1581.
- [204] S. Canaguier, V. Artero, M. Fontecave, *Dalton Trans.* **2008**, 315–325.
- [205] Y. Ohki, K. Tatsumi, *Eur. J. Inorg. Chem.* **2011**, 973–985.
- [206] R. Thauer, *Microbiology* **1998**, *144*, 2377–2406.
- [207] J. Schleucher, C. Griesinger, B. Schwörer, R. K. Thauer, *Biochemistry* **1994**, *33*, 3986–3993.
- [208] C. Zirngibl, R. Hedderich, R. Thauer, *FEBS Lett.* **1990**, *261*, 112–116.
- [209] C. Zirngibl, W. Van Dongen, B. Schwörer, R. Von Büнау, M. Richter, A. Klein, R. K. Thauer, *Eur. J. Biochem.* **1992**, *208*, 511–520.
- [210] E. J. Lyon, S. Shima, G. Buurman, S. Chowdhuri, A. Batschauer, K. Steinbach, R. K. Thauer, *Eur. J. Biochem.* **2004**, *271*, 195–204.
- [211] M. Schick, X. Xie, K. Ataka, J. Kahnt, U. Linne, S. Shima, *J. Am. Chem. Soc.* **2012**, *134*, 3271–3280.

- [212] T. Fujishiro, H. Tamura, M. Schick, J. Kahnt, X. Xie, U. Ermler, S. Shima, *Angew. Chem. Int. Ed.* **2013**, *52*, 12555–12558.
- [213] T. J. Lie, K. C. Costa, D. Pak, V. Sakesan, J. A. Leigh, *FEMS Microbiol. Lett.* **2013**, *343*, 156–160.
- [214] R. K. Thauer, A. R. Klein, G. C. Hartmann, *Chem. Rev.* **1996**, *96*, 3031–3042.
- [215] S. Shima, R. K. Thauer, *Chem. Rec.* **2007**, *7*, 37–46.
- [216] J. A. Wright, P. J. Turrell, C. J. Pickett, *Organometallics* **2010**, *29*, 6146–6156.
- [217] S. Shima, U. Ermler, *Eur. J. Inorg. Chem.* **2011**, 963–972.
- [218] M. J. Corr, J. A. Murphy, *Chem. Soc. Rev.* **2011**, *40*, 2279–2292.
- [219] S. Dey, P. K. Das, A. Dey, *Coordin. Chem. Rev.* **2013**, *257*, 42–63.
- [220] J. C. Escalante-Semerena, K. L. Rinehart, R. S. Wolfe, *J. Biol. Chem.* **1984**, *259*, 9447–9455.
- [221] P. Acharya, M. Goenrich, C. H. Hagemeyer, U. Demmer, J. A. Vorholt, R. K. Thauer, U. Ermler, *J. Biol. Chem.* **2005**, *280*, 13712–13719.
- [222] B. H. Geierstanger, T. Prasch, C. Griesinger, G. Hartmann, G. Buurman, R. K. Thauer, *Angew. Chem. Int. Ed.* **1998**, *37*, 3300–3303.
- [223] S. Bartoschek, G. Buurman, R. K. Thauer, B. H. Geierstanger, J. P. Weyrauch, C. Griesinger, M. Nilges, M. C. Hutter, V. Helms, *ChemBioChem* **2001**, *2*, 530–541.
- [224] S. Bartoschek, G. Buurman, B. H. Geierstanger, J. Lapham, C. Griesinger, *J. Am. Chem. Soc.* **2003**, *125*, 13308–13309.
- [225] K. Ceh, U. Demmer, E. Warkentin, J. Moll, R. K. Thauer, S. Shima, U. Ermler, *Biochemistry* **2009**, *48*, 10098–10105.
- [226] T. Hiromoto, E. Warkentin, J. Moll, U. Ermler, S. Shima, *Angew. Chem. Int. Ed.* **2009**, *48*, 6457–6460.
- [227] O. Pilak, B. Mamat, S. Vogt, C. H. Hagemeyer, R. K. Thauer, S. Shima, C. Vonrhein, E. Warkentin, U. Ermler, *J. Mol. Biol.* **2006**, *358*, 798–809.
- [228] G. Buurman, S. Shima, R. K. Thauer, *FEBS Lett.* **2000**, *485*, 200–204.
- [229] M. T. Stiebritz, A. R. Finkelmann, M. Reiher, *Eur. J. Inorg. Chem.* **2011**, 1163–1171.
- [230] S. Shima, O. Pilak, S. Vogt, M. Schick, M. S. Stagni, W. Meyer-Klaucke, E. Warkentin, R. K. Thauer, U. Ermler, *Science* **2008**, *321*, 572–575.
- [231] F. A. Armstrong, J. C. Fontecilla-Camps, *Science* **2008**, *321*, 498–499.
- [232] S. Shima, M. Schick, H. Tamura, *Methods Enzymol.* **2011**, *494*, 119–137.
- [233] T. Hiromoto, E. Warkentin, J. Moll, U. Ermler, S. Shima, *Angew. Chem.* **2009**, *121*, 6579–6582.
- [234] E. J. Lyon, S. Shima, R. Boecher, R. K. Thauer, F.-W. Grevels, E. Bill, W. Roseboom, S. P. J. Albracht, *J. Am. Chem. Soc.* **2004**, *126*, 14239–14248.

- [235] S. Shima, E. J. Lyon, R. K. Thauer, B. Mienert, E. Bill, *J. Am. Chem. Soc.* **2005**, *127*, 10430–10435.
- [236] S. Shima, E. J. Lyon, M. Sordel-Klippert, M. Kauss, J. Kahnt, R. K. Thauer, K. Steinbach, X. Xie, L. Verdier, C. Griesinger, *Angew. Chem. Int. Ed.* **2004**, *43*, 2547–2551.
- [237] M. Korbas, S. Vogt, W. Meyer-Klaucke, E. Bill, E. J. Lyon, R. K. Thauer, S. Shima, *J. Biol. Chem.* **2006**, *281*, 30804–30813.
- [238] X. Wang, Z. Li, X. Zeng, Q. Luo, D. J. Evans, C. J. Pickett, X. Liu, *Chem. Commun.* **2008**, 3555–3557.
- [239] Y. Guo, H. Wang, Y. Xiao, S. Vogt, R. K. Thauer, S. Shima, P. I. Volkers, T. B. Rauchfuss, V. Pelmeshnikov, D. A. Case, E. E. Alp, W. Sturhahn, Y. Yoda, S. P. Cramer, *Inorg. Chem.* **2008**, *47*, 3969–3977.
- [240] H. Tamura, M. Salomone-Stagni, T. Fujishiro, E. Warkentin, W. Meyer-Klaucke, U. Ermler, S. Shima, *Angew. Chem. Int. Ed.* **2013**, *52*, 9656–9659.
- [241] T. Hiromoto, K. Ataka, O. Pilak, S. Vogt, M. S. Stagni, W. Meyer-Klaucke, E. Warkentin, R. K. Thauer, S. Shima, U. Ermler, *FEBS Lett.* **2009**, *583*, 585–590.
- [242] M. Salomone-Stagni, F. Stellato, C. Whaley, S. Vogt, S. Morante, S. Shima, T. Rauchfuss, W. Meyer-Klaucke, *Dalton Trans.* **2010**, *39*, 2972–2983.
- [243] S. Shima, M. Schick, J. Kahnt, K. Ataka, K. Steinbach, U. Linne, *Dalton Trans.* **2012**, *41*, 767–771.
- [244] B. Schwörer, V. M. Fernandez, C. Zirngibl, R. K. Thauer, *Eur. J. Biochem.* **1993**, *212*, 255–261.
- [245] A. Berkessel, R. Thauer, *Angew. Chem. Int. Ed. Engl.* **1995**, *34*, 2247–2250.
- [246] A. Berkessel, *Curr. Opin. Chem. Biol.* **2001**, *5*, 486–490.
- [247] X. Yang, M. B. Hall, *J. Am. Chem. Soc.* **2008**, *130*, 14036–14037.
- [248] X. Yang, M. B. Hall, *J. Am. Chem. Soc.* **2009**, *131*, 10901–10908.
- [249] A. Dey, *J. Am. Chem. Soc.* **2010**, *132*, 13892–13901.
- [250] A. R. Finkelmann, M. T. Stiebritz, M. Reiher, *J. Phys. Chem. B* **2013**, *117*, 4806–4817.
- [251] S. Shima, S. Vogt, A. Göbels, E. Bill, *Angew. Chem. Int. Ed.* **2010**, *49*, 9917–9921.
- [252] S. Vogt, E. J. Lyon, S. Shima, R. K. Thauer, *J. Biol. Inorg. Chem.* **2008**, *13*, 97–106.
- [253] M. L. Ghirardi, A. Dubini, J. Yu, P.-C. Maness, *Chem. Soc. Rev.* **2009**, *38*, 52–61.
- [254] B. E. Barton, M. T. Olsen, T. B. Rauchfuss, *Curr. Opin. Biotech.* **2010**, *21*, 292–297.
- [255] B. Friedrich, J. Fritsch, O. Lenz, *Curr. Opin. Chem. Biol.* **2011**, *22*, 358–364.
- [256] C. Greco, *Inorg. Chem.* **2013**, *52*, 1901–1908.
- [257] F. A. Armstrong, *Science* **2013**, *339*, 658–659.
- [258] T. Liu, D. L. DuBois, R. M. Bullock, *Nat. Chem.* **2013**, *5*, 228–233.

- [259] T. Liu, X. Wang, C. Hoffmann, D. L. DuBois, R. M. Bullock, *Angew. Chem. Int. Ed.* **2014**, *53*, 5300–5304.
- [260] M. R. DuBois, D. L. DuBois, *Chem. Soc. Rev.* **2009**, *38*, 62–72.
- [261] M. L. Helm, M. P. Stewart, R. M. Bullock, M. R. DuBois, D. L. DuBois, *Science* **2011**, *333*, 863–866.
- [262] S. E. Smith, J. Y. Yang, D. L. DuBois, R. M. Bullock, *Angew. Chem. Int. Ed.* **2012**, *51*, 3152–3155.
- [263] M. O'Hagan, M.-H. Ho, J. Y. Yang, A. M. Appel, M. R. DuBois, S. Rauegi, W. J. Shaw, D. L. DuBois, R. M. Bullock, *J. Am. Chem. Soc.* **2012**, *134*, 19409–19424.
- [264] D. L. DuBois, R. M. Bullock, *Eur. J. Inorg. Chem.* **2011**, 1017–1027.
- [265] A. M. Royer, T. B. Rauchfuss, S. R. Wilson, *Inorg. Chem.* **2008**, *47*, 395–397.
- [266] B. Li, T. Liu, C. V. Popescu, A. Bilko, M. Y. Darensbourg, *Inorg. Chem.* **2009**, *48*, 11283–11289.
- [267] B. V. Obrist, D. Chen, A. Ahrens, V. Schünemann, R. Scopelliti, X. Hu, *Inorg. Chem.* **2009**, *48*, 3514–3516.
- [268] T. Liu, B. Li, C. V. Popescu, A. Bilko, L. M. Pérez, M. B. Hall, M. Y. Darensbourg, *Chem. Eur. J.* **2010**, *16*, 3083–3089.
- [269] D. Chen, A. Ahrens-Botzong, V. Schünemann, R. Scopelliti, X. Hu, *Inorg. Chem.* **2011**, *50*, 5249–5257.
- [270] A. M. Royer, T. B. Rauchfuss, D. L. Gray, *Organometallics* **2009**, *28*, 3618–3620.
- [271] A. M. Royer, M. Salomone-Stagni, T. B. Rauchfuss, W. Meyer-Klaucke, *J. Am. Chem. Soc.* **2010**, *132*, 16997–7003.
- [272] P. J. Turrell, J. A. Wright, J. N. T. Peck, V. S. Oganessian, C. J. Pickett, *Angew. Chem. Int. Ed.* **2010**, *49*, 7508–7511.
- [273] P. J. Turrell, A. D. Hill, S. K. Ibrahim, J. A. Wright, C. J. Pickett, *Dalton Trans.* **2013**, *42*, 8140–8146.
- [274] L.-C. Song, Z.-J. Xie, M.-M. Wang, G.-Y. Zhao, H.-B. Song, *Inorg. Chem.* **2012**, *51*, 7466–7468.
- [275] L.-C. Song, G.-Y. Zhao, Z.-J. Xie, J.-W. Zhang, *Organometallics* **2013**, *32*, 2509–2512.
- [276] D. Chen, R. Scopelliti, X. Hu, *Angew. Chem. Int. Ed.* **2010**, *49*, 7512–7515.
- [277] D. Chen, R. Scopelliti, X. Hu, *Angew. Chem. Int. Ed.* **2011**, *50*, 5671–5673.
- [278] M. D. Wodrich, X. Hu, *Eur. J. Inorg. Chem.* **2013**, 3993–3999.
- [279] D. Chen, R. Scopelliti, X. Hu, *Angew. Chem. Int. Ed.* **2012**, *51*, 1919–1921.
- [280] B. Hu, D. Chen, X. Hu, *Chem. Eur. J.* **2012**, *18*, 11528–11530.
- [281] B. Hu, D. Chen, X. Hu, *Chem. Eur. J.* **2013**, *19*, 6221–6224.

- [282] B. Hu, D. Chen, X. Hu, *Chem. Eur. J.* **2014**, *20*, 1677–1682.
- [283] K. M. Schultz, D. Chen, X. Hu, *Chem. Asian J.* **2013**, *8*, 1068–1075.
- [284] M. T. Stiebritz, M. Reiher, *Inorg. Chem.* **2010**, *49*, 5818–5823.
- [285] M. W. Anderson, R. C. F. Jones, J. Saunders, *J. Chem. Soc. Chem. Commun.* **1982**, 282.
- [286] H. Bieräugel, R. Plemp, H. C. Hiemstra, U. K. Pandit, *Tetrahedron* **1983**, *39*, 3971–3979.
- [287] M. W. Anderson, R. C. F. Jones, J. Saunders, *J. Chem. Soc. Perkin Trans. 1* **1986**, 1995–1998.
- [288] A. Salerno, V. Ceriani, I. Perillo, *J. Heterocyclic Chem.* **1992**, *29*, 1725–1733.
- [289] A. Salerno, V. Ceriani, I. Perillo, *J. Heterocyclic Chem.* **1997**, *34*, 709–716.
- [290] K. F. Kalz, *diploma thesis*, University of Göttingen, **2009**.
- [291] K. Hirano, S. Urban, C. Wang, F. Glorius, *Org. Lett.* **2009**, *11*, 1019–1022.
- [292] I. Pravst, M. Zupan, S. Stavber, *Tetrahedron Lett.* **2006**, *47*, 4707–4710.
- [293] J. M. Berg, J. L. Tymoczko, L. Stryer, *Biochemistry*, 5th vol., W. H. Freeman and company, New York, **2002**.
- [294] R. G. Matthews, J. T. Drummond, *Chem. Rev.* **1990**, *90*, 1275–1290.
- [295] S. J. Benkovic, W. P. Bullard, P. A. Benkovic, *J. Am. Chem. Soc.* **1972**, *94*, 7542–7549.
- [296] B. Fernández, I. Perillo, S. Lamdan, *J. Chem. Soc. Perkin Trans. 2* **1978**, 545–550.
- [297] D. R. Robinson, W. P. Jencks, *J. Am. Chem. Soc.* **1967**, *89*, 7088–7098.
- [298] D. R. Robinson, *J. Am. Chem. Soc.* **1970**, *92*, 3138–3146.
- [299] C. Kang, D. Feng, C. Qi, W. Zhao, Z. Cai, *Int. J. Quantum. Chem.* **2002**, *87*, 152–157.
- [300] U. Pandit, H. Bieräugel, *J. Chem. Soc. Chem. Comm.* **1979**, 117–119.
- [301] K. Singh, H. Singh, *Adv. Heterocyclic. Chem.* **2006**, *91*, 159–188.
- [302] M. Iglesias, D. J. Beetstra, J. C. Knight, L.-L. Ooi, A. Stasch, S. Coles, L. Male, M. B. Hursthouse, K. J. Cavell, A. Dervisi, I. a. Fallis, *Organometallics* **2008**, *27*, 3279–3289.
- [303] S. Saba, A. Brescia, M. Kaloustian, *Tetrahedron Lett.* **1991**, *32*, 5031–5034.
- [304] A. Arduengo, R. Krafczyk, R. Schmutzler, H. Craig, J. Goerlich, W. Marshall, M. Unverzagt, *Tetrahedron* **1999**, *55*, 14523–14534.
- [305] K. Arentsen, S. Caddick, F. G. N. Cloke, *Tetrahedron* **2005**, *61*, 9710–9715.
- [306] L. Delaude, M. Szypa, A. Demonceau, A. F. Noels, *Adv. Synth. Catal.* **2002**, *344*, 749–756.
- [307] B. Yigit, *Transition Met. Chem.* **2012**, *37*, 183–188.
- [308] A. Aidouni, S. Bendahou, A. Demonceau, L. Delaude, *J. Comb. Chem.* **2008**, *10*, 886–892.

- [309] K. M. Kuhn, R. H. Grubbs, *Org. Lett.* **2008**, *10*, 2075–2077.
- [310] E. M. McGarrigle, S. P. Fritz, L. Favereau, M. Yar, V. K. Aggarwal, *Org. Lett.* **2011**, *13*, 3060–3063.
- [311] R. Jazzar, H. Liang, B. Donnadiou, G. Bertrand, *J. Organomet. Chem.* **2006**, *691*, 3201–3205.
- [312] J. Zhang, X. Su, J. Fu, M. Shi, *Chem. Commun.* **2011**, *47*, 12541–12543.
- [313] W. Y. Lu, K. J. Cavell, J. S. Wixey, B. Kariuki, *Organometallics* **2011**, *30*, 5649–5655.
- [314] J. Zhang, X. Su, J. Fu, X. Qin, M. Zhao, M. Shi, *Chem. Commun.* **2012**, *48*, 9192–9194.
- [315] L. Jaenicke, E. Brode, *Liebigs Ann. Chem.* **1959**, *624*, 120–136.
- [316] E. Rabe, H.-W. Wanzlick, *Liebigs Ann. Chem.* **1973**, 40–44.
- [317] E. Rabe, H.-W. Wanzlick, *Liebigs Ann. Chem.* **1975**, 195–200.
- [318] A. Salerno, C. Caterina, I. Perillo, *Synthetic Commun.* **2000**, *30*, 3369–3382.
- [319] V. Jurcik, R. Wilhelm, *Org. Biomol. Chem.* **2005**, *3*, 239–244.
- [320] M. C. Caterina, M. A. Figueroa, I. A. Perillo, A. Salerno, *Heterocycles* **2006**, *68*, 701–712.
- [321] A. Paczal, A. C. Bényei, A. Kotschy, *J. Org. Chem.* **2006**, *71*, 5969–5979.
- [322] G. V. Boyd in *The Chemistry of Amidines and Imidates* (Eds.: S. Patai, Z. Rappoport), 2nd vol., John Wiley & Sons Ltd, Chichester, **1991**, pp. 367–324.
- [323] P. Ahlberg, L. Swahn in *The Chemistry of Amidines and Imidates* (Eds.: S. Patai, Z. Rappoport), 2nd vol., John Wiley & Sons Ltd, Chichester, **1991**, pp. 749–788.
- [324] R. Shriner, F. Neumann, *Chem. Rev.* **1944**, *35*, 351–425.
- [325] J.-A. Gautier, M. Miocque, C. C. Farnoux in *The Chemistry of Amidines and Imidates* (Ed.: S. Patai), 1st vol., John Wiley & Sons Ltd, London, **1975**, pp. 283–348.
- [326] V. G. Granik, *Russ. Chem. Rev.* **1983**, *52*, 377–393.
- [327] G. V. Boyd in *The Chemistry of Amidines and Imidates* (Eds.: S. Patai, Z. Rappoport), 2nd vol., John Wiley & Sons Ltd, Chichester, **1991**, pp. 339–366.
- [328] S. Ogata, A. Mochizuki, M. Kakimoto, Y. Imai, *Bull. Chem. Soc. Jpn.* **1986**, *59*, 2171–2177.
- [329] K. Yamamoto, H. Watanabe, *Chem. Lett.* **1982**, 1225–1228.
- [330] T. Imamoto, H. Yokoyama, M. Yokoyama, *Tetrahedron Lett.* **1981**, *22*, 1803–1804.
- [331] S. Bambirra, D. van Leusen, A. Meetsma, B. Hessen, J. H. Teuben, *Chem. Commun.* **2003**, *1*, 522–523.
- [332] S. Bambirra, E. Otten, D. van Leusen, A. Meetsma, B. Hessen, *Z. Anorg. Allg. Chem.* **2006**, *632*, 1950–1952.

- [333] F. Kurzer, K. Douraghi-Zadeh, *Chem. Rev.* **1967**, *67*, 107–152.
- [334] M. P. Coles, D. C. Swenson, R. F. Jordan, V. G. Young, *Organometallics* **1997**, *16*, 5183–5194.
- [335] M. Findlater, N. J. Hill, A. H. Cowley, *Dalton Trans.* **2008**, 4419–4423.
- [336] M. P. Spee, J. Boersma, M. D. Meijer, M. Q. Slagt, G. van Koten, J. W. Geus, *J. Org. Chem.* **2001**, *66*, 1647–1656.
- [337] C. Jones, S. J. Bonyhady, N. Holzmann, G. Frenking, A. Stasch, *Inorg. Chem.* **2011**, *50*, 12315–12325.
- [338] J. B. Lambert, D. E. Huseland, G.-T. Wang, *Synthesis* **1986**, 657–658.
- [339] G. W. Nyce, S. Csihony, R. M. Waymouth, J. L. Hedrick, *Chem. Eur. J.* **2004**, *10*, 4073–4079.
- [340] A. P. Blum, T. Ritter, R. H. Grubbs, *Organometallics* **2007**, *26*, 2122–2124.
- [341] F. H. Allen, O. Kennard, D. G. Watson, L. Brammer, A. G. Orpen, R. Taylor, *J. Chem. Soc. Perkin Trans. 2* **1987**, S1–S19.
- [342] J. R. Aranzaes, M.-C. Daniel, D. Astruc, *Can. J. Chem.* **2006**, *84*, 288–299.
- [343] I. Perillo, S. Lamdan, *J. Chem. Soc. Perkin Trans. 1* **1975**, 894–896.
- [344] B. A. Burdick, P. A. Benkovic, S. J. Benkovic, *J. Am. Chem. Soc.* **1977**, *99*, 5716–5725.
- [345] K. F. Kalz, A. Brinkmeier, S. Dechert, R. A. Mata, F. Meyer, *J. Am. Chem. Soc.* **2014**, *136*, 16626–16634.
- [346] S. Patai (Ed.), *The Chemistry of Amidines and Imidates*, 1st vol., John Wiley & Sons Ltd, London, **1975**.
- [347] S. Patai, Z. Rappoport (Eds.), *The Chemistry of Amidines and Imidates*, 2nd vol., John Wiley & Sons Ltd, Chichester, **1991**.
- [348] R. J. Grout in *The Chemistry of Amidines and Imidates* (Ed.: S. Patai), 1st vol., John Wiley & Sons Ltd, London, **1975**, pp. 255–281.
- [349] S. Bureiko, N. Golubev, S. Kucherov, A. Shurukhina, *J. Mol. Struct.* **2007**, *844-845*, 70–76.
- [350] G. Häfeli, F. K. H. Kuske in *The Chemistry of Amidines and Imidates* (Eds.: S. Patai, Z. Rappoport), 2nd vol., John Wiley & Sons Ltd, Chichester, **1991**, pp. 1–100.
- [351] M. P. Coles, *Dalton Trans.* **2006**, 985–1001.
- [352] C. L. Perrin in *The Chemistry of Amidines and Imidates* (Eds.: S. Patai, Z. Rappoport), 2nd vol., John Wiley & Sons Ltd, Chichester, **1991**, pp. 147–229.
- [353] A. F. Hegarty, A. Chandler, *J. Chem. Soc. Chem. Commun.* **1980**, 130–131.
- [354] J. Oszczapowicz, E. Raczynska, J. Osek, *Magn. Reson. Chem.* **1986**, *24*, 9–14.
- [355] R. T. Boeré, V. Klassen, G. Wolmershäuser, *J. Chem. Soc. Dalton Trans.* **1998**, 4147–4154.

- [356] H. Komber, C. Klinger, F. Böhme, *Polymer* **1997**, *38*, 2603–2608.
- [357] J. A. R. Schmidt, J. Arnold, *J. Chem. Soc. Dalton Trans.* **2002**, 2890–2899.
- [358] R. J. Baker, C. Jones, *J. Organomet. Chem.* **2006**, *691*, 65–71.
- [359] I. Wawer, *Magn. Reson. Chem.* **1989**, *27*, 1031–1038.
- [360] G. Häfelinger in *The Chemistry of Amidines and Imidates* (Ed.: S. Patai), 1st vol., John Wiley & Sons Ltd, London, **1975**, pp. 1–84.
- [361] E. D. Raczynska, C. Laurence, *Analyst* **1992**, *117*, 375–378.
- [362] I. Busko-Oszczapowicz, J. Oszczapowicz in *The Chemistry of Amidines and Imidates* (Eds.: S. Patai, Z. Rappoport), 2nd vol., John Wiley & Sons Ltd, Chichester, **1991**, pp. 231–299.
- [363] I. D. Cunningham, J. S. Blanden, J. Llor, L. Munoz, A. P. Sharratt, *J. Chem. Soc. Perkin Trans. 2* **1991**, 1747–1750.
- [364] I. Wawer, *Magn. Reson. Chem.* **1988**, *26*, 601–607.
- [365] I. Wawer, *J. Mol. Liq.* **1988**, *38*, 1–10.
- [366] I. Wawer, *Magn. Reson. Chem.* **1989**, *27*, 577–581.
- [367] J. Oszczapowicz in *The Chemistry of Amidines and Imidates* (Eds.: S. Patai, Z. Rappoport), 2nd vol., John Wiley & Sons Ltd, Chichester, **1991**, pp. 623–688.
- [368] L. Meschede, H.-H. Limbach, *J. Phys. Chem.* **1991**, *95*, 10267–10280.
- [369] B. Clement, T. Kämpchen, *Chem. Ber.* **1986**, *119*, 1101–1104.
- [370] J. Halliday, E. Symons, P. Binder, *Can. J. Chem.* **1978**, *56*, 1470–1476.
- [371] L. M. Jackman, T. Jen, *J. Am. Chem. Soc.* **1975**, *97*, 2811–2817.
- [372] H. Sieveking, W. Lüttke, *Liebigs Ann. Chem.* **1977**, 189–203.
- [373] E. Raczynska, C. Laurence, M. Berthelot, *Analyst* **1994**, *119*, 683–687.
- [374] D. Prevorsek, *J. Phys. Chem.* **1962**, *66*, 769–778.
- [375] J. Krechl, S. Smrcková, M. Ludwig, J. Kuthan, *Collect. Czech. Chem. Commun.* **1990**, *55*, 469–478.
- [376] S. Bureiko, I. Chernyshova, *J. Mol. Struct.* **1991**, *263*, 37–44.
- [377] J. Krechl, S. Smrcková, J. Kuthan, *Collect. Czech. Chem. Commun.* **1990**, *55*, 460–468.
- [378] A. Kraft, L. Peters, H. Powell, *Tetrahedron* **2002**, *58*, 3499–3505.
- [379] T. M. Krygowski, K. Wozniak in *The Chemistry of Amidines and Imidates* (Eds.: S. Patai, Z. Rappoport), 2nd vol., John Wiley & Sons Ltd, Chichester, **1991**, pp. 101–145.
- [380] W. H. Prichard in *The Chemistry of Amidines and Imidates* (Ed.: S. Patai), 1st vol., John Wiley & Sons Ltd, London, **1975**, pp. 157–188.
- [381] L. Xing, C. Wiegert, A. Petitjean, *J. Org. Chem.* **2009**, *74*, 9513–9516.

- [382] S. Hartmann, V. Brecht, A. W. Frahm, *Magn. Reson. Chem.* **1999**, *37*, 69–72.
- [383] J. Keeler, *Understanding NMR Spectroscopy*, 1st vol., John Wiley & Sons Ltd, Chichester, **2007**.
- [384] J. K. M. Sanders, B. K. Hunter, *Modern NMR Spectroscopy: A Guide for Chemists*, 2nd vol., Oxford University Press, Oxford, **2007**.
- [385] F. Neese, *WIREs Comput. Mol. Sci.* **2012**, *2*, 73–78.
- [386] A. Schäfer, H. Horn, R. Ahlrichs, *J. Chem. Phys.* **1992**, *97*, 2571–2577.
- [387] S. Sinnecker, A. Rajendran, A. Klamt, M. Diedenhofen, F. Neese, *J. Phys. Chem. A* **2006**, *110*, 2235–2245.
- [388] P. C. Junk, M. L. Cole, *Chem. Commun.* **2007**, 1579–1590.
- [389] D. Stalke, M. Wedler, F. Edelmann, *J. Organomet. Chem.* **1992**, *431*, C1–C5.
- [390] F. T. Edelmann, *Coord. Chem. Rev.* **1994**, *137*, 403–481.
- [391] J. Grundy, M. P. Coles, P. B. Hitchcock, *J. Organomet. Chem.* **2002**, *662*, 178–187.
- [392] C. Jones, S. Aldridge, T. Gans-Eichler, A. Stasch, *Dalton Trans.* **2006**, *1*, 5357–5361.
- [393] S. S. Sen, A. Jana, H. W. Roesky, C. Schulzke, *Angew. Chem. Int. Ed.* **2009**, *48*, 8536–8538.
- [394] S. S. Sen, H. W. Roesky, D. Stern, J. Henn, D. Stalke, *J. Am. Chem. Soc.* **2010**, *132*, 1123–1126.
- [395] F. T. Edelmann, *Chem. Soc. Rev.* **2009**, *38*, 2253–2268.
- [396] S. Bambirra, M. W. Bouwkamp, A. Meetsma, B. Hessen, *J. Am. Chem. Soc.* **2004**, *126*, 9182–9183.
- [397] F. Chen, S. Fan, Y. Wang, J. Chen, Y. Luo, *Organometallics* **2012**, *31*, 3730–3735.
- [398] D. Dick, R. Duchateau, J. Edema, S. Gambarotta, *Inorg. Chem.* **1993**, *32*, 1959–1962.
- [399] K.-H. Thiele, H. Windisch, H. Windisch, F. T. Edelmann, U. Kilimann, M. Noltemeyer, *Z. Anorg. Allg. Chem.* **1996**, *622*, 713–716.
- [400] V. Volkis, E. Nelkenbaum, A. Lisovskii, G. Hasson, R. Semiat, M. Kapon, M. Botoshansky, Y. Eishen, M. S. Eisen, *J. Am. Chem. Soc.* **2003**, *125*, 2179–2194.
- [401] E. Nelkenbaum, M. Kapon, M. S. Eisen, *Organometallics* **2005**, *24*, 2645–2659.
- [402] T. J. J. Sciarone, C. a. Nijhuis, A. Meetsma, B. Hessen, *Dalton Trans.* **2006**, 4896–4904.
- [403] X.-G. Li, Z. Li, H. Li, R. G. Gordon, *Eur. J. Inorg. Chem.* **2007**, 1135–1142.
- [404] R. P. Rose, C. Jones, C. Schulten, S. Aldridge, A. Stasch, *Chem. Eur. J.* **2008**, *14*, 8477–8480.
- [405] L. Fohlmeister, S. Liu, C. Schulten, B. Moubaraki, A. Stasch, J. D. Cashion, K. S. Murray, L. Gagliardi, C. Jones, *Angew. Chem.* **2012**, *124*, 8419–8423.

- [406] H. Nagashima, H. Kondo, T. Hayashida, Y. Yamaguchi, M. Gondo, S. Masuda, K. Miyazaki, K. Matsubara, K. Kirchner, *Coord. Chem. Rev.* **2003**, *245*, 177–190.
- [407] T. J. J. Whitehorne, J. P. Coyle, A. Mahmood, W. H. Monillas, G. P. A. Yap, S. T. Barry, *Eur. J. Inorg. Chem.* **2011**, 3240–3247.
- [408] J. A. R. Schmidt, J. Arnold, *J. Chem. Soc. Dalton Trans.* **2002**, 3454–3461.
- [409] J. Barker, M. Kilner, *Coord. Chem. Rev.* **1994**, *133*, 219–300.
- [410] F. T. Edelmann, *Adv. Organomet. Chem.* **2008**, *57*, 183–352.
- [411] M. W. Hosseini, *Coord. Chem. Rev.* **2003**, *240*, 157–166.
- [412] M. Best, S. Tobey, E. Anslyn, *Coord. Chem. Rev.* **2003**, *240*, 3–15.
- [413] E. Smolensky, M. S. Eisen, *Dalton Trans.* **2007**, 5623–5650.
- [414] S. Collins, *Coord. Chem. Rev.* **2011**, *255*, 118–138.
- [415] Z. Li, S. T. Barry, R. G. Gordon, *Inorg. Chem.* **2005**, *44*, 1728–1735.
- [416] B. S. Lim, A. Rahtu, J.-S. Park, R. G. Gordon, *Inorg. Chem.* **2003**, *42*, 7951–7958.
- [417] I. D. Brown, J. D. Dunitz, *Acta Cryst.* **1961**, *14*, 480–485.
- [418] J. Beck, J. Strähle, *Angew. Chem. Int. Ed. Engl.* **1986**, *25*, 95–96.
- [419] S. J. Archibald, N. W. Alcock, D. H. Busch, D. R. Whitcomb, *Inorg. Chem.* **1999**, *38*, 5571–5578.
- [420] F. Cotton, X. Feng, M. Matusz, R. Poli, *J. Am. Chem. Soc.* **1988**, *110*, 7077–7083.
- [421] S. Radak, Y. Ni, G. Xu, K. Shaffer, T. Ren, *Inorg. Chim. Acta* **2001**, *321*, 200–204.
- [422] T. Ren, C. Lin, P. Amalberti, D. Macikenas, J. D. Protasiewicz, J. C. Baum, T. L. Gibson, *Inorg. Chem. Commun.* **1998**, *1*, 23–26.
- [423] P. van Vliet, G. van Koten, K. Vrieze, *J. Organomet. Chem.* **1979**, *179*, 89–100.
- [424] M. Risto, T. T. Takaluoma, T. Bajorek, R. Oilunkaniemi, R. S. Laitinen, T. Chivers, *Inorg. Chem.* **2009**, *48*, 6271–6279.
- [425] A. Bondi, *J. Phys. Chem.* **1964**, *68*, 441–451.
- [426] L. P. Olson, D. R. Whitcomb, M. Rajeswaran, T. N. Blanton, B. J. Stwertka, *Chem. Mater.* **2006**, *18*, 1667–1674.
- [427] A. Bayler, A. Schier, G. A. Bowmaker, H. Schmidbaur, *J. Am. Chem. Soc.* **1996**, *118*, 7006–7007.
- [428] F. Scherbaum, A. Grohmann, B. Huber, C. Krüger, H. Schmidbaur, *Angew. Chem. Int. Ed. Engl.* **1988**, *27*, 1544–1546.
- [429] H. Schmidbaur, *Gold Bull.* **1990**, *23*, 11–21.
- [430] H. Schmidbaur, *Gold Bull.* **2000**, *33*, 3–10.
- [431] H. Schmidbaur, *Nature* **2001**, *413*, 31–33.
- [432] H. Schmidbaur, A. Schier, *Chem. Soc. Rev.* **2008**, *37*, 1931–1951.

- [433] P. Mehrotra, R. Hoffmann, *Inorg. Chem.* **1978**, *17*, 2187–2189.
- [434] K. Merz, R. Hoffmann, *Inorg. Chem.* **1988**, *27*, 2120–2127.
- [435] M. Jansen, *Angew. Chem. Int. Ed. Engl.* **1987**, *26*, 1098–1110.
- [436] J. Li, P. Pyykkö, *Chem. Phys. Lett.* **1992**, *197*, 586–590.
- [437] P. Pyykkö, *Chem. Rev.* **1997**, *97*, 597–636.
- [438] P. Pyykkö, *Chem. Soc. Rev.* **2008**, *37*, 1967–1997.
- [439] P. Pyykkö, *Angew. Chem. Int. Ed.* **2004**, *43*, 4412–4456.
- [440] S. Sculfort, P. Braunstein, *Chem. Soc. Rev.* **2011**, *40*, 2741–2760.
- [441] H. L. Hermann, G. Boche, P. Schwerdtfeger, *Chem. Eur. J.* **2001**, *7*, 5333–5342.
- [442] K. Singh, J. Long, P. Stavropoulos, *J. Am. Chem. Soc.* **1997**, *119*, 2942–2943.
- [443] M.-L. Tong, X.-M. Chen, B.-H. Ye, L.-N. Ji, *Angew. Chem. Int. Ed.* **1999**, *38*, 2237–2240.
- [444] J. Zhang, D. C. Grills, K.-W. Huang, E. Fujita, R. M. Bullock, *J. Am. Chem. Soc.* **2005**, *127*, 15684–15685.
- [445] M. a. Omary, T. R. Webb, Z. Assefa, G. E. Shankle, H. H. Patterson, *Inorg. Chem.* **1998**, *37*, 1380–1386.
- [446] P. Pyykkö, N. Runeberg, F. Mendizabal, *Chem. Eur. J.* **1997**, *3*, 1451–1457.
- [447] P. Pyykkö, F. Mendizabal, *Chem. Eur. J.* **1997**, *3*, 1458–1465.
- [448] M. Andrejić, R. A. Mata, *Phys. Chem. Chem. Phys.* **2013**, *15*, 18115–18122.
- [449] C.-M. Che, M.-C. Tse, M. C. W. Chan, K.-K. Cheung, D. L. Phillips, K.-H. Leung, *J. Am. Chem. Soc.* **2000**, *122*, 2464–2468.
- [450] A. L. Johnson, A. M. Willcocks, S. P. Richards, *Inorg. Chem.* **2009**, *48*, 8613–8622.
- [451] P. Pyykkö, F. Mendizabal, *Inorg. Chem.* **1998**, *37*, 3018–3025.
- [452] E. O. Fischer, *Angew. Chem.* **1955**, *67*, 475–482.
- [453] E. O. Fischer, R. Böttcher, *Z. Naturforsch. B* **1955**, *10*, 600–601.
- [454] J. Kühn, K. Rück-Braun, *J. Prakt. Chem.* **1997**, *339*, 675–678.
- [455] R. Theys, M. Dudley, M. Hossain, *Coord. Chem. Rev.* **2009**, *253*, 180–234.
- [456] R. B. King, *Acc. Chem. Res.* **1970**, *3*, 417–427.
- [457] M. Bergamo, T. Beringhelli, G. Ciani, G. D'Alfonso, M. Moret, A. Sironi, *Inorg. Chim. Acta* **1997**, *259*, 291–303.
- [458] M. Tilset, V. Parker, *J. Am. Chem. Soc.* **1989**, *111*, 6711–6717.
- [459] J. R. Pugh, T. J. Meyer, *J. Am. Chem. Soc.* **1992**, *114*, 3784–3792.
- [460] R. Dessy, R. Pohl, R. King, *J. Am. Chem. Soc.* **1966**, *88*, 5121–5124.
- [461] D. P. Estes, A. K. Vannucci, A. R. Hall, D. L. Lichtenberger, J. R. Norton, *Organometallics* **2011**, *30*, 3444–3447.

- [462] J. A. Gladysz, G. M. Williams, W. Tam, D. L. Johnson, D. W. Parker, J. C. Selover, *Inorg. Chem.* **1979**, *18*, 553–558.
- [463] T. Ohishi, Y. Shiotani, M. Yamashita, *J. Org. Chem.* **1994**, *59*, 250.
- [464] A. Davison, J. A. McCleverty, G. Wilkinson, *J. Chem. Soc.* **1963**, 1133–1138.
- [465] T. Blackmore, M. I. Bruce, F. G. A. Stone, *J. Chem. Soc. A* **1968**, 2158–2162.
- [466] M. Brookhart, W. Studabaker, G. Husk, *Organometallics* **1987**, *6*, 1141–1145.
- [467] H. Stueger, M. Braunwarth, G. Fuerpass, J. Baumgartner, R. Saf, *Monatsh. Chem.* **2006**, *137*, 595–603.
- [468] S. Jacobson, A. Wojcicki, *J. Organomet. Chem.* **1974**, *72*, 113–120.
- [469] D. Gibson, W.-L. Hsu, F. Ahmed, *J. Organomet. Chem.* **1981**, *215*, 379–401.
- [470] J. C. Vites, B. D. Steffey, M. E. Giuseppetti-Dery, A. R. Cutler, *Organometallics* **1991**, *10*, 2827–2834.
- [471] M. F. Joseph, J. A. Page, M. C. Baird, *Inorg. Chim. Acta* **1982**, *64*, L121–L122.
- [472] M. F. Joseph, J. A. Page, M. C. Baird, *Organometallics* **1984**, *3*, 1749–1754.
- [473] K. F. Kalz, N. Kindermann, S.-Q. Xiang, A. Kronz, A. Lange, F. Meyer, *Organometallics* **2014**, *33*, 1475–1479.
- [474] J. P. Collman, *Acc. Chem. Res.* **1975**, *8*, 342–347.
- [475] J. P. Collman, R. G. Finke, J. N. Cawse, J. I. Brauman, *J. Am. Chem. Soc.* **1977**, *99*, 2515–2526.
- [476] J. A. Gladysz, W. Tam, *J. Org. Chem.* **1978**, *43*, 2279–2280.
- [477] C. Cundy, *J. Organomet. Chem.* **1974**, *69*, 305–310.
- [478] H. Schumann, J. Opitz, *J. Organomet. Chem.* **1979**, *166*, 233–239.
- [479] C. Amatore, P. J. Krusic, S. U. Pedersen, J.-N. Verpeaux, *Organometallics* **1995**, *14*, 640–649.
- [480] J. J. Brunet, *Chem. Rev.* **1990**, *90*, 1041–1059.
- [481] D. E. Berning, B. C. Noll, D. L. DuBois, *J. Am. Chem. Soc.* **1999**, *121*, 11432–11447.
- [482] D. Wang, R. J. Angelici, *J. Am. Chem. Soc.* **1996**, *118*, 935–942.
- [483] T. Li, A. J. Lough, R. H. Morris, *Chem. Eur. J.* **2007**, *13*, 3796–3803.
- [484] K. H. Pannell, J. M. Rozell, W.-M. Tsai, *Organometallics* **1987**, *6*, 2085–2088.
- [485] D. J. Darensbourg, R. L. Gray, M. Pala, *Organometallics* **1984**, *3*, 1928–1930.
- [486] G. Bor, B. F. G. Johnson, J. Lewis, P. W. Robinson, *J. Chem. Soc. A* **1971**, 696–698.
- [487] G. Bor, *J. Organomet. Chem.* **1967**, *10*, 343–359.
- [488] E. Hey-Hawkins, H. G. von Schnering, *Z. Naturforsch.* **1991**, *46b*, 621–624.
- [489] K. H. Pannell, D. Jackson, *J. Am. Chem. Soc.* **1976**, *98*, 4443–4446.
- [490] M. Wojdyr, *J. Appl. Cryst.* **2010**, *43*, 1126–1128.

- [491] A. P. Humphries, S. A. R. Knox, *J. Chem. Soc. Dalton Trans.* **1975**, 1710–1714.
- [492] T. E. Bitterwolf, J. C. Linehan, J. E. Shade, *Organometallics* **2001**, *20*, 775–781.
- [493] T. Blackmore, J. D. Cotton, M. I. Bruce, F. G. A. Stone, *J. Chem. Soc. A* **1968**, 2931–2936.
- [494] P. J. Bailey, M. J. Duer, B. F. G. Johnson, J. Lewis, G. Conole, M. McPartlin, H. R. Powell, C. E. Anson, *J. Organomet. Chem.* **1990**, *383*, 441–461.
- [495] J. W. Gleeson, R. Vaughan, *J. Chem. Phys.* **1983**, *78*, 5384–5392.
- [496] S. Aime, M. Botta, R. Gobetto, A. Orlandi, *Magn. Reson. Chem.* **1990**, *28*, S52–S58.
- [497] G. E. Hawkes, K. D. Sales, S. Aime, R. Gobetto, L.-Y. Lian, *Inorg. Chem.* **1991**, *30*, 1489–1493.
- [498] L. Reven, E. Oldfield, *Inorg. Chem.* **1992**, *31*, 243–252.
- [499] H. C. Canuto, A. Masic, N. H. Rees, S. J. Heyes, R. Gobetto, S. Aime, *Organometallics* **2006**, *25*, 2248–2252.
- [500] J. T. Armstrong, *Microbeam Anal.* **1995**, *4*, 177–200.
- [501] K. E. Inkrott, S. G. Shore, *J. Am. Chem. Soc.* **1978**, *100*, 3954–3955.
- [502] J. F. Burnett, R. E. Zahler, *Chem. Rev.* **1951**, *49*, 273–412.
- [503] R. B. King, M. B. Bisnette, *J. Organomet. Chem.* **1964**, *2*, 38–43.
- [504] M. I. Bruce, F. G. A. Stone, *Angew. Chem. Int. Ed.* **1968**, *7*, 747–753.
- [505] G. Artamkina, P. Sazonov, V. Ivushkin, I. Beletskaya, *Chem. Eur. J.* **1998**, *4*, 1169–1178.
- [506] V. Ivushkin, P. Sazonov, G. Artamkina, I. Beletskaya, *J. Organomet. Chem.* **2000**, *597*, 77–86.
- [507] R. A. Rossi, A. B. Pierini, A. B. Peñéñory, *Chem. Rev.* **2003**, *103*, 71–167.
- [508] P. Krusic, P. Fagan, *J. Am. Chem. Soc.* **1977**, *99*, 250–252.
- [509] N. G. Connelly, W. E. Geiger, *Chem. Rev.* **1996**, *96*, 877–910.
- [510] D. Brown, W. Glass, M. M. Salama, *J. Organomet. Chem.* **1994**, *474*, 129–132.
- [511] H. Carr, E. Purcell, *Phys. Rev.* **1952**, *88*, 415–416.
- [512] E. J. Moore, J. M. Sullivan, J. R. Norton, *J. Am. Chem. Soc.* **1986**, *108*, 2257–2263.
- [513] W. Beck, A. Melnikoff, R. Stahl, *Chem. Ber.* **1966**, *99*, 3721–3727.
- [514] P. S. Braterman, R. Bau, H. D. Kaesz, *Inorg. Chem.* **1967**, *6*, 2097–2102.
- [515] D. J. Darensbourg, *Inorg. Chem.* **1972**, *11*, 1606–1609.
- [516] R. H. Crabtree, *The Organometallic Chemistry of the Transition Metals*, 4th vol., John Wiley & Sons, Hoboken (New Jersey), **2005**.
- [517] J. Burdon, W. B. Hollyhead, J. C. Tatlow, *J. Chem. Soc.* **1965**, 5152–5156.
- [518] R. B. King, F. G. A. Stone, *Inorg. Synth.* **1963**, *7*, 110.

- [519] G. R. Fulmer, A. J. M. Miller, N. H. Sherden, H. E. Gottlieb, A. Nudelman, B. M. Stoltz, J. E. Bercaw, K. I. Goldberg, *Organometallics* **2010**, *29*, 2176–2179.
- [520] J. C. Cobas, M. Martín-Pastor, *EXSYCalc*, Mestrelab Research, **2007**.
- [521] G. M. Sheldrick, *Acta Cryst.* **2008**, *A64*, 112–122.
- [522] *X-RED*, STOE & CIE GmbH, Darmstadt, Germany, **2007**.
- [523] N. M. Doherty, S. A. R. Knox, M. J. Morris, *Inorg. Syn.* **1990**, *28*, 189–191.
- [524] A. D. Becke, *J. Chem. Phys.* **1993**, *98*, 5648–5652.
- [525] S. Grimme, J. Antony, S. Ehrlich, H. Krieg, *J. Chem. Phys.* **2010**, *132*, 154104.
- [526] S. Grimme, S. Ehrlich, L. Goerigk, *J. Comput. Chem.* **2011**, *32*, 1456–1465.
- [527] F. Weigend, R. Ahlrichs, *Phys. Chem. Chem. Phys.* **2005**, *7*, 3297–3305.
- [528] D. Andrae, U. Häußermann, M. Dolg, H. Stoll, H. Preuß, *Theor. Chim. Acta* **1990**, *77*, 123–141.
- [529] F. Neese, F. Wennmohs, A. Hansen, U. Becker, *Chem. Phys.* **2009**, *356*, 98–109.
- [530] A. Klamt, G. Schüürmann, *J. Chem. Soc. Perkin Trans. 2* **1993**, 799–805.

List of Abbreviations

<i>i</i> Pr	iso-propyl
<i>t</i> Bu	<i>tert</i> -butyl
Fp ⁻	[CpFe(CO) ₂] ⁻
Rp ⁻	[CpRu(CO) ₂] ⁻
ALD	atomic layer deposition
ATR	attenuated total reflectance
BSE	backscattered electrons
CD	circular dichroism
cod	cyclooctadiene
CP	cross-polarization
Cp	cyclopentadienyl, C ₅ H ₅
Cp*	pentamethylcyclopentadienyl, C ₅ Me ₅
CSA	chemical shift anisotropy
CV	cyclic voltammetry
CVD	chemical vapor deposition
Cys	cysteine
DBDMH	1,3-dibromo-5,5-dimethylhydantoin
DCM	dichloromethane
DDQ	2,3-dichloro-5,6-dicyano-1,4-benzoquinone
depe	1,2-bis(diethylphosphino)ethane
DFT	density functional theory
DME	1,2-dimethoxyethane
DMF	dimethylformamide
DMSO	dimethyl sulfoxide
DOSY	diffusion-ordered spectroscopy
dppe	1,2-bis(diphenylphosphino)ethane
EI	electron ionization/electron impact

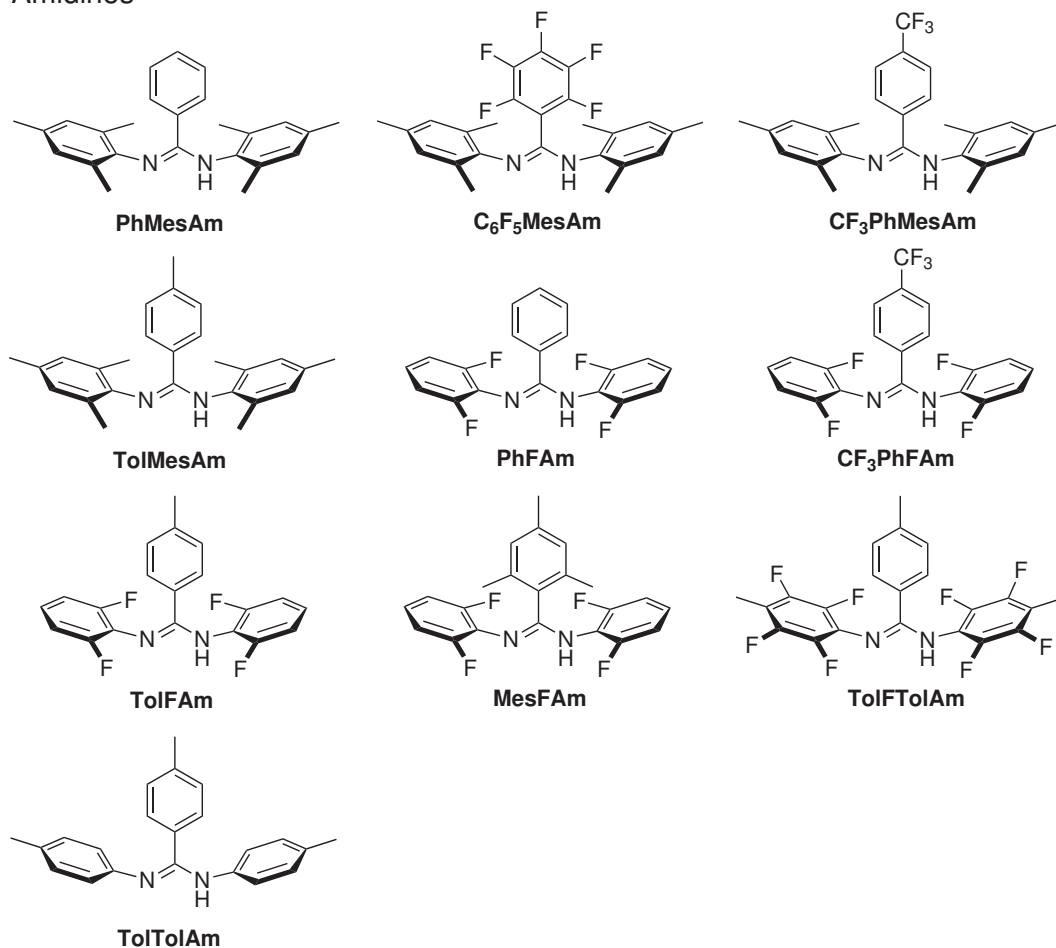
EMPA	electron microprobe analysis
EPR	electron paramagnetic resonance
ESI	electrospray ionization
ET	electron transfer
EXSY	exchange spectroscopy
Fc	ferrocene
FD	field desorption
FeGP cofactor	iron guanylylpyridinol cofactor
FLP	frustrated Lewis pair
Fp ₂	[CpFe(CO) ₂] ₂
H ₄ MPT	Tetrahydromethanopterin
HFp	HFeCp(CO) ₂
Hmd	H ₂ -forming methylenetetrahydromethanopterin dehydrogenase
HMDSO	hexamethyldisiloxane
HME	halogen–metal exchange
HRp	HRuCp(CO) ₂
IR	infrared
KFp	K[CpFe(CO) ₂]
KRp	K[CpRu(CO) ₂]
MALDI	matrix-assisted laser desorption/ionization
MAS	magic angle spinning
Me	methyl
MeCN	acetonitrile
Mes	2,4,6-trimethylphenyl
methenyl-H ₄ MPT ⁺	N ⁵ ,N ¹⁰ -methenyltetrahydromethanopterin
methylene-H ₄ MPT	N ⁵ ,N ¹⁰ -metylenetetrahydromethanopterin
NAD(P) ⁺	(oxidized form of) nicotinamide adenine dinucleotide (phosphate)
NBA	N-bromoacetamide
NBS	N-bromosuccinimide
NHC	N-heterocyclic carbene
NIR	near-infrared
NIS	N-iodosuccinimide
NMR	nuclear magnetic resonance
NOE	nuclear Overhauser effect
NOESY	nuclear Overhauser enhancement spectroscopy
NRVS	nuclear resonance vibrational spectroscopy
Ph	phenyl

PPSE	polyphosphoric acid trimethylsilyl ester
Rp ₂	[CpRu(CO) ₂] ₂
rt	room temperature
SEI	secondary electron imaging
SEM	scanning electron microscope
SET	single electron transfer
THF	tetrahydrofuran
Tol	tolyl
UV/Vis	ultraviolet–visible (spectroscopy)
XAS	X-ray absorption spectroscopy

Appendix

Structures of Important Compounds

Amidines



Bisamidinatodisilver(I) Complexes

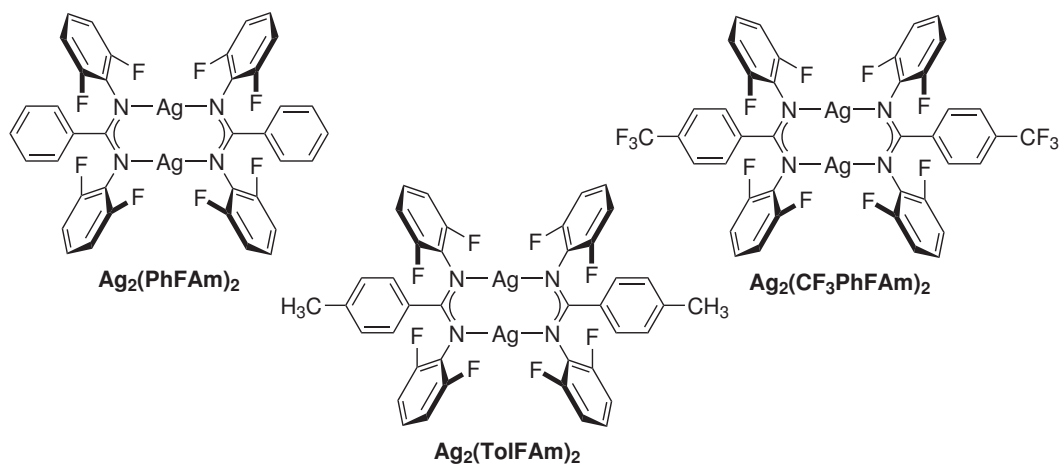
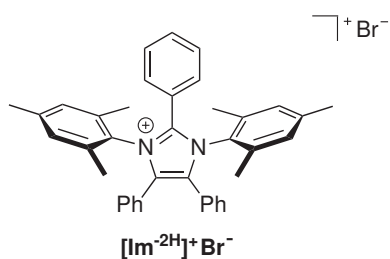


Figure A1. Overview of amidines and bisamidinatodisilver(I) complexes.

Imidazolium Salt



Imidazolium Salts

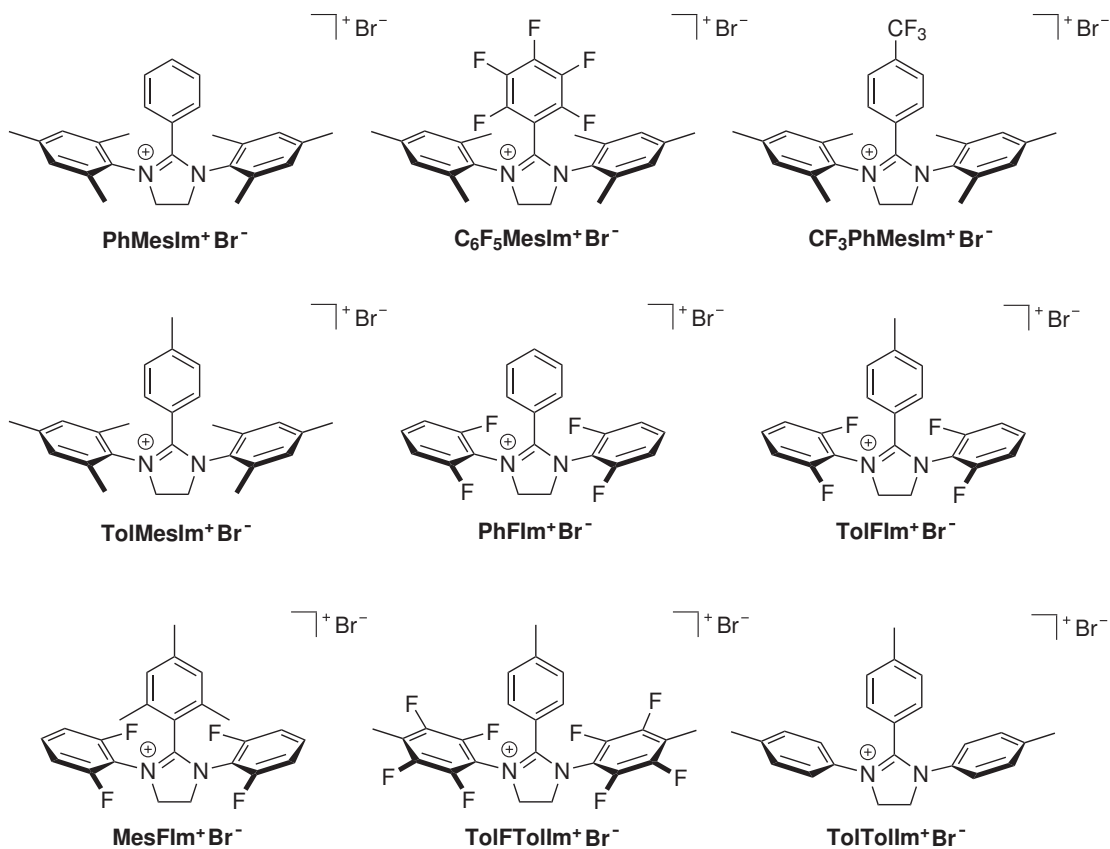
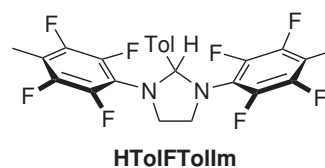
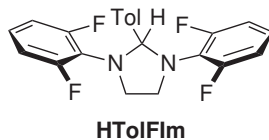
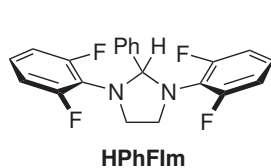
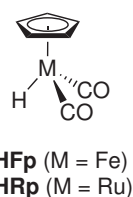
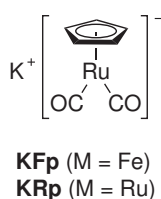
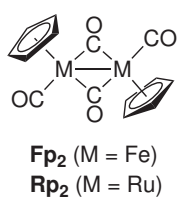


Figure A2. Overview of imidazolium and imidazolium salts.

Imidazolidines



Carbonyl Complexes, Metalates, Lewis Pairs, and Reaction Products



unknown structure
(see chapter 4.3)

Rs

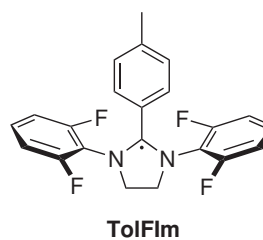
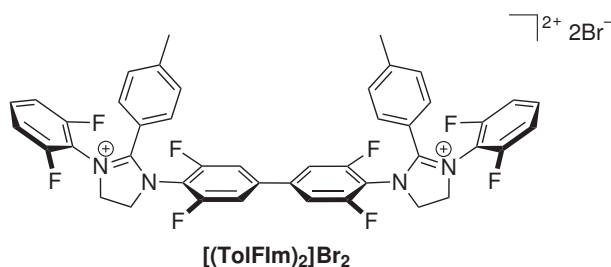
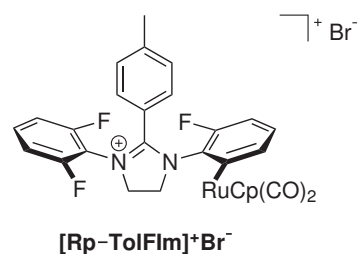
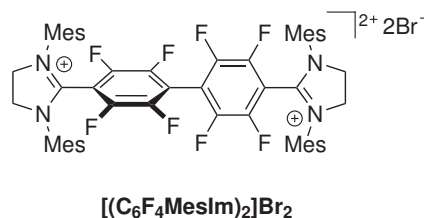
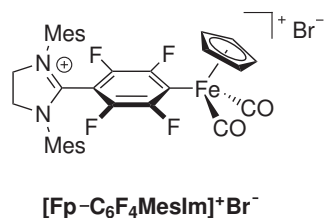
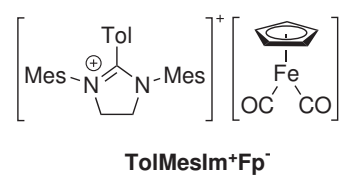
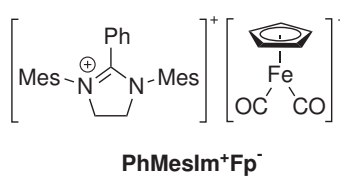
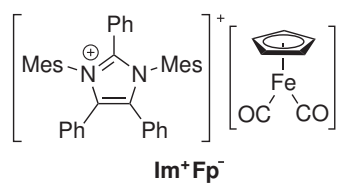


Figure A3. Overview of imidazolidines and other compounds.

Crystallographic Data

Table A1: Crystal data and refinement details.

compound	PhMesAm	C ₆ F ₅ MesAm	CF ₃ PhMesAm
empirical formula	C ₂₅ H ₂₈ N ₂	C ₂₅ H ₂₃ F ₅ N ₂	C ₂₆ H ₂₇ F ₃ N ₂
formula weight	356.49	446.45	424.51
<i>T</i> [K]	133(2)	133(2)	133(2)
crystal size [mm ³]	0.41 × 0.17 × 0.06	0.50 × 0.50 × 0.46	0.44 × 0.15 × 0.14
crystal system	monoclinic	monoclinic	orthorhombic
space group	<i>C2/c</i>	<i>C2/c</i>	<i>P2₁2₁2₁</i>
<i>a</i> [Å]	28.7595(16)	20.5125(7)	10.7826(6)
<i>b</i> [Å]	8.7326(3)	13.4309(3)	18.8601(9)
<i>c</i> [Å]	18.4758(12)	16.6149(6)	22.5082(10)
<i>α</i> [°]	90.00	90.00	90.00
<i>β</i> [°]	113.359(5)	106.455(3)	90.00
<i>γ</i> [°]	90.00	90.00	90.00
<i>V</i> [Å ³]	4259.8(4)	4389.9(2)	4577.3(4)
<i>Z</i>	8	8	4
<i>ρ</i> [g cm ⁻³]	1.112	1.351	1.232
<i>F</i> (000)	1536	1856	1792
<i>μ</i> [mm ⁻¹]	0.065	0.109	0.089
<i>T</i> _{min} / <i>T</i> _{max}	0.8013 / 0.9716	0.8098 / 0.9598	– / –
<i>θ</i> -range [°]	1.54 – 26.73	1.84 – 26.72	1.41 – 25.68
<i>hkl</i> -range	–36 ≤ <i>h</i> ≤ 36 –11 ≤ <i>k</i> ≤ 11 –23 ≤ <i>l</i> ≤ 22	–25 ≤ <i>h</i> ≤ 25 –16 ≤ <i>k</i> ≤ 16 –20 ≤ <i>l</i> ≤ 20	–13 ≤ <i>h</i> ≤ 13 –22 ≤ <i>k</i> ≤ 22 –23 ≤ <i>l</i> ≤ 27
measured refl.	20050	29454	40365
unique refl. [<i>R</i> _{int}]	4506 [0.0611]	4650 [0.0258]	8623 [0.1201]
obs. refl. (<i>I</i> > 2σ(<i>I</i>))	2779	4076	6238
data / res. / param.	4506 / 70 / 256	4650 / 0 / 301	8623 / 0 / 608
goodness-of-fit (<i>F</i> ²)	0.904	1.047	1.016
<i>R</i> 1, <i>wR</i> 2 (<i>I</i> > 2σ(<i>I</i>))	0.0463, 0.0912	0.0396, 0.1059	0.0489, 0.0987
<i>R</i> 1, <i>wR</i> 2 (all data)	0.0910, 0.1033	0.0459, 0.1094	0.0712, 0.1056
resid. el. dens. [e Å ⁻³]	–0.168 / 0.156	–0.222 / 0.223	–0.173 / 0.171

Table A2: Crystal data and refinement details.

compound	PhFAm	TolFAm	MesFAm
empirical formula	C ₁₉ H ₁₂ F ₄ N ₂	C ₂₀ H ₁₄ F ₄ N ₂	C ₂₂ H ₁₈ F ₄ N ₂
formula weight	344.31	358.33	386.38
<i>T</i> [K]	133(2)	133(2)	133(2)
crystal size [mm ³]	0.53 × 0.45 × 0.33	0.49 × 0.37 × 0.33	0.28 × 0.23 × 0.14
crystal system	monoclinic	monoclinic	monoclinic
space group	<i>Cc</i>	<i>P2₁/n</i>	<i>C2/c</i>
<i>a</i> [Å]	19.438(4)	10.3066(3)	46.8826(12)
<i>b</i> [Å]	10.114(2)	9.5516(2)	12.1413(4)
<i>c</i> [Å]	17.811(4)	33.7798(11)	31.8845(8)
α [°]	90.00	90.00	90.00
β [°]	116.93(3)	97.362(2)	124.558(2)
γ [°]	90.00	90.00	90.00
<i>V</i> [Å ³]	3121.8(11)	3298.02(16)	14946.8(7)
<i>Z</i>	8	8	32
ρ [g cm ⁻³]	1.465	1.443	1.374
<i>F</i> (000)	1408	1472	6400
μ [mm ⁻¹]	0.121	0.117	0.109
<i>T</i> _{min} / <i>T</i> _{max}	0.8082 / 0.9665	0.8991 / 0.9756	0.7712 / 0.9489
θ -range [°]	2.33 – 26.71	2.01 – 26.75	1.55 – 25.64
<i>hkl</i> -range	–24 ≤ <i>h</i> ≤ 24 –12 ≤ <i>k</i> ≤ 12 –22 ≤ <i>l</i> ≤ 22	–13 ≤ <i>h</i> ≤ 13 –12 ≤ <i>k</i> ≤ 12 –42 ≤ <i>l</i> ≤ 42	–49 ≤ <i>h</i> ≤ 56 –14 ≤ <i>k</i> ≤ 14 –38 ≤ <i>l</i> ≤ 37
measured refl.	15578	26149	68377
unique refl. [<i>R</i> _{int}]	6122 [0.0285]	6944 [0.0423]	14073 [0.0753]
obs. refl. (<i>I</i> > 2σ(<i>I</i>))	5721	6179	7602
data / res. / param.	6122 / 2 / 457	6944 / 0 / 479	14073 / 6 / 1039
goodness-of-fit (<i>F</i> ²)	1.059	1.051	1.017
<i>R</i> 1, <i>wR</i> 2 (<i>I</i> > 2σ(<i>I</i>))	0.0286, 0.0748	0.0360, 0.0859	0.0561, 0.1069
<i>R</i> 1, <i>wR</i> 2 (all data)	0.0308, 0.0755	0.0416, 0.0886	0.1180, 0.1197
resid. el. dens. [e Å ⁻³]	–0.133 / 0.222	–0.209 / 0.250	–0.209 / 0.405

Table A3: Crystal data and refinement details.

compound	TolTolAm	Ag ₂ (PhFAM) ₂	Ag ₂ (CF ₃ PhFAM) ₂
empirical formula	C ₂₂ H ₂₂ N ₂	C ₃₈ H ₂₂ Ag ₂ F ₈ N ₄ · 3 CHCl ₃	C ₄₀ H ₂₀ Ag ₂ F ₁₄ N ₄
formula weight	314.42	1260.44	1038.34
T [K]	133(2)	133(2)	133(2)
crystal size [mm ³]	0.22 × 0.20 × 0.09	0.19 × 0.18 × 0.12	0.43 × 0.33 × 0.31
crystal system	monoclinic	monoclinic	orthorhombic
space group	<i>P</i> 2 ₁ / <i>c</i>	<i>P</i> 2 ₁ / <i>c</i>	<i>Pbca</i>
<i>a</i> [Å]	13.0595(6)	22.5110(10)	11.3583(3)
<i>b</i> [Å]	15.5485(7)	16.5658(8)	14.7048(6)
<i>c</i> [Å]	9.0203(4)	12.0370(5)	22.1947(6)
α [°]	90.00	90.00	90.00
β [°]	97.919(4)	91.787(4)	90.00
γ [°]	90.00	90.00	90.00
<i>V</i> [Å ³]	1814.16(14)	4486.6(3)	3707.0(2)
<i>Z</i>	4	4	4
ρ [g cm ⁻³]	1.151	1.866	1.860
<i>F</i> (000)	672	2472	2032
μ [mm ⁻¹]	0.067	1.480	1.164
<i>T</i> _{min} / <i>T</i> _{max}	– / –	0.6795 / 0.8275	0.6549 / 0.7471
θ -range [°]	1.57 – 26.73	1.53 – 26.18	1.84 – 26.74
<i>hkl</i> -range	–16 ≤ <i>h</i> ≤ 16 –19 ≤ <i>k</i> ≤ 19 –11 ≤ <i>l</i> ≤ 11	–27 ≤ <i>h</i> ≤ 27 –20 ≤ <i>k</i> ≤ 20 –14 ≤ <i>l</i> ≤ 14	–14 ≤ <i>h</i> ≤ 14 –18 ≤ <i>k</i> ≤ 18 –28 ≤ <i>l</i> ≤ 28
measured refl.	24162	68258	33892
unique refl. [<i>R</i> _{int}]	3856 [0.0978]	68258 [0.0000]	3934 [0.0363]
obs. refl. (<i>I</i> > 2σ(<i>I</i>))	2799	34116	3464
data / res. / param.	3856 / 0 / 223	68258 / 0 / 578	3934 / 0 / 271
goodness-of-fit (<i>F</i> ²)	1.017	1.056	1.041
<i>R</i> 1, <i>wR</i> 2 (<i>I</i> > 2σ(<i>I</i>))	0.0510, 0.1156	0.0656, 0.1286	0.0212, 0.0526
<i>R</i> 1, <i>wR</i> 2 (all data)	0.0777, 0.1245	0.1298, 0.1380	0.0273, 0.0544
resid. el. dens. [e Å ⁻³]	–0.207 / 0.204	–0.700 / 1.996	–0.376 / 0.341

Table A4: Crystal data and refinement details.

compound	$\text{Ag}_2(\text{TolFam})_2$	$[\text{Im}^{-2\text{H}}]^+\text{PF}_6^-$	$\text{PhMesIm}^+\text{Br}^-$
empirical formula	$\text{C}_{40}\text{H}_{26}\text{Ag}_2\text{F}_8\text{N}_4$ · 2 DCM	$\text{C}_{39}\text{H}_{37}\text{F}_6\text{N}_2\text{P}$	$\text{C}_{27}\text{H}_{31}\text{BrN}_2$
formula weight	1100.24	678.68	463.45
T [K]	133(2)	133(2)	133(2)
crystal size [mm^3]	$0.36 \times 0.16 \times 0.11$	$0.13 \times 0.12 \times 0.10$	$0.50 \times 0.40 \times 0.32$
crystal system	monoclinic	monoclinic	trigonal
space group	$C2/c$	$P12/n1$	$P3_121$
a [Å]	16.6060(5)	11.1082(9)	11.6076(16)
b [Å]	21.7809(6)	11.8758(7)	11.6076(16)
c [Å]	11.9174(4)	15.9382(12)	14.991(3)
α [°]	90	90.000	90.00
β [°]	108.087(3)	91.189(6)	90.00
γ [°]	90	90.000	120.00
V [Å ³]	4097.5(2)	2102.1(3)	1749.2(5)
Z	4	2	3
ρ [g cm^{-3}]	1.784	1.866	1.320
$F(000)$	2176	2472	726
μ [mm^{-1}]	1.291	1.480	1.778
$T_{\text{min}} / T_{\text{max}}$	0.6672 / 0.8503	0.6795 / 0.8275	0.4778 / 0.6374
θ -range [°]	1.593 – 26.730	1.53 – 26.18	2.03 – 26.72
hkl -range	$-20 \leq h \leq 20$ $-25 \leq k \leq 27$ $-15 \leq l \leq 15$	$-27 \leq h \leq 27$ $-20 \leq k \leq 20$ $-14 \leq l \leq 14$	$-14 \leq h \leq 14$ $-14 \leq k \leq 14$ $-18 \leq l \leq 18$
measured refl.	25168	68258	19326
unique refl. [R_{int}]	4345 [0.0479]	68258 [0.0000]	2471 [0.0317]
obs. refl. ($I > 2\sigma(I)$)	3923	34116	2451
data / res. / param.	4345 / 0 / 277	68258 / 0 / 578	2471 / 0 / 141
goodness-of-fit (F^2)	1.019	1.056	1.064
$R1, wR2$ ($I > 2\sigma(I)$)	0.0198, 0.0459	0.0656, 0.1286	0.0197, 0.0537
$R1, wR2$ (all data)	0.0241, 0.0472	0.160, 0.1380	0.0200, 0.0538
resid. el. dens. [e Å^{-3}]	-0.470 / 0.418	-0.700 / 1.996	-0.271 / 0.217

Table A5: Crystal data and refinement details.

compound	C ₆ F ₅ MesIm ⁺ Br ⁻	CF ₃ PhMesIm ⁺ Br ⁻	PhFlm ⁺ Br ⁻
empirical formula	C ₂₇ H ₂₆ BrF ₅ N ₂ · 0.25 Et ₂ O	C ₂₈ H ₃₀ BrF ₃ N ₂ · CHCl ₃ , · 0.5 Et ₂ O	C ₂₁ H ₁₅ BrF ₄ N ₂
formula weight	571.94	687.88	451.26
<i>T</i> [K]	293(2)	133(2)	133(2)
crystal size [mm ³]	0.39 × 0.26 × 0.25	0.35 × 0.22 × 0.21	0.5 × 0.5 × 0.36
crystal system	triclinic	orthorhombic	monoclinic
space group	<i>P</i> $\bar{1}$	<i>Pbca</i>	<i>P2</i> ₁ / <i>c</i>
<i>a</i> [Å]	10.505(2)	14.6158(3)	9.9328(3)
<i>b</i> [Å]	10.524(2)	10.3915(2)	18.4913(8)
<i>c</i> [Å]	14.887(3)	43.9148(10)	10.6863(3)
α [°]	77.47(3)	90.00	90.00
β [°]	78.34(3)	90.00	95.917(3)
γ [°]	66.56(3)	90.00	90.00
<i>V</i> [Å ³]	1461.7(5)	6669.8(2)	1952.30(12)
<i>Z</i>	2	8	4
ρ [g cm ⁻³]	1.299	1.370	1.535
<i>F</i> (000)	585	2824	904
μ [mm ⁻¹]	1.456	1.514	2.151
<i>T</i> _{min} / <i>T</i> _{max}	0.6226 / 0.7349	0.4857 / 0.6317	0.2525 / 0.5110
θ -range [°]	1.41 - 26.85	1.85 - 25.64	2.06 - 26.86
<i>hkl</i> -range	-12 ≤ <i>h</i> ≤ 13 -13 ≤ <i>k</i> ≤ 13 -18 ≤ <i>l</i> ≤ 18	-17 ≤ <i>h</i> ≤ 17 -12 ≤ <i>k</i> ≤ 11 -53 ≤ <i>l</i> ≤ 53	-11 ≤ <i>h</i> ≤ 12 -23 ≤ <i>k</i> ≤ 23 -13 ≤ <i>l</i> ≤ 13
measured refl.	18977	53887	25601
unique refl. [<i>R</i> _{int}]	6231 [0.0926]	5951 [0.0839]	4160 [0.0559]
obs. refl. (<i>I</i> > 2σ(<i>I</i>))	3637	5001	3830
data / res. / param.	6231 / 24 / 357	5951 / 4 / 369	4160 / 0 / 253
goodness-of-fit (<i>F</i> ²)	1.001	1.034	1.124
<i>R</i> 1, <i>wR</i> 2 (<i>I</i> > 2σ(<i>I</i>))	0.0687, 0.1821	0.0404, 0.1061	0.0330, 0.0769
<i>R</i> 1, <i>wR</i> 2 (all data)	0.1095, 0.2116	0.0501, 0.1115	0.0382, 0.0791
resid. el. dens. [e Å ⁻³]	-0.430 / 0.748	-0.350 / 0.334	-0.404 / 0.417

Table A6: Crystal data and refinement details.

compound	TolFIm ⁺ Br ⁻	MesFIm ⁺ Br ⁻	TolFTolIm ⁺ Br ⁻
empirical formula	C ₂₂ H ₁₇ BrF ₄ N ₂ · H ₂ O	C ₂₄ H ₂₁ BrF ₄ N ₂	C ₂₄ H _{15.75} BrF _{8.25} N ₂ · 0.5 H ₂ O
formula weight	483.30	493.34	577.80
<i>T</i> [K]	133(2)	133(2)	133(2)
crystal size [mm ³]	0.46 × 0.45 × 0.15	0.41 × 0.3 × 0.08	0.65 × 0.34 × 0.06
crystal system	triclinic	monoclinic	triclinic
space group	<i>P</i> $\bar{1}$	<i>P</i> 2 ₁ / <i>c</i>	<i>P</i> $\bar{1}$
<i>a</i> [Å]	10.3885(5)	10.0129(3)	7.8445(8)
<i>b</i> [Å]	10.4707(5)	22.7057(9)	10.6861(10)
<i>c</i> [Å]	10.6706(5)	10.3495(3)	14.1239(14)
α [°]	111.553(4)	90.00	85.586(8)
β [°]	96.864(4)	112.720(2)	83.356(8)
γ [°]	102.719(4)	90.00	76.014(8)
<i>V</i> [Å ³]	1027.04(8)	2170.38(12)	1139.68(19)
<i>Z</i>	2	4	2
ρ [g cm ⁻³]	1.563	1.510	1.684
<i>F</i> (000)	488	1000	576
μ [mm ⁻¹]	2.053	1.941	1.889
<i>T</i> _{min} / <i>T</i> _{max}	0.3849 / 0.7487	0.4735 / 0.8108	0.4284 / 0.9187
θ -range [°]	2.06 – 26.72	1.79 – 26.75	1.45 – 26.82
<i>hkl</i> -range	-13 ≤ <i>h</i> ≤ 13 -13 ≤ <i>k</i> ≤ 13 -13 ≤ <i>l</i> ≤ 13	-12 ≤ <i>h</i> ≤ 12 -28 ≤ <i>k</i> ≤ 28 -13 ≤ <i>l</i> ≤ 11	-9 ≤ <i>h</i> ≤ 9 -11 ≤ <i>k</i> ≤ 13 -17 ≤ <i>l</i> ≤ 17
measured refl.	13660	18058	14662
unique refl. [<i>R</i> _{int}]	4340 [0.0374]	4607 [0.0311]	4837 [0.0530]
obs. refl. (<i>I</i> > 2σ(<i>I</i>))	4091	4056	3593
data / res. / param.	4340 / 2 / 278	4607 / 0 / 283	4837 / 31 / 348
goodness-of-fit (<i>F</i> ²)	1.039	1.055	1.129
<i>R</i> 1, <i>wR</i> 2 (<i>I</i> > 2σ(<i>I</i>))	0.0240, 0.0596	0.0333, 0.0806	0.0629, 0.1367
<i>R</i> 1, <i>wR</i> 2 (all data)	0.0261, 0.0605	0.0400, 0.0834	0.0901, 0.1479
resid. el. dens. [e Å ⁻³]	-0.365 / 0.372	-0.691 / 0.321	-0.256 / 0.604

Table A7: Crystal data and refinement details.

compound	TolTolIm ⁺ Br ⁻	HTolFlm	KRp
empirical formula	C ₂₄ H ₂₅ BrN ₂	C ₂₂ H ₁₈ F ₄ N ₂	C ₇ H ₅ KO ₂ Ru · THF
formula weight	421.37	386.38	333.38
<i>T</i> [K]	133(2)	133(2)	133(2)
crystal size [mm ³]	0.28 × 0.26 × 0.22	0.50 × 0.28 × 0.15	0.33 × 0.29 × 0.12
crystal system	orthorhombic	triclinic	orthorhombic
space group	<i>Pna</i> 2 ₁	<i>P</i> $\bar{1}$	<i>Pbca</i>
<i>a</i> [Å]	19.2736(5)	9.0488(17)	8.7374(17)
<i>b</i> [Å]	10.0987(3)	9.7465(18)	11.492(2)
<i>c</i> [Å]	10.4938(4)	11.796(2)	24.169(5)
α [°]	90.00	106.091(15)	90
β [°]	90.00	92.927(15)	90
γ [°]	90.00	110.799(14)	90
<i>V</i> [Å ³]	2042.50(11)	921.4(3)	2426.9(8)
<i>Z</i>	4	2	8
ρ [g cm ⁻³]	1.370	1.393	1.825
<i>F</i> (000)	872	400	1328
μ [mm ⁻¹]	2.023	0.111	1.623
<i>T</i> _{min} / <i>T</i> _{max}	0.4955 / 0.6973	0.9643 / 0.9875	0.2958 / 0.7075
θ -range [°]	2.11 – 26.74	1.82 – 26.87	1.685 – 25.705
<i>hkl</i> -range	-24 ≤ <i>h</i> ≤ 24 -12 ≤ <i>k</i> ≤ 12 -13 ≤ <i>l</i> ≤ 13	-11 ≤ <i>h</i> ≤ 11 -12 ≤ <i>k</i> ≤ 12 -14 ≤ <i>l</i> ≤ 14	-10 ≤ <i>h</i> ≤ 10 -13 ≤ <i>k</i> ≤ 13 -29 ≤ <i>l</i> ≤ 29
measured refl.	24856	11628	21384
unique refl. [<i>R</i> _{int}]	4347 [0.0580]	3931 [0.0945]	2284 [0.0982]
obs. refl. (<i>I</i> > 2σ(<i>I</i>))	3926	2363	2029
data / res. / param.	4347 / 1 / 247	3931 / 0 / 254	2284 / 0 / 145
goodness-of-fit (<i>F</i> ²)	1.017	0.915	1.073
<i>R</i> 1, <i>wR</i> 2 (<i>I</i> > 2σ(<i>I</i>))	0.0294, 0.0611	0.0474, 0.1052	0.0249, 0.0637
<i>R</i> 1, <i>wR</i> 2 (all data)	0.0346, 0.0626	0.0898, 0.1224	0.0300, 0.0659
resid. el. dens. [e Å ⁻³]	-0.273 / 0.529	-0.196 / 0.140	-0.585 / 0.522

Table A8: Crystal data and refinement details.

compound	17	[Rp–TolFlm] ⁺ Br ⁻
empirical formula	C ₃₉ H ₃₈ N ₂ O	C ₂₉ H ₂₂ BrF ₃ N ₂ O ₂ Ru · MeCN
formula weight	550.71	709.52
<i>T</i> [K]	133(2)	133(2)
crystal size [mm ³]	0.39 × 0.27 × 0.24	0.21 × 0.16 × 0.07
crystal system	monoclinic	triclinic
space group	<i>P</i> 2 ₁ / <i>c</i>	<i>P</i> $\bar{1}$
<i>a</i> [Å]	16.7008(9)	9.6121(5)
<i>b</i> [Å]	8.7947(4)	11.8218(5)
<i>c</i> [Å]	20.9993(13)	13.3728(6)
α [°]	90	76.337(4)
β [°]	90.935(5)	87.560(4)
γ [°]	90	84.662(4)
<i>V</i> [Å ³]	3083.9(3)	1469.84(12)
<i>Z</i>	4	2
ρ [g cm ⁻³]	1.186	1.603
<i>F</i> (000)	1176	708
μ [mm ⁻¹]	0.071	1.944
<i>T</i> _{min} / <i>T</i> _{max}	0.7732 / 0.9483	0.6853 / 0.8580
θ -range [°]	1.940 – 26.832	1.567 – 26.756
<i>hkl</i> -range	-21 ≤ <i>h</i> ≤ 21 -11 ≤ <i>k</i> ≤ 10 -26 ≤ <i>l</i> ≤ 26	-12 ≤ <i>h</i> ≤ 11 -14 ≤ <i>k</i> ≤ 14 -16 ≤ <i>l</i> ≤ 16
measured refl.	25194	18033
unique refl. [<i>R</i> _{int}]	6343 [0.0469]	6212 [0.0451]
observed refl. (<i>I</i> > 2σ(<i>I</i>))	4422	5139
data / restraints / param.	6343 / 0 / 385	6212 / 0 / 372
goodness-of-fit (<i>F</i> ²)	1.031	1.011
<i>R</i> 1, <i>wR</i> 2 (<i>I</i> > 2σ(<i>I</i>))	0.0544, 0.1282	0.0309, 0.0669
<i>R</i> 1, <i>wR</i> 2 (all data)	0.0852, 0.1420	0.0423, 0.0699
resid. el. dens. [e Å ⁻³]	-0.350 / 0.279	-0.393 / 0.693

Electron Microprobe Analysis

Table A9: Details of EMPA measurements of the black solid **Rs**. The table includes values obtained from measurements at different positions on the sample surface and their mean values (\emptyset). Recalculating the raw data using CITZAF^[500] (see Experimental Section) and assuming that the unassigned content is carbon, leads to minor deviations represented as well in the table (\emptyset_{corr}).

No.	mass percentage (wt%)				normalized atomic percentage (at%)				standard deviations (relative %) (1-sigma by counting statistics)				
	O	Si	Ru	K	O	Si	Ru	K	O	Si	Ru	K	
1	11.8	0.6	44.0	14.1	47.4	1.4	28.0	23.2	100	1.41	2.23	0.67	0.62
2	12.0	0.8	43.9	12.8	48.6	1.9	28.2	21.3	100	1.40	1.81	0.67	0.65
3	12.6	0.4	45.6	13.2	49.6	1.0	28.3	21.2	100	1.36	2.87	0.66	0.64
4	11.7	0.5	44.4	14.2	47.3	1.0	28.3	23.4	100	1.42	2.70	0.66	0.62
5	13.1	0.8	43.1	12.7	51.3	1.8	26.6	20.3	100	1.32	1.79	0.68	0.65
6	14.8	0.5	43.6	12.4	54.7	1.1	25.5	18.8	100	1.23	2.45	0.67	0.66
7	18.0	1.3	40.6	12.7	59.3	2.4	21.2	17.1	100	1.07	1.38	0.70	0.65
8	14.6	0.7	41.8	13.0	54.1	1.5	24.6	19.8	100	1.23	1.99	0.69	0.64
9	13.2	0.5	43.1	12.9	51.5	1.2	26.7	20.6	100	1.31	2.39	0.68	0.65
10	17.4	0.9	41.6	12.6	58.7	1.7	22.3	17.4	100	1.09	1.74	0.69	0.65
11	14.7	0.6	43.9	12.2	54.4	1.3	25.8	18.6	100	1.22	2.21	0.67	0.66
\emptyset	14.0	0.7	43.2	13.0	52.4	1.5	26.0	20.2	100	1.28	2.14	0.68	0.64
\emptyset_{corr}	13.6	0.7	44.2	12.9	21.1	0.6	10.9	8.2	100*	1.28	2.14	0.68	0.64

(*) The estimated carbon content which is not included in this table was taken into account.

Additional NMR Data

The H₂ splitting reaction described in chapter 5.5.3 performed by mixtures of **TolFI_m⁺Br⁻** and **Rs** was examined by means of NMR spectroscopy. In this section, detailed views of the time-dependent evolution of the signals are provided.

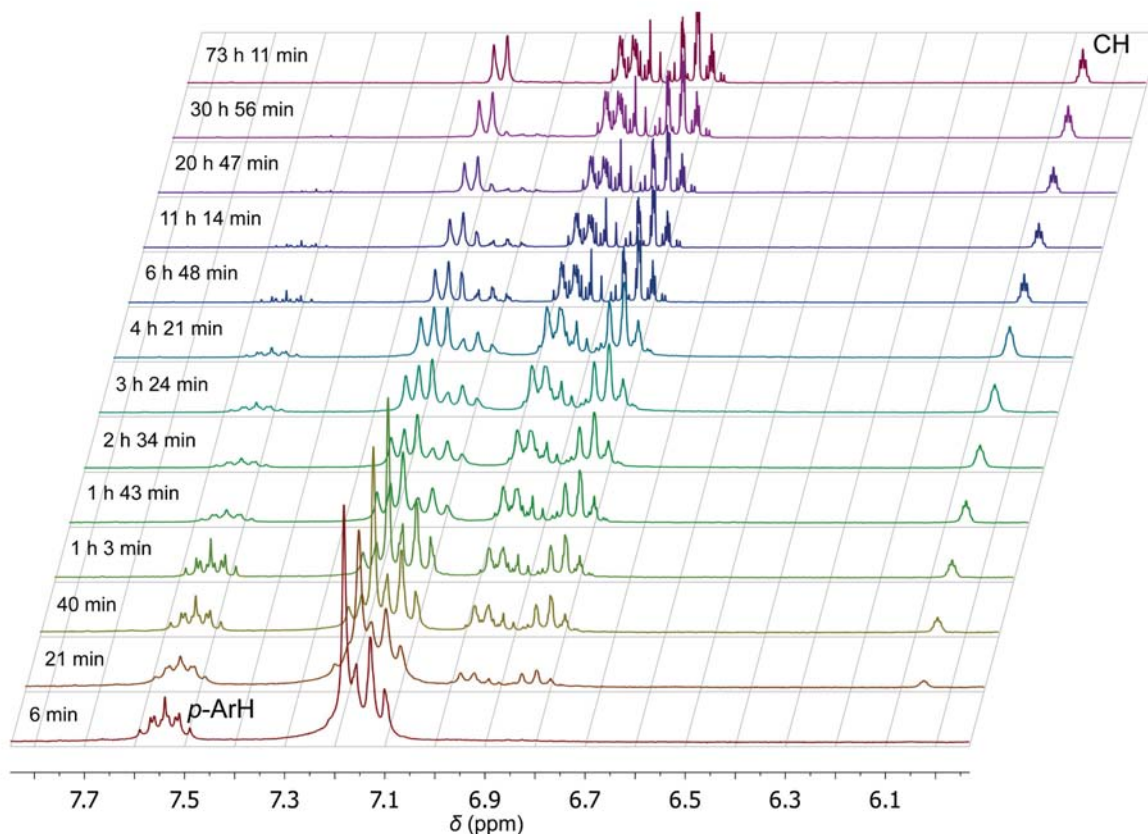


Figure A4. Superposition of ¹H NMR spectra (300 MHz, CD₃CN) acquired at different times in the region of 7.85 to 5.95 ppm. The decrease of the *p*-ArH signal of **TolFI_m⁺Br⁻** at 7.60 – 7.50 ppm and the increase of the CH signal for **HTolFI_m** at 6.07 ppm are visible.

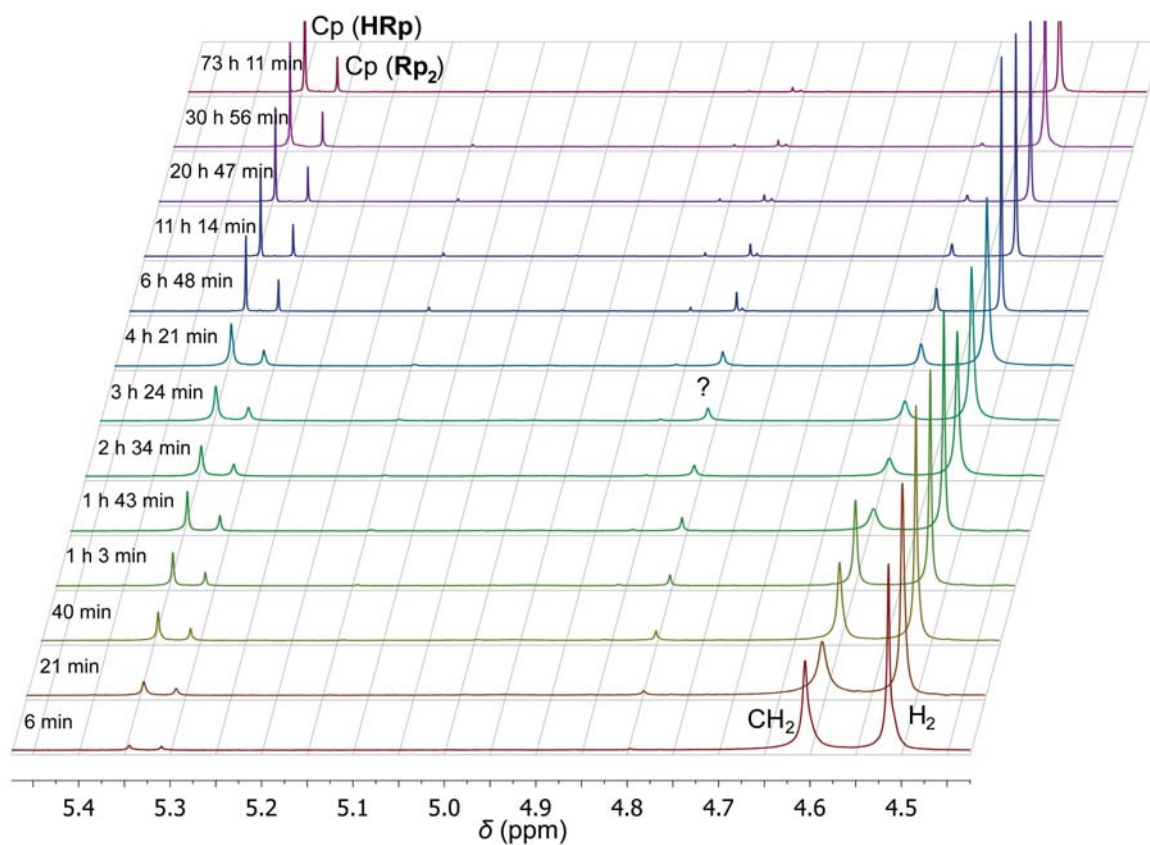


Figure A5. Superposition of ^1H NMR spectra (300 MHz, CD_3CN) acquired at different times in the region of 5.49 to 4.45 ppm. Cp signals for **HRp** (5.40 ppm) and **Rp₂** (5.36 ppm) increase, while the CH_2 signal of **TolFIm⁺Br⁻** at 4.67 ppm decreases. At a chemical shift of 4.86 ppm, a temporarily formed species is observed. The species could not be identified unambiguously until now.

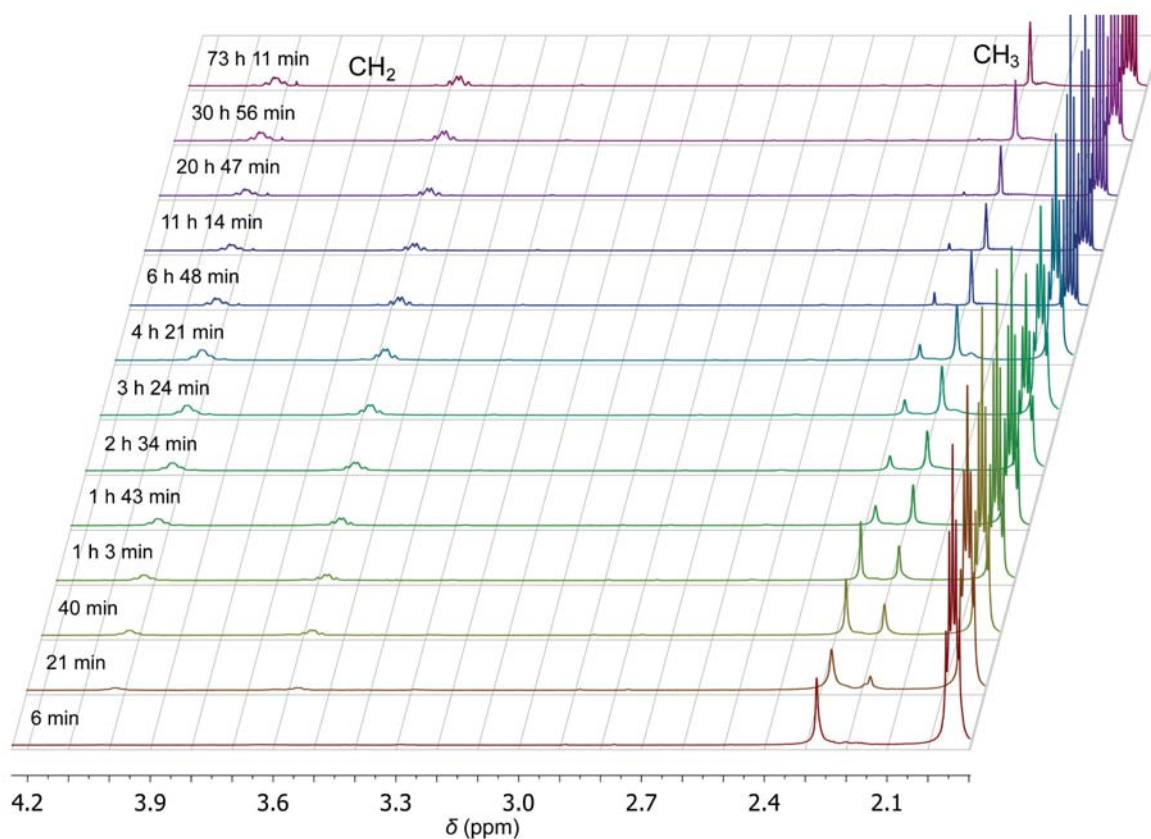


Figure A6. Superposition of ^1H NMR spectra (300 MHz, CD_3CN) acquired at different times in the region of 4.25 to 1.09 ppm. CH_2 signals (4.09–3.97 and 3.64–3.52 ppm) and a CH_3 signal at 2.18 ppm attributable to **HTolFI**m appear while the CH_3 signal for **TolFI**m $^+$ **Br** $^-$ at 2.27 ppm decreases.

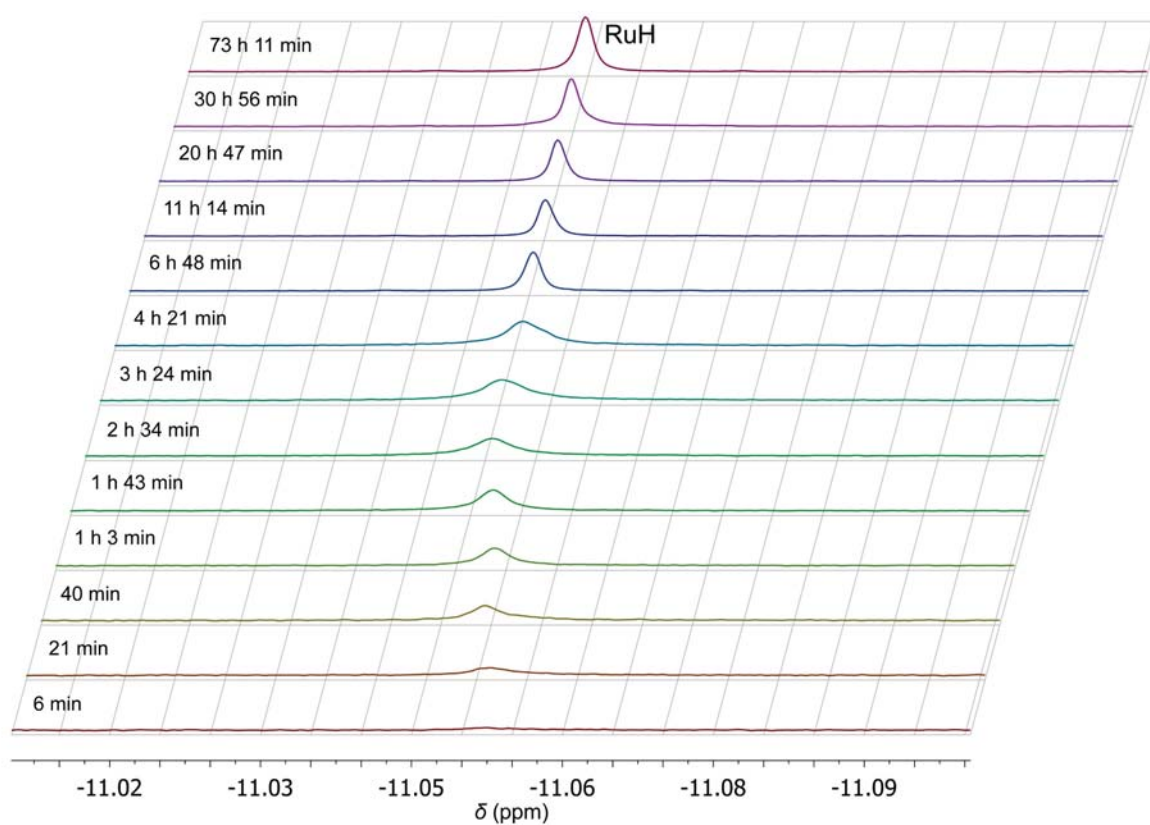


Figure A7. Superposition of ¹H NMR spectra (300 MHz, CD₃CN) acquired at different times in the region of -11.01 to -11.10 ppm. The intensity of the signal corresponding to the metal hydride **HRp** (-11.05 ppm) increases.

List of Scientific Contributions

Publications

K. F. Kalz, N. Kindermann, S.-Q. Xiang, A. Kronz, A. Lange, F. Meyer, "Revisiting the Synthesis and Elucidating the Structure of Potassium Cyclopentadienyldicarbonylruthenate, $K[CpRu(CO)_2]$ ", *Organometallics* **2014**, *33*, 1475–1479.

K. F. Kalz, A. Brinkmeier, S. Dechert, R. A. Mata, F. Meyer, "Functional Model for the [Fe] Hydrogenase Inspired by the Frustrated Lewis Pair Concept", *J. Am. Chem. Soc.* **2014**, *136*, 16626–16634.

Material from these publications was reprinted or adapted with permission in this thesis. © 2014 American Chemical Society.

Presentations at Conferences and Workshops

K. F. Kalz, "Mimicking the [Fe] Hydrogenase Active Site – Frustrated Lewis Pairs for the Heterolytic Cleavage of H_2 ", *Joint Workshop of the International Research Training Group 1422 "Metal Sites in Biomolecules: Structures, Regulation and Mechanisms" and the Emerging Fields Initiative "Medicinal Redox Inorganic Chemistry"*, Homberg (Hülsa), Germany, May 23rd to 25th, **2013**.

K. F. Kalz, "Mimicking the [Fe] Hydrogenase Active Site – Frustrated Lewis Pairs for the Heterolytic Cleavage of H_2 ", *6. Göttinger Chemie-Forum*, Göttingen, Germany, June 05th, **2013**.

Posters at Conferences and Workshops

K. F. Kalz, S. Dechert, F. Meyer, "Mimicking the [Fe] Hydrogenase Active Site: Frustrated Lewis Pairs for the Heterolytic Cleavage of Dihydrogen", *Workshop of the International Research Training Group 1422 "Metal Sites in Biomolecules: Structures, Regulation and Mechanisms"*, Lund, Sweden, February 9th to 11th, **2011**.

K. F. Kalz, A. Brinkmeier, C. Schiwiek, F. Meyer, "Mimicking the [Fe] Hydrogenase Active Site: Frustrated Lewis Pairs for the Heterolytic Cleavage of Dihydrogen", *Joint Workshop of the International Research Training Group 1422 "Metal Sites in Biomolecules: Structures, Regulation and Mechanisms" and the FOR 1405 "Dynamics of Electron Transfer Processes within Transition Metal Sites in Biological and Bioinorganic Systems"*, Hofgeismar, Germany, April 11th to 13th, **2012**.

K. F. Kalz, A. Brinkmeier, S. Dechert, F. Meyer, "Mimicking the [Fe] Hydrogenase Active Site: Frustrated Lewis Pairs for the Heterolytic Cleavage of H₂", *Zing Conference – Bioinorganic Chemistry*, Lanzarote, Spain, February 19th to 22nd, **2013**.

K. F. Kalz, A. Brinkmeier, S. Dechert, F. Meyer, "Mimicking the [Fe] Hydrogenase Active Site: Frustrated Lewis Pairs for the Heterolytic Cleavage of H₂", *Joint Workshop of the International Research Training Group 1422 "Metal Sites in Biomolecules: Structures, Regulation and Mechanisms" and the Emerging Fields Initiative "Medicinal Redox Inorganic Chemistry"*, Homberg (Hülsa), Germany, May 23rd to 25th, **2013**.

Acknowledgments

First of all I would like to thank my supervisor Prof. Dr. Franc Meyer for his guidance and for giving me the opportunity to work on an exciting topic relevant to one of the most urgent issues of the present time, the world's energy problem. His optimistic and motivating attitude fueled my own ambition to search for solutions to seemingly desperate situations. Thank you Franc for granting great academic freedom, the proper equipment, and a positive working atmosphere. Special thanks I address to my co-supervisors Prof. Dr. Ulf Diederichsen and Prof. Dr. Ebbe Nordlander, and the whole examination board.

Many thanks I owe to my colleagues and external cooperation partners who contributed to this work: Dr. Adam Lange, Sheng-Qi Xiang, and Brigitta Angerstein (Max Planck Institute for Biophysical Chemistry) for the solid-state NMR measurements; Dr. Andreas Kronz (Geowissenschaftliches Zentrum, Georg-August-University Göttingen) for the wavelength dispersive electron microprobe analysis of **Rs**; Prof. Dr. Ricardo Mata (Institute of Physical Chemistry, Georg-August-University Göttingen) for the DFT calculations concerning the mechanism of dihydrogen splitting by the FLP **ToIFIm⁺Rp⁻**; Dr. Michael John, Ralf Schöne, and Wolfgang Zolke for their help with numerous NMR measurements and interpretation of NMR data; Dr. Sebastian Dechert for performing X-ray diffraction experiments and X-ray data refinements, for his help with computer programs and DFT calculations, and for his advice I appreciated very much; Nicole Kindermann, Steffen Meyer, and Kevin Pröpper for further X-ray diffraction experiments and corresponding structure refinements; Dr. Claudia Stückl for EPR measurements; Jörg Teichgräber for cyclic voltammetry measurements; Angelika Wraage and the analytical laboratory for elemental analyses; Dr. Holm Frauendorf and Thomas Schuchardt for questions and problems related to mass spectrometry; Jörg Teichgräber, Andreas Schwarz, Petra Unger, Dr. Claudia Stückl, and the workshops of the institute for tackling all kinds of technical and administrative issues. Thank you all for your continuous support and patience which were essential for the success of this work!

Furthermore, I would like to thank my bachelor students Christoph Schiwiek, Alexander Brinkmeier, and Artur Kochanke, as well as the research students who supported me with their experimental work. For a wonderful time in the laboratory I am truly grateful to Lina, Adam, Olli, Jörg, and Claudia. The perfect teamwork and the many – not always scientific – discussions were essential ingredients for the completion of this PhD thesis. I thank all present and former members of the Meyer group, especially the “old-school members” Markus, Felix, Iris, Anett, Adam, Anne B., Kristian, Dennis, Sven, Beni, Lina, Toni, and Steffen. The great atmosphere and the many group activities made the workplace an entertaining place. Special thanks I would like to address to Felix Klinke. The mutual support and helpful discussions during the final stages of this PhD thesis facilitated the challenges I faced at that time. For corrections and improvements of this

document I thank Dr. Michael John, Anne Bretschneider, Nicole Kindermann, Dennis Manz, Sven Neudeck, and Markus Steinert.

I gratefully acknowledge research fellowships including financial support from the DFG (International Research Training Group 1422 “Metal Sites in Biomolecules: Structures, Regulation and Mechanisms”) and the “Fonds der Chemischen Industrie”. Furthermore, I thank all IRTG members for the pleasant time we spent in seminars, at workshops, and at conferences.

I would like to express my special thanks to all my friends in Göttingen, especially to the “core” of the summer semester 2005: Nils, Tim, Dennis, Johannes, Sven, and Markus. Thank you for a wonderful time in Göttingen and for being true friends.

Finally, I thank my parents and my brothers for their unlimited support in every aspect of life.

Curriculum Vitae

Personal Data

Name: Kai Felix Kalz
Date of Birth: September 9th 1984
Place of Birth: Celle
Nationality: German
Marital Status: Unmarried

Pre-Academic Education

08/1991–06/1995 Grundschule Klein Berßen
08/1995–06/2004 Gymnasium Marianum Meppen
06/2004 *Abitur*, cumulative grade 1.3

Civilian Service

7/2004–03/2005 Bürgerhilfe e. V., Meppen

Academic Career

04/2005–04/2007 Undergraduate student at the Faculty of Chemistry, Georg-August-Universität Göttingen
04/2007 *Diplomvorprüfung*
04/2007–04/2009 Diploma student at the Faculty of Chemistry, Georg-August-Universität Göttingen
04/2009–11/2009 Diploma thesis “Bioinspirierte frustrierte Lewis-Paare für die heterolytische Wasserstoffspaltung” supervised by Prof. Dr. F. Meyer, Institute of Inorganic Chemistry, Georg-August-Universität Göttingen
02/2010 *Diplomprüfung*, cumulative grade: 1.05
04/2010–07/2014 PhD thesis “Mimicking the [Fe] Hydrogenase Active Site: Transition Metal Frustrated Lewis Pairs for the Heterolytic Cleavage of Dihydrogen” supervised by Prof. Dr. F. Meyer, Institute of Inorganic Chemistry, Georg-August-Universität Göttingen

